High temperature abrasion in sinter plants and their cost efficient wear protection

Hochtemperatur-Abrasion in Sinteranlagen und
deren wirtschaftlicher Verschleißschutz

Markus Varga, MSc

A dissertation submitted to the
Department of Product Engineering
Montanuniversität Leoben
January 2016

Affidavit

I declare in lieu of oath, that I wrote this thesis and performed the associated research myself, using only literature cited in this volume.

Leoben, January 2016, Markus Varga, MSc

Author

Markus Varga, MSc
msva@gmx.net
AC2T research GmbH
Viktor-Kaplan-Straße 2 C
A-2700 Wiener Neustadt
Tel: +43 2622 816 00 - 132
Fax: + 43 2622 816 00 - 99

Shun no toil, to make yourself remarkable by some talent or other. Yet do not devote yourself to one branch exclusively. Strive to get clear notions about all. Give up no science entirely, for science is but one.

Seneca

To Nina

Acknowledgments

First I want to acknowledge the “Excellence Centre of Tribology”, Wiener Neustadt, Austria, which made this work possible within the frame of Austrian COMET Programme (Project K2, XTribology, 849109). Of my colleagues, Ewald Badisch is thanked for fruitful discussions and scientific input. Reinhard Polak is acknowledged for his expertise in project acquisition and wear protection by hardfacings. Hector Torres deserves thanks for his input of high temperature sliding expertise and English corrections as well as Stefan Eder for the latter. Michael Buranich helped with knowledge of maintenance strategies and economic assessment of wear protection. Harald Rojacz and Christian Katsich are acknowledged for their expertise and help with material analysis. Many thanks go to Frank Schütze for performing high-stress abrasive and impact/abrasive tests and Maksim Antonov for erosive wear experiments. Werner Tschirk is thanked for preparing cross sections and Christian Jogl for operating SEM.

At the Montanuniversität Leoben, Florian Grün and Robert Danzer are greatly acknowledged for their support during preparation of this thesis.

The company partner voestalpine steel deserve thanks, especially Karl Adam for initialisation and support of the projects, Manfred Griesinger for help in understanding the details of the sinter plant and Rudolf Wimberger for making the holistic maintenance approach possible. Castolin is acknowledged for their project support and expertise in hardfacings, especially Johann Hornung for providing samples and Martin Kirchgaßner for scientific input.

Further I would like to thank all the people in my family environment who made it possible for this work to be written. These people are especially my parents who helped me through my university life through financial support. Further thanks go out to my siblings for their backup and my partner who supported me with scientific input and encouragement.

Abstract

Abrasive wear at high temperatures (HT) is a serious issue in many industrial applications. Within this work, on the example of an iron ore sinter plant, maintenance tasks were analysed and abrasive wear was found to be the most frequent tribological failure. Core components like the grate bars of the sinter belt, the sinter crusher system and the hot sieve suffer from abrasion at HT, with various forms of abrasion present. Failure analysis pointed out that high-stress abrasion, impact-abrasion and erosion are of major concern, hence these abrasion modes were studied in detail at temperatures up to 550°C-700°C. The influence of the various forms of abrasion on prospective HT wear-resistant materials was investigated. Relative soft cast materials with low amount of hardphases (<20 %) turned out to show beneficial high-stress abrasive and normal erosive wear behaviour due to the in-situ formation of wear-protective mechanically mixed layers (MML) with the abrasive. The wear rates are lower, up to a factor of 2.3 at high-stress abrasion and up to 3.3× at normal erosion, compared to hardphase-rich materials which do not form MMLs. On the other hand, high hardphase content (>40 %) and high hardness at application temperature are necessary to withstand impact-abrasion, because low hardphase containing materials showed up to 17× higher wear loss. MML formation is strongly dependent on the microstructure of the material: hardfacings with more than 40 % hardphases do not show significant MML formation. Temperature-induced material softening and severe abrasive contact encourage massive MML formation on low hardphase containing materials. In this case, wear protection of in-situ formation of MML was pronounced at HT. Linear correlation of abrasive wear rates with hot hardness was especially evident at high-stress abrasion and oblique erosion (30°). Further, the ratio of normal and oblique erosion follows a linear relationship with the hot hardness for nearly all materials and temperatures investigated.

Keywords

- tribology
- abrasion
- high temperature
- hardfacing
- sinter plant
- maintenance

Kurzfassung

Abrasion bei Hochtemperatur (HT) ist ein kritischer Verschleißmechanismus in vielen industriellen Anwendungen. In dieser Arbeit wurden am Beispiel von Eisenerz-Sinteranlagen Instandhaltungstätigkeiten analysiert und Abrasion zeigte sich als der häufigste tribologische Schadensmechanismus. Kernkomponenten wie die Roststäbe am Sinterband, der Sinterbrecher und das Heißsieb werden durch verschiedene Formen von Abrasion bei HT geschädigt. Schadensanalysen zeigten Hochlast-Abrasion, Schlagabrasion und Erosion als Hauptlast, daher wurden diese Abrasionsformen im Detail bei Temperaturen bis zu 550°C-700°C erforscht. Der Einfluss dieser verschiedenen Abrasionsformen auf unterschiedliche verschleißbeständige HT Werkstoffe wurde untersucht. Relativ weiche Gusswerkstoffe mit geringem Hartphasenanteil (<20 %) zeigten günstige Eigenschaften bei Hochlast-Abrasion und 90°-Erosion aufgrund der in-situ Ausbildung einer verschleißschützenden mechanischen Mischschicht (mechanically mixed layer - MML) mit dem Abrasiv. Die Verschleißraten waren geringer, um einen Faktor von 2,3 bei Hochlast-Abrasion und bis zu 3,3× bei 90°-Erosion, verglichen mit hartphasenreichen Werkstoffen, welche keine MML ausbilden. Andererseits erwiesen sich ein hoher Hartphasenanteil (>40 %) und hohe Härte bei Anwendungstemperatur als unerlässlich um Schlagabrasion zu widerstehen: Werkstoffe mit geringem Hartphasenanteil zeigten bis zu 17× höheren Verschleiß. MML Bildung ist stark abhängig von der Mikrostruktur des Werkstoffes: Hartauftragungen mit über 40 % Hartphasenanteil bilden keine signifikante MML aus. Materialerweichung durch steigende Temperatur und abrasives Hochlastregime begünstigen die Ausbildung dicker MML bei Werkstoffen mit geringem Hartphasenanteil. Der Verschleißschutz durch in-situ Bildung von MML war besonders bei Hochtemperatur ausgeprägt. Ein linearer Zusammenhang zwischen den Verschleißraten und der Warmhärte ist besonders bei Hochlast-Abrasion und 30° Erosion zu finden. Weiters folgt das Verhältnis aus 90° und 30°-Erosion einem linearen Zusammenhang mit der Warmhärte bei nahezu alle getesteten Werkstoffen und Temperaturen.

Schlüsselwörter

- Tribologie
- Abrasion
- Hochtemperatur
- Hartauftragung
- Sinteranlage
- Instandhaltung

Scientific contribution of this work

- Plant maintenance often lacks scientific investigations of causes of failure. A holistic approach is introduced to identify tribological failure criteria based on maintenance records.
- Present wear mechanisms in the sinter crusher system of sinter plants were successfully simulated in lab-scale using high temperature impact-abrasion testing. Wear mechanisms for high temperature sieves were reproduced by erosion testing.
- Different equipments for high temperature abrasion testing were combined with advanced analytical techniques for microscopic examination.
- Abrasive wear was studied at various abrasion modes (high-stress abrasion, impact-abrasion and solid particle erosion) disclosing critical regimes for wear resistant alloys.
- Temperature dependence of abrasive wear for the evaluated abrasion modes is presented up to 550°C-700°C, offering a broad data source for the choice of suitable high temperature wear protection and further material improvement.
- For the materials tested critical temperatures which can lead to changing wear mechanisms under abrasive loads were identified.
- The in-situ formation of wear-protective mechanically mixed layers was proven to significantly lower wear loss for materials with low hardphase content (<20 %) especially at high-stress abrasion and normal erosion (90° impact). This beneficial effect is enhanced at higher temperatures.
- Factors influencing the extent of mechanically mixed layers were identified as follows: energy input (energy/abrasive particle) during the test as well as hot hardness, hardphase content and distribution of the material.
- In impact-abrasive environment, a high hardphase content (>40 %) was found to be necessary for sufficient wear resistance.
- For several test conditions various materials exhibeted a linear correlation of hot hardness with high temperature wear rates. These were especially evident at high-stress abrasion and oblique erosion (30°).
- The ratio of 90° and 30° erosion (erosion response) was found to follow a linear relationship with hot hardness for nearly all materials investigated.

List of abbreviations

bcc	body-centred cubic
CIP	continuous improvement process
EDX	energy dispersive X-ray diffraction
fcc	face-centred cubic
GMAW	gas metal arc welding
hcp	hexagonal close-packing
HHT	hot hardness test
HT	high temperature
HT-CAT	high temperature-continuous abrasion test
HT-CIAT	high temperature-cyclic impact-abrasion test
HT-ET	high temperature-erosion test
LM	light microscopy
MML	mechanically mixed layer
NI	nano indentation
PTA	plasma transferred arc
RT	room temperature
SEM	scanning electron microscope
SEM-BSE	SEM-back scattered electron mode
SEM-SE	SEM-secondary electron mode
XRD	X-ray diffraction

Contents

1. Introduction

Failure of core components in industrial plants can often be put down to wear – the material loss due to mechanical interaction between two bodies. When hard particles or protuberances are present within the system, this can lead to increased material loss, namely abrasive wear. So the quantification of wear resistance for components is required for successful plant maintenance. Furthermore, many industrial applications operate at high temperatures (HT), e.g. plants in steel industry or cement industry. Hence the role of temperature needs to be studied in order to find solutions with better wear resistance/lower maintenance costs.

In this work, a holistic approach was undertaken to identify core components causing high maintenance efforts and their underlying failure mechanisms. Abrasive applications were modelled with various testing techniques in order to simulate in laboratory the wear modes found in application. The focus lies mainly on the influence of temperature on the different forms of abrasion for various materials, extending the scientific knowledge of material behaviour at HT abrasive load.

In detail, the sinter plant for pig iron production was chosen for investigation. This plant is necessary to process raw materials for optimal use in the blast furnace, i.e. ore fines and coke breeze are sintered with additions to the so called sinter cake. This agglomeration than is broken to the desired size for the blast furnace and fines are removed by a sieve and recycled. This processing takes place at HT: sintering at up to 1400°C, crushing at ~700°C and screening at 300-500°C.

Evaluations of the maintenance records and unplanned downtimes pointed out abrasion as the most expensive/significant maintenance cause of core components, hence systematic research of HT abrasion is necessary in order to minimise maintenance expenses of these aggregates. For this purpose, different mechanisms of abrasion found in the application were simulated in laboratory, namely high-stress abrasion (breaking up of the abrasive), impact-abrasion (abrasion with impact component) and solid particle erosion (abrasion without counter body). Temperatures simulated were up to 700°C in order to map plant conditions sufficiently and broaden the available data-basis of HT abrasion for the scientific community.

Several material groups suitable for an HT wear environment were chosen for investigation, most of them metal matrix composites (MMCs), i.e. materials with hard precipitations embedded in a metallic matrix. Cast alloys are compared with hardfacings (local deposition of wear protection by welding technique). The material groups were (i) cast alloys (due to their

cost-efficient production), (ii) hardfacings with Co content (HT stability) and (iii) hardfacings with high hardphase content (improved wear resistance). In the group of cast alloys, a Fe-base material was compared with a Ni-base material, both with a ~15 % hardphase content, in order to investigate the role of the matrix. In the Co-group, a Fe-base material with Co-addition was compared to a Co-base hardfacing to investigate the influence of Co content on the HT stability. In the group of the hardphase-rich hardfacings, the influence of chemical composition and microstructure was studied. Furthermore, the processing technology by two different welding techniques was investigated for one of the hardfacing alloys. By this comprehensive test- and material-matrix, critical abrasion modes and temperature ranges for the various materials should be identified to aid proper material selection for plant specific demands.

Furthermore, the scientific study of the underlying wear mechanisms at different temperatures is a major goal of this work. The basic forms of abrasive wear mechanisms: microploughing, microcutting, microfatigue and microcracking, affect the various phases present in MMCs in different way. Also wear protecting effects are known, especially the in-situ formation of mechanically mixed layers (MML) with the abrasive during tribological interaction. The influence of this MML-formation on wear rates at the various forms of abrasion and its temperature dependence should be studied in detail.

The calculation of wear loss from material and system properties is the goal of every tribologist. Also in this work the correlation of material parameters with wear rates at the different forms of abrasion is attempted, in order to predict the lifetime of components under abrasive load.

This work is structured in **State of the art**, where the sinter process, maintenance concepts and wear of core components in sinter plants are described. Furthermore, the theoretical background for different forms of abrasion is pointed out. In **Methodology** and **Results**, the approach of the analyses and results are presented for maintenance costs in the sinter plant, materials for HT abrasive environment and various abrasion tests applied. The **Discussion** gives a critical evaluation of maintenance records and comparison of wear mechanisms of the core components with abrasive wear tests. Furthermore, the wear rates and mechanisms are elucidated, especially the function of in-situ formed layers with the abrasive as wear protection. In a last step, the economic aspects of material choice for certain plant conditions are discussed.

2. State of the art

This work is focused on the investigation of typical wear mechanisms present in the HT field of sinter plants and strategies to minimise wear loss by improving wear protection. For this purpose, an overview on the setup of sinter plants and maintenance concepts is given, followed by the description of common wear phenomena of core components. As abrasion is of major concern, systematic classification of abrasive wear and experimental simulation thereof is presented. Wear mechanisms in abrasion are described and temperature influence as reported in literature is summarised.

2.1. Sinter plants in pig iron production

Mined lump iron ores are mostly accompanied by a large fraction of fines due to the mining and breaking to a suitable size for the blast furnace. These fine ores would impede the gas flow in the blast furnace entailing reduced productivity. The fine ores get agglomerated by sintering or pelletising to achieve an economic blast furnace process. [VDE71]

For the agglomeration of ores the continuous sintering process (Dwight-Lloyd process) is mostly used. This down-draft principle is superior to discontinuous sinter processes using pans (e.g. Greenawalt process) or rotary kilns, which cause higher costs [AVH61]. A schematic of the continuous sinter plant is given in Fig. 1. From the bunkers ore fines, limestone, coke breeze and returned sinter are weighed and mixed in a rotating drum (Fig. 1/4). Additionally blending beds can feed intermediate bunkers, which are piled from the raw material bunkers and homogenise the ores beforehand [CAP73]. As particle size is very important for the sinter process a separate granulating drum (5) is used. The fines adhere to larger particles by water spray addition to the drum. Hereby, the particle size of ~5 mm is desired for an optimal sinter process. [BOG71, VDE71] Optimal water and limestone content is required, as a too high amount may lead to a clogging of the sinter grate [BOG71].

The sinter mix is fed to a continuous sinter belt with moving grates (Fig. 2). First, a small layer of coarse finished sinter (15-25 mm) is applied on the grate (Fig. 2/2) to avoid loss of fine particles and to protect the grate from highest temperatures and oxidation. Then the sinter mix is added in a layer of ~250-500 mm (1). The top of the sinter mix is ignited (3) and air is sucked through the mixture (5). The downward air flow leads to a progress of the burning sinter mix frontline towards the grate. Typical temperatures in the reaction zone are 1200-1400°C and sintering is complete when the fuel in the mixture has been burnt. The speed of the belt is adjusted so that the process is completed at the end of the sinter belt. The HT

during the process lead to an agglomeration of the ore fines and a spongy cake is formed, the so called sinter. [BOG71, CAP73, VDE71]

The downward sucked exhaust gas is collected in the suction boxes and gathered in a gas collecting pipe. Depending on the ores exhaust gas temperatures can reach >600°C and contain corrosive elements, e.g. sulphur, chlorine or fluorine. Hot exhaust gas circulation is utilised to save energy. Further, extensive gas cleaning is necessary in state of the art plants with various filter systems to meet environmental requirements. [CAP73]

The sinter cake is of large size after drop-off of the sinter belt, which makes the use of a crusher necessary (Fig. 1/between 6-7). A toothed crusher is utilised to break the HT sinter cake. For this purpose, a massive shaft with teeth shears the sinter through a grate. As the hot sinter is rigid and tough the minimal distance between the crusher grate bars is 200-250 mm, which entails sinter chunks in the range of 200 mm. With increasing plant size the loading of the crusher system worsens, especially the teeth show extensive wear and must be equipped with wear protection. [CAP73]

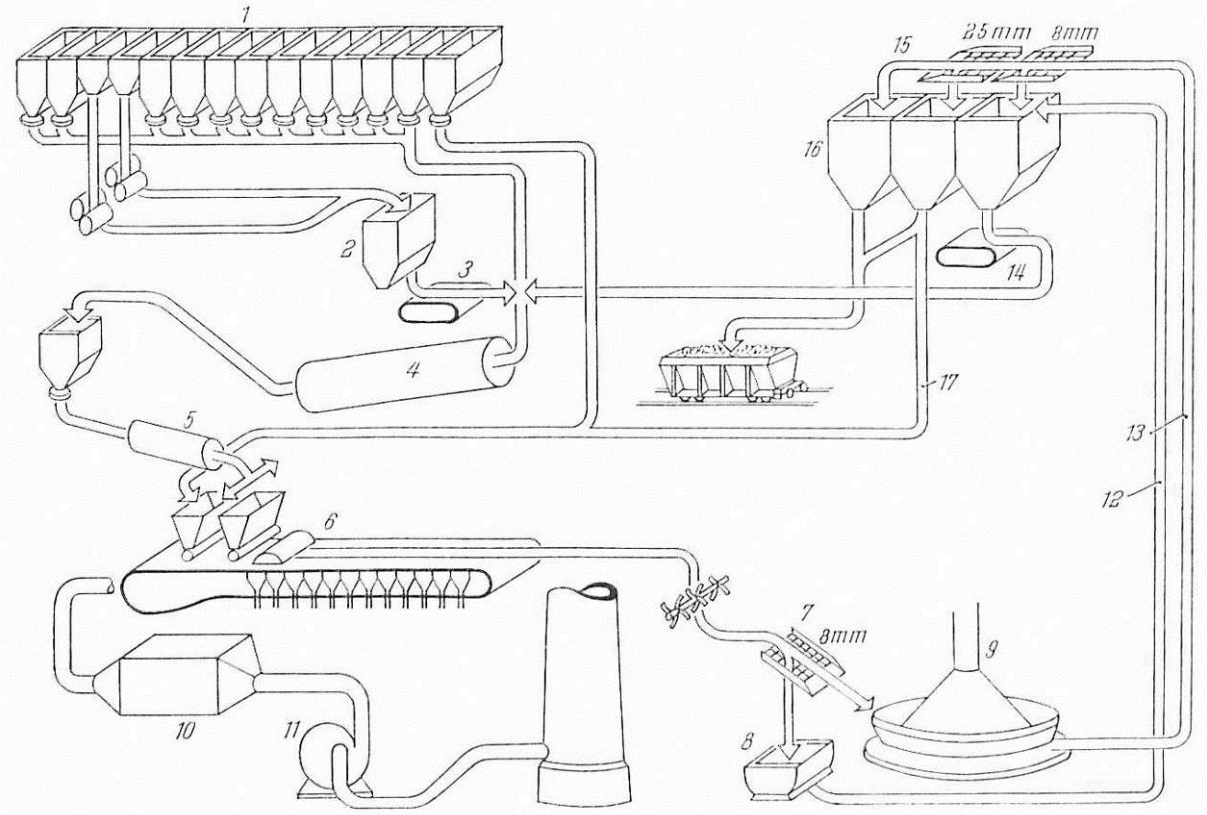

1 Two bins for coke breeze, eleven for ore fines, one for hearth layer, *2* Coke breeze minus 3 mm, *3* Regulating belt feeder for coke breeze, *4* Pre-mixing drum, *5* Secondary mixing drum, *6* Sinter machine: 2.5 m wide, 37.5 m long, 93.75 m² suction area, *7* Hot screening, *8* Return fines cooler, *9* Sinter cooler: (255000 m³ of cooling air per hour, 180 mm wg, *10* Dust content after the two-stage electrofilters below 0.100 g/m³, *11* Fan: 150°C, 1100 mm wg, 550000 m³/h, *12* Cooled return fines, *13* Cooled sinter, *14* Regulating belt feeder for return fines, *15* Cold screening, *16* Finished sinter, *17* Hearth layer

Fig. 1: Flow diagram of the continuous sintering process [BOG71]

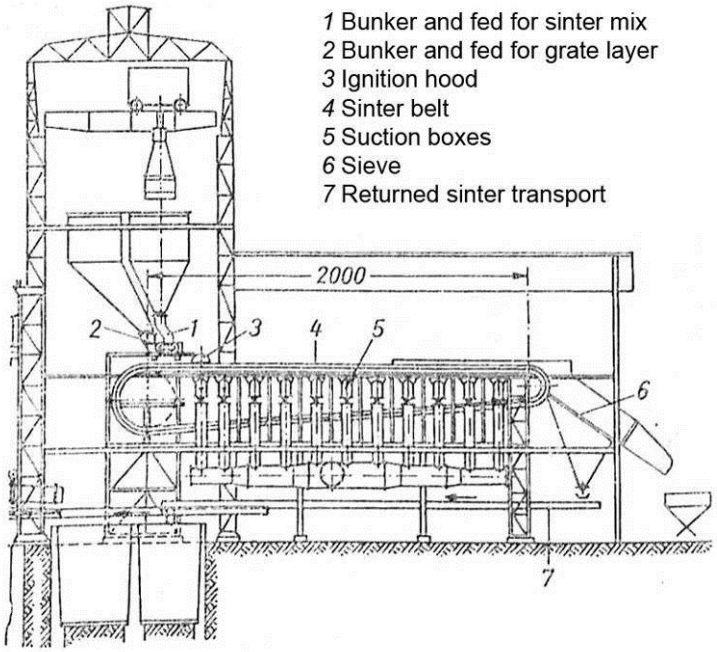

Fig. 2: Scheme of the Dwight-Lloyd sinter belt [cf. AVH61]

After crushing a HT sieve screens the sinter (Fig. 1/7). Particles and dust <5 mm are removed in order to keep the performance of the following sinter cooler at a high level [CAP73]. The fine fraction after sieving is returned to the sinter mix and the coarse sinter is fed to the sinter cooler (9). In the cooler air is blown through the sinter until temperatures are reached, which makes the transport by rubber conveyor belts possible. Before the use in the blast furnace a further breaking and screening is performed as the mechanical and chemical properties of the sinter are directly influencing the blast furnace process and coke consumption thereof. Ideal sinter fraction should be in the range of 8-50 mm. [BOG71, VDE71] For the breaking roller crushers are used and after cold screening the sinter is transported to the blast furnace by conveyor belts [CAP73].

2.2. Maintenance concepts

In steel industry high plant availability is essential in order to keep production costs at a minimum. In the pig iron production cokery, sinter plant and blast furnace are bottleneck plants and their continuous production is essential, as each production loss entails additional costs for compensation of raw materials. To avoid this, maintenance strategies are presented here.

"*Driven by the continuous improvement process (CIP), maximisation of plant availability at high process stability and reduction of maintenance costs are crucial.*" [VAR13-3] Currently the economic growth goes hand in hand with complex, automated and effective manufactur-

ing plants. A breakdown, e.g. by wear processes, construction mistakes, human influences, inevitably leads to substantial economic losses. [OEN98, VAR13-3, VDI02, VDI06].

Concerning sinter plants maintenance costs can be up to 20 % of the total costs of sinter production (40 % involve fuel, 10 % electricity), hence the minimizing of maintenance costs is of major importance. [CAP73] "*On the one hand maintenance has the function to ensure sufficient plant availability and on the other hand it has to secure cost effectiveness. This can be reached by prevention of unscheduled breakdowns, optimizing the availability, assurance of competitiveness, protection of natural capabilities and reduction of maintenance costs. Maintenance activities do not only cover reinstatement work, servicing, inspections, and plant improvements but also include the prevention of breakdowns, analysis of the failure performance and improving the recognisability of potential faults. Maintenance actions may have positive effects on the value added by reducing expenditures through optimisation of maintenance strategies, replacement investment with reduced maintenance costs or prevention of breakdowns and failures as well as increasing revenue by ensuring all functions required of a technical plant and increasing the utilisation level.*" [VAR13-3]

Four different maintenance strategies are commonly used to reach the various aims of maintenance. In these strategies the kind and time of action required for optimal outcome is regulated. For choosing the specific maintenance strategy, technical, economic, legal and safety-related aspects have to be balanced. These types are (i) Corrective-, (ii) Preventive-, (iii) Predictive-, and (iv) Reliability Centred Maintenance. [SCH10, VAR13-3]

(i) Corrective Maintenance: here the maintenance activities are triggered by a breakdown of a plant or component failure. Fast and spontaneous work is required for efficient repair, hence it is also known as fire-fighting or breakdown maintenance. Production loss is inevitable here. [SLA15, VAR13-3]

(ii) Preventive Maintenance: all activities are scheduled and take place regardless of the condition of the component, i.e. repairs take place before failure occurs. The aim of this strategy is to avoid unnecessary inspections, maintenance and downtime. It is usually applied for the most critical items. The drawback of this strategy is unnecessary and expensive maintenance, if the component in question is not worn completely. [SLA15, VAR13-3].

(iii) Predictive Maintenance: takes use of plant condition monitoring. Actual plant data of the condition of components are utilised to plan maintenance tasks, only required repairs are conducted. In contrast to preventive maintenance the actions are not scheduled, but changes of the plant condition trigger maintenance actions. [SLA15, VAR13-3].

(iv) Reliability Centred Maintenance: "*identifies the most effective and suitable maintenance actions for all facilities and also contains the establishment or development of a maintenance program in the most cost-efficient and technically accomplishable approach*" [VAR13-3]. The consequences of possible breakdowns are used to structure a systematic method for maintenance duties. Time-based maintenance schedules are replaced by a study of a functional significance of components, their breakdown and maintenance history to plan maintenance actions. [SLA15, VAR13-3].

2.3. Wear of core components of the sinter plant

Within this section the most wear affected components within the sinter plant are presented. The **grate bars** of the sinter wagons are by far the most numerous in use with a number of several thousand pieces – already small improvements in wear resistance/lifetime can give a noticeable economical advantage. Secondly, the **crusher system** is heavily worn, due to the falling and crushing of the hot, abrasive sinter. The hot, crushed sinter is further transported by HT chutes and afterwards screened. Chutes and sieve are identical aggregates, except the sieve cavities. Therefore, the more wear sensitive **HT sieve** will be investigated here.

2.3.1. Grate bars

The grate bars are the flooring of the sinter belt. They are arranged parallel on the sinter wagons, approximately 120 pieces for each wagon. A drawing is given in Fig. 3: on the upper surface lies sinter mixture during the sinter process. Both heads protect the wagon from the sinter, while the notch in between must maintain the downward airflow, which is necessary for the sinter process. The feet hold the grate bar in position during the return of the sintering belt, when the wagons are hanging upside down.

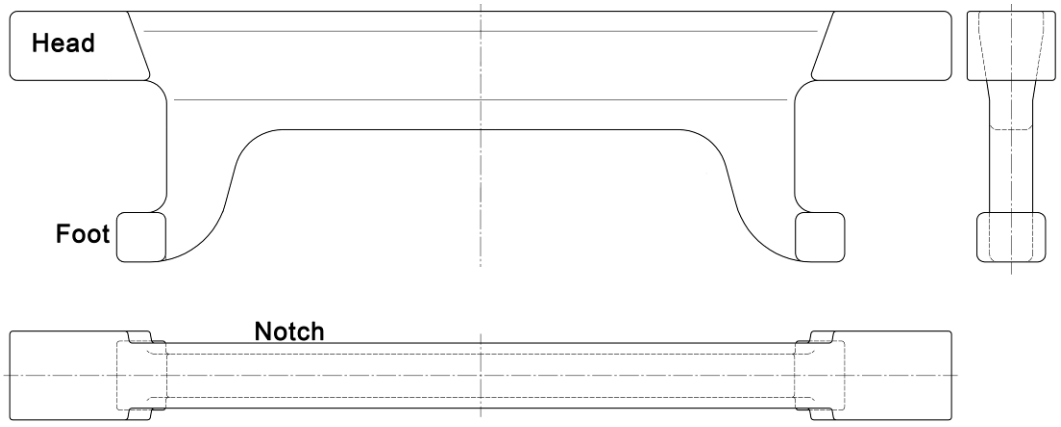

Fig. 3: Drawing of the grate bars

The current maintenance interval of the sintering belt is seven weeks. After this period, the cleaning of the ventilation slots (notches) in between of the grate bars is necessary to keep the productivity of the plant at high level. The main reason for the closing of the notches are corrosion and deposit build-up [BOG71, CAP73]. Currently, the grate bars are casted of a heat resistant high Cr-alloyed steel. The microstructure shows a Cr-carbide network along the grain boundaries of the ferrite grains. This material will serve as reference material (FeCrC) for all investigations within this work and is presented in detail in chapter 3.2 and 4.2. Although this material is relativly corrosion-resistant, in the aggressive environment of the sinter belt even this material corrodes. During the sinter process aggressive components are released from the ores and a corrosive gas atmosphere is built. Depending on the ore composition significant amounts of sulphur, chlorine and fluorine can be present [CAP73]. Some components additionally condense on the colder zones of the grate bars and corrosive salts are formed (Fig. 4a). Corrosion is the main reason leading to the necessity of cleaning intervals, as the corrosion products close the ventilation slots and promote the clogging by sinter deposit and build-up.

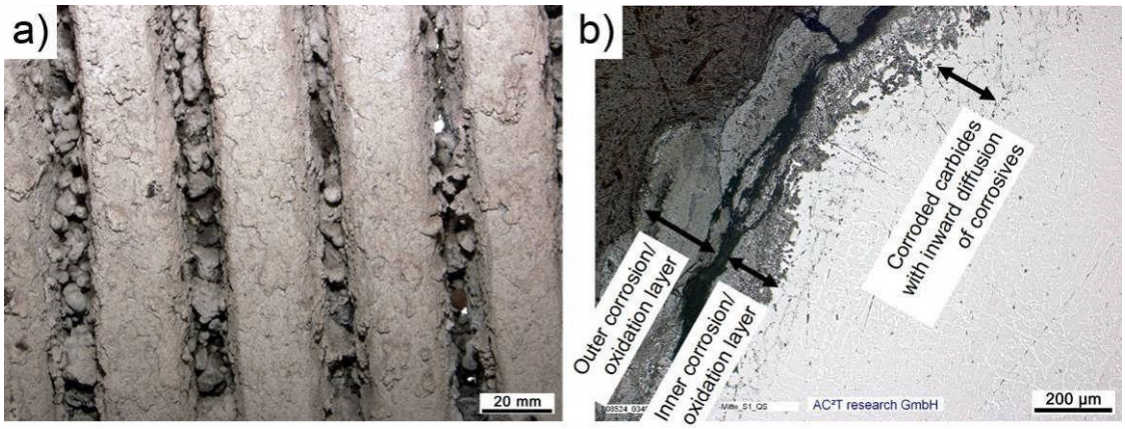

Fig. 4: Corrosion of the grate bars: a) section of several grate bars from below: massive salt deposition and clogged ventilation slots; b) cross section of a worn grate bar: transition from the top to the flanks

A cross section of a worn grate bar is shown in Fig. 4b. Massive corrosive attack can be seen, thick corrosion scales are found on the side walls, which easily detach. Furthermore, a deep penetration of corrosives into the microstructure is found, especially alongside the Cr-carbides. Detailed information on the corrosion processes under this environment can be found in [ROJ15]. While the corrosion is the dominant damage mechanism at the flanks and bottom of the grate bars, indicated by thick scales, the upper surface shows just minor corrosion products on the surface, but penetration of the microstructure as seen in Fig. 4b. This difference can be put down to the additional contact with the sinter on the upper surface.

The sinter is very sharp-edged and hard, thus making abrasion possible under relative movement. Especially at the drop-off into the crusher system, the hot finished sinter slides and abrades over the surface of the sinter wagon, i.e. the grate bars. The abrasive wear loss is firstly obvious at the drop-off edge of the sinter wagon. Fig. 5 shows the worn edges of grate bars after several months in use. Scratches in the drop direction are clearly visible, as well as geometry loss: the original grate bars have rectangular head shape (Fig. 3), while in the photograph they are almost triangular.

Fig. 5: Worn heads of the grate bars at the drop-off edge of the sinter wagon

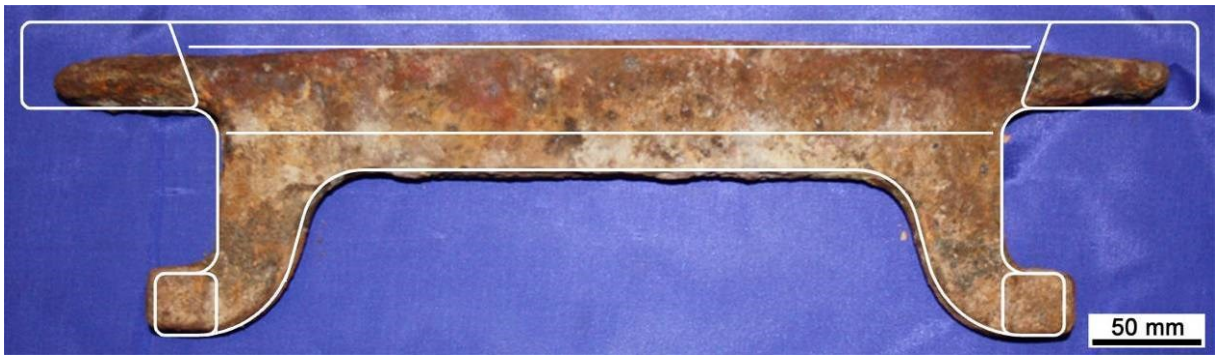

Fig. 6: Comparison of worn grate bar with the technical drawing (white lines)

One grate bar at the end of his lifetime is compared in Fig. 6 with the original geometry. With prolonged use, additionally to the wear of the drop-off edge, the whole surface gets abraded and the grate bar loses height. The wear gradually increases from the centre to the head. The symmetric wear loss to both heads is caused by the maintenance changes of the grate bars: when one side is worn too much, the grate bar is turned around. Corrosion products are visible at the entire surface of the grate bar, also white areas of salt depositions. The feet of the grate bar almost maintain their geometry during use. Flank zones in the vicinity of the contact with the sinter have to endure much higher temperatures and more pronounced material loss due to

tribo-corrosion, indicated by thinner grate bars. This also comes with a reduction of the notches and impaired air flow. The highest material loss can be found at the upper surface, where the interaction with the hot sinter takes place. There abrasion is supposed to be the major wear mechanism, likely accelerated by corrosion in the aggressive atmosphere of the sinter belt.

2.3.2. Crusher system

In the crusher system (Fig. 7) the hot sinter cake slides every ~30 s from the turning sinter belt. The falling sinter first hits the pre-breaker, which should lessen the impact on the crusher grate. There the sinter cake breaks in smaller chunks, which fall onto the crusher grate. The rotating sinter crusher presses the sinter through the grate, entailing maximal chunk size of ~200 mm [KAT07]. The sinter crusher's lifetime has to be as long as possible, as it is difficult to replace. Pre-breakers and crusher grate bars are easier to replace, which can be done at each regular maintenance plant downtime.

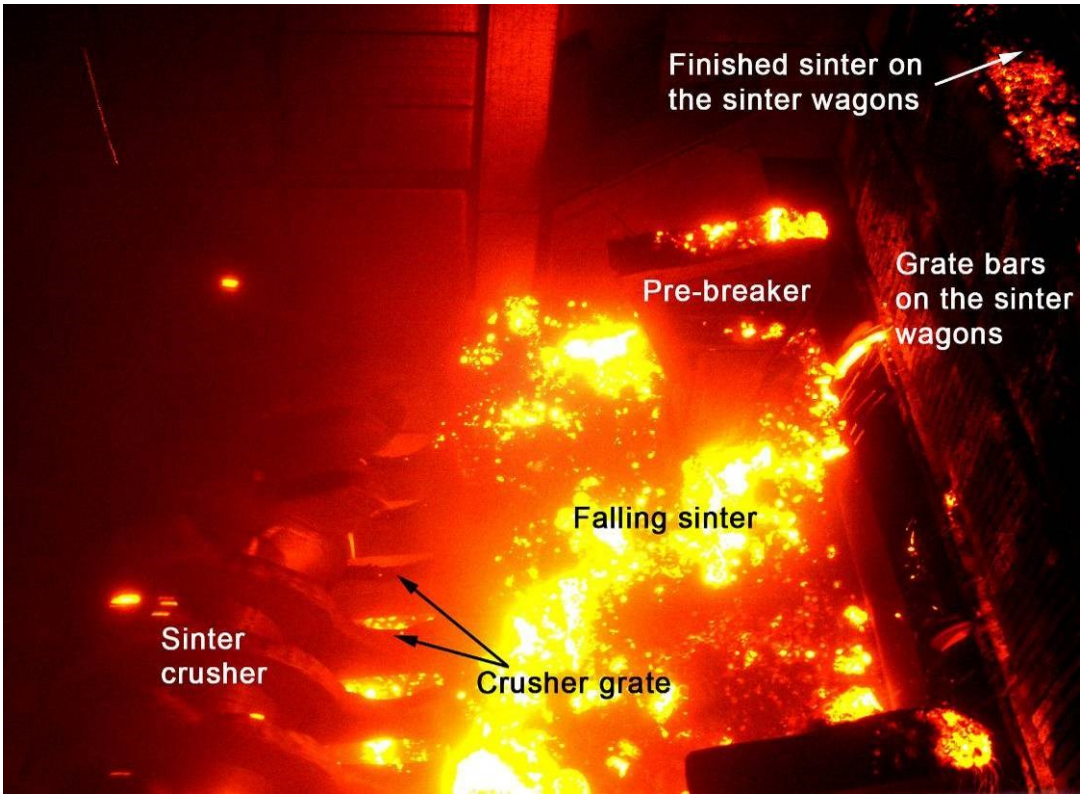

Fig. 7: Photograph of the crusher system in operation

As already visible in the photograph (Fig. 7) temperatures are high in the crusher system. Thermal imaging (Fig. 8) in [KAT07, WIN09-3, WIN09-1] measured 970°C for the hot sinter at this position. The highest surface temperatures for the crusher grate were in the range of 470°C, but local temperatures of 720°C were found, where a sinter chunk remained. The

crusher showed average temperature of ~400°C and much higher local temperatures during crushing must be expected.

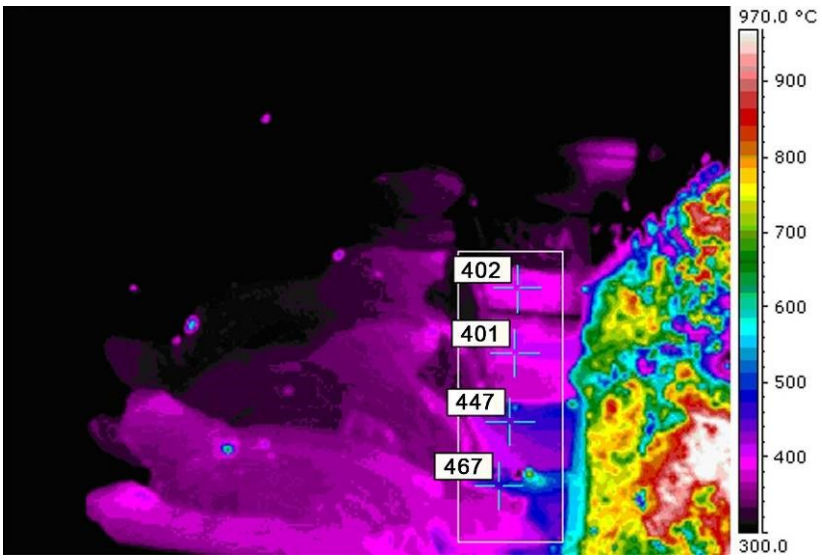

Fig. 8: Thermal imaging of the crusher system [cf. WIN09-1], temperatures in [°C]

2.3.2.1. Sinter crusher

The sinter crusher is a highly sophisticated spike crusher of three-pointed teeth segments. The teeth are mounted on an axis and welded together. Replacement is difficult, because the side walls of the crusher system have to be removed before the crusher could be replaced. For longer service the segments are covered by a wear protection [CAP73]. As temperatures at the crusher can reach the 700°C-range a complex alloyed hardfacing [KAT07] is in use for wear protection. This material is named “FeCrCNbBWC” within this work. Worn edges of the teeth are repair-welded at the maintenance intervals.

Damage analyses of this system are not known, but a sketch of the dominating loads was presented by a supplier of sinter crushers [SHA14]: Fig. 9a shows large areas of the crusher loaded by the impacting sinter. At the crusher tooth pressure due to the rotation of the crusher is dominating. An impact/abrasive wear mechanism can be expected there. On the side walls of the crusher tooth abrasion is dominating.

Macroscopical investigations at the maintenance intervals (Fig. 9b) showed highest wear loss at the border between “pressure” side and “abrasion” flanks of the teeth, which is in accordance with [CAP73]. Most intensively worn is the outermost tip of the teeth, where highest velocity and specific load can be expected.

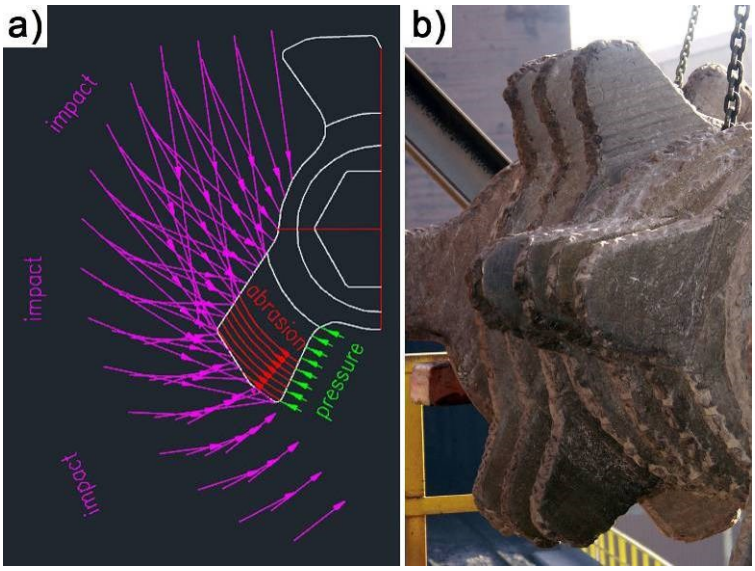

Fig. 9: Sinter crusher: a) load zones [SHA14] b) worn section after prolonged use

2.3.2.2. Crusher grate

At the time of the damage analysis of Winkelmann [WIN09-3] and Katsich [KAT07] stacked wear plates were in use at the crusher grate. The wear plates consisted of a hypereutectic hardfacing welded onto a mild steel substrate. Fig. 10 gives cross sections of the crusher grate after usage. Fig. 10a shows the hardfacing on top of the grate, where the impacting sinter hits the grate. The surface shows uniform wear loss and minor oxidation. The primary hardphases and also smaller carbides in the matrix show fracture up to a depth of ~50 µm. Deeper lying wear plates do not show carbide fracture, but enhanced selective oxidation of the matrix zones. Hence, the impact/abrasive wear loss is dominating in this environment as at large areas of the crusher teeth. Further, a significant hardness loss of the hardfacing was detected: while the uppermost wear plates with direct contact to the hot sinter showed ~590 HV10, less thermal affected wear plates had ~800 HV10. I.e. thermal material degradation is expected on the tribological stressed surface. [KAT07]

On the flanks of the crusher grate wear has exposed the mild steel substrate (Fig. 10b). Plastic deformation and scale formation is visible. A ploughing wear mechanisms can be expected. Detailed analyses of the mild steel substrate at different positions found pearlite nodules at the uppermost wear plates. This soft annealing effect occurs after long-term thermal exposure in the range of 650-700°C, which indicates that this temperature range is present at the crusher grate. [KAT07]

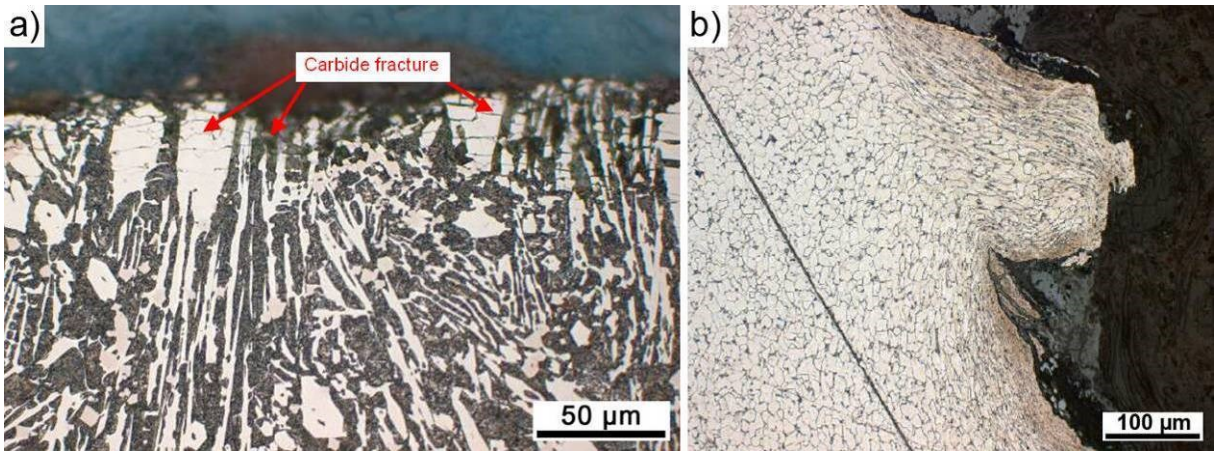

Fig. 10: Cross sections of crusher grate after use: a) hardfacing on top of the grate; b) mild steel substrate on the flanks [cf. KAT07, WIN09-3]

The main damaging mechanisms in the crusher system are:

- impact where the falling sinter hits the components
- impact-abrasion, when the sinter is additionally pressed through the crusher
- high-stress abrasion on the flanks of the crusher grate and crusher teeth
- solid particle erosion on side walls and exhaust system
- high temperatures up to 700°C exacerbate the wear loss

2.3.3. Sinter sieve

A HT sieve is used for screening the fine fraction of the crushed sinter caused by the sinter crusher. Particles <5 mm should be removed and are returned to the sinter process as it would impair the cooling performance of the sinter cooler [CAP73]. For screening a fishbone structure with 5 mm cavities is cut in plates. The plates consist of a HT wear protection hardfacing of hypereutectic structure and FeCrNbC composition, welded onto a mild steel substrate. Detailed investigations of process temperatures and wear mechanisms are published in [VAR15-2].

Thermal imaging of the sinter flow reveals much lower temperatures of the sinter than in the crusher system (Fig. 11a). Surface temperatures on smaller sinter particles are in the range of 200-300°C. This drastic reduction in temperature can be put down to the long transport route from the crusher system to the HT sieve, during which the sinter cools down. Nevertheless, larger chunks of sinter were found with temperatures up to 600°C. Although this punctual HT load average temperatures of the sieve plates were measured by thermocouples as ~200-250°C (Fig. 11b).

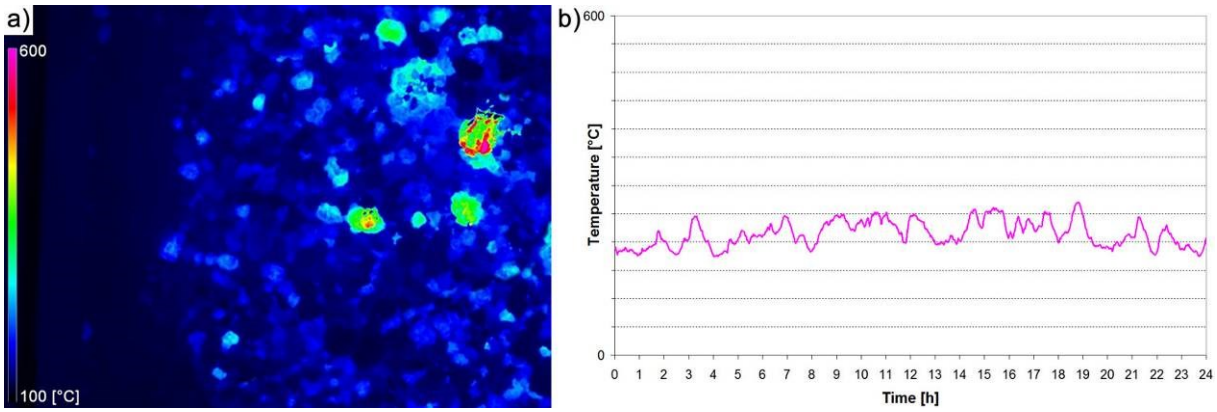

Fig. 11: Thermal investigations of the HT sieve: a) thermography of sinter flow;
b) thermocouple measurement of sieve plate temperature on the bottom [VAR15-2]

The productivity of the sinter plant is reduced by increased returned sinter due to widening of the sieve cavities. Hence, wear of the HT sieve is of major importance. The original geometry of the sieve cavities is cut by plasma cutting with a single stroke from the backside of the plates (i.e. from the substrate side). The plasma cut geometry is not ideally constant, because the hardfacing has varying thickness and inhomogeneous microstructure, resulting in inconstant cavity width. Furthermore, the heat input by the thermal cutting technique alters the microstructure in cavity-near zones. Fig. 12 depicts a cross section of a cavity after use. In Fig. 12a an overview is given, which shows on the left the original microstructure of the hardfacing. On the right the cavity was cut and in its vicinity a clearly different microstructure can be seen after etching. Many pores are visible and large carbides are absent.

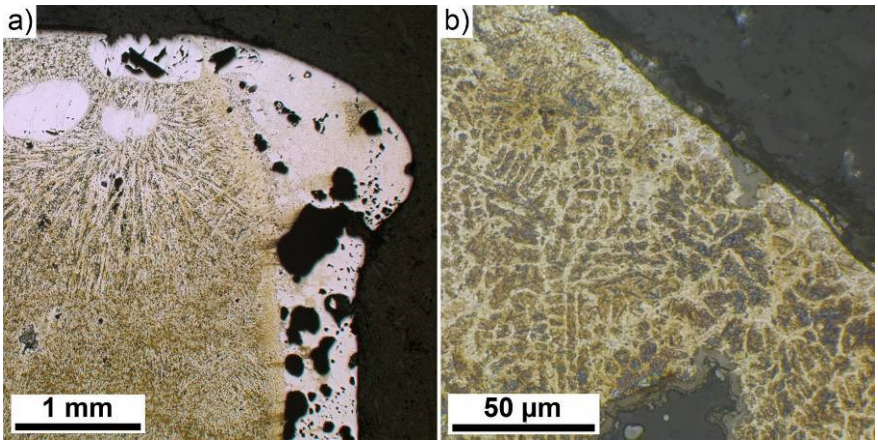

Fig. 12: Cross section of sieve cavity: a) blunted edge and side wall of sieve cavity;
b) detail of hypoeutectic zone [cf. VAR15-2]

Fig. 12b gives a detail of this zone showing hypoeutectic microstructure. Through the thermal cutting process from the substrate side intermixing of the hypereutectic microstructure with

the mild steel substrate takes place, entailing hypoeutectic chemistry and microstructure. Further micro hardness measurements in [VAR15-2] show clearly reduced hardness of 400 HV0.5 in this zone, compared to 800-900 HV0.5 of the hypereutectic hardfacing.

Abrasive wear on the sieve's surface was of minor importance. The lifetime of the HT sieve is limited by the widening of the cavities. In the work of the author et al. [VAR15-2] a detailed wear history over the lifetime of the HT sieve is given. Blunting of the cavities' edges is the major wear loss. Fig. 13 gives quantitative results of the measurements of the sieve cavity geometry. Measurement was done at 0.5 mm intervals from the top of the sieve as shown in Fig. 13a. Seven intervals within the lifetime of the sieve of ~1 year were investigated and changes of the minimal width are given in Fig. 13b. Rapid blunting on the very edge was found at the first interval, the sharp edges lose their geometry significantly. Ongoing wear of the edges widens the cavity by ~4 mm within the lifetime of the sieve. Due to the brittle hardfacing larger break-outs were found at several occasions. The minimal cavity width, limiting the size of the screened sinter, was usually found in a depth <2.5 mm. Here a widening of ~1 mm was observed.

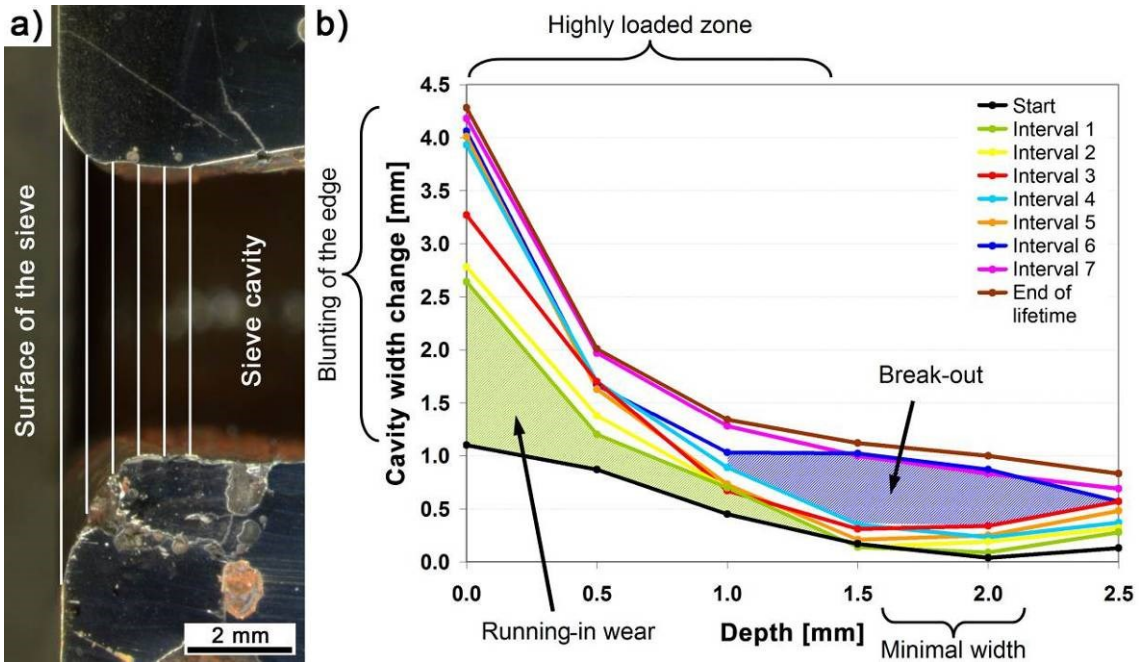

Fig. 13: Quantitative cavity width change over the lifetime of the HT sieve: a) measurement positions from the surface to the depth (stereo microscopy); b) width change evolution [VAR15-2]

The wear regime within the HT sieve is suspected to be mild but lasting for thousands of cycles. Abrasive wear on the sieve plates' surface is minor, only the cavity edges and cavities are affected. At these positions only free moving small sinter particles are present, what leads to the conclusion that the major abrasion mode is erosion.

2.4. Abrasive wear and experimental simulation

Abrasive wear as part of tribological interaction of surfaces causes substantial efforts in maintenance as presented in the previous section. Within this chapter the fundamentals of abrasive wear loss are presented. The experimental simulation, wear mechanisms and, of special importance for this work, influence of temperature on abrasive wear are emphasised.

Tribology is defined *as "the science and technology of interacting surfaces in relative motion and of the practices related thereto"* [GAH87]. This includes investigation of friction, lubrication and wear. [GAH87] The DIN standard [DIN79] defines wear as *"the progressive loss of material from the surface of a solid body due to mechanical action, i.e. the contact and relative motion against a solid, liquid or gaseous counterbody"*. Wear may entail dimensional changes of components and surface damage and in extreme cases fracture of the component. Further the formation of wear debris may be detrimental for the operation of the tribosystem [GAH87]. "*Of the various factors that produce surface damage, impact and abrasion are usually most severe. Heat, friction, corrosion and the cyclic stresses that cause fatigue may also play important parts, but for most mining, construction and related earth handling work, the dominant wear mechanism is abrasion.*" [AVE61] Abrasion is defined as *"A process in which hard particles or protuberances are forced against and move along a solid surface"* [KEN01], i.e. the interaction with the hard particles taking place. Abrasive wear on the other hand, is defined as *"Wear due to hard particles or hard protuberances forced against and moving along a solid surface"* [KEN01], i.e. the result of abrasion.

Summarising the previous section wear of core components of the sinter plant is indeed mainly caused by abrasive interaction at HT. Oxidative and corrosive mechanism may also accelerate the wear of materials, but should not be of major focus within this work. Abrasive interaction is present at various loads and conditions like abrasion, impact-abrasion or erosion. Wear of the grate bars is driven by abrasion at high loads, the crusher system suffers impact/ abrasion, while in the HT sieve erosive mechanisms dominate.

Abrasive wear causes serious maintenance efforts in mining and mineral processing. The extraction and transport of hard materials inevitably leads to relative movement and tribological interactions leading to wear of components. [HAW01, KAO01, REN09, TYL92] Wear is not only defined by load, interaction components and relative velocities but is also often exacerbated by elevated temperatures, e.g. in materials processing or steel industry [STO02].

It is widely known that wear is not a material property, but a response to the conditions present in the tribosystem and wear resistance is strongly related to current wear mechanism [ADA03, KAO01]. Hence, despite its technological importance the notion of abrasion resistance as a material property remains elusive [ZOK07]. In spite of the lack of linking abrasion resistance to material properties, methods for controlling wear are known also for complex tribosystems, albeit users and tribologists are not aware of all details of wear mechanisms occurring there [KAO00]. Avery [AVE61] already states in 1961: "*There is no universal wear test. Instead, it is necessary to analyze the factors that are most important in a given wear situation and to evaluate these separately or in simple combinations. Such evaluations or tests have the aim of making possible the wise selection of materials and the prediction of service performance.*"

2.4.1. Classification of abrasive wear

Terminology is not always consistent in literature on abrasion. Here the most detailed terminology proposed by Gates [GAT98] shall help to correctly name present wear mechanisms.

In abrasive wear two basic mechanisms can be identified: two-body abrasion (grooving abrasion) and three-body abrasion (rolling abrasion). Grooving abrasion is present, when abrasive particles do not move relative to the counter surface and are "fixed" there. Rolling abrasion takes place, when the abrasive particles can move "freely" between the two surfaces. [ADA03, ALL01, AXE94, TRE99] A detailed study of parameters influencing wear modes on the example of micro-scale abrasion test are given by Adachi and Hutchings in [ADA03]: Main parameters influencing wear mode were applied load, abrasive material and content, surface condition of the counter body and used materials. It is important to say that the presence of a "third body", e.g. abrasive particles, does not necessarily lead to three-body abrasion [ADA03, GAT98, TRE99]. Adachi and Hutchings [ADA03] also found out that the hardness ratio between sample and counter body is essential for establishment of the different abrasive wear modes.

Three-body abrasion does not necessarily need a counter surface. Forces also can be created by the "abrasive" itself, e.g. when digging into a pile of loose rock, or at solid particle erosion no rigid counter surface is present. The "third body" can be defined as any loose abrasive, hence these cases can also be seen as three-body abrasion. [GAT98, MIS80]

Further classification can be done by the severity of contact. Four categories are known hereby [AVE61, GAT98, HAW01, MUT88, NOR80]: (i) gouging abrasion, at very high stress levels, e.g. when sharp rock edges cut and tear the material (Fig. 14a). (ii) High-stress abrasion when breaking of the abrasive occurs: abrasive particles are compressed between two solid surfaces, e.g. in grinding mills (Fig. 14b). Hawk and Wilson [HAW01] state: "*High stress abrasion is sometimes referred to as three-body abrasion, although two-body, high stress conditions can sometimes exist. High stress abrasion implies that the abrasive particle is fractured and broken apart during the wear process.*" (iii) Low-stress abrasion (Fig. 14c) generally results from low forces, which cause no fracture or microcracking of hardphases and the microstructure. This is typical when dealing with slurries. (iv) Solid particle erosion takes place with loose abrasives. Wear is caused by the impact of abrasive, i.e. by the inertia of the abrasive particle alone [GAT98, MIS80].

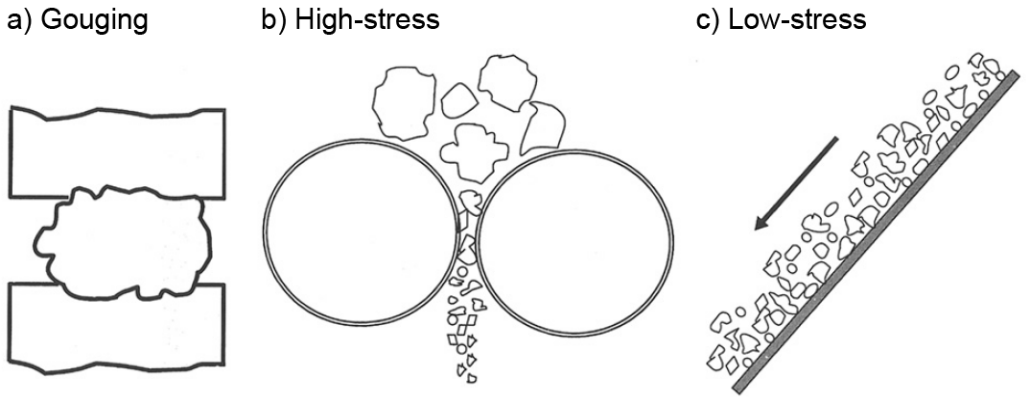

Fig. 14: Schematic diagram for wear involving three-body abrasion processes [cf. CHA10]

Gates gives in his publication "Two-body and three-body abrasion: A critical discussion" [GAT98] further possibilities of a more accurate classification of abrasive wear. Detailing the above mentioned classification based on the abrasive movement and fracture he suggests a situation-based classification given in Tab. 1. This classification has the advantage that plant engineers can immediately identify the abrasion mode according to the scheme. Two- and three-body conditions are implied as free and constraint abrasive within this classification. The fracture of abrasives is not only system related but also to the properties of the abrasive itself. The contact stress leading to particle fracture is also used within this scheme, i.e. low- and high-stress conditions as well as gouging are represented (gouging is limited to a fixed abrasive). The drawback of this classification is that just two parameters (free or loose abrasive and contact stress) are used for classification and many others are neglected.

Tab. 1: Situation-based classification for abrasive wear according Gates [GAT98]

		Contact stress		
		Low (particles do not fracture)	High (particles fracture)	Extreme (gross deformation)
Abrasive particles	Free	Low-stress free-abrasive	High-stress free-abrasive	
	Constrained	Low-stress fixed-abrasive	High-stress fixed-abrasive	Extreme-stress fixed-abrasive

Gates [GAT98] introduces a further detailed classification according abrasive wear mode and dominant debris-generation mechanism given in Tab. 2. This severity-based classification features the wear modes mild, severe and extreme, entailing the typical wear mechanisms microploughing, microcutting and microcutting/microfracture. The wear modes are comparable to the above mentioned, but also include details on the abrasive size, shape and fracture. Nevertheless, a quantitative classification remains elusive as the values are too strongly dependent on other variables, including the worn material.

Tab. 2: Severity-based classification for abrasive wear according Gates [GAT98]

Typical[a] situations	Abrasive wear mode		
	Mild	Severe	Extreme
Particle size	Small	Moderate	Large
Constraint	Unconstraint	Partially constrained by counterface	Strongly constrained
Particle shape	Rounded	Sharp	Sharp
Contact stress	Low-insufficient to fracture particles	Moderate-sufficient to fracture particles	Very high-may cause macroscopic deformation or brittle fracture of material being worn
Dominant[b] mechanism	Microploughing	Microcutting	Microcutting and/or Microfracture
Equivalent terms	Low-stress abrasion	High-stress abrasion	Gouging abrasion
	Scratching abrasion	Grinding abrasion	
	Low-stress three-body	High-stress three-body	High-stress two-body
		Low-stress two-body	

[a]Not all aspects of "typical" situation necessarily apply simultaneously
[b]Debris-removal mechanisms are highly material-dependent

2.4.2. Experimental simulation of abrasion modes

As previously stated abrasive wear is not a material property but a response to the tribosystem. This makes material testing under application-near conditions inevitable in order to select suitable materials for plant specific demands and reported tests simulating abrasive conditions are presented in this section.

For utilisation of test methods to quantify abrasive or erosive wear resistance, the test must be reproducible and the sample must be subjected well-defined to abrasion or erosion [ADA03, HUT98]. It is important that the test reproduces the practical application as far as possible. Furthermore, an accurate measurement of the extent of wear is necessary. The most common method for abrasive and erosive wear loss quantification is the determination of mass loss. [HUT98] However, also the present wear mechanisms have to be identified and it has to be assured that the wear mechanisms of the test are identical with the given application and service conditions, otherwise lab-scale wear tests are irrelevant for material selection [HUT98, WIR00]. Often a single model test gives a limited view on material behaviour and a combination of tests can be done to generate a 'tribological profile' [HUT98]. Frequently scratch testing is utilised to simulate single abrasive phenomena [JAC92]. These are also reported recently up to 1000°C on nanoscale by Beake et al. [BEA14] and at high loads up to 500 N by the author et al. [VAR15-3]. Although useful insight in wear behaviour can be gained by simulating a single fundamental abrasive event, this work should concentrate on the cumulative action of multiple abrasives like in plant operation. Most tests are limited to ambient conditions without heating possibility, within this work the focus lies on HT test possibilities.

2.4.2.1. Three-body abrasion

In order to simulate wear mechanisms comparable to the application it is crucial to model the abrasive movement. Constrained abrasive (two-body condition) leads to fundamental other mechanisms than free abrasive (three-body condition). E.g. two-body abrasion was found to produce about one order of magnitude higher wear loss than three-body abrasion under comparable loading conditions [RAB61], even 3 orders of magnitude were reported in [GAT98].

Various abrasion tests are published in literature and studies on the wear mode resulting from changing conditions of the tribosystem are known [e.g. RAB61, TRE99]. Nowadays the most common are the dry sand/rubber wheel test according ASTM G65 [AST10], the taber abraser [AST15, DIN99] and the microscale abrasion test, also known as ball crater test [TRE99]. Many wear-protective solutions base on coatings so generally also a separation of bulk material and coating testing is necessary, as applicable test devices and/or parameters vary greatly. Within this work thin films are not of importance, but thick wear-protective coatings are investigated. According Hutchings [HUT98] thick coatings can be treated as if they were effectively a bulk material, hence test devices and parameters can be chosen accordingly.

The contact surface stays constant in typical polishing and grinding tests, where a plane specimen is pressed against a flat surface and abrasive is introduced between the two surfaces. Both rotary and vibratory movement has been used with a variety of abrasives and abrasive size. [HUT98] Also fixed abrasive (two-body condition) is reported by grinding against an abrasive paper, but this requires low temperatures [BER01].

Some simpler test rigs are working with a moving sample against a counter body in a bed of (heated) abrasive. [JON09] uses a reciprocating sliding movement in an abrasive bed heated up to 350°C. A mixed wear mode is suspected from the given wear scars, but the condition of the abrasive is questionable, as it is more or less tracked in the wear zone and interchange with the compartment is not probable. A three-body abrasive test (without counter body) in a heated abrasive up to 750°C is reported in [BIR10]: a specimen is rotating in an abrasive filled cup, which enables better flow of abrasive. A similar setup is a drum, partly filled with abrasive, where samples rotate through. A heated test chamber capable of 1000°C is reported in [ANT09].

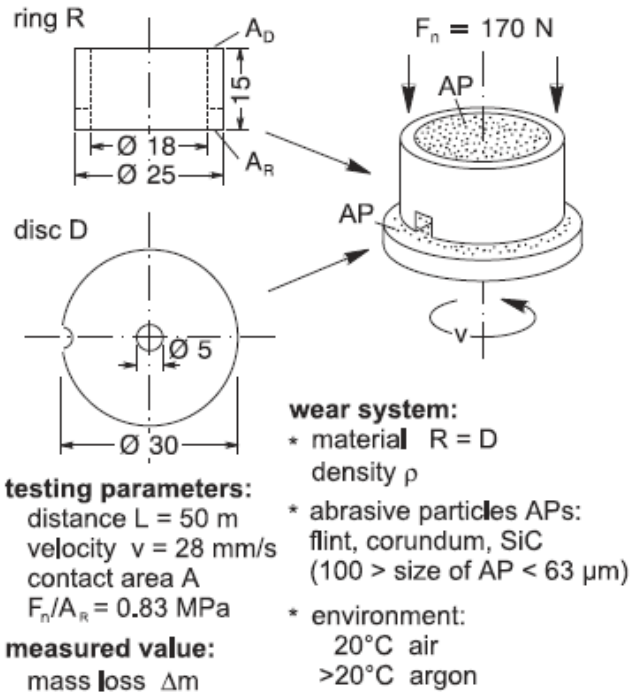

Fig. 15: Schematic of HT sliding abrasion test up to 900°C of ring-on-disc structure [BER99-2]

Another possibility keeping contact area constant is of ring-on-plate geometry. This setup is usually used for sliding experiments, but also abrasive tests are reported [AXE97]: this test works with a tube rotating against a specimen with abrasive slurry in between (tube drill test). A similar setup was already published in 1961 by Rabinowicz [RAB61] and Fischer [FIS92]

introduces also HT testing possibility. He uses an abrasive filled tube, which is notched at the contact surface, which enables the feed with abrasive in the contact zone. This system could be heated and worked up to 750°C, which was extended to 900°C later [BER01, BER97, BER99-1]. Argon atmosphere is used for HT testing. A schematic of the test setup is given in Fig. 15. A similar setup is reported in [VEN97] operating in air up to 600°C.

The micro-scale abrasion wear test also known as ball-cratering test [ADA03, ADA05, BAD03, CES06, COZ11, RUT96], uses a flat specimen pressed against a rotating ball as displayed in Fig. 16. The abrasive is usually fed in slurry condition and wear is quantified easiest by the diameter of the wear scar, or topographical measurement of the wear volume. (A very similar setup uses a rotating disc as counter body [GAL97].) Like in ASTM G65 also a decreasing contact pressure with ascend of wear has to be kept in mind.

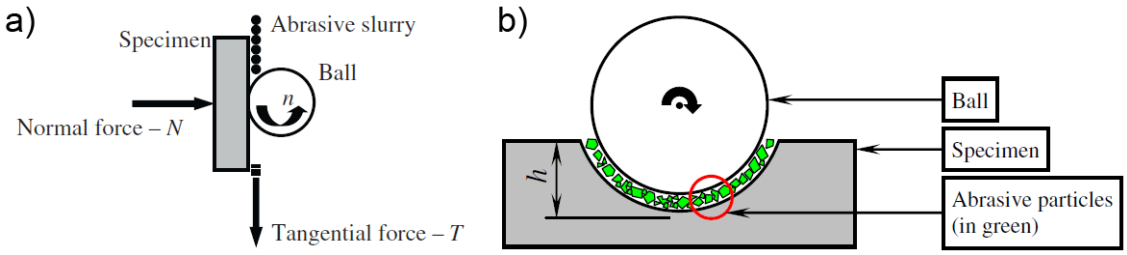

Fig. 16: Schematic of a micro-scale abrasion test [COZ11]

Ball-cratering tests were reported at elevated temperature by Allsopp and Hutchings [ALL01] up to 350°C. Hereto the specimen is placed onto a heated block and abrasive powder is used instead of slurry. The counter body is not heated actively.

Detailed studies of wear modes are available for the micro-scale abrasion setup. A transition in wear modes from two-body to three-body abrasion can be found when changing conditions slightly [ADA03, ADA05]. Free rolling abrasive, i.e. three-body conditions show more reproducible test results and should be preferred for characterisation of wear resistance according Adachi and Hutchings [ADA05].

The ASTM G65 [AST10] is used for abrasion testing of bulk materials and is predated by the Brinell abrasion apparatus [BRI21, WIR00]. It is of block-on-ring structure with abrasive feed in between. Within the standard fixed test parameters are given, nevertheless, load, sliding velocity and abrasive can be changed easily. The standard works with a rubber wheel, which leads to low-stress three-body condition. Some modifications with steel wheel are known, e.g. by Antonov et al. [ANT12] which makes with a further heating system also HT testing up to 450°C possible. The steel wheel results in much severer conditions than rubber wheel testing

and massive abrasive breakage, i.e. high-stress conditions, is found already at low loads. A drawback of this method is the increasing contact surface due to wear, entailing decreasing contact pressures over time, which also means less severe contact. To keep comparable results wear scars of similar size have to be ensured [ANT12, HUT98]. Further test details of this setup are given in the Methodology chapter 3.4.1.

Differences between ASTM G65 and micro-scale abrasion tests or others using rigid counter bodies are discussed by Hutchings [HUT98]: "*The important distinction between all these methods and the rubber wheel abrasion test lies in their use of a much more rigid counter body. Elastic deformation of a rubber wheel results in displacements of the wheel rim which are comparable to the depth of the wear scar in the specimen. The shape of the scar is thus determined by both the distortion of the wheel and the wear resistance of the specimen. With a rigid counter body, in contrast, any local reduction in wear resistance in the specimen will lead to a local increase in wear rate, which will, however, increase the gap between the specimen and counter body at that point, reducing the contact pressure and thus reducing the wear rate. This mechanical feedback results in a wear scar with a conformal geometry which almost precisely replicates the shape of the counter body.*"

Hutchings [HUT98] proposes the use of the specific wear rate to quantify abrasive wear loss: $mm^3/(m \cdot N)$, i.e. the wear volume divided by the sliding distance and the test load. This makes comparison of test conditions with varying loads and sliding distances possible.

2.4.2.2. Solid particle erosion

"*Solid particle erosion is defined as material degradation due to the impact of particles travelling with some significant velocity*." [ROY06] The difference between erosion and abrasion can be defined by the following: in erosion the force exerted by the particles is due to their deceleration; in abrasion the force is externally applied and kept constant [AXE94]. Erosion does not generally take place in inert media and also oxidation has to be considered. Although at RT oxidation influence can be ignored. [AXE94, ROY06]

Generally two test types for solid particle erosion are widely used: a jet type setup, e.g. standardised in ASTM [AST13] and a centrifugal accelerator setup, e.g. GOST standard [GOS79]. Both test principles are also reported for elevated temperature testing and a comprehensive review is given by Roy [ROY06], who elucidates wear of metallic materials including erosive wear tests. Jet type setups accelerate the particles by a gas flow and shoot them on the sample. Two types are known: the isothermal setup with heated abrasive in

comparison to tests where just the sample is placed in a heated chamber and cold abrasive is used. [ROY06] Here always one sample can be investigated at a time [ROY06, SHI95]. Another type of HT erosion test is reported from Tallinn University of Technology using a centrifugal accelerator [ZIK13] similar to the GOST standard [GOS79], but placed in a heated test chamber. This setup is reported to work at temperatures up to 700°C [KUL05] and has the advantage of simultaneously testing of multiple samples. Also the impinging angle can be varied for each sample individually by its rotation to the sand stream. Particle velocity is set by the rotation speed of the centrifugal accelerator. Details of this test are given in the Methodology chapter 3.4.3.

2.4.2.3. Impact-abrasion

Already Avery highlights 1961 in [AVE61]: "*Impact is a prominent factor that can ruin predictions* [of abrasive wear resistance]. *Since abrasion resistance and toughness are usually opposing properties, most choices of alloy require some compromise.*"

Impact-abrasion is a serious wear mechanism in mining and material transport and is commonly tested with a paddle wear test [REN09] or impeller-tumbler wear test [GEI05, RAT13, SUN01], also called continuous impact-abrasion test [BAD09]. These tests use a turning tumbler to stir the abrasive and a fast rotating sample which hits the abrasive flow (Fig. 17). The circumference velocity and the particle weight define the impact load. These tests offer a wide range of possible abrasives, as it is just limited through maximal size useable in the drum. To the present day, only applications at ambient temperature are known.

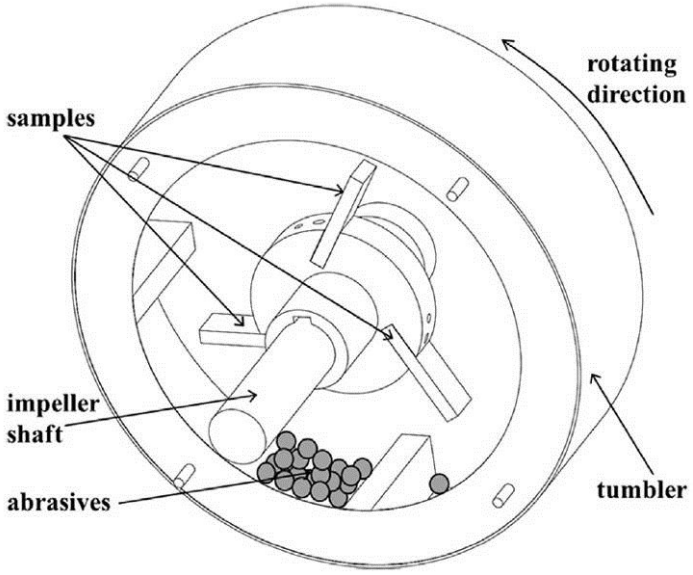

Fig. 17: Schematic of an impeller-tumbler impact-abrasion test [RAT13]

Another test published is an impact-abrasion tester cyclically hitting a wheel with abrasive in between [QIA97]. A dropping hammer is hitting the wheel surface and abrasive is fed in between, operating at RT. A similar principle is used at the HT cyclic impact-abrasion test, a unique test rig at AC2T, allowing investigation of combined impact-abrasive conditions [WIN09-1]. It also uses a dropping hammer, cyclically hitting a sample from a certain height with abrasive flow in between. Normal or 45° impact are possible. The later allows a distinct abrasive component of wear. HT testing of impact-abrasion is scarcely published, solely this last test described is reported to be able to test under temperatures up to 750°C [WIN10]. Details are given in the Methodology chapter 3.4.2.

2.4.3. Wear mechanisms at high temperature abrasive load

This chapter gives an overview on possible strategies to overcome massive abrasive wear loss. In the next chapters fundamental wear mechanisms and wear phenomena present at MMCs are summarised, followed by their changes with increasing temperature, also the influence of the abrasive media is given. By aid of the literature temperature influence on three-body abrasive, erosive and impact-abrasive wear is summarised and forms the basis for investigation of HT abrasive wear in this work. As MML formation plays a crucial role at some materials investigated within this work, published literature is also presented here.

2.4.3.1. Fundamental wear mechanisms

Various theories and models describing the material loss are published since tribology is studied. Well known are the **Archard's wear law** and micro mechanisms of abrasive wear presented by Zum Gahr.

The first widely known theory for wear removal is given by Archard in 1953 [ARC53]. He proposes an adhesion model for wear: the theory postulates when asperities come into contact they may adhere strongly to each other. At subsequent movement the adhesive bond breaks at the weaker asperity in one single action. The transferred particles may become free and weight loss occurs. If the real contact area is given as the normal load L divided by the hardness H, the volume loss V after a sliding distance S can be calculated according Eq. 1:

$$V = K\frac{LS}{3H} \qquad \text{Eq. 1}$$

Where K is a coefficient which gives the probability of the formation of a wear particle from an asperity junction. [ARC53, JAH75] This theory implies that the hardness is the most important material factor in wear loss and softer materials wear more than harder ones.

[JAH75] Further disadvantages of this theory are that it completely ignores the physics of metal deformation, and also different sliding conditions are not taken into account. [SUH73]

Suh proposes in 1973 [SUH73] a delamination theory of wear which especially considers deformation mechanisms present for metals, thought to be the most important mechanism in sliding wear. More important for this work are the possible wear mechanisms in abrasion as proposed by Zum Gahr in 1987 [GAH87]. Four different basic wear mechanisms can be distinguished in abrasive contact: (i) microploughing, (ii) microcutting, (iii) microfatigue and (iv) microcracking. They are displayed in Fig. 18. (i) if at a single pass of abrasive plastic deformation takes place and no material is removed it is called **microploughing**: in front of the abrasive a prow is formed and ridges to the sides. (iii) due to microploughing material removal can occur when many particles are acting and plough aside the wearing material repeatedly, **microfatigue** occurs. (ii) during **microcutting** a material loss equal to the wear scar volume occurs. Microploughing and microcutting are the dominant mechanisms in more ductile materials. (iv) **microcracking** takes place when highly concentrated stresses are caused by the abrasive particles. This is especially evident in brittle materials and large debris may be detached by crack formation and propagation.

A very general probability of the mechanisms is given by Zum Gahr [GAH87]: "*Predominant microploughing changes to predominant microcutting with increasing hardness of the material worn. Further increase in hardness of the wearing material may result in the transition from microcutting to microcracking.*"

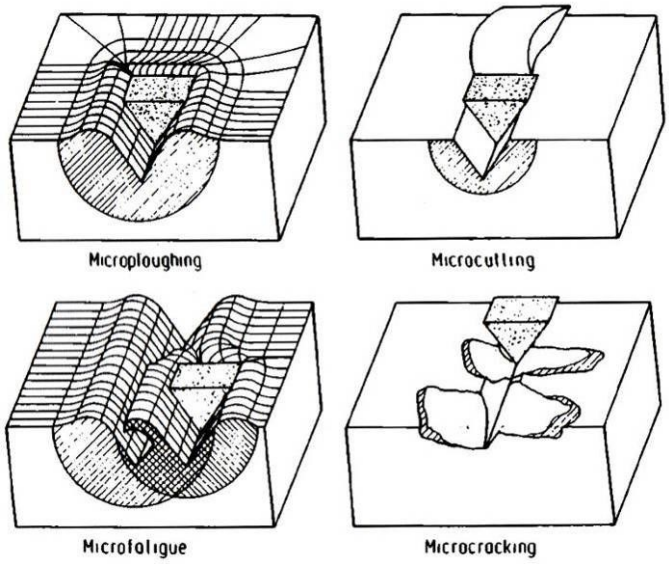

Fig. 18: Basic wear mechanisms in abrasive contact [GAH87]

2.4.3.2. Wear phenomena at abrasive load

There are several known material groups, which should withstand wear at conditions present at the real-field application. Certain hardphase content is often added to improve wear resistance. Fig. 19 gives an overview of typical materials for wear applications sorted by their hardphase content. Important material properties in wear are given on the right side. Toughness and plasticity is generally high for metals with no hardphases. On the other hand, hardness generally increases with increasing hardphase content. The term "wear resistance" has to be treated carefully and depends largely on the present conditions. [KLE05, KUL05] For this work especially the groups alloy tool steel up to coatings with ~55 % hardphase content are relevant.

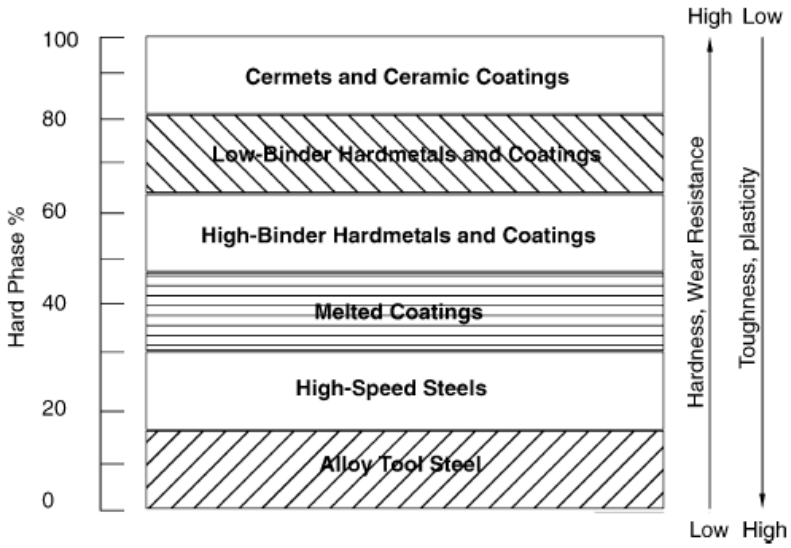

Fig. 19: Wear resistance to oblique erosion of various material groups [KUL05]

A high hardness influence on abrasive wear is documented [e.g. GAH87]. Abrasive wear dominates when the hardness of the particles is in the range or higher than the surface hardness of the worn material. A sharp increase of wear in homogeneous materials is reported from equal hardness of abrasive and surface, flattening at a higher wear level (Fig. 20). For materials with hardphases the matrix is softer than the abrasive at equal compound hardness, i.e. abrasive wear starts earlier. The transition to the high wear level starts when the hardness of the abrasive exceeds both the matrix and the hardphase hardness. [GAH87]

Hard and soft abrasives are distinguished by Zum Gahr [GAH87]: soft abrasives are softer than the hardphases in the MMC, while hard abrasive particles exceed the hardness of all hardphases within the material. Studies on white cast irons with different volume fraction of carbides show decreasing wear loss with increasing carbide content at soft abrasive particles.

On the other hand, hard, large abrasive particles were able to cut and crack massive carbides, which entailed increased wear loss with increasing carbide content. The wear volume was found to decrease with increasing hardness of hardphases when microcracking does not occur. Microcracking can result in massive wear loss in structures with large volume content of carbides. [GAH87]

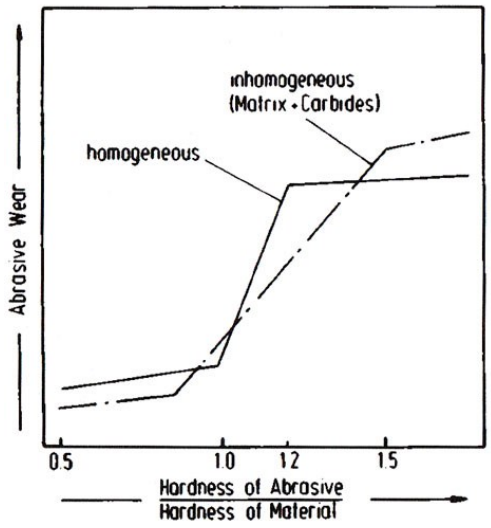

Fig. 20: Hardness influence on abrasive wear of homogenous and reinforced materials [GAH87]

Hardfacings were mainly developed to withstand abrasive wear, hence their wear resistance in the special loading condition is their central property. Generally, the above mentioned micro mechanisms apply also for the wear by multiple events, e.g. in two-body abrasion. Micro-ploughing and microcutting dominate wear in the soft matrix regions, while depending on the abrasive hardness microcutting or microcracking of the hardphases occur, when it exceeds the hardness of the hardphases. [BER98]

On a larger scale, wear in MMC can generally be described by digging out, cutting, cutting and cracking, pulling out of hardphases and maybe wearing of the abrasive particles. These mechanisms are shown schematically in Fig. 21. "*Hard abrasive particles can easily dig out small carbides. Ductile carbides which are larger than the average wear grooves are cut by hard abrasives. Brittle carbides are cut and cracked. Soft abrasive particles are able to dig out small carbides or produce large pits. The indentation depth of the soft abrasive particles is substantially reduced by hard carbides. Large carbides deficiently bonded to the matrix can be pulled out by sliding soft abrasive particles. Large carbides strongly bonded to the matrix can blunt or fracture soft abrasive particles, i.e. abrasive particles can only attack the softer matrix. This may result in protruding carbides which are finally fractured due to lack of support by the matrix.*" [GAH87] A combination of these mechanisms can occur. Geiderer

[GEI05] found in impact abrasive environment the breakage of large hardphases within the MMC as well as removal of the matrix by the soft abrasive particles, i.e. the impact energy of the soft abrasive particles can also destroy hard hardphases.

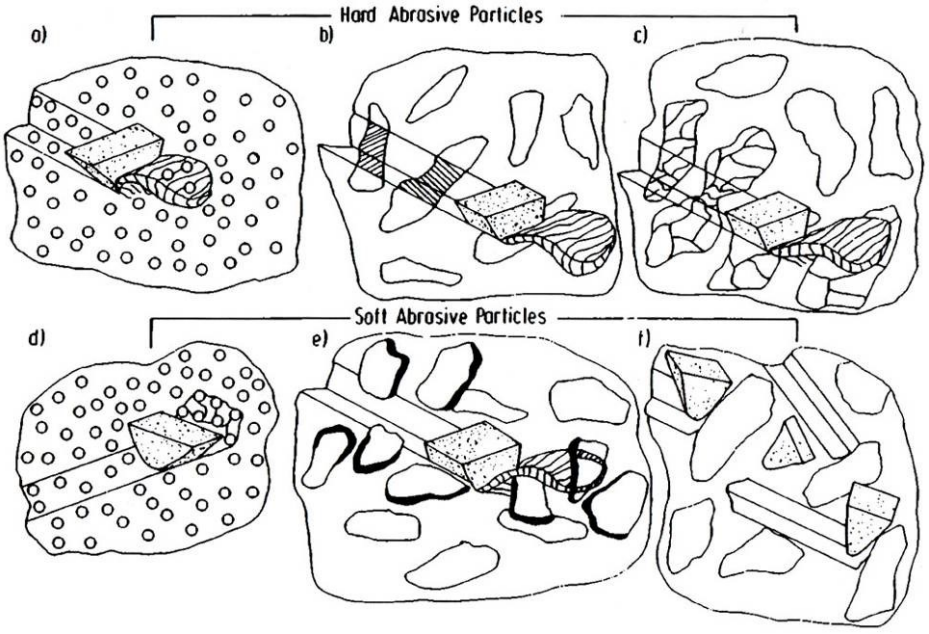

Fig. 21: Abrasive wear of MMCs: possible wear mechanisms [GAH87]

The matrix microstructure is also known to influence abrasive wear behaviour. The abrasive wear behaviour is dependent on the matrix properties, the properties of the hardphases and of all constituents together. Abrasive wear resistance of single phases was studied in the past and found to be mostly dependent on stacking fault energy of alloys. Also work hardening was found to be important. Generally, higher matrix hardness was found to be more abrasion resistant. Especially martensites showed superior wear resistance compared to ferritic-pearlitic structures. Fig. 22 gives an overview of wear resistance in two-body regime of common steels. [GAH87] In this work the focus lies on MMC materials and hardphase influence is thought to dominate the wear behaviour and is studied in greater detail.

Transitions in wear mechanisms in sliding abrasion of brittle materials were investigated by Moore and King [MOO80], which can be put down to applied load and properties of the abrasive. For materials with low toughness, wear is primarily a mechanism of brittle fracture, hence increasing the toughness leads to reduced wear rates. High toughness materials show ductile wear behaviour and fracture does not occur. Under these circumstances the wear rate is determined primarily by the hardness of the material. However, most materials feature a decrease in fracture toughness, when increasing hardness, hence a transition between these two phenomena can occur. Then transition is highly related to applied parameters, like load

and abrasive. [GAH87, HUT92] Rabinowicz et al. [RAB61] found that the effect of hardening a metallic surface for increased wear resistance does not follow a linear hardness dependence, but has less effect. One reason may be the increased brittleness accompanied by hardening, and wearing may entail larger wear volumes due to brittle spalling than to plastic grooving. A further factor is fatigue, as abrasive wear is of repetitive nature a high fatigue strength would be beneficial.

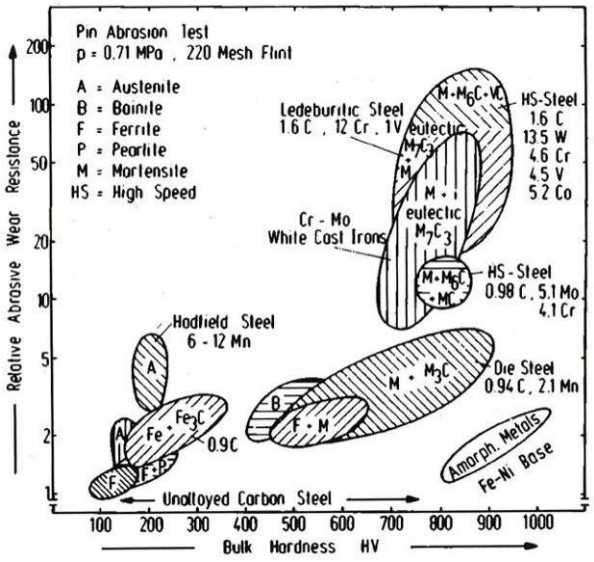

Fig. 22: Abrasive wear resistance of steels in two-body abrasion [GAH87]

"*Abrasion occurs via various mechanisms, including plasticity and cracking, under single or multiple (fatigue) load cycles. It can also involve adhesion and subsequent decohesion, as well as oxidation.* […] *Even in seemingly simple geometric configurations (e.g. two flat contacting plates), the stress states in the contact regions are complex because of surface asperities. The stresses that govern abrasion are highly localized and decay rapidly with distance from the contact sites.*" [ZOK07] Idealised contact regimes are displayed in Fig. 23 with normal and combined normal and tangential load. The first line (a,b) illustrates conditions at round abrasives with no cracking. The second (c,d) leads to cracking against round abrasives and the last line (e,f) depicts stress regions against sharp abrasives. Wear maps of materials withstanding these conditions and combinations of them are given in [ZOK07], but are of low concern here, as materials range from polymers to ceramics in this study with low attention to steels. The localised stresses in the tribocontact can further result in residual stresses, which may have detrimental influence on wear resistance and cracks are formed and propagate during cyclic loading [DAN08, LIN13].

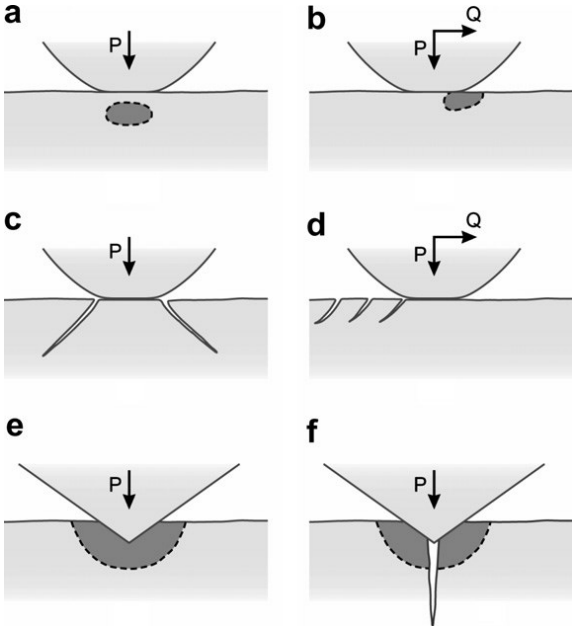

Fig. 23: Damage mechanisms during contacts with blunt and sharp abrasives.
Shaded areas represent yielding. [ZOK07]

2.4.3.3. Temperature influence on wear resistance

As material hardness is a crucial factor influencing wear, the knowledge of the hardness at application temperature is necessary to understand wear behaviour [BER98], thus hardness measurement techniques should be introduced here. While standard methods for measuring hardness are commonly in use [e.g. AST11, ISO05], HT devices are rare. Berns [BER95] describes a hot hardness test based on the Vickers-standard in the 1990s, where it was possible to determine the hardness of single phases in a composite up to 900°C [BER99-1]. Highest temperatures are reached nowadays at 1500°C [MAR14] and it is mainly used for ceramics. Better reported is a test device up to 800°C used for metallic materials and MMCs at AC2T [VAR11, VAR13-1, ZIK13] which works with 10 kg load and determines the "macro-hardness" change at increasing temperature. A new setup allows hardness testing with variable loads up to 1000°C [VAR15-3].

Berns (editor) concentrates in [BER98] on hardfacings, their microstructure and wear properties. Metal matrices with decreasing stacking fault energy show increased work hardening during plastic deformation, which is utilised in Ni- and Co-base hardfacings. Hardphases mostly are carbides, nitrides and borides, which generally show much higher hardness than the matrix. Pure ceramic hardphases like Cr_7C_3 generally dilute other elements from the alloy entailing decreased micro hardness, e.g. with increasing Fe-content. Hardphases show generally higher resistance to scratching, but breakage of the hardphases may occur above a critical

load (Fig. 24a), while at lower loads microcutting dominates (Fig. 24b). Also hardphases which are not directly scratched and in the range of plastic deformation may crack. Scratch resistance of hardphases is, contrary to the matrices, driven by microcracking instead of hardness dependency. At HT microcracking may change to microcutting. [BER98]

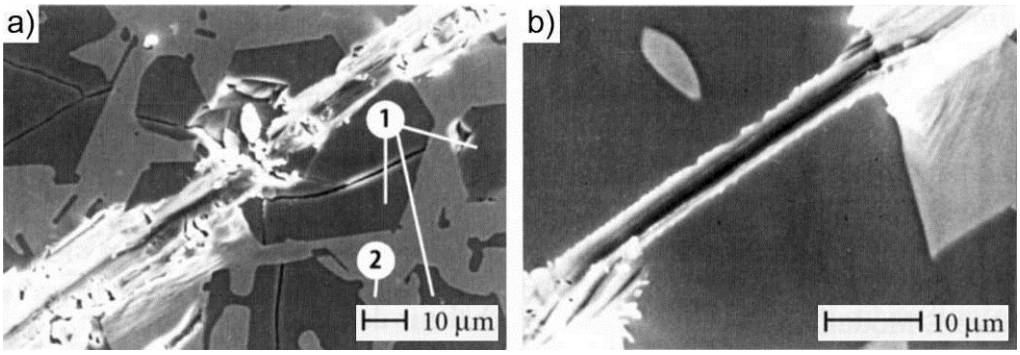

Fig. 24: Carbide wear during scratching: a) microcracking at higher load (1-Cr_7C_3 hardphases, 2-Ni-matrix); b) microcutting at low load [cf. BER98]

Temperature influence of MMCs was studied by Berns (editor) [BER98] in greater detail. With increasing temperature the hardness of all phases and also that of the abrasive decreases. Work hardening ability drops and recrystallisation starts at ~0.3 times the melting temperature. Hardness curves for several metal matrices are shown in Fig. 25a. Especially Fe-base matrices soften because of annealing effects. For martensitic tool steels this effect is shifted to temperatures >600°C leading to a rapid hardness drop exceeding this temperature. The metallic matrix must embed the hardphases and backup them sufficiently at loading, i.e. both high hardness and toughness is required. This is especially difficult when different temperature regimes are present. E.g. an annealed martensitic structure meets these requirements at low temperatures, but hardness rapidly drops >600°C and backup worsens. Contrary to these body-centred cubic (bcc) structures the face-centred cubic (fcc) materials do not show a rapid drop in this temperature range. This was put down to the higher packing factor of the fcc structure which exacerbates diffusion. The Co-alloy features hexagonal close-packing (hcp) at RT, which changes to fcc at HT. This entails higher hardness at RT, which stays at a higher level than the NiCr20 alloy because of its lower stacking fault energy. The stacking fault formation of the Co-alloy also results in a higher resistance to scratching at HT compared to the other matrices. Fe-base alloys show prominent recrystallisation phenomena >700°C.

Also the hardphases suffer softening with ascending temperature. Here the reason is the reduced binding energy, only very tough hardphases (e.g. Ni_3B) feature dislocation driven softening. Fig. 25b depicts the temperature-micro hardness curves of different hardphases.

The order of the hardphases does not change within the investigated temperature range. Softer carbides (M_3C, M_7C_3 and Cr_7C_3) soften >600°C distinctly. [BER98]

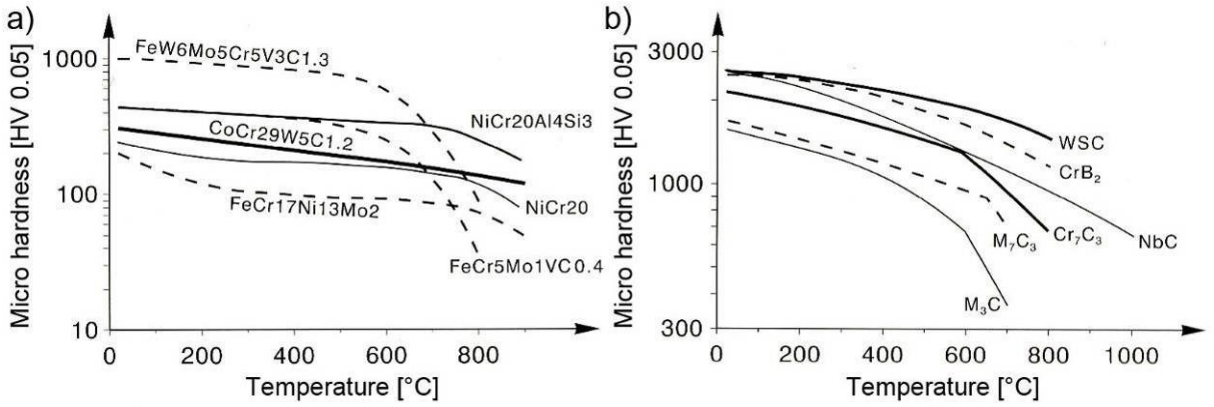

Fig. 25: Temperature dependence of micro hardness: a) metal matrices, b) hardphases [cf. BER98]

2.4.3.4. Influence of abrasive properties on wear

Also the abrasive is an important part of the tribosystem. While most tests deal with standardised abrasive media (e.g. ASTM G65 [AST10]), Kelly and Hutchings [KEL01] investigated the influence of the abrasivity of different media and found that the shape of the particles has the highest influence, while the size seems to be less important. Large particles are most likely broken at the entrance to the wear scar. Influence of abrasive's hardness was investigated by Badisch and Mitterer [BAD03]. They observed highest abrasive wear loss by the hardest abrasive (SiC), which was able to damage both, the matrix and the hardphases, while a soft abrasive (ZrO_2) affects only the matrix of high speed steels. Wear mechanisms also vary: while the softest abrasive ZrO_2 leads to mainly microploughing wear of high speed steels, Al_2O_3 entailed microcutting and SiC prominent microcracking. Hence, in order to simulate real applications, it is important to deal with similar abrasives. Often quartz and hard silicates are used as abrasive as they induce severe service conditions and are easy available and provide reproducibility of the test, while customer specific abrasives often alters during wear testing [AVE61, KEL01]. Rabinowitz presents in [RAB61] an investigation of abrasive size influence, where he found a distinct increase of three-body wear rate with increasing particles up to a threshold where wear rates stay constant with further increasing abrasive size. In steel-steel contact this was observed at ~50 µm.

Particle fracture of abrasive is of major importance for the wear mechanism. High-stress conditions entail fracturing of particles, leading to more, small, sharp particles after fracture, which increase wear loss. The extent of particle fracture is most often neglected, but some studies are published [ANT12, DUB99]. The fracture is strongly related to particle size,

shape, applied loads and used abrasive as well as abraded materials. The effect of particle size is detailed investigated by Chacon-Nava et al. [CHA10]. They observed that generally smaller, sharp particles cause more damage than larger ones in abrasive conditions.

Temperature influence on abrasives is scarcely investigated. Together with micro properties of phases in hardfacings Berns (editor) [BER98] presents hardness dependence of common abrasives. Fig. 26 compares the temperature - micro hardness dependence of common abrasives with different metal matrices and hardphases. Additional to higher hardness than the abrasive the size of the hardphases have to be at least the size of the abrasive to offer wear protection (cf. Fig. 21). E.g. at RT taking a martensitic matrix (700 HV0.05) with M_7C_3 (1600 HV0.05) carbides of sufficient size, flint with a hardness of 1200 HV0.05 can scratch the matrix, but not the hardphases. With increasing temperature flint losses hardness rapidly and reaches lower hardness at 700°C than the martensitic matrix. If the abrasive is corundum on the other hand, it stays very hard also at HT, thus damaging both matrix and hardphases in all temperature ranges investigated. Hardness of abrasives generally is slightly lower than of the hardphases, thus breaking of the abrasives is present and many sharp edged smaller particles are formed [BER98] and higher abrasivity can be suspected [KEL01].

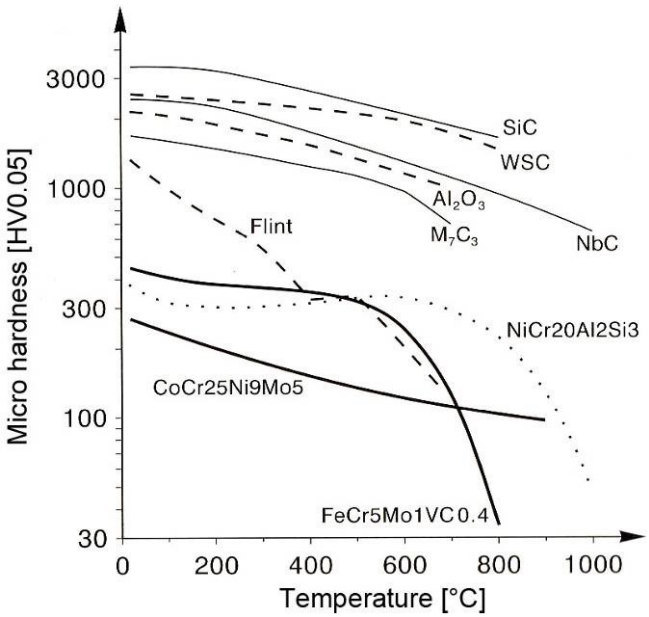

Fig. 26: Micro hardness' temperature dependence of metal matrices, hardphases and abrasives [cf. BER98]

Some studies can be utilised to investigate the abrasive decay in block-on-ring configuration. Higher abrasion rates with steel wheel were observed compared to the rubber wheel ASTM G65 configuration [CHE98], crushing of abrasive in steel wheel test is evident [ANT12,

GOR97]. Wear coefficients in high-stress condition are independent of original particle size [WIR00]. Particle fracture occurs, which leads to the assumption of higher forces promoting wear. However, particle embedding occurs and may lead to increasing wear resistance. Particle fracture results in smaller abrasives of highly angular shape.

2.4.3.5. Three-body abrasive wear

As mentioned above, hardphases which are much smaller than the abrasives are removed by the chip (Fig. 21). For optimal scratch resistance the hardphase should be larger than the abrasive and form a "barrier". It has to be noted, that too large hardphases also entail disadvantages, as an increase in microcracking was observed at larger hardphases. A homogeneous distribution of sufficient large carbides was found superior to hardphase networks with larger matrix areas in between. The decreasing wear resistance with soft matrices (or softening with temperature) can be balanced with larger hardphases. However hardphase cracking increases, when matrix back-up worsens. [BER98]

Berns (editor) [BER98] also investigated cumulative effects in MMCs on the basis of two-body abrasion tests. With decreasing abrasive particle size the applied load is carried on a larger amount of particles, i.e. the load on a single abrasive reduces. This produces also smaller scratches and sufficient wear protection can be reached by smaller hardphases. This further brings the benefit of lower sensitivity to microcracking. In a test rig aimed for the simulation of three-body abrasion (Fig. 15) the embedding of abrasives in the surface was observed at soft alloys (until ~300 HV30). The metal matrix was found to wear more easily than the hardphases. [BER98] Other abrasive contact situations are not investigated in detail. For HT wear the same tests were applied. Generally mechanisms are very similar, but the different phases have diverged temperature dependence. During scratching of white cast iron at RT mainly microcutting of the primary M_7C_3 carbides was observed, which changes to microcracking at 700°C. At the matrices of MMCs the plasticity increases with temperature, while the work hardening ability decreases. Above 500°C matrices can be sorted by their stacking fault energy. Ni-base alloys generally are soft and the metallic matrix offers poor wear resistance. Nevertheless, they are used as wear protection, because their properties do not change significantly in a wide temperature range. At 700°C these alloys were found to surpass hardened Fe-base alloys regarding wear resistance. At 900°C it was observed that wear resistance of alloys with different hardphase content is similar. Berns (editor) [BER98] assumes that at increasing temperature the influence of hardphases on wear resistance decreases. At HT abrasion tests the embedding of broken abrasive particles was observed in

matrix areas, which may also reduce wear. At lower temperatures this was especially evident at materials with low initial hardness or hardphase content. At materials with high initial hardness or sufficient hardphase content, the improvement through abrasive embedding was minor. Despite the formation of these layers the matrix is removed by abrading larger particles. In a critical temperature regime hardphases may break due to increased contact stress, as the surrounding matrix is worn or they break beneath the surface due to deformation gradients. At HT of approximately >0.6 times the melting temperature, mechanisms are mostly driven by the matrix properties. Work hardening ability is lost and dynamic recrystallisation takes place beneath the wear track. The back-up of the matrix worsens, pointed out by largely decreased hardness, and especially smaller eutectic hardphases break under load. [BER98] Low-stress HT-abrasion (700°C) of high Cr-alloys (2.9C-25Cr-0.5Ni-0.5Mo) was studied by Liu et al. [LIU01]: "*The primary γ-phase* [fcc] *that was softer at the test temperature was worn rapidly, leaving the eutectic phase carbide that was harder and wear resistant forming the hills of the worn surface. The micro grooving and deformation were considered to be the dominant mechanisms of the wear of the primary γ-phase, while the brittle fracture process was considered to be the process of the wear of eutectic carbides.*" The hypereutectic Cr-alloy (4.5C-40Cr-8Ni-9Nb-5Mo) shows brittle fracture of primary carbides and eutectic zones, but higher wear resistance than the hypoeutectic alloy [LIU01]. Addition of Al_2O_3 to the hypoeutectic alloy (36Cr-9Ni-5Mo-2.2C) by powder metallurgy increases HT low-stress abrasive wear resistance [SAT05].

Especially when dealing with hardfacings samples have to be kept constant during a test series and must be comparable to service condition. "*Hard facing alloys are influenced by welding method, dilution from the base material, cooling rates, reheating from subsequent weld deposition, and by contact with molten fluxes. [...] Cast and wrought parts are also subject to metallurgical variables, particularly chemical composition, section size, heat treatment and cooling rates.*" [AVE61] The production also influences the orientation of hardphases. Doğan et al. [DOG95-1, DOG95-2] studied the influence of carbide orientation of Cr white cast iron in high-stress abrasive conditions. A high dependence of carbide orientation was found: longitudinal arranged hardphases showed lower wear rates than transverse hardphases. Although this is worth knowing, processing of ideal microstructures is especially difficult in application and is mostly limited to optimise process parameters for, e.g. welding procedure found in lab-scale tests [KAT11].

2.4.3.6. Erosive wear

The second abrasive wear mode widely investigated is erosive wear. Three types of variables are influencing erosion behaviour: impingement variables describing the particle flow, particle variables, and material parameters [AXE94]. Studied in greater detail within this work is the angle of incidence as it is of great importance on wear phenomena experienced by ductile and brittle alloys. Materials are often separated in erosion literature to ductile and brittle by their erosion dependence on angle of incidence. Ductile materials generally have a maximal erosion rate at oblique angles, typically 15-30°. For brittle materials the maximum of erosive wear is mostly observed at normal impact. [AXE94, HUT92, KAT09, VAR13-2] In this context even hardened steels show brittle behaviour. Data of elevated temperature erosion of metals are reviewed by Roy [ROY06]. It was found that almost all (pure) metals, irrelevant of temperature, show ductile behaviour with a maximum erosion rate at oblique impact of 10-30°.

It was found that there often exist a threshold velocity resulting in severe wear [HUT92, WIN09-2]. At HT (up to 650°C) erosive wear of MMCs similar mechanisms to abrasion were found: the hardphases break beneath the surface and may fall out, if their bonding to the matrix is poor. It is also assumed that fatigue of the hardphases is especially critical during erosion. Wear maps for erosive and abrasive wear of brittle materials, especially ceramics are introduced by Hutchings [HUT92]. Wear rates increase largely when wear mechanisms change from plastic deformation to brittle fracture [MOO80], hence it is desirable that these materials are used at conditions where brittle fracture is avoided. Badisch et al. [BAD10] compares Fe-base hardfacings with an austenite up to 650°C. Contrary to the hardfacings, the austenite shows almost no temperature dependence at normal impact and wear rates stay at a low level, while the high hardphase containing materials drastically increase their wear rate. At oblique impact all materials showed increasing wear with temperature. For the austenite wear protection through abrasive particle embedding was observed.

Materials operating at HT are often afflicted by enhanced oxidation, leading to changes in wear mechanism exceeding critical temperatures. This is studied in great detail at erosive wear. Roy points in his review [ROY06] out that accelerated wear occurs by erosion-oxidation synergism. This goes conform with a change in wear mechanism from mainly abrasive wear to oxidation [BIR10] and is also present at the microscale, i.e. also hardphases needs sufficient oxidation resistance. E.g. the for wear protection commonly used tungsten carbides tend to oxidation above 600°C [WIN10]. For the highly alloyed materials and short term investigations within this work oxidation influence is thought of minor importance. This

is supported by a study of abrasion-oxidation synergy [ANT09] where a major finding concerning the stainless steel reference AISI 316 is that the corrosion taking place is negligible compared to the abrasive wear loss.

2.4.3.7. Impact-abrasive wear

Impact-abrasion is scarcely investigated, especially at elevated temperature. Qian and Chao-chang [QIA97] found increased impact-abrasive wear loss with ascending volume fraction of eutectic carbides in low alloyed white cast irons at RT. An optimum at ~10 % carbides was found. Gouging, fatigue spalling craters, microcut grooves and microcracks were found, as well as macroscopic cracking in areas with large amount of carbides. Abrasive embedding was found to cause microcracking in their vicinity. Katsich and Badisch [KAT11] compare low-stress abrasion of MMCs with spherical W-carbides with impact-abrasion. While the hardphases offer good wear resistance in the low-stress rubber wheel test, their behaviour under high impact-abrasive load with corundum was inferior. Brittle fracture of the carbides was the dominating wear mechanism. Kirchgaßner et al. investigated a series of Fe-base hardfacings also under low-stress abrasion and impact-abrasion with two sizes of abrasives. While the high content of larger hardphases entailed best wear results at low-stress abrasion their behaviour at impact-abrasion was diverse. At low impact load high hardness was beneficial, while at high impact load a good combination of hardness and toughness is necessary, e.g. martensitic materials. In impact-abrasive environments hardness was found of major importance for martensites also in [RAT13]. However instead of bulk hardness, the hardness of the worn/plastically deformed surface layer should be taken to assess wear resistance [SUN01]. "*However, in conditions with dominating impact load, an improvement in wear resistance can be obtained by applying ductile matrices with fine uniformly distributed hardphases*." [ZIK13] MMCs with Cr_3C_2 carbides in Ni-base matrix were found less wear resistant in impact-abrasion up to 700°C compared to TiC reinforced ones. Trans- and inter-granular cracking of the Cr-carbides is dominating the wear, especially at highest temperatures. The TiC withstands the load better and mainly the matrix is worn. At HT also particle embedding in the matrix zones gets pronounced and could even be found at the hardphases. [ZIK13] Badisch et al. [BAD10] compared two hardfacings with an austenite also at HT impact-abrasion. At RT the hardfacings show very good wear resistance. At 600°C the higher alloyed complex hardfacing shows best wear resistance. The austenite is distant with double to triple wear loss at both conditions, albeit massive MML formation is observed at 600°C. Similar was found in [WIN09-1], where the austenite shows highest wear at RT and

600°C. A tool steel shows similar wear rate at RT as the austenite, despite its manifold hardness, whereas high hardphase-containing materials are superior. It can be concluded that hardphase reinforcement is beneficial in (HT) impact-abrasive environment at lower impact loads.

2.4.3.8. Influence of in-situ built layers

Although hardness has a crucial influence on wear behaviour, wear rates go not always in relation with hardness, e.g. [GAH87, XUX13]. Especially at HT other phenomena can dominate the wear loss in abrasive conditions, e.g. oxidation or MML formation [JON09, VAR11, VAR13-1, WIN11-2, WIN11-1, XUX13]. HT wear behaviour in respect to microstructural properties of metal alloys is scarcely investigated.

Wear of MMCs increases due to matrix softening at elevated temperatures [VAR11, WIN10]. However ductile materials or matrix regions, e.g. austenitic steels, can **form surface layers during tribological contact**, which may reduce wear. This tribolayer formation is largely dependent on the tribosystem conditions, e.g. counter body material, abrasives and especially temperature [PAU03]. "*Three different layers can be formed in a tribological contact: (i) transfer layers are built up when the worn surface shows the same chemical composition as the mating surface where oxidation does not take place; (ii) mechanically mixed layers are formed when the chemical composition of the debris is a mixture of the wearing and the mating materials, and no oxidation takes place; (iii) composite layers build up in combination with wear and oxidation at higher temperatures. These layers consist of both mating and wearing materials with mixed oxides.*" [VAR13-1]

Early investigations in HT abrasion are published by Fischer [FIS92] who studied three-body abrasion up to 750°C. The formation of tribolayers with the abrasive, which were found strongly adhering to the surface, was present especially at HT. These layers result in low wear rates at abrasion. [FIS92, VAR13-1] Three-body abrasion in hot forging dies was studied by Venkatesan et al. [VEN97]. The investigated temperature range was RT to 600°C. Testing leaded to MML formation for soft materials, but also oxidation was found. Contrary to three-body abrasion in two-body low-stress condition of a high hardphase containing hypereutectic MMC no MML formation was observed at 650°C. [LIU01] Eventually the stresses were too low to lose abrasive particles and embed them. High-stress three-body abrasion up to 450°C was studied by Antonov et al. [ANT12]. The steel AISI 316 formed a pronounced MML with the broken abrasives. The formation of so called glaze-layers at HT due to oxidation is known [STO02] which offer excellent wear resistance in sliding conditions, however resistance to abrasion may be insufficient.

Impact-abrasion at HT was studied in [WIN09-1, WIN10, ZIK13]. MML formation was found for low hardphase containing alloys, especially austenite. In erosion testing composite layers with the abrasive (MML) were found at ductile materials, which were more pronounced at low hardphase content and higher temperature. [WIN09-2] On the other hand, hardfacings with high hardphase content were found to not form MML in contrast to tool steel [KAT09]. Zikin et al. [ZIK13] investigated Ni-base alloys in erosive and impact-abrasive environment. He observed the formation of MML in the matrix zones with broken abrasives as well as broken hardphase particles and gives a schematic of the formed microstructure (Fig. 27). The figure shows large cermet phases (consisting of smaller ceramic grains) embedded in a matrix. During wear the surface near cermet phases break and abrasive sticks to it. Intermixing of broken ceramic grains with abrasive and oxides takes place in matrix areas. I.e. also in the hardphase surface some intermixing was observed. Oxidation was found, albeit very thin layers.

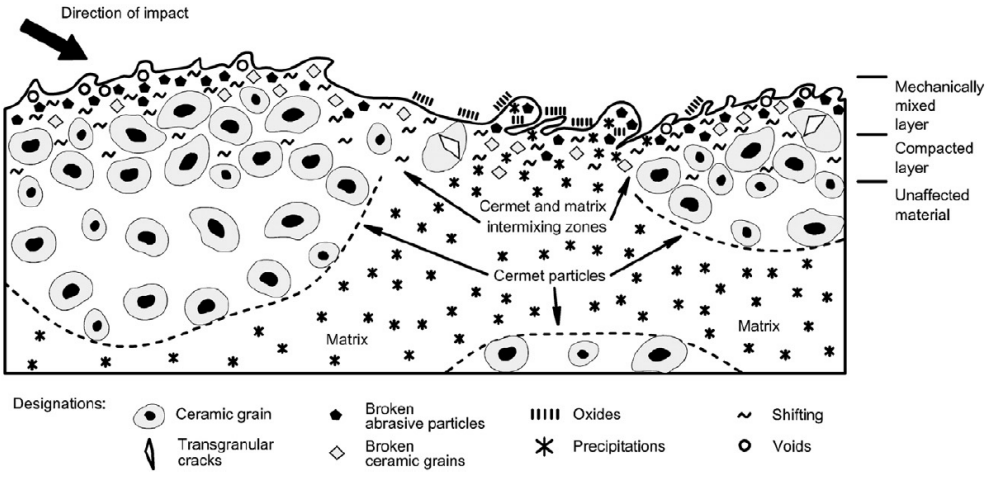

Fig. 27: Surface degradation and MML formation of MMC during HT erosive wear [ZIK13]

It can be expected that MML will form preferentially on soft materials, increasing with temperature induced material softening. Interaction with MMC microstructure and resistance to different forms of abrasive wear remain unknown after comprehensive literature review. There has been significant progress exceeding the test methods described in the review by Hutchings [HUT98] in the last 15 years, especially in the HT regime. The aim of this work is to combine the data found using various HT abrasive methods to build tribological profiles for common materials usable at HT at abrasive particle loaded environments. The focus lies on cost-efficient systems and compares different types of hardfacings with cast bulk materials.

3. Methodology

Within this chapter, the test and analysing methods utilised are described in detail. At first methods for economic evaluation of maintenance costs are given to determine core components worth of tribological investigation in the field of sinter plants. Prospective materials which were chosen for systematic investigation and methods for experimental simulation at HT of found abrasive wear modes are shown in detail. Further quantitative and qualitative investigation methods of wear experiments are presented.

3.1. Determination of core components

The identification of core components which cause most of the expenses is a necessary first step in order to further identify components worth of tribological improvement. Three sources need to be considered: (i) plant priority; (ii) unplanned downtime costs and (iii) scheduled maintenance expenses. This is illustrated in Fig. 28. [VAR13-3]

(i) Plant priority: plants of priority A are crucial for the production process and are not redundant: an unplanned downtime immediately leads to production loss. Hence improvement focuses on the reliability of plants of priority A. Nevertheless, plants of priority B or C also should not be neglected. They may not directly influence the production process, but also are necessary, e.g. for safety or environmental reasons. Typical examples are redundant conveyor belts or emission control aggregates. [VAR13-3] The priority of aggregates is generally available at the customer and do not need further investigation.

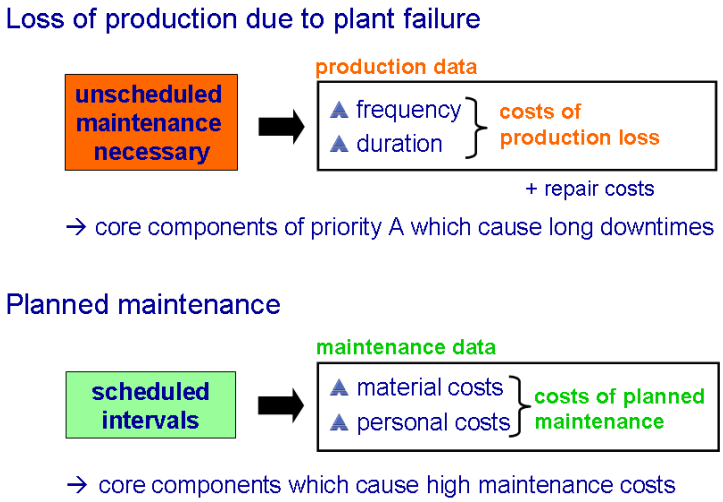

Fig. 28: Identification of core components on the basis of downtime and maintenance data [VAR13-3]

(ii) Downtime costs of priority A plants exceed mostly planned maintenance costs by far. Additionally to the repair costs, the costs of production loss have to be added. I.e. each minute

of downtime is valued with the production loss. The production staff normally has comprehensive knowledge of frequent downtime causes and durations. Unplanned downtime often is accompanied by a severe endangerment of staff, especially in the surrounding of steel production plants. [VAR13-3]

(iii) Scheduled maintenance costs are normally well available within the plant's database. Generally these costs are both personal and material costs. In order to oversee all relevant costs, a long period has to be investigated, as some components may have a lifetime of several years. Further, a clustering of similar components is advisable, e.g. conveyor belts, because many small amounts also can entail high overall costs and are often overlooked in maintenance considerations. [VAR13-3]

"If all these data are correctly assessed costs of unplanned downtimes and scheduled maintenance can be added and overall costs of plant maintenance can be calculated. It is crucial that this assessment is accomplished by a business economist and a plant engineer, because only the knowledge of the plant engineer allows a reasonable classification of aggregates. E.g. many similar production units are in use and have similar bearing problems, the costs per unit due to bearing change may be low, but summarising them, expenses justify a deeper and fundamental investigation of this failure." [VAR13-3]

Within this work, the maintenance efforts of the sinter plant are evaluated. As system boundary at the delivery of raw materials the blending beds were chosen. On the other side of the sinter plant, the entrance of finished sinter via conveyor belt to the stock house of the blast furnace was chosen. This includes the main aggregates:

- Blending beds for sinter mixture
- Sinter mixture transport, mostly conveyor belts, and drum loader
- Pug mills for sinter mixture homogenisation
- Sinter belt with sinter wagons and crusher system for sinter production
- HT chutes and HT sieve for hot sinter transport and screening
- Apron conveyors for transport of hot sinter and returned sinter
- Sinter cooler for cooling down of the hot sinter
- Sinter transport to the stock house, mostly conveyor belts
- Emission control: ventilation, filters, chemical gas cleaning
- Electrical installation, measurement and control systems

3.1.1. Review of maintenance records

All tasks required for maintenance are recorded within the database system of the plant. When a task is accomplished the amount of working time, repair parts, external costs, etc. are accounted to the specific task number. As an example, the replacement of a broken lamp should be taken here: A task is created in the database that the lamp has to be repaired. Then the maintenance staff takes a lamp from the stock and replaces it on site. They record their time and material needed in the database and close the task. Additional information like task start and end, technical place of the work and short description of the work are recorded.

That means that the database system from the plant also can be utilised for reviewing the maintenance costs. For this work an observation period of three business years was chosen (4.2008-3.2011). All tasks within the technical place "sinter plant" with all subgroups were investigated. This means several thousand maintenance tasks/records were evaluated.

To overcome this data flood, data were grouped. At first a clustering according technical place subgroups was undertaken, e.g. sinter plant-infrastructure, sinter plant-sinter belt, sinter plant-exhaust extraction system, etc. Secondly, similar aggregates, like conveyor belts, were grouped, although they have different technical places. This is advisable, as they suffer similar failure causes and should be analysed together. After this, similar failure causes of the groups were clustered manually by analysing their short description, e.g. change of lamp, service air conditioning, repair of conveyor belt damage, etc. This assures that frequent tasks, with maybe lower costs, are not neglected.

Sometimes problems with the database structure occurred. Eventually costs of tasks which overstep the observation period are not correctly calculated. This small amount of tasks was considered of minor importance compared to the remaining tasks and was neglected. A problem of higher impact is bad description quality. The database relies on tasks created by the staff – when no meaningful description is added, it is impossible to figure out what was done exactly. In this case the tasks were added to the nearest possible group with the addition "remains". For all the grouped tasks the total costs and frequency within the three years were analysed. For privacy reasons, the results can only be given in percentage of the total maintenance costs of the sinter plant within this time period.

3.1.2. Review of standstill causes

The downtime costs are more difficult to evaluate. The total unplanned downtime costs, sum the repair and staff costs explained in the previous section plus the production loss. In case of

the sinter plant this is the purchase of iron pellets at the amount of the production loss. I.e. an unplanned downtime of the sintering belt of, e.g. 10 min can be valued as loss of 10 min of the planned sinter production. This amount has to be bought externally in form of iron pellets and entails additional costs of some thousand Euros an hour (the exact value is confidential). For planned repair downtimes the costs can be calculated with half of the amount of iron pellets, because the blast furnace process gets adapted before the downtime for lower consumption of sinter for this time.

As example, the breakage of a sinter grate bar should be explained here. The breakage causes a hole within the sinter wagon, and needs immediate repair. The sinter belt stops when the affected wagon is at the position of the maintenance door. There the remains of the grate bar will be removed and a replacement bar is positioned. The whole procedure takes about 2 min, i.e. also 2 min of sinter production are lost. Also the costs of the replacement bar and the staff for changing is recorded in the database, i.e. these costs are counted in the previous section. Here just the time of plant downtime is evaluated. Further the scheduled downtimes are not considered here; just unplanned standstills of the plant due to failure were evaluated.

Generally all aggregates in the priority A-line can cause a downtime of the sinter belt and in further consequence a production loss. This starts at the conveyor belts, which transport the raw materials, pug mills, sinter belt, sinter breaker and ongoing aggregates like sinter sieves. The basis for this evaluation is a list of sinter belt downtimes, which is kept by the production stuff. There each standstill, planned and unplanned, is recorded. Start time and duration, as well as a short description of the failure/downtime is given. The aggregate causing the failure is also noted, as far as known.

As for the maintenance records, the downtimes were accounted to technical places and similar causes were added: e.g. breakage of a grate bar, or failure of a sieve due to loss of a sieve plate. When this was not possible because of missing information, the downtime was added to the nearest group with the addition “remains”. Like before for all the grouped failures the downtime costs and frequency within three years were analysed. The costs than can be added to the maintenance costs, which gives the total costs of a certain aggregate. Also here results can just be given as percentage of total downtime and costs, respectively.

3.1.3. Tribological assessment of core components

Additionally to the economical assessment of maintenance, as described in the previous sections, a rating of tribological optimisation potential is necessary. There is no direct possibility

to extract this from the database or cost evaluations, but the short description given with the tasks may give useful information. All tasks with high costs or frequent downtime causes were analysed in detail for their tribological relevance. For this purpose, detailed task descriptions were taken from the database and discussed with the responsible plant engineers. [VAR13-3]

Tribological optimisation is often possible when the failure is caused due to wear or lubrication problems, whereas failures, e.g. in the control system and wiring cannot be approached within this work. I.e. frequent tasks or high costs were investigated in detail according their tribological relevance [VAR13-3]. These results are discussed in chapter 5.1.

3.2. Materials investigated

A wide range of HT alloys was chosen for investigation in abrasive environment according current use in sinter plants or their prospective HT properties. Tab. 3 gives an overview of the materials and their processing technology and the reason for their selection is given.

The two chosen bulk materials (blue) are high alloyed Fe- and Ni-base cast alloys. The FeCrC is currently used as material for the grate bars and the reference alloy.

The hardfacings are deposited by two different welding techniques: Plasma Transferred Arc (PTA) welding and Gas Metal Arc Welding (GMAW). While PTA welding allows a good control of process parameters and hardfacing quality, it is more time consuming and pricier. GMAW is also commonly used at large scale production of hardfacings. PTA materials were deposited in one-layer technique, which leads to higher dilution with the substrate and may dissolve substrate in the hardfacing. The faster GMAW allowed the deposition of two-layer systems, which generally show no significant dilution in the second layer. [BAD08]

Tab. 3: Summary of the investigated cast and hardfacing alloys

	Name	Technology	Investigation goal
Bulk	**FeCrC**	Casting	Influence of Fe and Ni-Matrix
	NiCrW	Casting	
Hardfacings	**FeCrCoC**	PTA hardfacing, 1-layer	Influence of Co-content
	CoCrWC	PTA hardfacing, 1-layer	
	FeCrNbC	PTA hardfacing, 1-layer	Influence of microstructure and hardness due to chemical composition and welding procedure
	FeCrNbBWC	PTA hardfacing, 1-layer	
	FeCrNbBWC	GMAW hardfacing, 2-layer	
	FeCrNbBC	GMAW hardfacing, 2-layer	

The second alloying group (green) should highlight the influence of Co. While FeCrCoC is Fe-based with high amount of Co, CoCrWC is Co-based.

The last group (orange) represents different Fe-base hardfacings with high amount of carbide forming elements. FeCrNbBWC is deposited via both welding techniques to investigate their influence on wear behaviour.

Tab. 4 gives the chemical compositions of the materials investigated. The FeCrC is a Fe-base white cast iron which is highly Cr alloyed with 27-30 wt.%. The combination of both, Cr and C cause precipitations of Cr-carbides. Samples of this alloy are taken from grate bars from large scale cast production. NiCrW has the same amount of Cr, but in a Ni-base matrix. It is a commercial HT material and additionally alloyed with W. W enhances HT strength and is also a carbide forming element. This material was produced by ingot casting on lab-scale.

Tab. 4: Chemical composition of the materials [wt.%] and etchants used

	Cast materials		Co-family		Carbide rich hardfacings		
	FeCrC	NiCrW	FeCrCoC	CoCrWC	FeCrNbC	FeCrNbBWC	FeCrNbBC
C	1.2-1.4	0.35-0.55	0.15	1.8	5.5	1.3	1.2
Si	1.0-2.5	1.0-2.0	0.6	1.0	0.8	0.5	0.5
Mn	0.5-1.0	<1.5	0.4	0.4	0.2	0.2	0.2
Cr	27-30	27-30	13	30	21	15.4	10.2
Nb	-	-	-	-	7	4.2	3.1
B	-	-	-	-	-	4.2	4.1
others [Mo, W, V]	<0.5	4.0-6.0	<2.5	<12.9	<1.5	<11.5	<7.9
Ni	-	balance	-	-	-	-	-
Co	-	-	12.5	balance	-	-	-
Fe	balance	15	balance	<3	balance	balance	balance
Etchant	V2A	Murakami	Pikral	Murakami	Murakami	Murakami	Murakami

The following materials where deposited on 5 mm austenitic sheet metal (1.4301). An austenitic substrate is known to entail different hardfacing properties compared to mild steel substrates. This origins from the lower thermal conductivity of the austenite, which lowers the cooling of the hardfacing and influences its microstructure. Austenitic substrates were necessary for HT investigations, to ensure thermal stability of the substrate and minimise the influence of the substrate on HT wear behaviour of the hardfacings, such as substrate oxidation and thermal softening. Deposition parameters for PTA-hardfacings were optimised in the lab and samples deposited in one-layer structure, hence dilution may alters the microstructure slightly. GMAW samples were deposited by a large scale production unit in two-layer structure. At this technology the dilution of the substrate was too high in the first layer, which influences the microstructure and the resulting hardness. Hence a second layer was necessary to avoid distorted results by the substrate influence.

FeCrCoC contains ~13 wt.% Co and Cr, C-content is with 0.15 wt.% relatively low. In combination with rapid cooling of the hardfacing, martensitic microstructure without large carbides due to the low C-content is expected. CoCrWC is a Co-base alloy with high amount of Cr (30 wt.%) and W. In combination with the high C-content of 1.8 wt.% the precipitation of Cr/ W-carbides can be expected. Both Co-alloys were one-layer deposited via PTA technology.

FeCrNbC has hypereutectic composition due to the high C-content of 5.5 wt.%. Main alloying elements are Cr (21 wt.%) and Nb (7 wt.%), which are strong carbide forming elements. It is expected to form coarse primary carbides and a ledeburitic matrix. This hardfacing is also deposited via PTA welding in one-layered structure.

FeCrNbBWC is a complex alloyed hardfacing with high amount of various alloying elements. Main alloying elements are Cr, Nb and W. Due to the high C- and B-content the formation of various carbides and carboborides can be expected. This alloy was both deposited with PTA and GMAW in one-layer and two-layer structure, respectively to show the influence of different processing technologies on one material and the resulting HT wear behaviour.

FeCrNbBC is also a complex alloy with lower amount of alloying elements to reduce its price. C- and B-content is in the same range as the material before, hence the formation of carbides and carboborides is expected. Especially the comparison with the wear results of FeCrNbBWC is of great interest, as this alloy will have slightly lower amount of hardphases, but still at a very high level. This material was deposited via GMAW in two-layer structure.

3.3. Analysing techniques

To investigate materials' microstructures and wear scars, classical metallographic and microscopic methods were used. Further, quantitative image analysis was carried out on cross sections to determine present fractions of phases within the materials. Cross sections of wear scars were used to determine built MML and broken hardphases during abrasive testing. Hot hardness measurement was utilised to investigate hardness progress with temperature and nano indenter (NI) measurements give mechanical properties of the various material's phases.

3.3.1. Optical microscopy

To reveal material's microstructure, microstructural change and wear mechanisms cross sections of the samples were prepared. First, the samples were cut. When dealing with samples for microstructural investigation the samples were taken from a suitable position, e.g.

in the middle of the cast block. For hardfacing samples the whole weld bead was investigated, with concentration to the top layer, where the wear takes place. Samples after wear testing are usually cut normal to the loading direction, in the middle of the wear scar. After cutting, samples are embedded in plastics, grinded and polished up to 1 µm diamond grain size. Most samples were etched with the etchants given in Tab. 4, section 3.2 to highlight the hardphases and investigate the microstructure and possibly deformed zones. Pores and foreign matter, e.g. abrasive particles, may be better visible in unetched condition.

Optical light microscopy (LM) was carried out on a reflected light microscope Leica® MEF4. Interesting zones are photographed by the integrated camera and can then be measured. This was especially important when dealing with wear scars. E.g. the depth of interaction and embedding of abrasive can well be measured. This was used, e.g. when determining the maximum depth of MML as shown in Fig. 29 (embedding plastic is brightened for better visibility). For this purpose, on the cross section the maximum depths of the MML is measured at several points, in this example it is in the range of 20 µm. Similar measurements can be done regarding maximum depth of carbide breakage, but this was more accurate at SEM-images, see section 3.3.2. Also the coverage of the MML was measured on cross sections, for this purpose the covered length was measured and the percentage of the total lenght calculated. In the example in Fig. 29 coverage is 100 %.

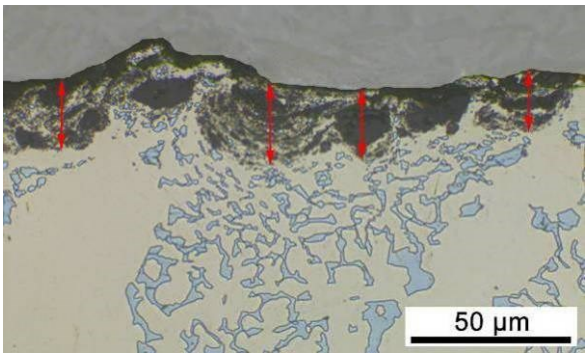

Fig. 29: Cross section of NiCrW after 550°C HT-CAT testing

3.3.2. Scanning electron microscopy

In addition to LM most of the samples were investigated by Scanning Electron Microscopy (SEM - Zeiss® Supra 55 VP). With SEM-SE mode (Secondary Electrons detector) wear scars can be evaluated in more detail. Especially the high depth of focus allows the investigation of heavily worn surfaces and identification of major wear mechanisms. SEM-BSE mode (Back Scattered Electrons detector) gives useful information on the present phases: light elements (like C or O in carbides or oxides) appear dark, while heavy elements are depicted bright (e.g.

the metallic matrix). This material contrast can be used for quantitative image analysis, which is introduced in the next section. The SEM is equipped with an energy dispersive X-ray diffraction device (EDX - EDAX®). With EDX the chemical composition of the different phases can be evaluated. When dealing with known materials, the various phases can well be matched with the EDX data. SEM images of wear scars were utilised to measure the affected depth by abrasive testing. Like at LM MML formation or cracking depth can be investigated. This method was used for quantitative description of affected depths do to its higher magnification and better contrast in BSE-mode compared to LM.

3.3.3. Quantitative image analysis

The area fraction of phases can be measured by Quantitative Image Analysis. Leica QWin® software was used on this behalf [cf. POL08]. The software can separate different phases by its grey value or colour.

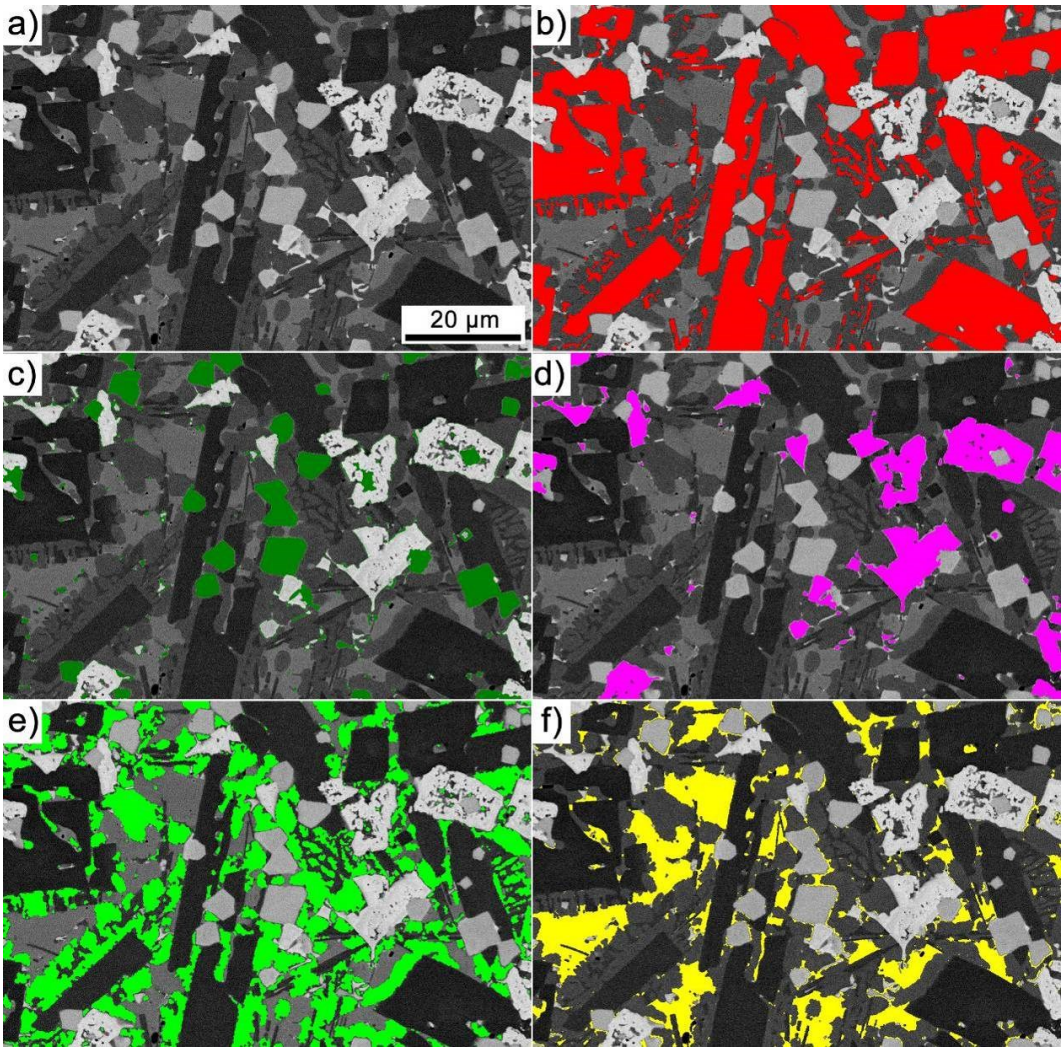

Fig. 30: Cross section of FeCrNbBWC-PTA with different phases coloured:
a) original SEM-BSE; b) Cr-carbides; c) Nb-carbides; d) W-carbides; e) W-rich matrix; f) matrix

In this work mostly the area fraction was analysed, i.e. the fraction of the two dimensional image occupied by a definite colour. For the materials with low hardphase content also the distances between the hardphases were analysed, as they were found to be of major importance for abrasive wear resistance [POL08]. This was not possible for the materials with very high hardphase content, as most of the hardphases are interlinked. In order to obtain reliable results good contrast between the phases is necessary. This either can be reached by etching the samples (over-etching can be useful) and analysing the LM image. For this work, mostly the material contrast gained by SEM-BSE was utilised to quantify the fraction of different hardphases within a material. For this purpose, SEM-BSE images of cross sections were taken and the material contrast was analysed with QWIN. This is much more difficult than measurement of silica, because different hardphases may have similar chemical composition and show insufficient contrast. In this case also the particle shape was used to determine between phases, e.g. it is known that Nb-carbides show triangular shape and are a little darker, while W-carbides are squarer-shaped and brighter [KIR08]. Fig. 30 shows the various phases detected on a high magnification image of FeCrNbBWC-PTA. In order to obtain representative results, the analysed area should be as large as possible with high image resolution: It is advisable to take pictures at lower magnification but with high resolution to cover a large area and receive a reliable average value. Also the embedding of abrasive in wear scars can be studied on SEM images using QWIN. Additional studies for some similar materials are published in [VAR11, VAR15-1].

3.3.4. Hot hardness testing

As the hardness is an important material parameter for wear, the knowledge of the hardness at application temperature is of major importance. The author developed a hot hardness test rig at AC2T [VAR10] capable of hardness testing up to 800°C, which is in the typical application range for Fe-base alloys.

The main components of the test rig are given in Fig. 31a. A sample of ~50×22×6 mm is placed onto a sample holder. Within this sample holder an infrared heater is placed, which heats up the sample from the bottom. Temperature control is done via a ø 0.5 mm type K thermocouple in a drilled hole, placed as close to the test surface as possible. As test method typically Vickers method is chosen, which gives the best measurable indents at HT testing. Test load is fixed at 10 kg (98.1 N) by a dead weight, which is lowered by a pneumatic actuator. Loading and holding time are according the Vickers standard for RT testing [ISO05]. A second pneumatic actuator can move the sample linearly in the sample holder to

allow multiple indents on the same sample up to a maximum of 18 indents. The whole set-up is placed in a vacuum vessel under low vacuum conditions, to prevent massive oxidation of the sample and diamond-indenter damage. The test parameters are summarised in Tab. 5.

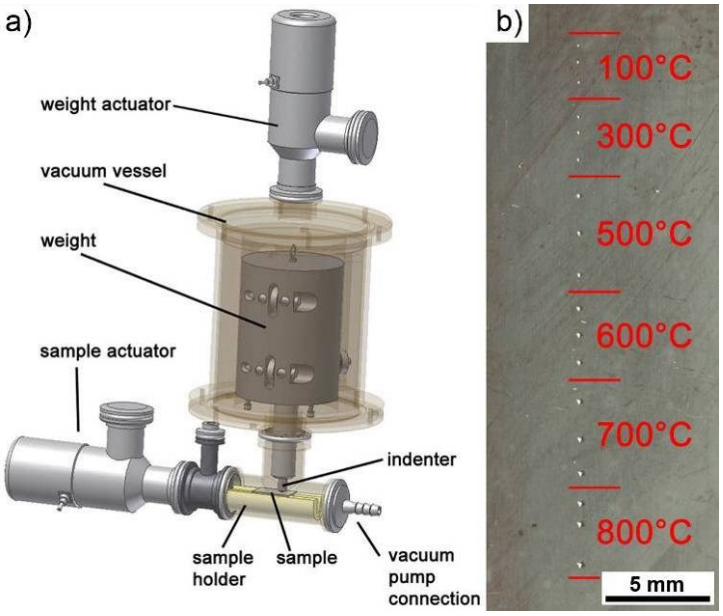

Fig. 31: Hot Hardness Test rig (HHT): a) main components;
b) typical row of indents after HHT [VAR10]

Tab. 5: HHT parameters

Parameter	Value
Temperature	RT, 100°C, 300°C, 500°C, 600°C, 700°C, 800°C
Test method	Vickers [ISO05]
Load	F=98.1 N (10 kg)
Indenter	Diamond Vickers-pyramid
Indentation time	13 s
Measurement	LM measurement of the two diagonals, $d = \frac{d_1 + d_2}{2}$ [mm]
	calculation according $HV = \frac{0.102 \cdot 2 \cdot F \cdot \sin\frac{136°}{2}}{d^2}$ [ISO05] Eq. 2

The test is automatised and controlled via a LabView® software. A typical test cycle runs from 100°C to 800°C (100, 300, 500, 600, 700, 800°C) with three indents for each temperature. This produces a line of indents as shown in Fig. 31b, which can be measured after cooling down of the test rig by light microscopy. For statistical coverage, two samples of each material are tested. RT hardness measurements are done before HHT on the same sample within the test rig. After evaluating the hardness at the various temperatures, hardness-temper-

ature curves for the material can be plotted. These indicate critical temperature ranges where the material softens due to microstructural change and wear mechanism may change rapidly.

A few remarks on the reliability of the test method should be given here. The largest uncertainty when dealing with multiphase alloys is the position of the indent. When approaching a hardphase-rich region the resulting indent is small, an area of matrix with less hardphases yields too large indents and lower hardness, respectively. This problem was overcome by using the large test load of 98.1 N, which entails relatively large indents, averaging over a wide area of the microstructure. Nevertheless, when dealing with structures exceeding ~50 µm, very high standard deviations of hardness values are the result. With the current test set-up this can only be minimised by a large number of indents and removal of invalid measurements (e.g. pores).

By measuring the indent at RT a failure due to the thermal contraction occurs. The maximal failure from a material with high thermal expansion and indentation at 800°C was calculated to < 3 %. Details on the calculation are given in the Master thesis of the author [VAR10] and [VAR15-3]. Due to the fact that failure because of inhomogeneity of the material is for the most materials much larger, the failure due to thermal expansion was neglected. Although tests are done in vacuum, some degradation of the sample's surface is inevitable. This can lead to "blurred" tips of the indents, especially at very HT, which makes them difficult to measure by LM. Best results were obtained by dark field lightning, which emphasises edges. In the worst case reliable measurement is impossible and the indent needs to be repeated.

3.3.5. Nano indentation

Nano Indentation (NI, Hysitron®) was carried out to determine the mechanical properties of different phases within the microstructure. For this purpose, cross sections of several materials were prepared and etched. Then the different phases were measured at 10 mN load with minimal five indents each. Indentation is done with a Berckovich indenter and load-displacement curves are recorded during penetration. From these curves hardness and reduced Young's modulus are calculated. Due to the limited stiffness of the measurement device just a reduced Young's modulus can be derived, nevertheless for comparative measurements this is sufficient. Differences in hardness and reduced Young's modulus between matrix regions and hardphases can easily be measured. Unfortunately NI was just possible at RT, while it can be assumed that differences between matrix and hardphases get even more pronounced at elevated temperatures, as the carbides are very temperature stable compared to the matrix (cf. Fig. 26) [BER98].

3.4. Abrasion testing

Various test rigs were used to simulate the different abrasion modes found in the sinter plant. All tests allow the investigation of wear behaviour at enhanced temperatures. Several steps up to the maximum possible temperature at the different tests were used. A high-stress abrasion test, an impact-abrasion test and an erosion test were utilised for comprehensive characterisation of the wear resistance of the various materials.

3.4.1. Continuous abrasion test

In order to test the abrasion resistance of the various materials a modified ASTM G65 apparatus [AST10] was utilised (Fig. 32). The test parameters chosen for this HT-Continuous Abrasion Test (HT-CAT) are given in Tab. 6. Like in the dry sand/rubber wheel standard a sample is pressed against a turning wheel and an abrasive flow is introduced in between (Fig. 32b). Some modifications were necessary to allow HT-abrasion testing. First of all a possibility to heat the samples was introduced by an inductive heating coil (see Fig. 32a). Further the rubber wheel was replaced by a steel wheel, to allow higher temperatures. First tests with steel wheel showed major breaking of the abrasive in the contact zone, i.e. high-stress contact condition [DUB99] as needed for simulation of the applications (cf. with the low-stress condition using rubber wheel). As wheel material Hardox 400® with a diameter of 232 mm and 12 mm thickness was used. The hardness of the wheel was measured as ~360 HV10 at RT. In order to obtain well measurable wear scars and avoid too much wear loss at HT the load from the standard set-up (130 N) was reduced to 45 N.

In the set-up just heating of the sample is possible, the wheel and the abrasive cannot be heated. First tests show excessive drop of the sample temperature when the abrasive flow was turned on. As abrasive standard Ottawa silica sand with a grain size of 212-300 µm is used (according ASTM G65 [AST10]), introduced between specimen and wheel. The ASTM G65 standard works with 300-400 g/min abrasive flow. It was found that most of the abrasive passes the sample without any interaction [ANT12, DUB99], but the cooling of the sample. Therefore, the flow was reduced to 180 g/min. The sliding speed was set, by the rotational speed of the wheel, to 1 m/s (83 min^{-1}). Sliding distance was chosen as 600 m, i.e. test time is 10 min. With these parameters it was possible to achieve shallow wear tracks (Fig. 32c) with similar contact conditions for all tests, while the wear loss is still measurable and materials revealed clear differences. HT abrasive tests were performed at RT, 300 and 550°C, representing a typical application range for Fe-base hardfacings. For temperature control a hole of ø 0.7 mm was drilled near the contact zone in the side wall of the sample. Within this

hole a thermocouple (ø 0.5 mm, type K) was placed. Some further tests were performed at 700°C for other publications, but not with all of the materials from this study. As they may be interesting for insight in higher temperature range it is referred here to the publications by the author et al. [VAR13-1, VAR15-1]. A study of load influence was published in [VAR16] and HT sliding wear without abrasive in [TOR16].

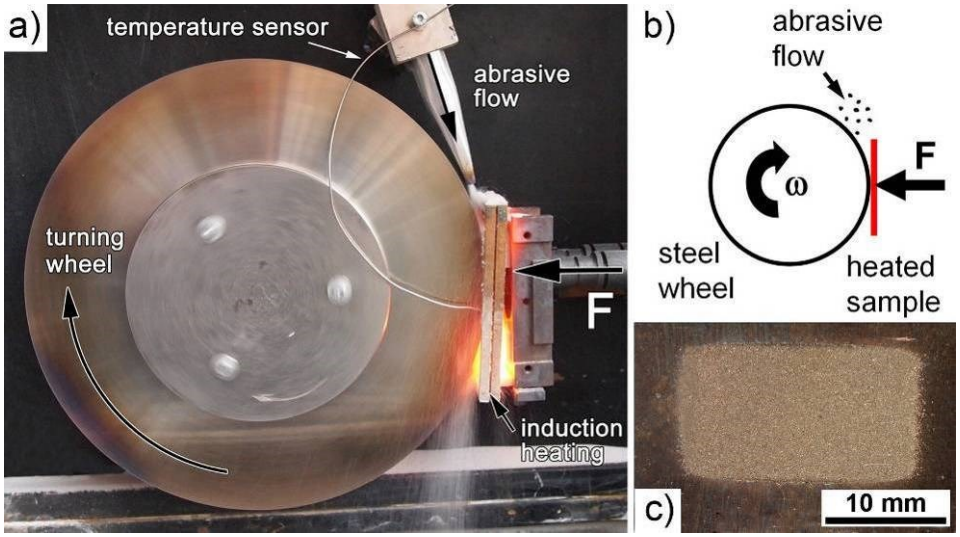

Fig. 32: High Temperature-Continuous Abrasion Test rig (HT-CAT): a) view of test rig [VAR13-1]; b) test principle; c) typical wear mark [cf. VAR13-1]

Tab. 6: Main parameters used in HT-CAT testing

Parameter	Value
Temperature	RT, 300°C, 550°C
Normal load	45 N
Sliding speed	1 m/s
Sliding distance	600 m
Test time	10 min
Counter body	Hardox 400, 360 HV10, ø 232 × 12 mm
Abrasive	Standard Ottawa silica sand, round, 212-300 µm [AST10] at 180 g/min flow rate
Wear quantification	Volume loss / sliding distance → wear rate [mm³/m]

For statistical reasons each conditions was repeated three times. The wear loss is determined gravimetrically after the test. For this purpose, the samples were cleaned in an ultrasonic bath with ethanol and weighted after drying. Volume loss is calculated by material's density. The volume loss is divided by the sliding distance to calculate the wear rate in [mm³/m] which is common in abrasive testing [HUT98]. Normalisation to the load was omitted, as just one load was studied here. Additionally wear analysis was done by microscopic methods on the worn surface and cross sections (3.3.1).

All tests were performed with the same Hardox 400® steel wheel counter body. After pre-tests a working surface on the steel wheel was established, which did not change significantly during a test series. Also the diameter stayed constant at 232 mm within this test series. As HT may degrade the martensitic structure of the Hardox 400® it was analysed after some test series [VAR13-1]: some loosely sticking particles were found on the surface. A cross section (Fig. 33, after 5 s etching with 10 % Fe_3Cl in aqueous solution) reveals still the typical martensitic structure of the Hardox 400®. No hardness difference comparing stressed surface near regions and bulk could be measured (360±12 HV1 for all regions). "*It can be assumed, that due to the small contact area compared to the large circumference of the wheel, heat transfer is limited, and the area in contact cools down before being in contact next time*." [VAR13-1]

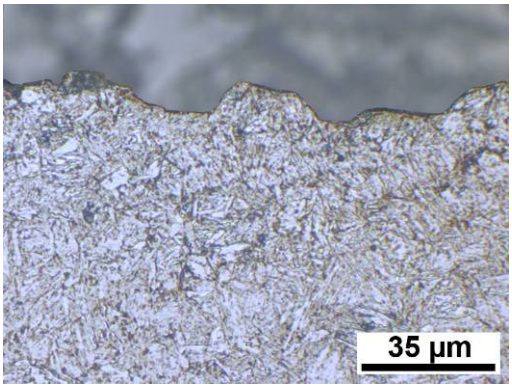

Fig. 33: Cross section of wheel counter body (Hardox 400®) after test series [VAR13-1]

This was also substantiated by temperature measurements of the wheel right after testing, where maximum temperatures of 100°C were found. This temperature increase will not significantly affect the microstructural and mechanical properties of the wheel during testing and material degradation is negligible. As also visible in Fig. 33 a pronounced working surface establishes on the wheel: deep grooves in rotating direction are visible. However as tests are done after the working surface of the wheel was established, no detrimental influence should be present for the test series.

3.4.2. Cyclic impact-abrasion test

To the present day, no standard test method or test rig for impact-abrasion testing is known. This work uses a test rig built at AC2T [WIN09-1]. The HT-Cyclic Impact-Abrasion Test (HT-CIAT, Fig. 34) mainly consists of a heated test chamber where the sample is mounted in 45° angle. The tilted sample is cyclically hit by a free falling plunger (dead weight) and abrasive is introduced between the two bodies. A schematic is given in Fig. 34b. Additionally

to the impacting component the plunger is able to slide a certain distance over the sample, resulting in an abrasive component. Two distinct zones can be seen on the sample afterwards (Fig. 34c): the impact zone, where the plunger directly hits the sample with abrasive in between, and the abrasion zone, where the plunger slides over the sample with the trapped abrasives in the contact zone.

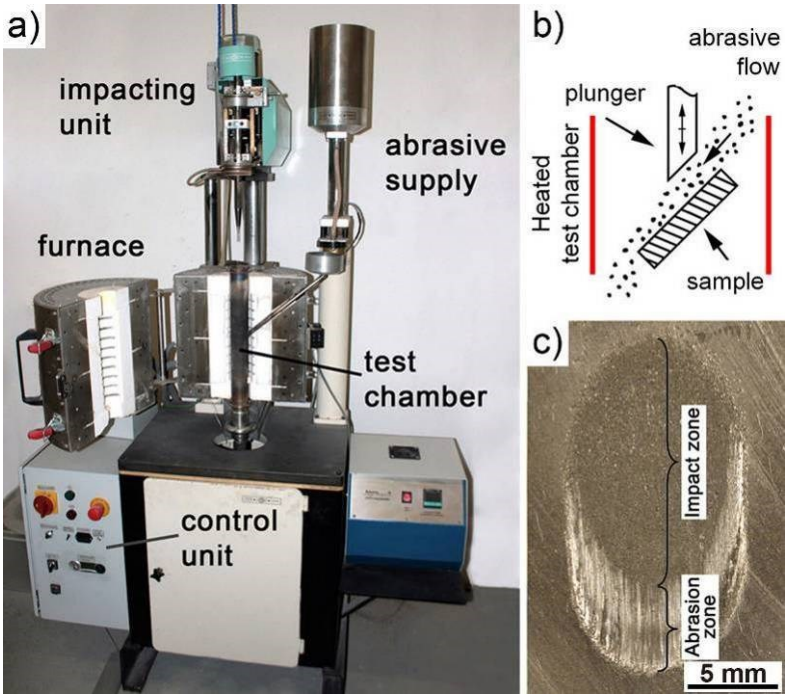

Fig. 34: High Temperature-Cyclic Impact-Abrasion Test rig (HT-CIAT):
a) view of test rig [WIN09-1]; b) test principle;
c) typical wear mark with impact and abrasion zone [VAR13-1]

As counter body a Co-rich HSS hardfacing (ø 5 mm) is used which shows high wear resistance at HT [WIN10]. The tip of the cylindrical plunger is grinded to 45° angle and aligned with the sample's angle within the test rig. Although the high wear resistance of the plunger material, wear of the counter body is not negligible. Therefore, the plunger is reground after a test series.

Due to comparability to the application impact energies of 0.8 J were chosen. The plunging frequency is 2 Hz, angular silica sand with a particle size of 0.4-0.9 mm is used as abrasive and fed at 90 g/min flow rate. The test time is 60 min, i.e. 7,200 impacts hit the sample. The test chamber is heated via resistance heating from outside. Temperature control is done via type K thermocouple (ø 1 mm) which is pressed to the sample by the sample holder in the test chamber. Temperatures from RT-700°C (RT, 300, 500, 650, 700°C) were tested with 3 samples each for statistical evaluation. The test parameters are summarised in Tab. 7.

Wear loss was determined gravimetrically after cleaning the samples in ultrasonic bath in ethanol and drying. Volume loss is calculated via material's density [mm³]. Additionally wear analysis was done on the worn surface and cross sections by microscopic methods (3.3.1). As the abrasion zone shows similar wear behaviour as in HT-CAT, further investigations concentrate on the impact zone.

Tab. 7: Main parameters used in HT-CIAT testing

Parameter	Value
Temperature	RT, 300°C, 500°C, 650°C, 700°C
Impact energy	0.8 J
Impact angle	45°
Impact frequency	2 Hz
Test time	60 min
Counter body	Co-rich HSS rod, ø 5 mm, 45° aligned
Abrasive	Angular silica sand, 0.4-0.9 mm at 90 g/min flow rate
Wear quantification	Volume loss [mm³]

3.4.3. Solid particle erosion test

Solid particle HT-Erosion Testing (HT-ET) was done with a centrifugal four-channel accelerator present at Tallinn University of Technology (Fig. 35). The test rig is similar to the GOST 23.201-78 standard [GOS79]. The abrasive is accelerated via four channels onto to samples (Fig. 35b). The samples can be mounted in different angles in order to test oblique or normal impact conditions. Up to twenty samples can be tested in one run, while it is advisable add several control samples. For these investigations Hardox 400® reference samples were used. When the reference samples don't show their typical results, the test must be repeated.

Relatively high impact velocities of 80 m/s were used to obtain severe erosive conditions and produce measurable wear loss on the highly sophisticated wear resistant hardfacings. In order to compare different impact angles normal impact (90°) and oblique impact (30°) were tested. In the application often even shallower impact angles are present, but they cannot be tested reliably with this set-up: the shallower the angle, the wider and shallower the wear tracks (Fig. 35c), which makes them difficult to measure. 30° was chosen as most ductile materials show a maximum of erosive loss in this range [ROY06].

As abrasive 6 kg of angular silica sand with 0.1-0.3 mm grain size was used [cf. KAT09]. Tests were performed from RT-650°C (RT, 300, 550, 650°C). Test time changes with temperature slightly, from ~40 min at low temperatures to ~60 min at 650°C. Weight loss was

measured and volume loss was calculated via material's density. The erosion rate was calculated by referring the volume loss to the abrasive weight [mm³/kg]. The main test parameters are summarised in Tab. 8. Further microscopic analyses were carried out on worn surfaces and cross sections according 3.3.1.

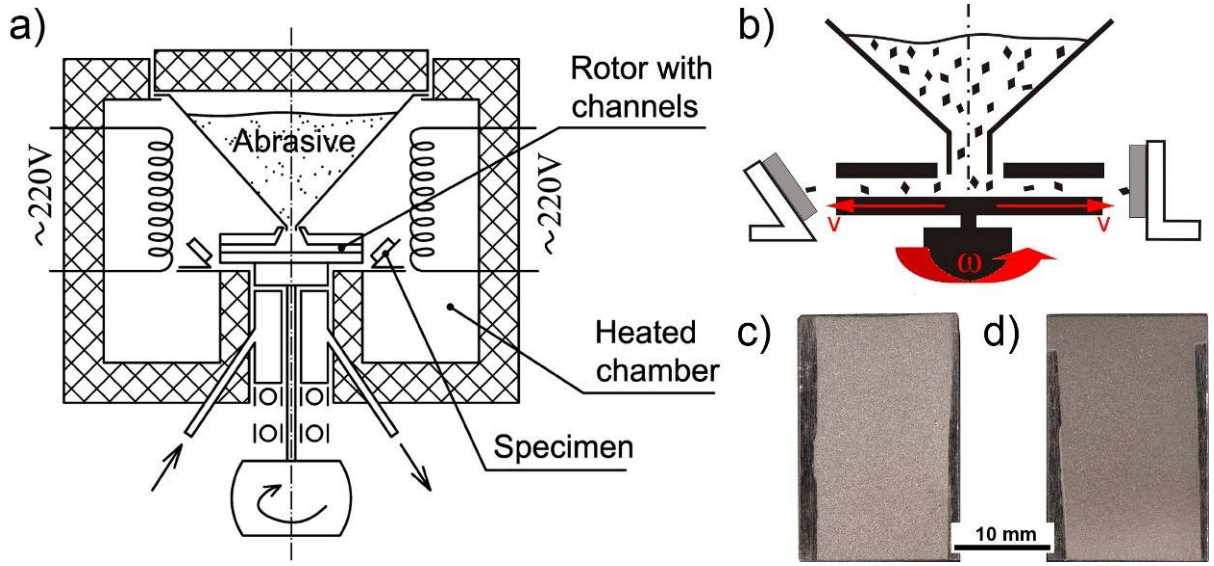

Fig. 35: High Temperature-Erosion Test rig (HT-ET): a) schematic of test rig [cf. WIN09-2]; b) test principle; typical wear marks at c) 30° and d) 90° impact

Tab. 8: Main parameters used in HT-ET testing

Parameter	Value
Temperature	RT, 300°C, 550°C, 650°C
Impact velocity	80 m/s
Test time	40-60 min
Impact angle	30°, 90°
Abrasive	Angular silica sand, 0.1-0.3 mm in total 6 kg
Wear quantification	Volume loss / abrasive weight → erosion rate [mm³/kg]

4. Results

In this section the results of the maintenance evaluations and wear tests are presented. First maintenance expenses are highlighted from different viewpoints, i.e. frequency of tasks and costs, downtimes and their combined evaluation in terms of total costs. Microstructures of the materials investigated are analysed in detail, including quantitative phase analysis. Finally, wear results of various abrasive tests and microscopic analysis of the wear scars are shown. The discussion of the maintenance records and combination of wear results is presented in chapter 5 Discussion.

4.1. Evaluation of maintenance records

At the begin of the research stands the evaluation of maintenance data and costs, in order to identify promising components worth of tribological improvement. The maintenance records and unplanned plant downtimes of the sinter plant were analysed over three years (4.2008-3.2011) regarding their costs and tasks which have been frequently necessary to be carried out. In a second step the reason for high costs and frequent necessity of these tasks was investigated and assessed regarding their tribological improvement possibilities, given in the next chapter 5 Discussion.

4.1.1. Maintenance costs and frequency

Within this section, the ten plants/aggregates which consume highest maintenance efforts and frequency within the sinter plant's system boundaries are presented. Fig. 36 displays the maintenance costs per plant/aggregate of the ten most important units. Here, costs of the maintenance tasks are evaluated, i.e. material costs, staff and external costs, without costs of production loss (this is analysed in the next chapter 4.1.2). Large plants are split in aggregates for more detailed understanding. This is indicated by the colour code within Fig. 36 and the next figures.

It is obvious that the main aggregate within the sinter plant, the sinter belt, requires most of the maintenance costs with >19 %. It is followed by the emission control with ~13 %. Conveyor belts and electronics (electrical installation, measurement and control systems) are in the range of 11 %. The HT sieve and chutes cover the 5th place with ~8 %. Following aggregates are <4 % of required maintenance costs within the sinter plant. It was suspected that the sinter belt as main aggregate of the sinter plant also consumes highest maintenance efforts. The maintenance costs for the following three places, emission control, conveyor belts and electronics, were not clear from the beginning. The emission control is calculated as the

sum of several plants. The single plants do not show high costs on their own, but when adding them, costs are significantly high. Also, the conveyor belts gain their significance in the sum. With over fifty conveyor belts in use within the system boundaries, the summarised costs are of great relevance. Electric installation, measurement and control are essential parts for the proper operation of the plants, which is reflected in the costs. HT sieves and chutes, three nearly identical aggregates, albeit relatively small machines, also entail substantial maintenance costs.

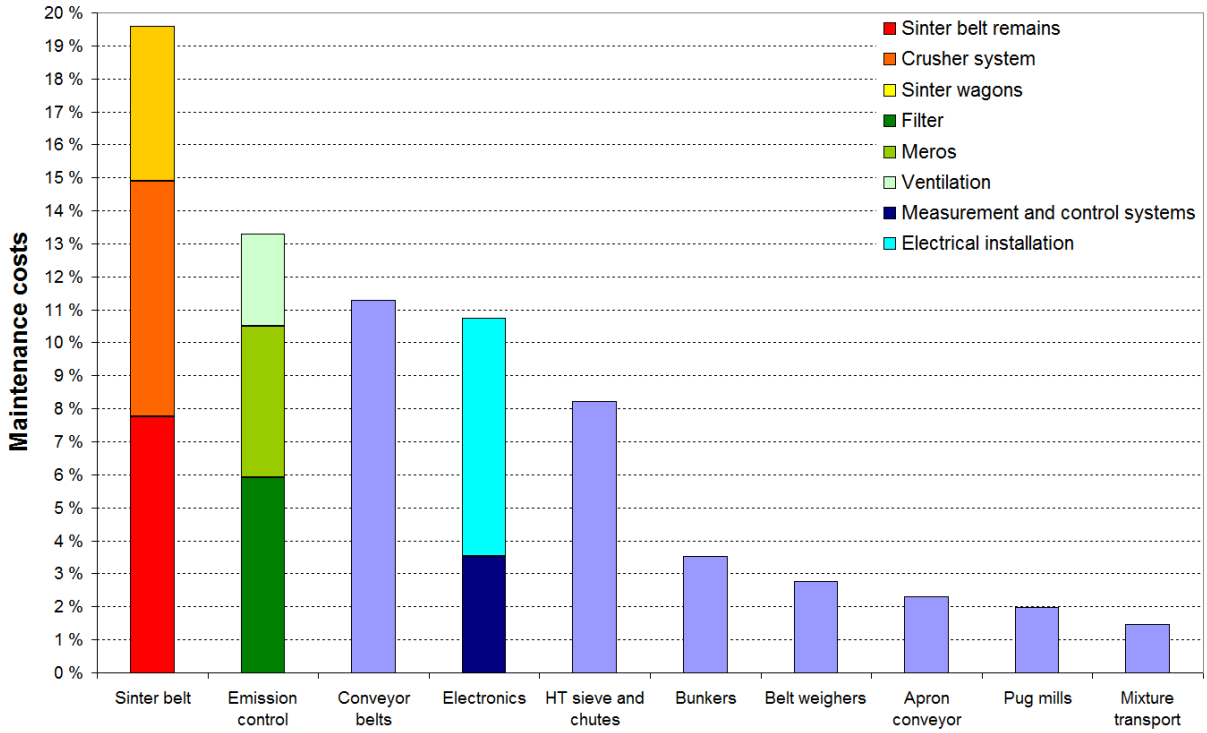

Fig. 36: Maintenance costs of the sinter plant

The ~19.5 % of the sinter belt consist of ~5 % expenses for the sinter wagons, 7 % for the crusher system and the rest for all other components including, e.g. the electrical drive, ignition system or rails. The emission control summarises 6 % filters, 4.5 % Meros plant (mechanical and chemical gas cleaning plant) and ~3 % ventilation. The amount for the ventilation is surprisingly low, as it is of major importance for the air flow in the sinter process. The electronics efforts are mainly spent for measurement and control (7 %) and the rest for electrical installation.

Detailed investigations of the sinter belt maintenance costs revealed by far the highest amount (**7 %**) for the **crusher system** with 2.9 % repair of crusher system, 2.8 % repair of spike crusher and 1.3 % pre-breaker. This was followed by the repair of **sinter wagons** with **4.2 %**. Costs for components of the emission control are significantly lower. Electrical installations

for ventilation were found to consume 1.4 %, filter hoses 1.1 %. Nevertheless, total costs add up to the second largest maintenance expenses. For the conveyor belt section, repair of the **belt** itself consumes highest costs with **4.4 %** of total maintenance costs. This is followed by 1.9 % for the drums, 1.2 % for security installations and 1.1 % for scrapers. Most of the measurement and control activities were done for the Meros system (2.8 %) and additionally 1.1 % for electrical installation. Surprisingly 1.5 % of total maintenance costs are spent for lightning maintenance. Sieves and chutes again consumed reasonable high amounts of maintenance expenses: **3.5 %** for **major renovations** and **2.9 %** for **replacement of screens and flooring**. The repair of bunker walls used 1.4 % of maintenance, belt weighers 1.6 % due to conveyor belt drift and 1.3 % electrical problems.

Fig. 37 displays the frequency of maintenance tasks. In this evaluation the costs play no role, but how often problems occur. It is obvious that conveyor belts need most of the maintenance tasks (~23 %), followed by electronics with ~13 % for measurement and control and 5 % for electrical installation. Emission control follows with ~11 % (5 % filters, 4 % Meros, 2 % ventilation). The sinter belt needs ~9 % of maintenance tasks, following aggregates are below 5 %.

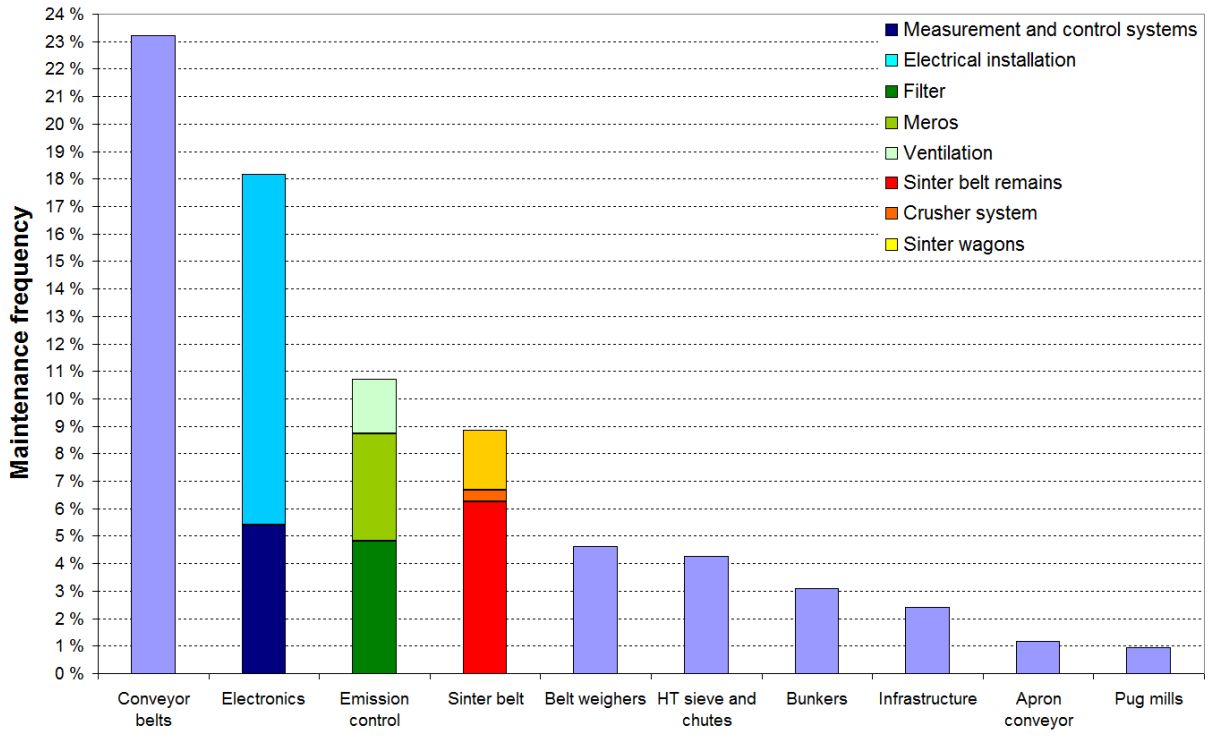

Fig. 37: Frequency of maintenance tasks

Detailed investigations showed that **9.3 %** are used for **control of conveyor belt** systems and **5.2 %** for maintenance of the **belt**, mainly **re-alignment of the belt**. Electronics require frequent maintenance: **4 %** for the **lightning**, **3.5 %** for **measurements of various process**

parameters (e.g. temperature, pressure, filling level) and 1.8 % for measurement of exhaust emissions. Electrical installations of the emission control need frequent maintenance with 1.8 % for filters and 1.3 % for ventilation.

The repair of sinter wagons is relatively often necessary (1.9 %). Also, the drive of the sinter belt needed 1.5 % of total maintenance tasks. Belt weighers consumed high frequency of 2.4 % because of misalignment of the conveyor belt and 2.3 % because of electrical failure. 1.3 % of maintenance tasks account for the floorings of HT sieve and chutes. 1.3 % are also used for control duties of the bunkers.

4.1.2. Downtimes and downtime frequency

Unplanned downtimes due to plant failure cause immediate production loss. The distribution of the duration of plant downtime is given in Fig. 38. Most of the downtime, nearly 23 % of the total downtime, is caused due to failure of the sinter belt itself. This is followed by electrical failures (20 %). After that, HT sieve and chutes and emission control caused both ~10 % of downtime each. Conveyor belts caused ~7 % and the apron conveyors slightly over 6 %. Sinter mixture transport lies at 4 % and pug mills at 3 %.

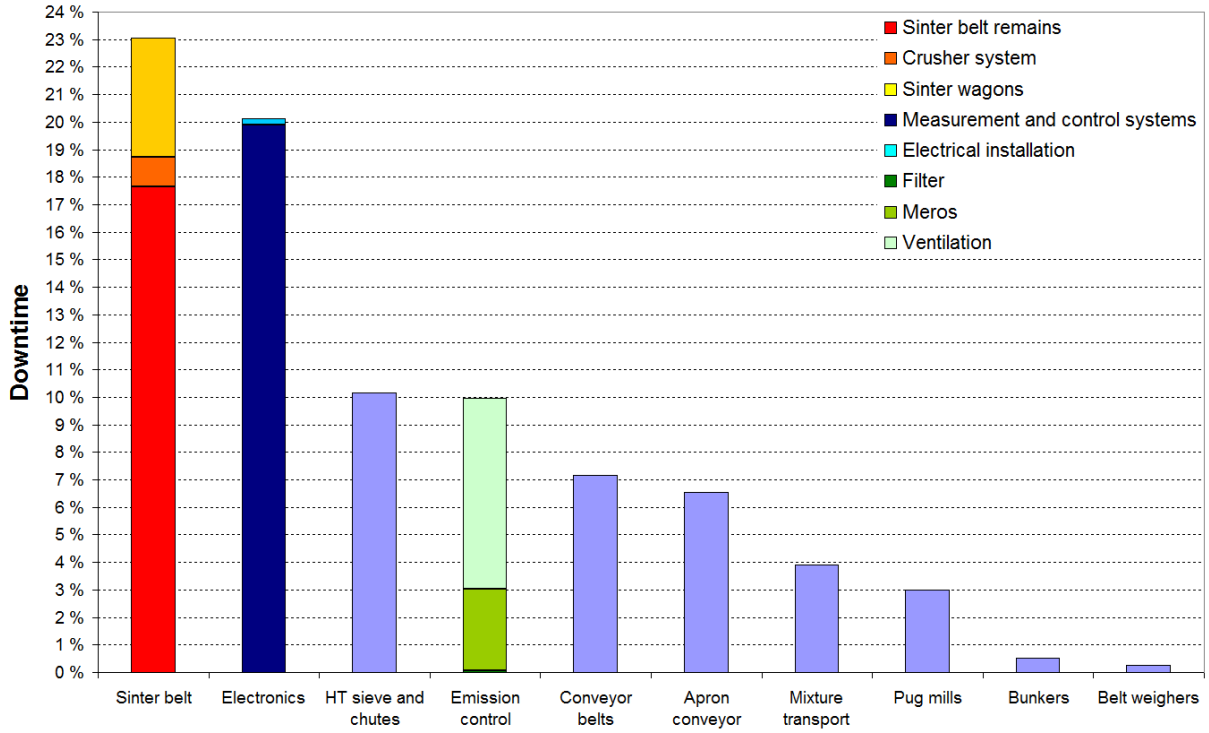

Fig. 38: Unplanned downtimes due to plant failure

Downtime of the sinter belt is caused to a high percentage by failure of the **rails** (**4.6 %**). problems with the **sinter wagons** (**4.3 %**) and the **electrical drive** (**2.9 %**). The clutch and the lifting wheel caused downtimes of 1.9 % and 1.7 %, respectively. The crusher system is

relatively seldom affected by severe failure (1.1 %). Electrical installations caused a huge amount of total downtime within the observation period. However **19.5 %** of the total 20.1 % was an unfortunate **cable fire** which took days to be repaired, because the whole control system of the sinter belt was affected. Concerning HT sieve and chutes, main problems were **bearing damages** (**3.7 %**) and **inconstant oscillation frequency** (**2.1 %**). The last issue exceeding 1 % at the HT sieve and chutes were the electrical drives with 1.8 %.

The main downtime problem within the emission control is caused by the **main ventilation for the sinter belt**. This huge aggregate of priority A caused **7 %** of total downtime. Other aggregates are of minor priority and caused seldom downtimes. A necessary cleaning of the **Meros** between scheduled downtimes caused **2.5 %** downtime.

Although relatively simple aggregates, conveyor belts can cause severe problems, as most of them are not redundant and the delivery of raw materials is necessary for the production process. Accidentally **cut conveyor belts** caused **3.6 %** of the downtime. Apron conveyors consist of many bearings and small components. Especially the **apron conveyor** for the returned sinter from the hot sieve is prone to unplanned failure due to its high time of operation. Axle- or bracket fracture or loss of small components caused in total **5.9 %** downtime. The drum loader for the sinter mixture consumed 2.7% and mechanical failure of the pug mills led to 1.4 % of total downtime.

The frequency of unplanned downtimes is displayed in Fig. 39. It is clearly visible that the sinter belt itself caused by far the most downtimes with ~48 %. Conveyor belts caused 10 %, HT sieve and chutes 8 %, apron conveyors 7 % and pug mills 6 %. The rest is at 4 % and lower frequency of downtimes.

The most downtimes are caused by the sinter wagons, 34 %, followed by other components of the sinter belt with 15 %, all other aggregates are below these two. **27 %** of the sinter wagons failures account to the **sinter grate bars**, and **4.1 %** to the necessary **cleaning** of them during operation. Additional 2.5 % were necessary for other sinter wagon problems. The **electric drive** of the sinter belt causes **3.1 %** and the **clutch 4.8 %** of unplanned downtimes frequency, 1.1 % was necessary for the rails and the same amount for the filling of the sinter belt with raw materials. At the conveyor belts 2.1 % was caused by irregular drive speed, 1.8 % by large clumps getting stuck and 1.1 % by triggering the emergency stop. At the HT sieve and chutes also 2.9 % were caused by irregular drive speed. From the apron conveyors almost everything can be accounted to the conveyor for returned sinter from the HT sieve (6.5 %). This can be divided in the loss of small components (1.8 %, e.g. screws), security stop

(1.3 %), break of brackets and failure of trailing wheels (1.1 % each). The pug mills also caused relatively frequent downtimes with 1.2 % of failure of water sprinklers and 1.1 % for removal of heavy build-up deposits. The sinter mixture transport lead to 1.1 % downtime frequency each because of starting problems and the drum loader. 2.3 % of downtimes were created by completely emptying of bunkers. All other components lie below 1 %.

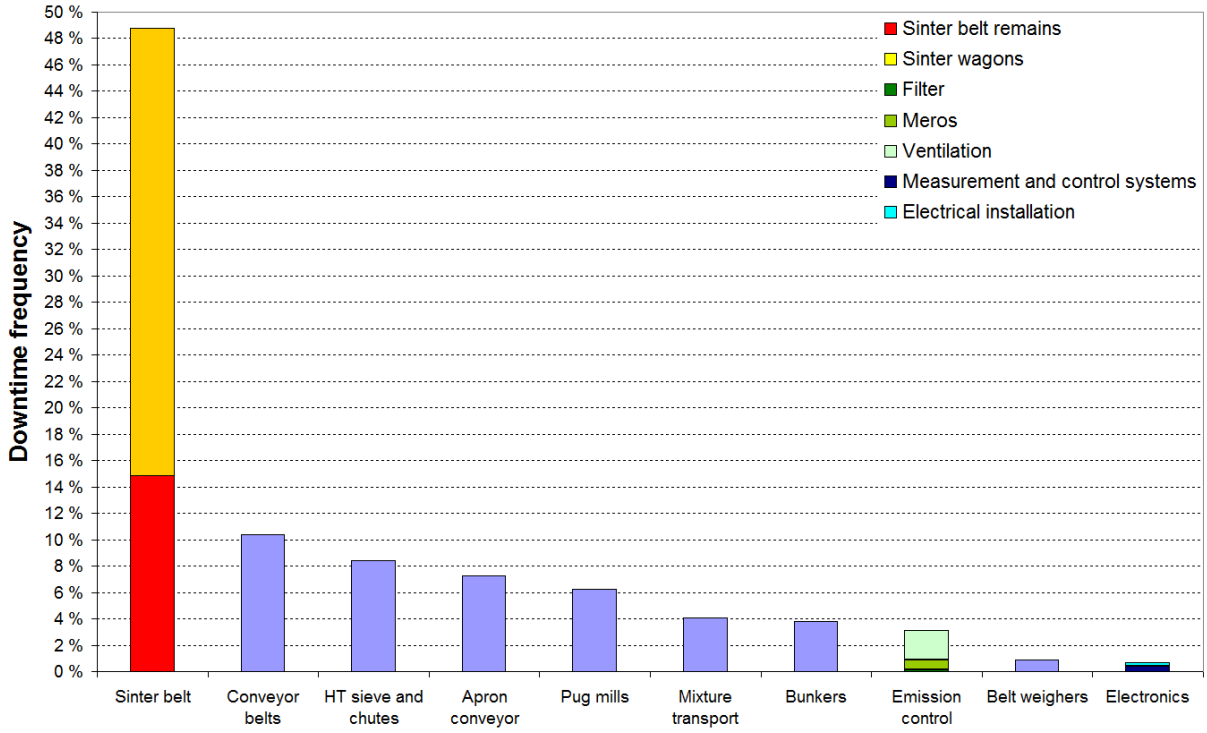

Fig. 39: Frequency of unplanned downtimes due to plant failure

4.1.3. Total costs of maintenance

By valuing the production loss due to downtime length with the costs for purchasing iron pellets, the downtime can be added to the maintenance costs. Fig. 40 presents these total costs of maintenance for the ten costliest aggregates.

Due to high maintenance costs and high downtime the sinter belt remains the most costly aggregate with nearly 18 % of total maintenance costs. The electronics are on place two with 11.5 %. The emission control needed 10.5 %, conveyor belts ~8.5 % and HT sieve and chutes 7.5 %. Following aggregates lie at 3 % and below.

At the sinter wagons (3.9 %) about three quarters are used by maintenance and one quarter by unplanned downtime. The crusher system (4.6 %) consumed relatively low downtime costs, the remaining components (9.1 %) on the other hand, needed about half maintenance and half downtime. However it has to be considered that downtimes which could not be assorted to any specific component of the sinter belt were placed there. Detailed analyses showed that the

sinter wagons consumed **3.9 %** of total costs due to high maintenance costs (2.9 %) and downtimes (1 %), albeit average individual downtime is very short: the replacement of a broken sinter grate bar needs just about a minute of standstill, but is often necessary (27 % of downtime frequency). The **4.6 %** of total costs for the **crusher system** are nearly entirely caused by maintenance expenses (4.4 %), downtimes are negligible. The rails of the sinter wagons needed 1.5 % and the electric drive 1.3 %, downtime which could not be matched 1.1 %.

The costs for electronics divide in **7 % for electrical installation** and 4.5 % for measurement and control. The electrical installations are downtime dominated because the before mentioned **cable fire** (70 % downtime, or **5 %** of total maintenance expenses). The measurement and control caused negligible downtimes.

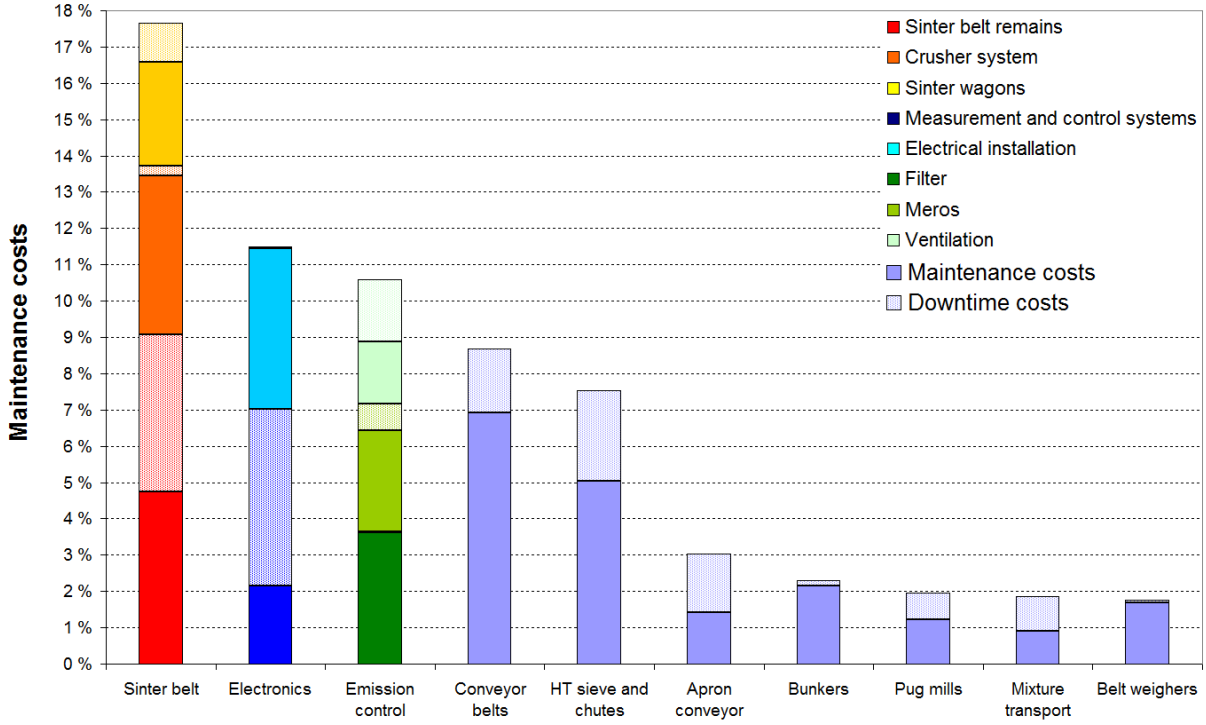

Fig. 40: Total costs split in maintenance costs (full colour) and downtime costs (transparent)

The emission control adds up 3.6 % for filters, 3.5 % for the Meros plant and 3.4 % for the ventilation systems. The filters caused almost no downtime. The Meros, albeit not directly necessary for the sinter process (priority B), caused some downtimes (0.7 % of total costs). Within this section the ventilation costs are half caused by maintenance and downtime, which means 1.7 % of total costs each.

The conveyor belts are dominated by maintenance costs, but also downtimes were reasonable (20 %): **3.8 %** of total costs fall on the **conveyor belts** itself (2.7 % maintenance, 1.1 % downtime) and 1.2 % on the drums.

At the HT sieves and chutes the downtimes are a third of total costs for the aggregate. The **electrical drive** consumed **2.2 %** of total costs, 1.9 % thereof due to unplanned downtimes. Also **2.2 %** were invested in **major renovations** of the chutes and 1.9 % for the floorings.

The costs for the apron conveyors are half for downtime and maintenance. **2.5 %** of total costs can be accounted to the **apron conveyor** for returned sinter from the HT sieve. 1.4 % thereof due to breakage or loss of components entailing unplanned downtime, i.e. leading to 1.1 % of the total costs.

Bunkers costs (**2.3 %**) are nearly not affected by downtimes. **Pug mills** costs (**2 %**) caused by downtimes are approximately one third, sinter mixture transport (1.9 %) half. At the belt weighers (1.8 %) downtimes are negligible.

4.2. Microstructure and hardness of the materials investigated

Microstructure and hardness of the materials have major influence on the wear behaviour under abrasive load. Hence it is essential to know the present phases, their distribution and mechanical properties. In the first section, the microstructure is evaluated with LM and SEM to identify present phases. Phase distribution is analysed by quantitative image analyses. Secondly, the hardness of typical present phases is evaluated with NI. Finally, the hardness evaluation of the phase compound (macro hardness) with increasing temperature is presented.

4.2.1. Microstructure

The microstructure of the cast materials is given in Fig. 41. The FeCrC cast alloy shows dendritic structure where large matrix areas are enclosed by carbide precipitations. The matrix area fraction as measured by QWIN image analysis (Fig. 42) is ~85 % and the rest accounts for large Cr-carbides (Fig. 43). The alloy has ferritic matrix as measured by XRD with typical grain size of 20-30 µm, surrounded by a Cr-carbide network. This entails a bimodal distribution of the inter-particle distance [cf. POL08] as seen in Fig. 44a: while the distance within the carbide network is in the range of 2-5 µm, the large matrix areas are mostly ~20-40 µm wide. A detail of the carbides is given in Fig. 41b as seen by SEM-BSE. The compound hardness of the material is ~280 HV10 at RT.

The microstructure of the Ni-cast NiCrW is shown in Fig. 41c. Cr-carbides appear blue after etching with Murakami-reagent. Also for this material a dendritic structure is visible with the carbides precipitating on the border of grain boundaries. As the FeCrC alloy also NiCrW shows a bimodal distribution of the inter-particle distance (Fig. 44a). Within the carbide network the distance is ~2-3 µm and slightly smaller as at FeCrC. Between the dendritic branches the distance is typically 20-30 µm. Nevertheless, large areas with >100 µm without hardphases are more frequent at this alloy compared to FeCrC. The matrix has austenitic structure as found by XRD-measurements. In addition to the Cr-carbides, W-carbides can be found scarcely. A detail of them is given in Fig. 41d (white zones). The area fraction of Cr-carbides is ~13 %, W-carbides are <1 %. The RT-hardness of this alloy is ~250 HV10.

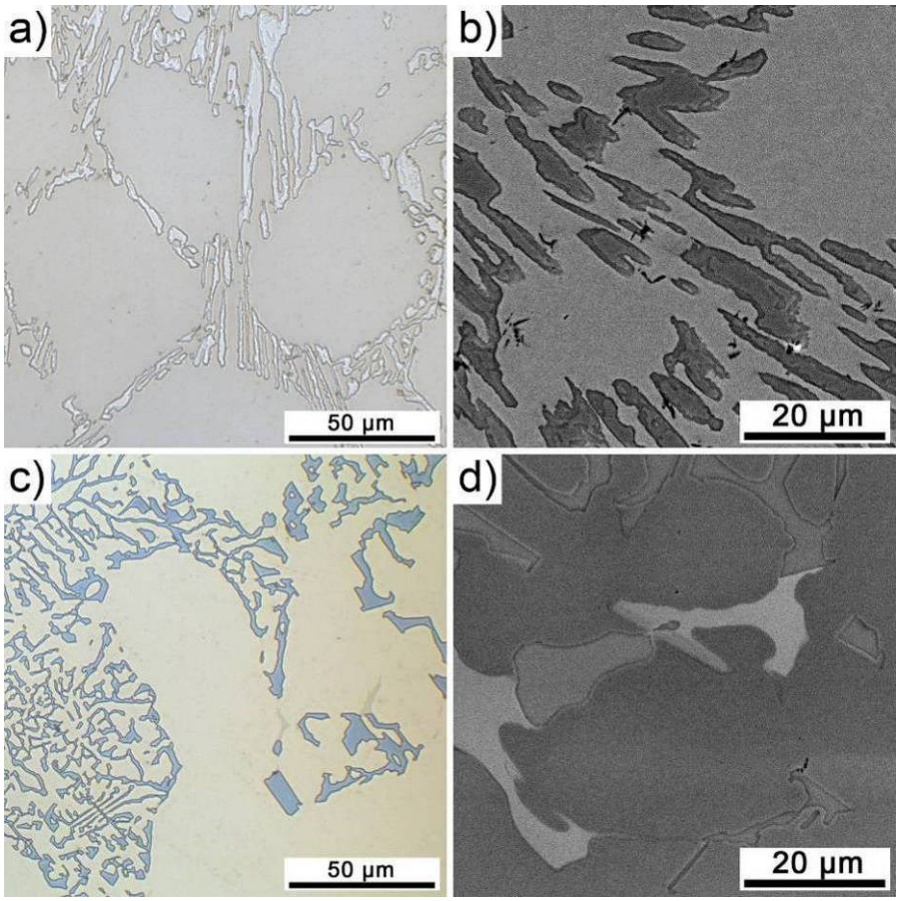

Fig. 41: Microstructure of the cast materials: a) LM and b) SEM-BSE of FeCrC;
c) LM and d) SEM-BSE of NiCrW.

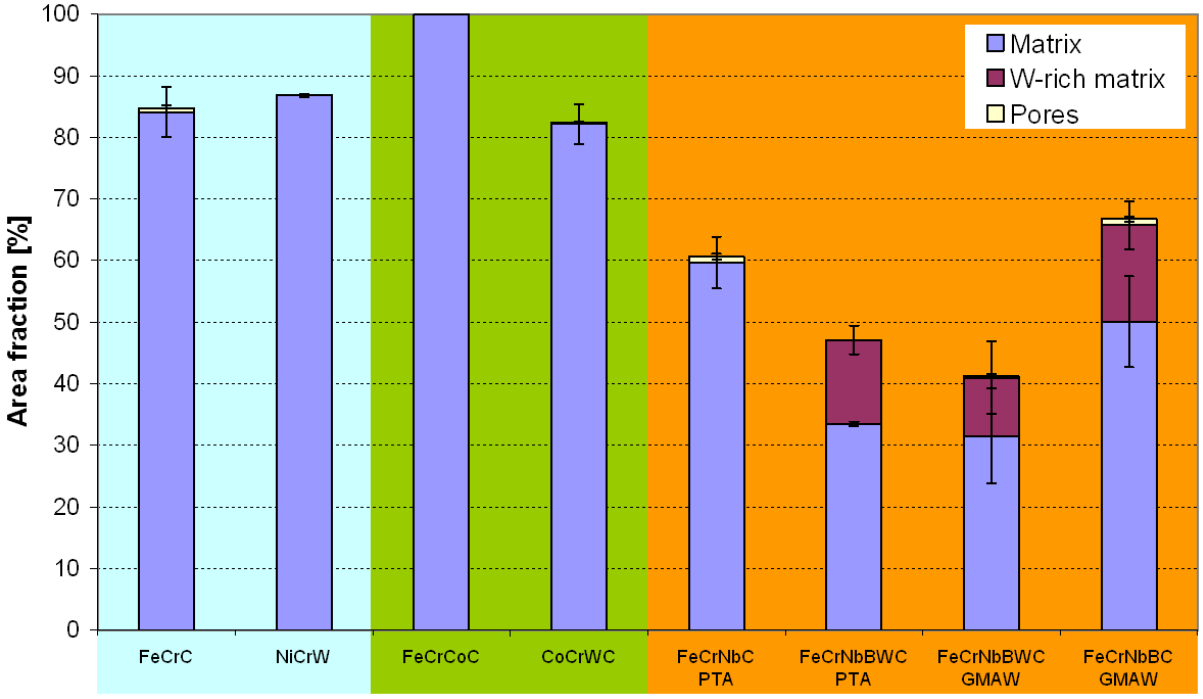

Fig. 42: Matrix fraction of the materials as measured by QWIN image analysis

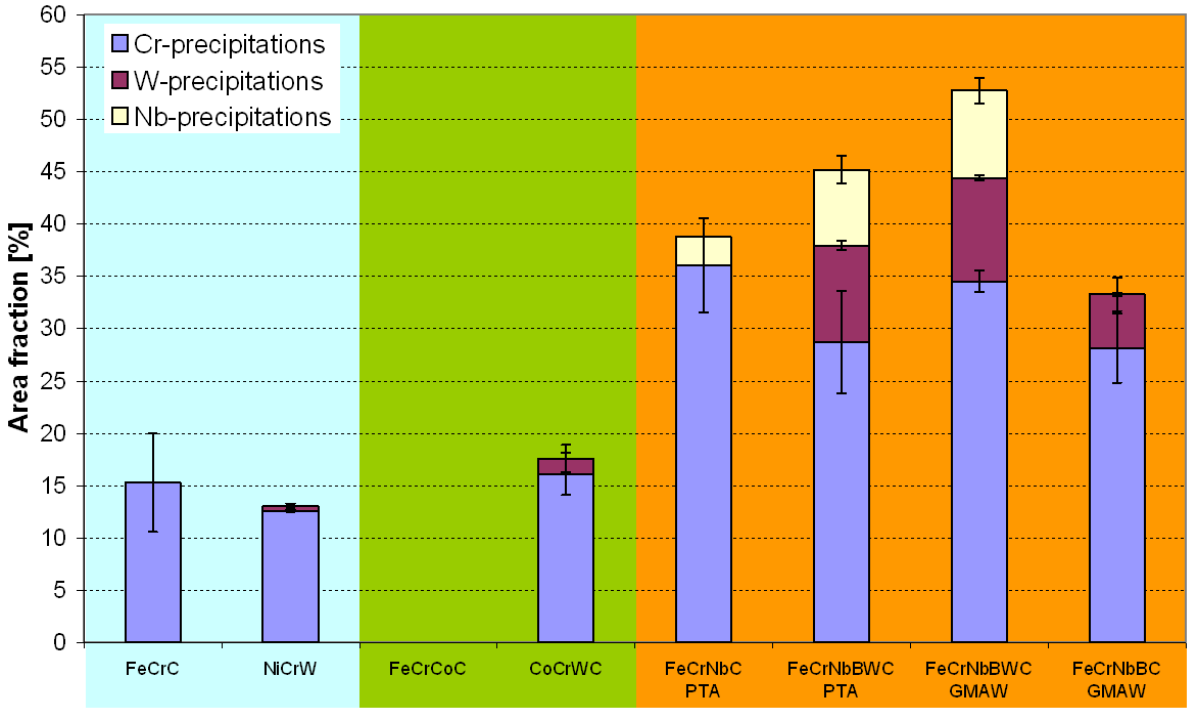

Fig. 43: Hardphase content of the materials as measured by QWIN image analysis

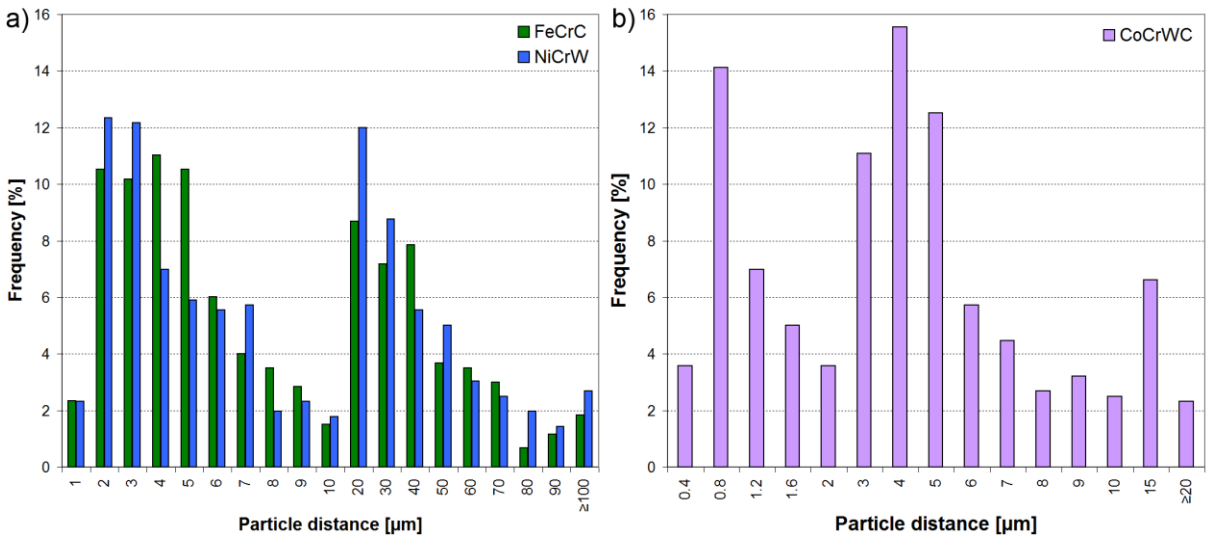

Fig. 44: Histogram of the hardphase particle distances for: a) cast alloys, b) CoCrWC

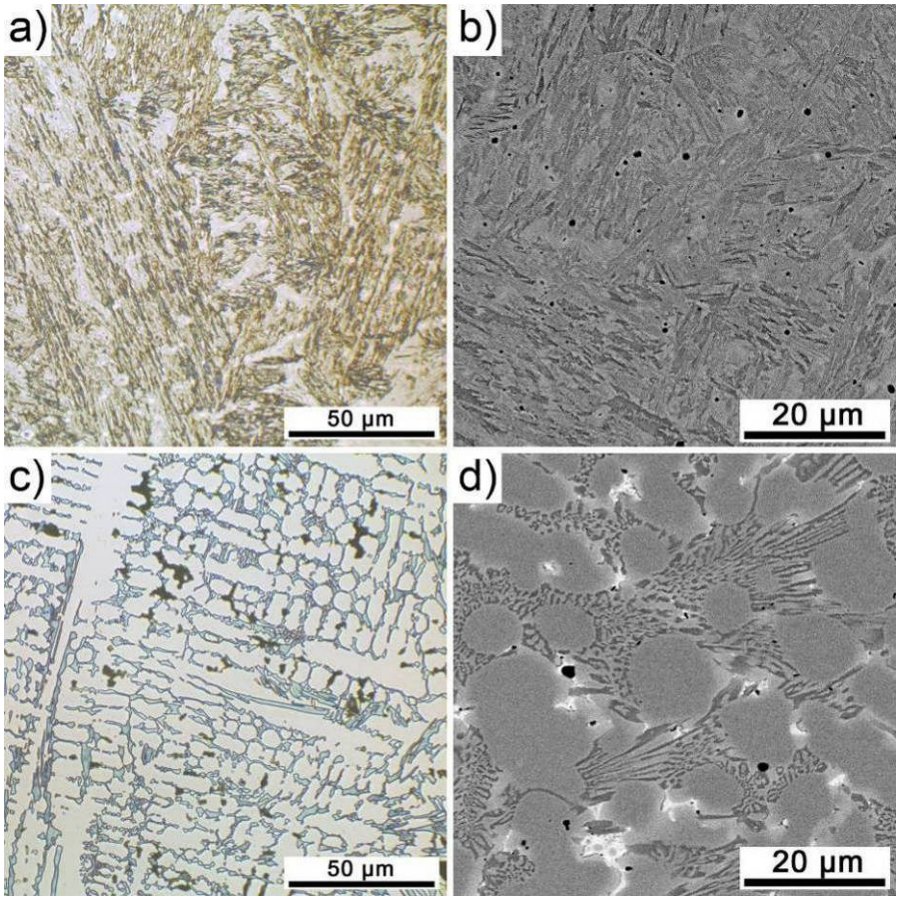

Fig. 45: Microstructure of the Co containing hardfacings, PTA welded: a) LM and b) SEM-SE of FeCrCoC; c) LM and d) SEM-BSE of CoCrWC.

The microstructures of the Co-group are given in Fig. 45. Materials are used as-deposited without further heat treatment. FeCrCoC hardfacing exhibits very fine martensitic micro-structure. Although some regions show less etching effect, no differences in chemical

composition were found using EDX-analysis, it may be originated to different grain orientations. This material is an exception within this work, as it contains no large hardphases; the martensitic matrix is 100 %. The hardness of this material is ~530 HV10 at RT.

The Co-base hardfacing CoCrWC is shown in Fig. 45c. It features dendritic Co-matrix structure with Cr-carbide precipitations around the grain boundaries. The structure is much finer than at the cast alloys, with a typical dendritic branch distance of 3-5 µm (Fig. 44b). Also the carbides are of smaller size and the distance between the carbides within the carbide network is ~0.8 µm. Due to the random spatial distribution of the dendritic structures also larger carbide-free areas ≥15 µm occur. The SEM-BSE in Fig. 45d further reveals W_xC-precipitations (white) between the Cr-carbides. A total of 18 % hardphases was measured by QWIN, with 16 % Cr- and 2 % W_xC-precipitations. The hardness of this material is 475 HV10 at RT.

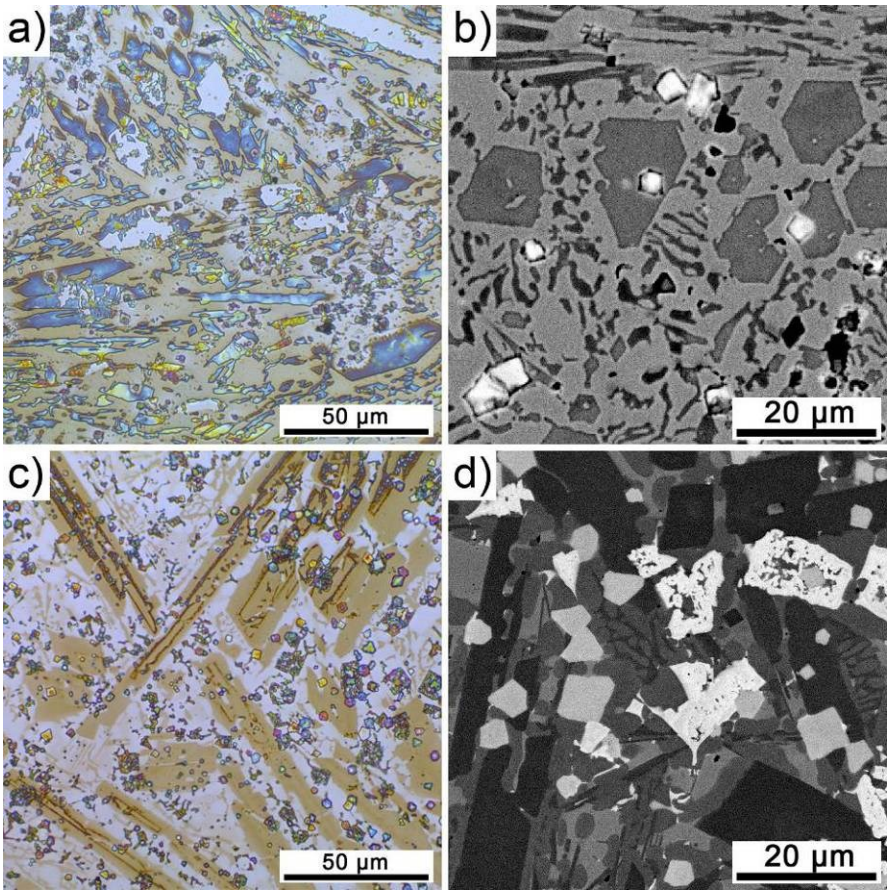

Fig. 46: Microstructure of the PTA-welded hardfacings: a) LM and b) SEM-BSE of FeCrNbC; c) LM and d) SEM-BSE of FeCrNbBWC.

The microstructures of the carbide-rich hardfacings are given in Fig. 46 and Fig. 47, where the first gives the PTA-welded and the second the GMAW materials. Fig. 46a shows the LM of FeCrNbC where the Cr-carbides are colourful highlighted after Murakami etching. They

are of large size with needle shape precipitations up to 100 µm length and exhibit typical hexagonal structure. The Nb-carbides are better visible in the SEM image in Fig. 46b. In this BSE image they are brightest within the microstructure and mostly of tetragonal shape. As visible in Fig. 42 and Fig. 43 the matrix is 60 %, 36 % Cr- and 3 % Nb-precipitations, the rest are some pores. A compound hardness of ~780 HV10 was measured at RT.

The FeCrNbBWC complex alloy after PTA welding is shown in Fig. 46c. After Murakami etching phases containing Fe appear brown, hence it can be assumed that the large Cr-precipitations contain also Fe. These large precipitations can reach a length up to 200 µm. Also within the matrix zones smaller Cr-precipitations can be detected. The different hardphases can be better seen in the SEM-BSE in Fig. 46d. Darkest areas represent the Cr-carboborides, brightest, blocky areas are W-carboborides. Tetragonal bright-grey are Nb-precipitations. As said before also Cr-carboborides of smaller size are located within matrix zones. The matrix itself shows two chemical compositions, a darker one with less W (33 %), and a brighter one with more W (~14 %). The hardphase content is ~45 % according QWIN analysis with ~30 % Cr-, 9 % W- and 7 % Nb-precipitations (the missing fraction to 100 % can be put down to fluctuations between the different measured samples). The RT hardness is 765 HV10.

The same alloy as deposited by GMAW is shown in Fig. 47a,b. This welding technique entailed generally finer carbides compared with the Fig. 46c after PTA welding. Nevertheless, the same types of carbides were found. Large hexagonal Cr-carboborides with lengths of several 100 µm, but narrower than at PTA welded samples, were observed. Also W- and Nb-precipitations as seen by SEM-BSE (Fig. 47b) are smaller, but at higher frequency. This leads to the conclusion that cooling was faster at GMAW. Also slightly higher total amount of precipitations was found by QWIN technique: 35 % Cr-, 10 % W- and 8 % Nb-precipitations. The two matrix zones were 41 %, whereof 9 % account for the W-rich matrix. The RT hardness is much higher as at PTA welded samples with ~1070 HV10, which stands also for the hardest alloy in this work.

The FeCrNbBC hardfacing (Fig. 47c) has lower amount of alloying materials, leading to less hardphases. Like before, also long hexagonal Cr-carboborides dominate the microstructure, which can reach several 100 µm length, but have limited width. In the SEM-BSE different hardphases can be detected. Bright areas have high W-content, but here different structures can be found: blocky carbides and needle-shaped structures. No distinct Nb-precipitations are detected. Like in the alloy before, two different matrix zones can be found, giving a total of 67 % matrix, whereof 16 % are W-rich. ~28 % Cr- and 5 % W-precipitations were measured by QWIN. The hardness of this alloy is ~1010 HV10 at RT.

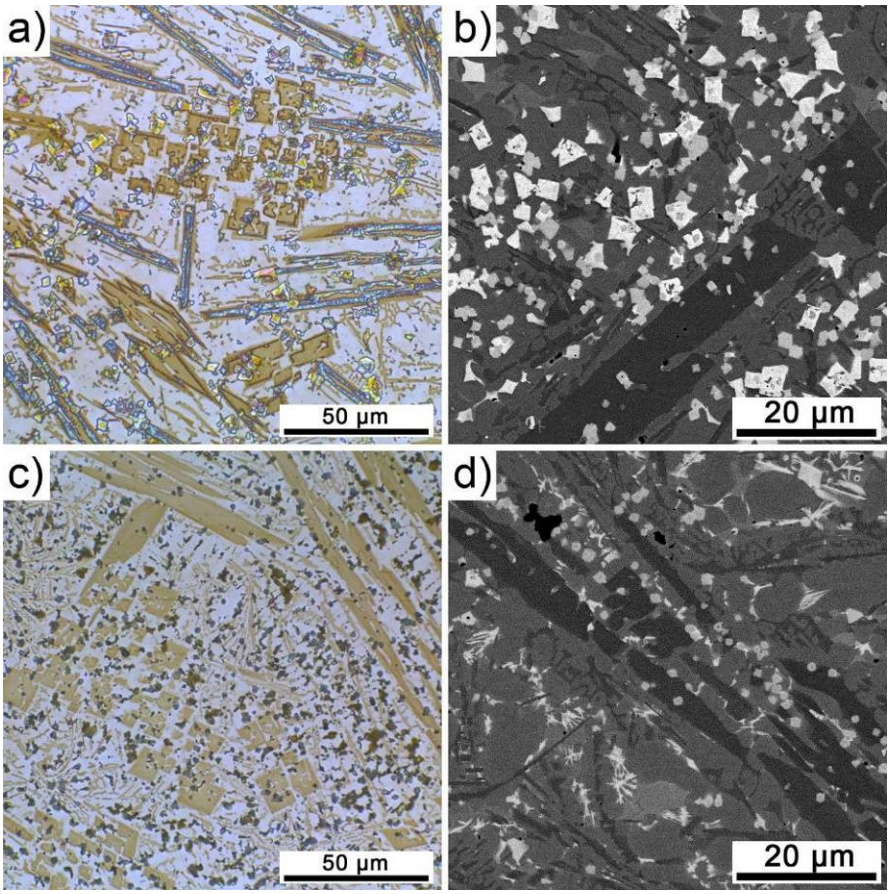

Fig. 47: Microstructure of the GMAW-welded hardfacings: a) LM and b) SEM-BSE of FeCrNbBWC; c) LM and d) SEM-BSE of FeCrNbBC.

4.2.2. Phase properties

Representative materials of all groups were investigated by NI. By this technique the differences between the various phases can be measured. One type of Fe-, Ni- and Co-matrix was chosen, as well as a complex alloyed carbide-rich hardfacing. Reduced Young's modulus and hardness were evaluated and results are displayed in Fig. 48. Measurements were only possible at RT.

Comparing the matrix, four types are present within Fig. 48. bcc ferritic matrix of FeCrC, fcc Ni-matrix of NiCrW and hcp Co-matrix of CoCrWC show similar hardness of ~4.5 GPa and ~185 GPa reduced Young's modulus. The ledeburitic matrix of the complex alloyed hardfacing has higher hardness of ~8 GPa and slightly increased reduced Young's modulus (205 GPa), due to the combination of ferrite and cementite.

The precipitations have generally higher hardness than the matrix; further the reduced Young's modulus is increased. Cr-carbides in cast alloys are hardest at FeCrC (~16 GPa), CoCrWC shows the softest Cr-precipitations (~8 GPa). The Cr-carboborides in the carbide-

rich hardfacing are harder (~20 GPa) than Cr-carbides of the other alloys, also the reduced Young's modulus is higher (~260 GPa). Differences between large precipitations (Cr-Carboborides) and small of the same type (Cr-Carboborides S) within the matrix are not significant. Nb-precipitations are of least hardness within this alloy with ~12 GPa, W-carboborides are in the same range as Cr-precipitations (~19 GPa). The reduced Young's modulus of all these precipitations lies within the measurement accuracy in the range of 210-260 GPa.

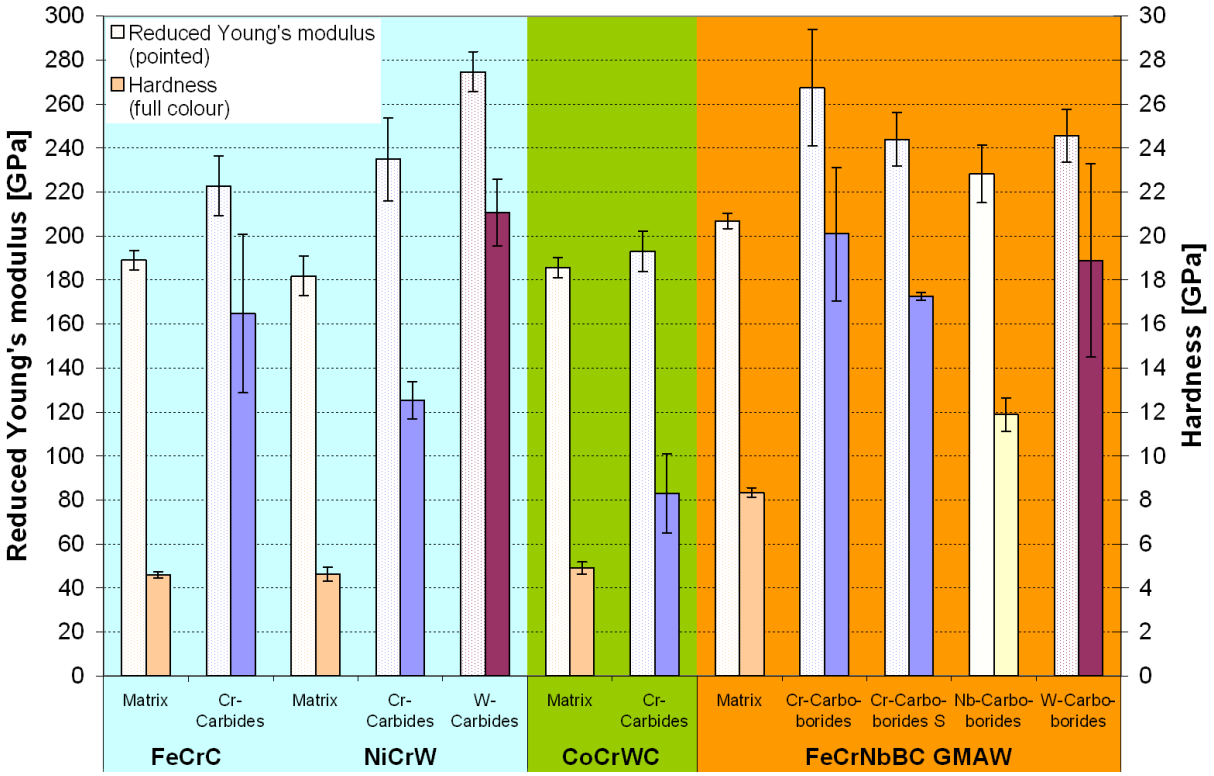

Fig. 48: Reduced Young's modulus and hardness of different phases of representative materials as measured by NI at RT

4.2.3. Hot hardness

The hot hardness of all investigated materials is displayed Fig. 49. The cast alloys (blue) show relatively low hardness due to their comparatively low amount of hardphases and matrix structure. The Fe-base material FeCrC (blue dotted line) has ~280 HV10 at RT, which drops almost linearly to 150 HV10 at 600°C. Above 600°C the hardness loss is more pronounced resulting in ~40 HV10 at 800°C, the lowest value within the test matrix. The second cast material, NiCrW shows different behaviour. Due to its Ni-base matrix, it is much more temperature stable, entailing less hardness decrease from ~250 HV10 at RT to ~130 HV10 at 800°C. This means a hardness loss of just ~48 % in the test range.

The Co containing hardfacings are highlighted green in Fig. 49. The Fe-base FeCrCoC hardfacing has ~530 HV10 initial hardness with moderate hardness loss until 500°C, followed by plummeting from ~390 HV10 at 500°C to ~100 HV10 at 800°C. Thus representing the annealing of the martensitic microstructure above 500°C. The Co-base CoCrWC is relatively temperature stable, like the Ni-base material. The hardness decrease is more pronounced from ~480 HV10 at RT to 310 HV10 at 500°C, followed by a stable temperature region up to 700°C. At 800°C a hardness of 250 HV10 was measured, which puts the alloy in a similar range than the hardphase-rich hardfacings at highest temperature investigated.

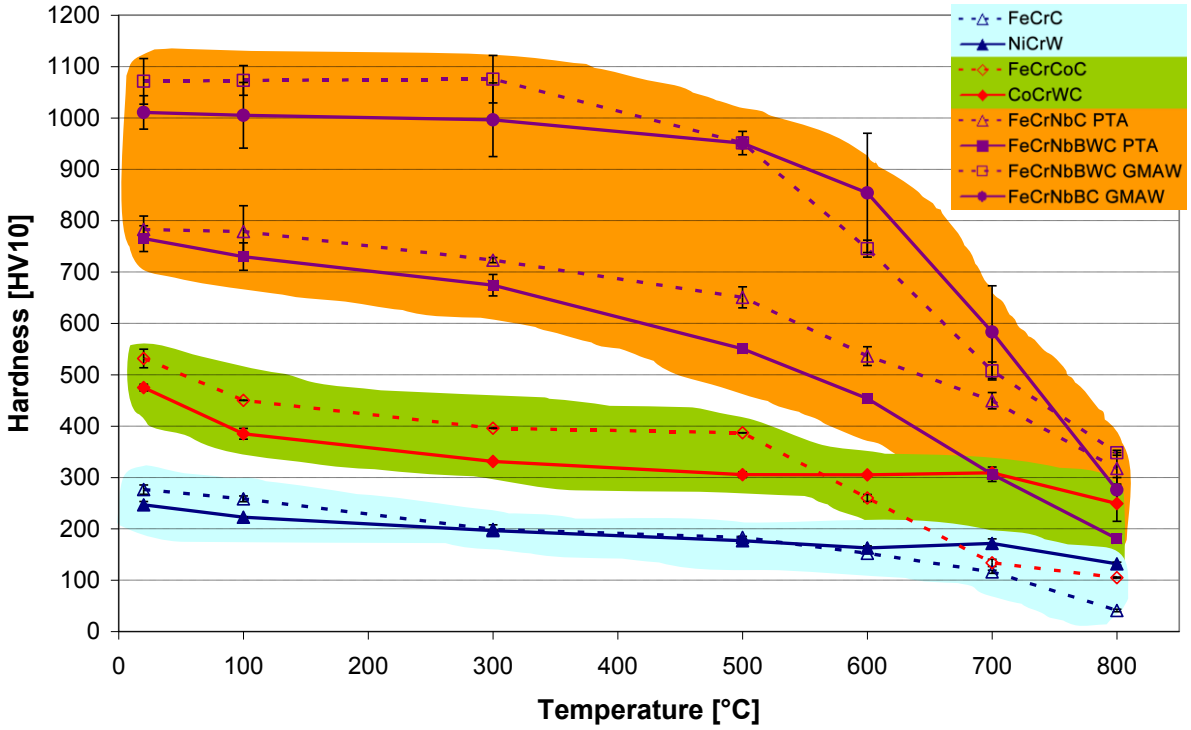

Fig. 49: Hot hardness results

Hardness curves of the carbide-rich Fe-base hardfacings are highlighted orange. Generally it has to be stated that maximum hardness values for these alloys are lower on austenite substrate, due to its lower thermal conductivity. This leads to decreased cooling rates and thus lower hardness of the deposit and is especially evident at the PTA-welded hardfacings. Further one-layered hardfacings feature lower hardness due to the dilution with the substrate [BAD08]. Nevertheless, hardness of the hardfacings is distinctly higher at low temperatures than of the other two material groups. PTA welded FeCrNbC starts at 780 HV10 and FeCrNbBWC at ~770 HV10, respectively. Hardness drop is nearly linear until 500°C and more pronounced above this temperature, especially for the FeCrNbBWC hardfacing, resulting in the lowest value of this group at 800°C of 180 HV10. Thus its hardness is at the

same level as the CoCrWC at 700°C and significantly lower at 800°C. On the other hand, despite the lower hardness of the FeCrNbC at RT, this hardfacing is in the superior range at highest temperature with ~320 HV10, which is comparable with the highest hardness measured (350 HV10 for FeCrNbBWC GMAW welded). This is a first indicator that RT hardness may be misleading when dealing with high temperature wear [cf. ALL01].

The two-layered GMAW welded FeCrNbBWC shows highest hardness at low temperatures in the tested field with ~1070 HV10, which keeps almost constant up to 300°C. A hardness drop to 950 HV10 at 500°C can be observed, followed by ~350 HV10 at 800°C. This stands for the highest value measured at 800°C within the tested materials. The FeCrNbBC shows a shallow decrease from ~1010 HV10 at RT to 950 HV10 at 500°C. Hardness stays at a very high level at 600 and 700°C, but the large scatter indicates ongoing microstructural changes at these temperatures. Nevertheless, in this temperature range this hardfacing has highest hardness in the test field. At 800°C the hardness drops beneath the two FeCrNbBWC alloys which show the temperature limit of this alloy.

4.3. Abrasive wear results

In this chapter the test results of the different abrasion modes are given. This includes quantitative results (wear rates) as well as microstructural analysis of wear mechanisms. The three abrasion modes were: i) high-stress three body abrasion tested by the Continuous Abrasion Test and simulating HT crusher applications; ii) impact-abrasion tested by the Cyclic Impact-Abrasion Test simulating falling and abrading goods and iii) erosion tested at two angles in the Erosion Test simulating abrasive wear without counter body, e.g. at the HT sieve. Discussion of microstructural influence, combined action of different wear modes and efficient wear protection is discussed in chapter 5.

4.3.1. Continuous abrasion test

The results of the abrasion test are given in Fig. 50 for the three tested temperatures. RT results are very similar (0.030-0.035 mm^3/m) for the FeCrC cast alloy, Co containing hardfacings and PTA welded hardfacings. The Ni-base cast alloy and GMAW welded hardfacings show higher RT wear rate of 0.037-0.042 mm^3/m. 300°C wear rates don't change significantly for the FeCrC and Co family, an increase could be measured for the Fe-base hardfacings and Ni-base cast alloy. At the highest testing temperature all alloys showed increased wear rates compared to 300°C. Nevertheless, for the Co-base alloy CoCrWC almost constant, low wear rates from RT to 550°C can be found, which entails the lowest abrasive wear loss at

550°C of the materials investigated. Highest wear rate was detected at the GMAW welded FeCrNbBWC, which is with 0.079 mm³/m 2.4-times more than for the best alloy CoCrWC.

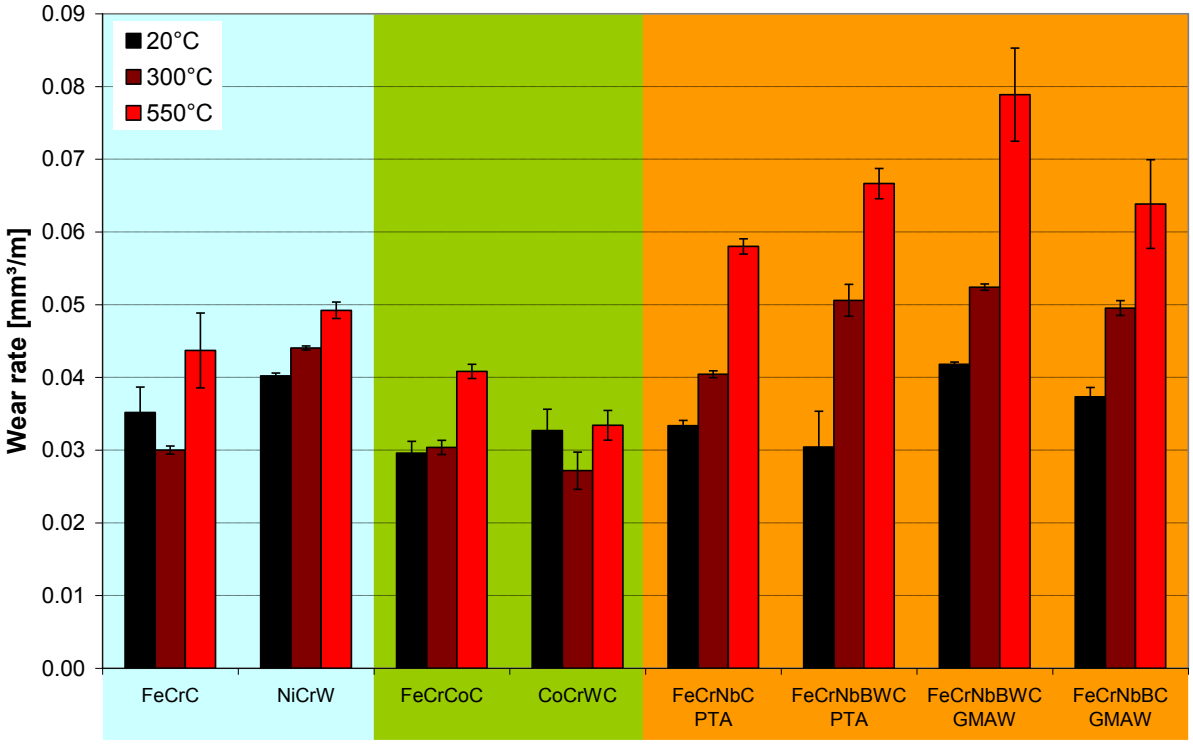

Fig. 50: High-stress three-body abrasion results

The FeCrC cast alloy shows no significant increase in wear rate from RT to 300°C. At 550°C wear rate is higher by 20 % compared to RT. The NiCrW cast alloy shows gradual increase in wear rate, also with 20 % increase from RT to 550°C. The martensitic FeCrCoC hardfacing shows constant wear rates up to 300°C and an increase by 38 % at 550°C. This goes conform to the hardness drop starting at 500°C for this alloy. The wear rates for the Co-base hardfacing stay at a similar, low level of 0.027 -0.033 mm³/m within the investigated temperature range. This also fits the hardness progress well, as there are no major changes until 700°C. Large increase with temperature could be observed for the carbide-rich hardfacings. Wear rates increase from RT to 550°C by a factor of 1.7 for FeCrNbC-PTA, 2.2 for FeCrNbBWC-PTA, 1.9 for FeCrNbBWC-GMAW and 1.7 for FeCrNbBC-GMAW, respectively. According the figures it can be assumed that the carbide-rich hardfacings are unbeneficial for HT high-stress abrasive conditions.

For more detailed understanding of wear rates in HT-CAT testing the damage mechanisms were examined on cross sections through the wear scars. Representative zones at RT and highest testing temperature of the various materials are given in Fig. 51-Fig. 54. SEM images were taken in BSE mode, i.e. abrasive intermixed in the surface appears dark, also precipi-

tations with light elements. Precipitations with heavy atoms (Nb, W) appear bright. Depth of cracking of hardphases, MML coverage and penetration depth were also measured and are given in Tab. 9 and Tab. 10. Deviations of penetration are generally high, due to the inhomogeneous microstructures. If single events were found in the observed area this is indicated by displaying this maximum value. For the carbide-rich hardfacings, different types of carbides and in some cases even the matrix were found to break.

Fig. 51 shows cross sections of the cast materials and Tab. 9 gives quantitative results measured on them. Fig. 51a shows FeCrC at RT, where a mixed layer with abrasive is visible at the majority of the surface. A MML up to 30 µm can be found, albeit it is mostly in the range of 15 µm. Larger carbide zones interfere MML formation as visible in the middle of the image. Carbide breaking is frequent up to ~80 µm depth, but can be found up to ~100 µm occasionally. At 550°C testing the MML covers almost the whole surface with a significant thickness up to 30 µm. Common carbide breakage exceeds 70-80 µm depth.

Tab. 9: Quantitative results of wear mechanisms during HT-CAT: cast- and Co-family

		Crack depth [µm]	MML depth [µm]	MML coverage [%]
FeCrC	RT	89±8 max. 97	16±9 max. 32	69
	550°C	86±12 max. 97	23±11 max. 32	88
NiCrW	RT	46±8 max. 56	12±2 max. 16	78
	550°C	106±7 max. 113	20±5 max. 24	96
FeCrCoC	RT	-	12±3 max. 16	90
	550°C	-	16±4 max. 23	97
CoCrWC	RT	21±8 max. 29	5±2 max. 6	26
	550°C	19±6 max. 27	6±2 max. 10	45

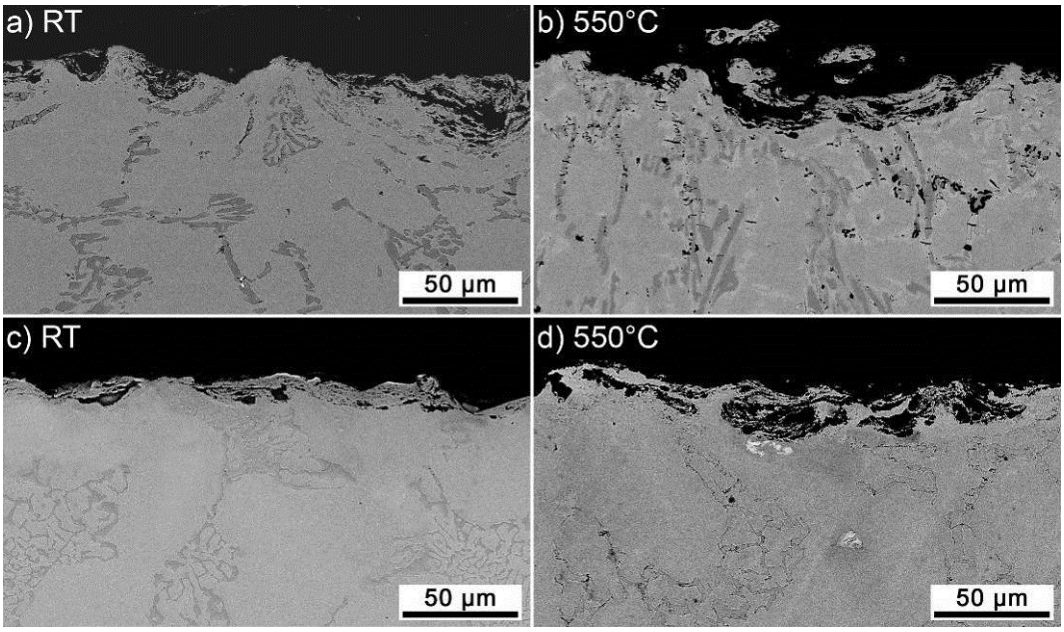

Fig. 51: SEM of cross sections through the HT-CAT wear scars of the cast materials: FeCrC: a) RT, b) 550°C; NiCrW: c) RT, d) 550°C

MML formation is already dominant for NiCrW at RT (Fig. 51c). The degree of intermixing with the matrix is much higher than at FeCrC, but the thickness of the layer is limited to ~12 µm. This may be put down to the larger, more stable matrix areas compared to FeCrC with a more frequent network of not interconnected carbides. Also the fcc structure may be deformed more easily than the bcc ferritic matrix of FeCrC leading to the increased wear rate. Carbide breakage can be detected up to ~55 µm, but at lower frequency compared to the ferritic alloy. At 550°C a pronounced surface covering MML (96 %) of ~20 µm thickness can be measured. Carbides scatter up to ~110 µm depth.

Cross sections of wear scars of the Co-family are displayed in Fig. 52, quantitative results are given in Tab. 9. Due to the lack of large hardphases FeCrCoC shows a very distorted surface. Intermixing with test abrasive is widely present already at RT (Fig. 52a) with a typical thickness of 10-15 µm. Because of the hard martensitic structure intermixing is slightly impeded. Nevertheless, plastic deformation of the surface is obvious, ~5 µm beneath the MML, a plastic deformed microstructure is clearly visible. At 550°C testing abrasive penetration is more pronounced with 15-20 µm depth. However, also here the penetration depth is limited due to the still hard martensitic matrix, albeit MML covers nearly the whole surface. The plastic deformed zone is in the range of 10 µm.

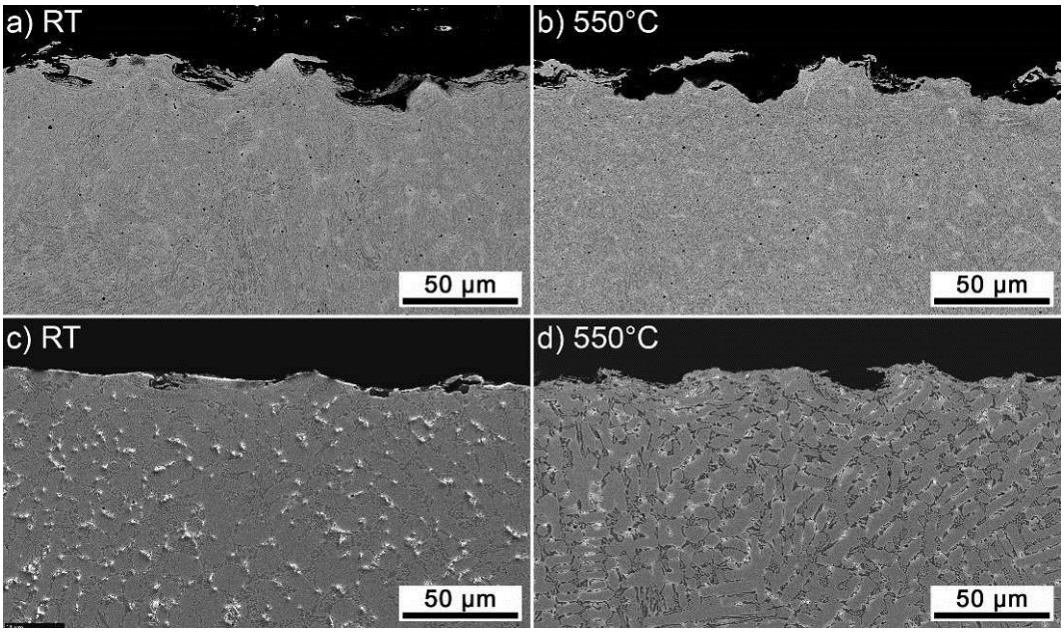

Fig. 52: SEM of cross sections through the HT-CAT wear scars of the Co-containing alloys: FeCrCoC: a) RT, b) 550°C; CoCrWC: c) RT, d) 550°C

The Co-base alloy CoCrWC shows almost no abrasive penetration at RT (Fig. 52c). Plastic deformation can be found in the range of 5 µm. Occasional carbide breakage was observed up

to 40 µm depth on high magnification images. Limited MML formation can be detected at 550°C samples. Sticking of abrasives reach thicknesses up to 10 µm and plastic deformed microstructure is visible also up to 10 µm. Carbide breakage is less pronounced at 550°C compared to RT and can be found up to 30 µm depth.

Entirely different behaviour can be found at the carbide-rich hardfacings. Quantitative results are given in Tab. 10, microstructures of the PTA welded ones are shown in Fig. 53. The hypereutectic FeCrNbC alloy is given in Fig. 53a, where large hexagonal primary Cr-carbides are obviously cracked multiple times. Cracking is visible throughout all large carbides (~30 µm depth), but can also be found within this depth at primary carbides which do not reach the surface. Smaller carbides within the matrix and other types of carbides (Nb) were just scarcely found to break at this condition. The wear behaviour is very similar at 550°C (Fig. 53b), large carbides break until ~30 µm depth. Limited plastic deformation in the first micrometres can be found.

Tab. 10: Quantitative results of wear mechanisms during HT-CAT: carbide-rich hardfacings

		Crack depth [µm]			MML	
		Large HP	Small HP	Matrix	Depth [µm]	Coverage [%]
FeCrNbC-PTA	RT	29±5 max. 32	max. 16	-	-	-
	550°C	32±7 max. 41	max. 13	-	-	-
FeCrNbBWC-PTA	RT	18±4 max. 20	4±0 max. 4	-	-	-
	550°C	24±1 max. 25	19±1 max. 19	7±0 max. 8	-	-
FeCrNbBWC-GMAW	RT	11±2 max. 14	-	max. 6	-	-
	550°C	20±2 max. 23	5±0 max. 6	-	-	-
FeCrNbBC-GMAW	RT	13±3 max. 15	-	max. 10	-	-
	550°C	18±1 max. 19	-	-	-	-

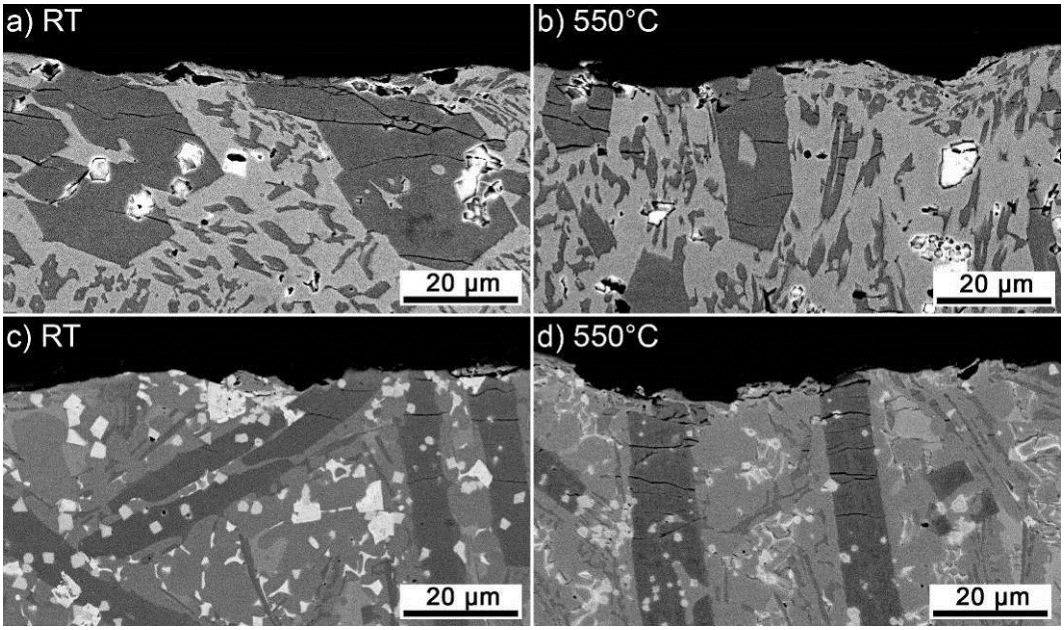

Fig. 53: SEM of cross sections through the HT-CAT wear scars of the PTA welded carbide-rich hardfacings: FeCrNbC: a) RT, b) 550°C; FeCrNbBWC: c) RT, d) 550°C

The complex alloyed FeCrNbBWC deposited by PTA welding can be seen in Fig. 53c. Brittle behaviour dominates the wear scars. Large Cr-carboborides break until ~20 µm depth at RT, where orthogonal oriented hardphases are affected most. Smaller Nb- and W-precipitations break just in surface near zones <5 µm. The extent of broken orthogonal carbides reaches ~25 µm at 550°C testing. Like for the FeCrNbC alloy at HT also smaller carbides within the matrix break, which can be found up to ~20 µm. Also W-rich matrix zones behave brittle and show cracks. No abrasive penetration or sticking abrasives could be found on the cross sections for this alloy.

The wear scars of GMAW hardfacings are displayed in Fig. 54. The hardest alloy under investigation, FeCrNbBWC-GMAW, shows similar behaviour as the PTA welded type at RT testing. The extent of carbide breakage in the primary Cr-carboborides is ~10 µm, which is slightly less than at the PTA welded one. This may be attributed to the higher hardness of the GMAW alloy. However unlike the PTA welded type here also smaller carbides as well as W-rich matrix zones show cracks. I.e. almost all phases show brittle behaviour, which may lead to the increased wear loss. At 550°C testing cracking is exacerbated, not just cracks parallel to the surface occur (like in all cases mentioned before) but surface-near hardphase zones scatter entirely up to ~10 µm depth. Single cracks in large hardphases can be found up to 20 µm depth. No plastic deformation is detectable at this alloy.

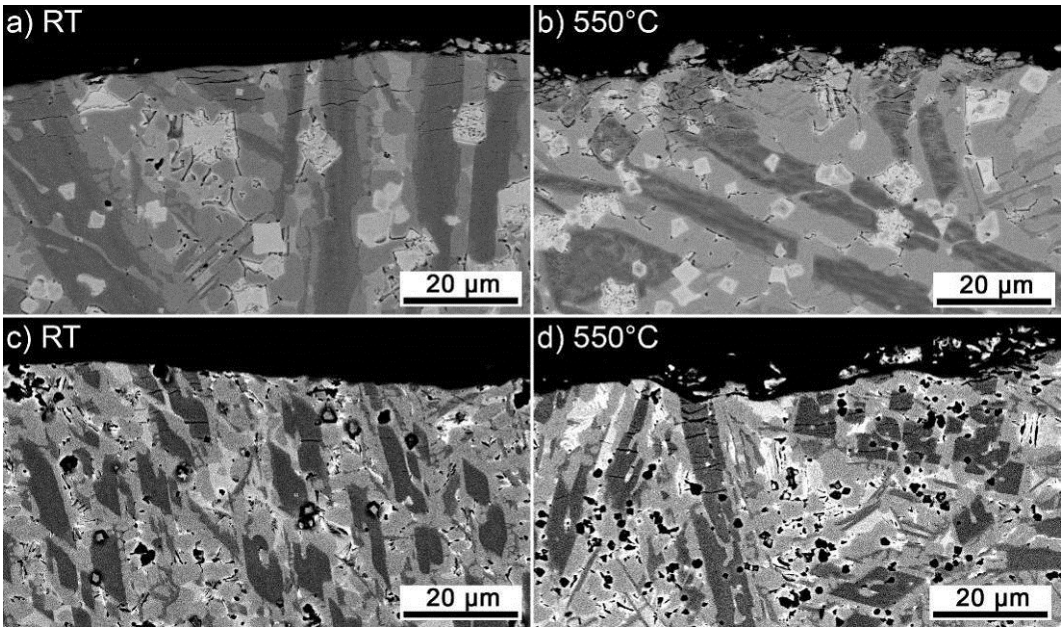

Fig. 54: SEM of cross sections through the HT-CAT wear scars of the GMAW carbide-rich hardfacings: FeCrNbBWC: a) RT, b) 550°C; FeCrNbBC: c) RT, d) 550°C

FeCrNbBC is given in Fig. 54c. Like at the other carbide-rich hardfacings, large Cr-precipitations show most cracking at RT up to ~15 µm depth. Also W-rich matrix zones show some cracks up to 10 µm depth. No abrasive penetration or plastic deformation can be found. The affected depth is similar at 550°C testing (~20 µm), albeit the frequency of cracks is much higher, which will encourage wear loss.

4.3.2. Cyclic impact-abrasion test

Wear tests with distinct impact component were carried out by the Cyclic Impact-Abrasion tests up to 700°C. The results of the experiments are given in Fig. 55 and are quite different from high-stress abrasion testing. Cast materials show highest wear loss and very hard carbide-rich and CoCrWC hardfacing lowest wear loss. All materials show a pronounced wear increase from RT to highest testing temperature of 700°C. At temperatures up to 500°C just minor wear loss <4 mm³ of the FeCrNbBWC-PTA and -GMAW and FeCrNbBC-GMAW hardfacing was measured. At higher temperatures wear loss increases more pronounced. Nevertheless, superior wear resistance of the GMAW and the CoCrWC at highest temperature could be detected with 8-11 mm³ wear loss.

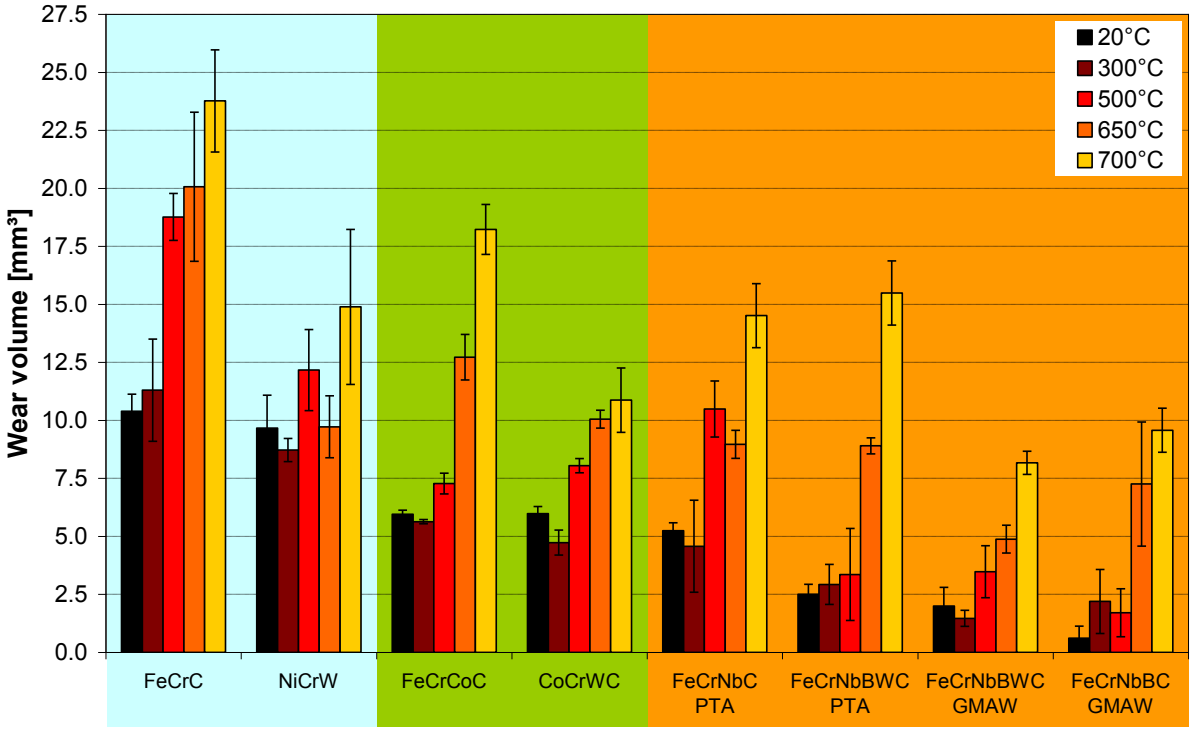

Fig. 55: Impact-abrasion results

The cast alloys start with relative high values of ~10 mm³ wear volume at RT. For FeCrC this distinctly increases at 500°C to ~19 mm³ and ~24 mm³ at 700°C, which represents the highest values at these temperatures within the test field. The Ni-base cast material shows no

significant increase in wear loss up to 650°C testing and stays in the range of 9-12 mm³. At 700°C ~15 mm³ was measured, which means an increase of ~50 % compared to RT.

Like at abrasion testing the FeCrCoC shows constant wear loss up to 300°C, but rockets afterwards: At 500°C, wear rates are still relatively low but increase to ~13 mm³ at 650°C and ~18 mm³ at 700°C, which means 3-times higher wear loss than at RT. Despite relative high wear loss at RT for the CoCrWC wear increase with temperature is modest. This leads to competitive performance of the alloy compared to the best carbide-rich hardfacings at 700°C with ~11 mm³. Increase in wear loss from RT to 700°C is ~80 % of this relative temperature stable material.

The FeCrNbC hardfacing starts with ~5 mm³ at RT, doubles to ~10 mm³ at 500 and 650°C and triples to ~15 mm³ at 700°C. The complex alloy FeCrNbBWC-PTA on the other hand, shows half wear loss at RT of ~2.5 mm³, which doesn't increase significantly up to 500°C. Above that temperature wear loss rockets to ~15 mm³ at 700°C, which is at the same level as FeCrNbC-PTA. The GMAW welded alloys show superior wear resistance up to 500°C with outstanding performance of the FeCrNbBC. Significant increase in wear loss can be detected >300°C for FeCrNbBWC-GMAW and >500°C for FeCrNbBC-GMAW. Nevertheless, wear loss of 8-10 mm³ at 700°C means superior impact-abrasive wear resistance at HT.

The wear mechanisms of the alloys were investigated on SEM images of length sections. Abrasive mechanisms (in the abrasion zone of the wear scar, Fig. 34c) are very similar to HT-CAT mechanisms, therefore this chapter concentrates on the impact zone of the wear marks. Also quantitative results measured on the length sections are given in the tables.

Tab. 11 gives quantitative results of the cast materials and Co-family. The FeCrC cast alloy is shown in Fig. 56a,b. At RT some abrasive particle embedding in carbide free zones can be found, maximal penetration depth is ~10 µm, but the covered surface is limited (~60 %). Some broken carbides can be found up to ~20 µm depth. Plastic deformation is notable in the surface near zones, which may lead to the high wear loss of this alloy. At 700°C a surface covering layer of embedded abrasive and MML can be found. Layer thickness reaches up to 30 µm. The MML consists of abrasive, metal oxide as well as FeCrC matrix and carbides from the original material. Like before MML reaches highest expansion in matrix zones. Broken carbides can be found up to ~90 µm depth in this impact-dominated environment.

Wear scars of the Ni cast alloy are shown in Fig. 56c,d. Wear behaviour is similar to the FeCrC, as they have similar hardphase content and structure. At RT some abrasive penetration and MML formation can be detected, reaching up to ~15 µm depth, surface coverage

is 76 %. Mostly matrix zones are affected by abrasive embedding. Broken carbides are common up to ~40 µm depth. At 700°C large areas are covered by abrasive (94 %). Large particles are embedded in carbide free zones and MML formation is evident. Penetration depth is up to ~30 µm. Surface near carbides are scattered and partly mixed in the MML. Broken carbides can be detected up to ~110 mm depth.

Tab. 11: Quantitative results of wear mechanisms during HT-CIAT: cast- and Co-family

		Crack depth [µm]	MML depth [µm]	MML coverage [%]
FeCrC	RT	18±7 max. 24	10±2 max. 13	62
	700°C	85±10 max. 97	22±8 max. 32	98
NiCrW	RT	38±11 max. 48	10±5 max. 18	76
	700°C	107±4 max. 113	25±11 max. 35	94
FeCrCoC	RT	-	19±4 max. 26	96
	700°C	-	42±16 max. 63	100
CoCrWC	RT	24±8 max. 32	10±5 max. 16	69
	700°C	29±5 max. 32	12±6 max. 19	100

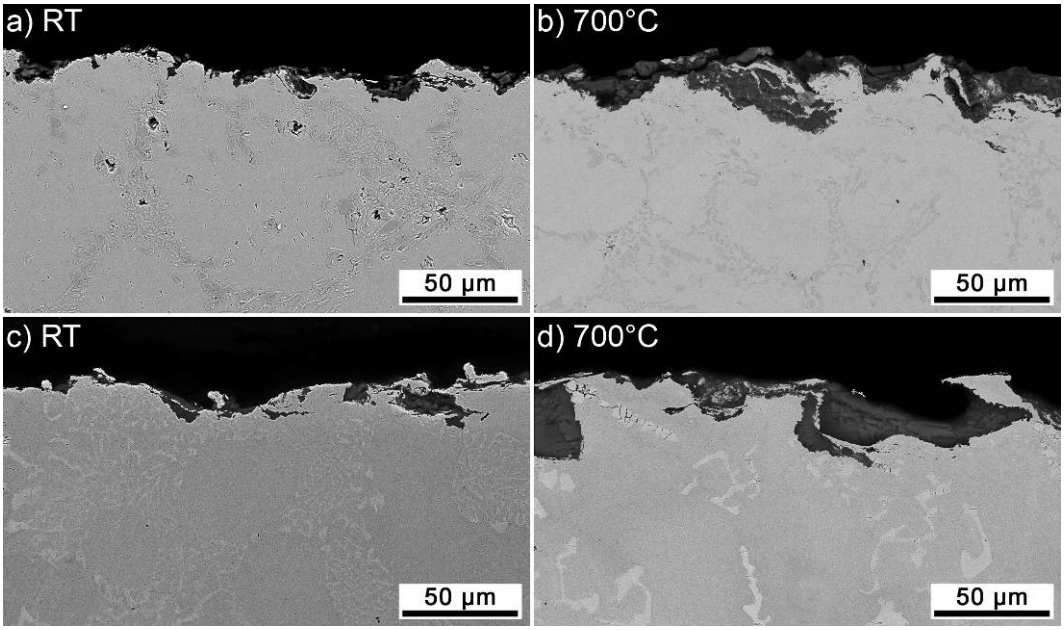

Fig. 56: SEM images of the HT-CIAT impact zone of the cast materials:
FeCrC: a) RT, b) 700°C; NiCrW: c) RT, d) 700°C

The wear zone of the martensitic FeCrCoC is dominated by MML formation. Already at RT (Fig. 57a) thick embedded pockets of ~20 µm are formed and a majority of the surface is covered (96 %). The degree of intermixing is high and plastic deformation of the martensitic matrix reaches ~5-10 µm beneath the MML. At 700°C MML formation is increased, and oxidation is evident, which exacerbates material loss significantly. The martensitic matrix show signs of annealing and is supposed to have reduced wear resistance. MML covers the whole surface and reaches max. 60 µm depth. Further massive cracking of large surface near

zones can be found. It may be caused by near MML zones. Oxidation plays a role in this relative long test (3 h heating-up, 1 h testing, 1 h cooling down) compared to CAT.

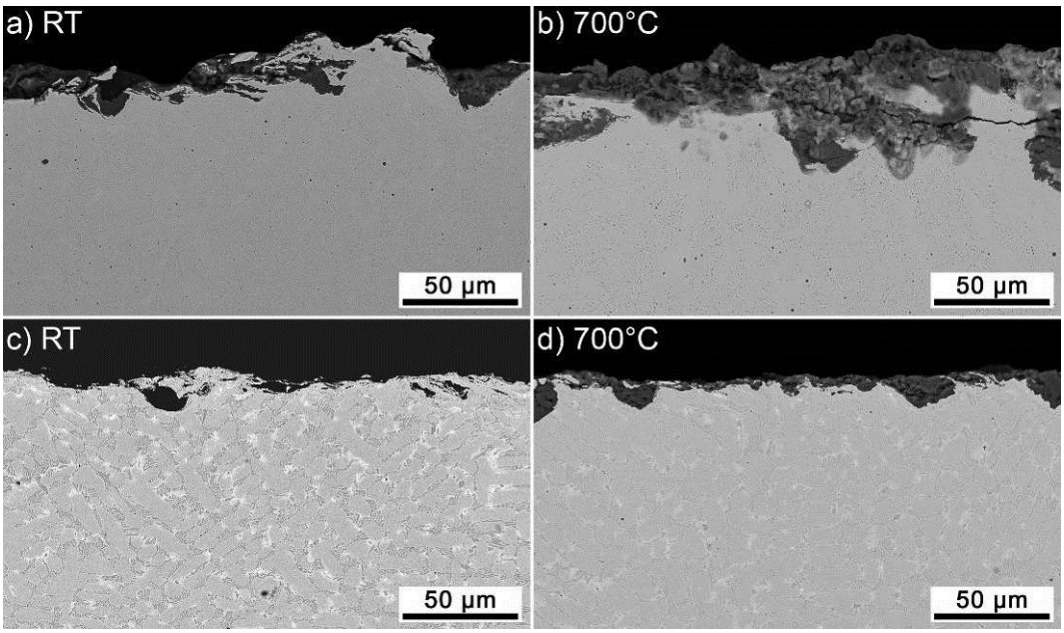

Fig. 57: SEM images of the HT-CIAT impact zone of the Co-containing alloys:
FeCrCoC: a) RT, b) 700°C; CoCrWC: c) RT, d) 700°C

The CoCrWC alloy (Fig. 57c) shows also some MML formation with abrasive, matrix and carbides. The depth of the MML reaches occasionally 10-15 µm (~70 % coverage). The zone of plastic deformation can be found for just a few µm beneath the MML/stressed surface. Broken carbides can be detected up to ~25 µm depth on high magnification images. A surface covering MML can be observed at 700°C testing (Fig. 57d), albeit the thickness is generally low (~12 µm), some spots of 20 µm can be found. It is assumed that the fine structured carbide network defines the MML structure and limits its thickness in this case. Broken carbides at HT have higher frequency than at RT, maximal affected depth is ~30 µm.

The PTA welded hardfacings are illustrated in Fig. 58 and quantitative results of all carbide-rich hardfacings are shown in Tab. 12. The hypereutectic FeCrNbC alloy (Fig. 58a) shows at RT broken large hardphases (Cr-carbides) up to 10 µm depth. Abrasive incorporation cannot be found at this temperature and brittle behaviour dominates the wear loss. At 700°C (Fig. 58b) carbide breaking is more pronounced in large primary Cr-carbides and can be found up to ~25 µm depth. The large carbides show a crack network in surface near zones, while cracks in deeper layers are mostly parallel oriented to the wear surface (up to 35 µm). Some sticking abrasive particles can be found, but no intermixing with the hardfacing. In the first micrometres beneath the surface some plastic deformation can be observed at 700°C.

The PTA welded FeCrNbBWC shows very brittle behaviour at RT (Fig. 58c), all hardphases break until 10-15 µm depth. This means large Cr-carboborides, Nb- and W-precipitations as well as W-rich matrix zones. Nevertheless, impact-abrasive wear resistance is quite optimal according to the wear results. At 700°C surface near zones are scattered to particles in the micrometre range. Larger hardphases show breakage until 10-15 µm depth.

Tab. 12: Quantitative results of wear mechanisms during HT-CIAT: carbide-rich hardfacings

		Crack depth [µm]			MML	
		Large HP	Small HP	Matrix	Depth [µm]	Coverage [%]
FeCrNbC-PTA	RT	9±4 max. 14	-	-	-	-
	700°C	25±8 max. 35	-	-	-	-
FeCrNbBWC-PTA	RT	13±2 max. 14	3±1 max. 3	max. 8	-	-
	700°C	11±2 max. 13	7±3 max. 10	max. 6	-	-
FeCrNbBWC-GMAW	RT	6±1 max. 7	3±1 max. 4	-	-	-
	700°C	17±7 max. 25	6±1 max. 7	10±4 max. 13	-	-
FeCrNbBC-GMAW	RT	11±5 max. 16	-	-	-	-
	700°C	18±3 max. 21	11±2 max. 13	-	7±1 max. 8	19

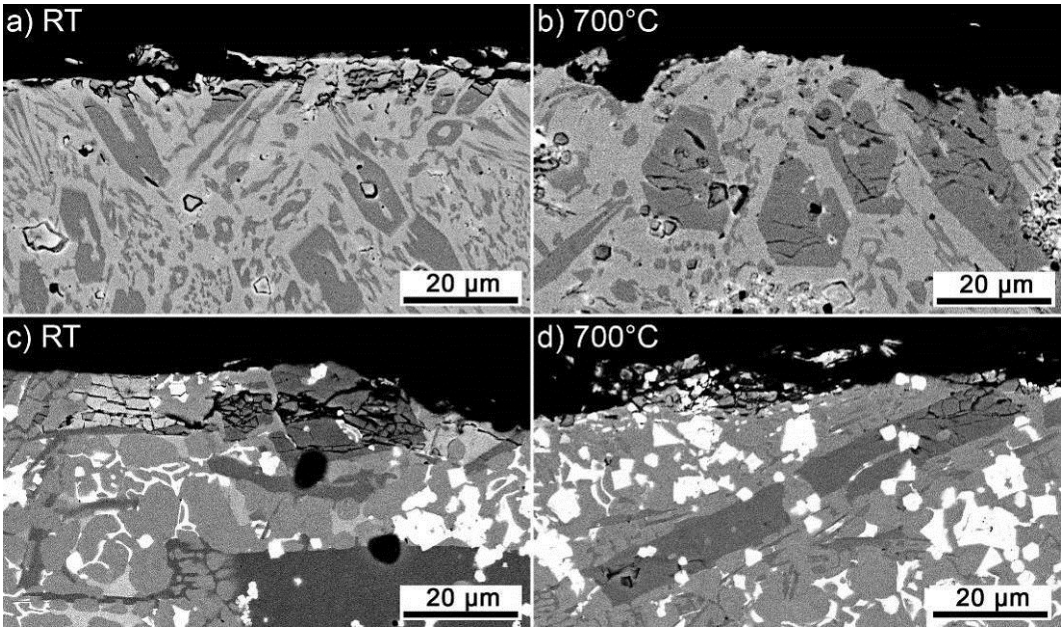

Fig. 58: SEM images of the HT-CIAT impact zone of the PTA welded carbide-rich hardfacings: FeCrNbC: a) RT, b) 700°C; FeCrNbBWC: c) RT, d) 700°C

The two-layered GMAW alloys with lowest wear loss of all materials investigated are displayed in Fig. 59. FeCrNbBWC shows few damaged areas at RT. Hardphases of all types are broken until ~7 µm at some points, but generally the surface is smooth and scarcely damaged. At 700°C spacious breaking can be observed. All phases are affected until ~10 µm depth, exceeding this depth mainly large carbides break until ~25 µm, albeit this massive brittle behaviour wear loss is very limited.

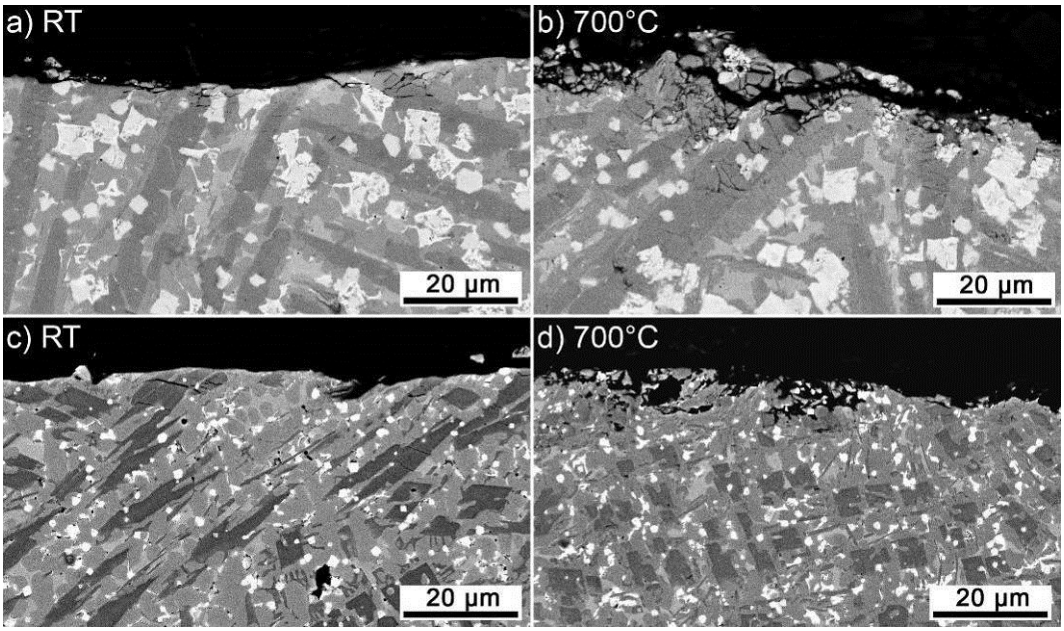

Fig. 59: SEM images of the HT-CIAT impact zone of the GMAW carbide-rich hardfacings: FeCrNbBWC: a) RT, b) 700°C; FeCrNbBC: c) RT, d) 700°C

The RT impact zone of FeCrNbBC is given in Fig. 59c. Like at the alloy before, the surface is smooth with just minor affected zones. However for this alloy breaking of large Cr-carboborides can be found until ~15 µm depth, while other carbides and different matrix zones are not distorted. At 700°C cracking of all hardphases can be observed up to 15-20 µm depth. Limited plastic deformation can be seen and beginning MML formation (20 % coverage) with the scattered particles and some abrasive in certain regions.

4.3.3. Solid particle erosion test

Erosion results of oblique and normal impact are displayed in Fig. 60 and Fig. 61. As observed for the other wear modes, also HT wear rates at ET are significantly higher than RT values, but also here distinct differences in the magnitude are obvious. Also opposing behaviour of the materials to the angle of impact can be figured out: while the cast alloys and FeCrCoC show lower wear rates at normal impact, whereas the other alloys show a contrary behaviour.

Lowest RT wear rates for oblique erosion (30°) were measured for the PTA hardfacings and FeCrNbBWC-GMAW with <15 mm³/kg. 650°C wear rate was lowest at FeCrNbBWC-PTA with 35 mm³/kg, albeit also FeCrC, CoCrWC and FeCrNbBWC-GMWA show good results with ~40 mm³/kg. Highest HT-wear rate at oblique impact was measured at the martensitic FeCrCoC. Interesting behaviour with almost constant wear rates at 300°C and 550°C indicate that for the cast alloys and CoCrWC, temperature increase in this range does not seem to

result in detrimental effects for these materials regarding wear rate. At FeCrC the increase of wear rate from RT to 300°C is ~30 %, stays at a constant level at 550°C and increases for another ~30 % at 650°C. For the Ni-cast wear rates worsen more with ascending temperature: + ~50 % at 300°C and 550°C and more than double at highest testing temperature. Even more extreme is the rise at FeCrCoC, it gains 70 % to 300°C and wear rates ramp with a factor of ~2.5 (58 mm³/kg) at 650°C compared to RT, which stands for the highest value measured at oblique impact. The Co-base alloy CoCrWC exhibits a huge increase at the first temperature step, it almost doubles from RT to 300°C. Further ascend is less pronounced, reaching a good value of 41 mm³/kg at 650°C.

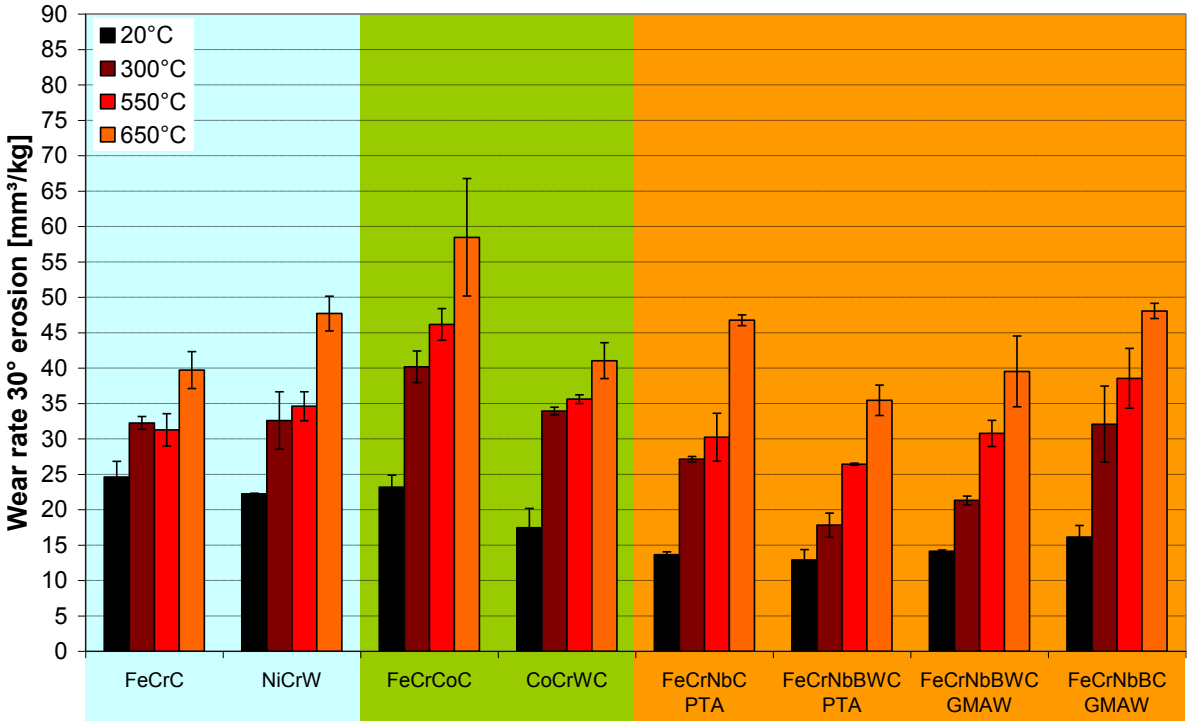

Fig. 60: Erosion results at oblique impact of 30° at 80 m/s particle velocity

The carbide-rich hardfacings show similar behaviour at oblique impact. Starting with very low wear rates at RT, they gradually increase with ascending temperature. For FeCrNbC-PTA and FeCrNbBC the first interval shows significant increase of ~50 %. For FeCrNbC-PTA the last interval is also pronounced, reaching 47 mm³/kg at 650°C, which means a 3.4-fold wear rate increase compared to RT. The complex alloyed FeCrNbBWC shows best performance in PTA-welded condition, but differences to GMAW are minor. It doubles its wear at 550°C, and the factor at 650°C is 2.8, entailing the lowest wear rate in the test field at oblique impact. FeCrNbBC reveals a steep increase, it doubles its wear rate already at 300°C and triples at 650°C compared to RT.

Normal erosion (90°) rates are displayed in Fig. 61. Lowest wear rates at all temperatures are measured for the cast alloys, while the hardfacings exhibit a dramatic increase at higher temperatures. Standard deviations for these hardfacings are generally very high at normal impact, indicating brittle behaviour with larger outbreaks. Lowest RT wear rate was found at FeCrC with 16.5 mm³/kg, which is in the range of the lowest wear rates of oblique impact testing. This is especially interesting, as the normal impact energy to the surface is doubled compared to 30° impact. Also low wear rates of ~20 mm³/kg at RT are found for NiCrW cast, and the two complex alloyed FeCrNbBWC. Wear rates generally increase with ascending temperature, albeit highest wear rates of FeCrNbC and FeCrNbBWC-GMAW are already reached at 300°C and do not worsen significantly at further rising temperature. Very good HT wear rates of ~30 mm³/kg at 650°C were found for the two cast alloys, which is even lower than the best performing alloy at oblique impact (i.e. FeCrNbBWC-PTA, ~35 mm³/kg at 30°).

The FeCrC alloy starts with lowest wear rate at RT, increase to 300°C and 550°C is 20-30 %, but the difference is insignificant. Comparing the 650°C wear rate with RT an increase of 80 % can be calculated in this temperature range. Thus, this alloy shows lowest wear rates at normal impact for all temperatures investigated. The NiCrW features ~5 mm³/kg higher wear rates than FeCrC at RT-550°C. At highest testing temperature they are approximately of the same excellent value of ~30 mm³/kg.

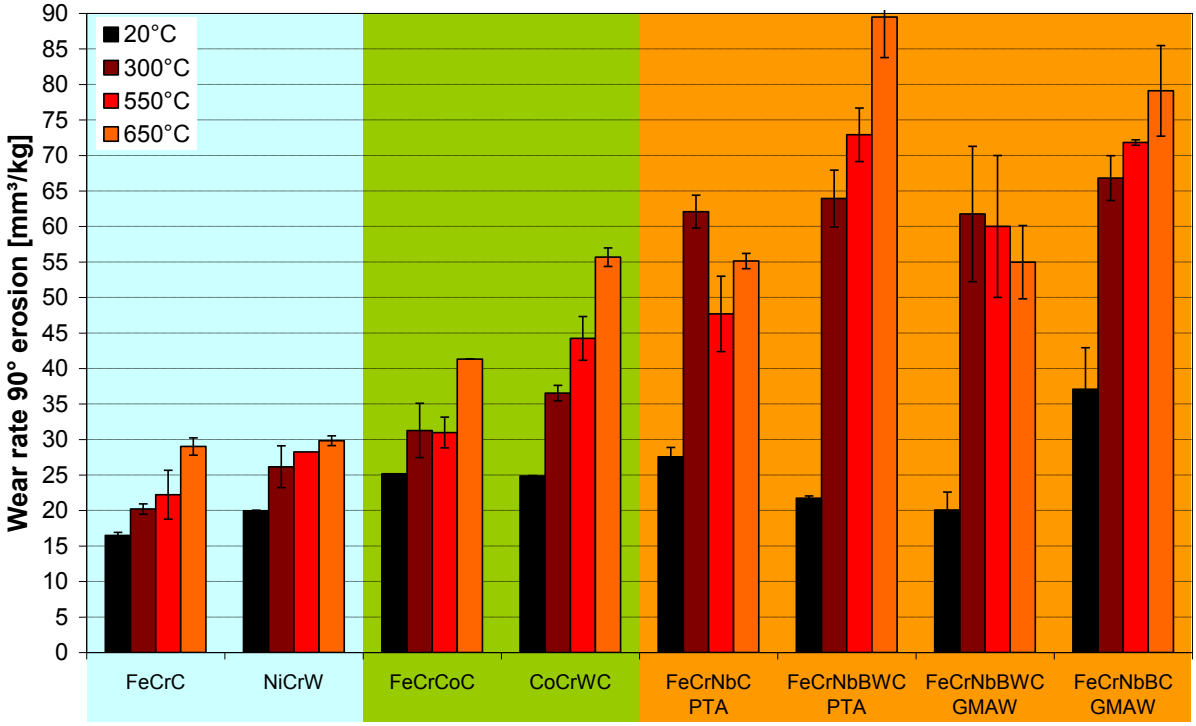

Fig. 61: Erosion results at normal impact (90°) at 80 m/s impact velocity

Both alloys of the Co-family start at 25 mm³/kg. FeCrCoC slowly increases to ~31 mm³/kg at 300°C and stays constant at 550°C. The 650°C erosion rate is ~41 mm³/kg, which means 60 % more than at RT. The wear rate of CoCrWC rapidly increases by 50 % at 300°C, 80 % at 550°C and 120 % at highest testing temperature, entailing ~56 mm³/kg at 650°C. The carbide-rich hardfacings all show high wear rates already at 300°C testing. For FeCrNbC wear rate rises from ~28 mm³/kg at RT to ~55 mm³/kg at 300°C, which then stays similar up to highest testing temperature. Hence increase is about twofold. The two complex FeCrNbBWC hardfacings show similar wear rates at RT (~20 mm³/kg) and 300°C (~60 mm³/kg), i.e. they almost triple in this first interval. The PTA welded one further worsens to ~90 mm³/kg at highest temperature, which is a factor of 4.1 of the RT value. The GMAW alloy does not significantly change with further increasing temperature, but standard deviations are extraordinary high. The FeCrNbBC-GMAW alloy has the highest RT wear rate of 37 mm³/kg. It rockets to 67 mm³/kg at 300°C (+80 %) and reaches 79 mm³/kg at 650°C, which is within the range of the highest value of FeCrNbBWC-PTA. Wear increase in the first interval (RT-300°C) may be put down to the reduction of beneficial residual stresses by temperature increase.

In search of changing wear mechanisms wear scars of all alloys were investigated at RT and 650°C at both impact angles. Cross sections through the wear zone were analysed in SEM and images are given in Fig. 62-Fig. 65, where the left column represents oblique impact and the right column normal impact results. Quantitative results are shown in Tab. 13 and Tab. 14.

Tab. 13: Quantitative results of wear mechanisms during HT-ET at oblique and normal impact: cast- and Co-family

		30° erosion		
		Crack depth [µm]	**MML depth [µm]**	**MML coverage [%]**
FeCrC	RT	22±2 max. 24	5±1 max. 6	42
	650°C	22±7 max. 31	6±4 max. 11	78
NiCrW	RT	24±3 max. 27	max. 5	8
	650°C	105±10 max. 116	3±1 max. 5	56
FeCrCoC	RT	-	2±1 max. 3	69
	650°C	-	6±2 max. 8	81
CoCrWC	RT	10±2 max. 11	3±1 max. 3	26
	650°C	6±1 max. 8	3±1 max. 5	32

		90° erosion		
		Crack depth [µm]	**MML depth [µm]**	**MML coverage [%]**
FeCrC	RT	56±8 max. 61	7±4 max. 13	78
	650°C	52±5 max. 56	19±10 max. 32	95
NiCrW	RT	59±7 max. 68	7±3 max. 11	56
	650°C	103±6 max. 110	11±4 max. 16	66
FeCrCoC	RT	-	2±2 max. 5	81
	650°C	-	21±7 max. 29	33
CoCrWC	RT	16±4 max. 19	4±1 max. 5	32
	650°C	4±1 max. 5	4±2 max. 8	33

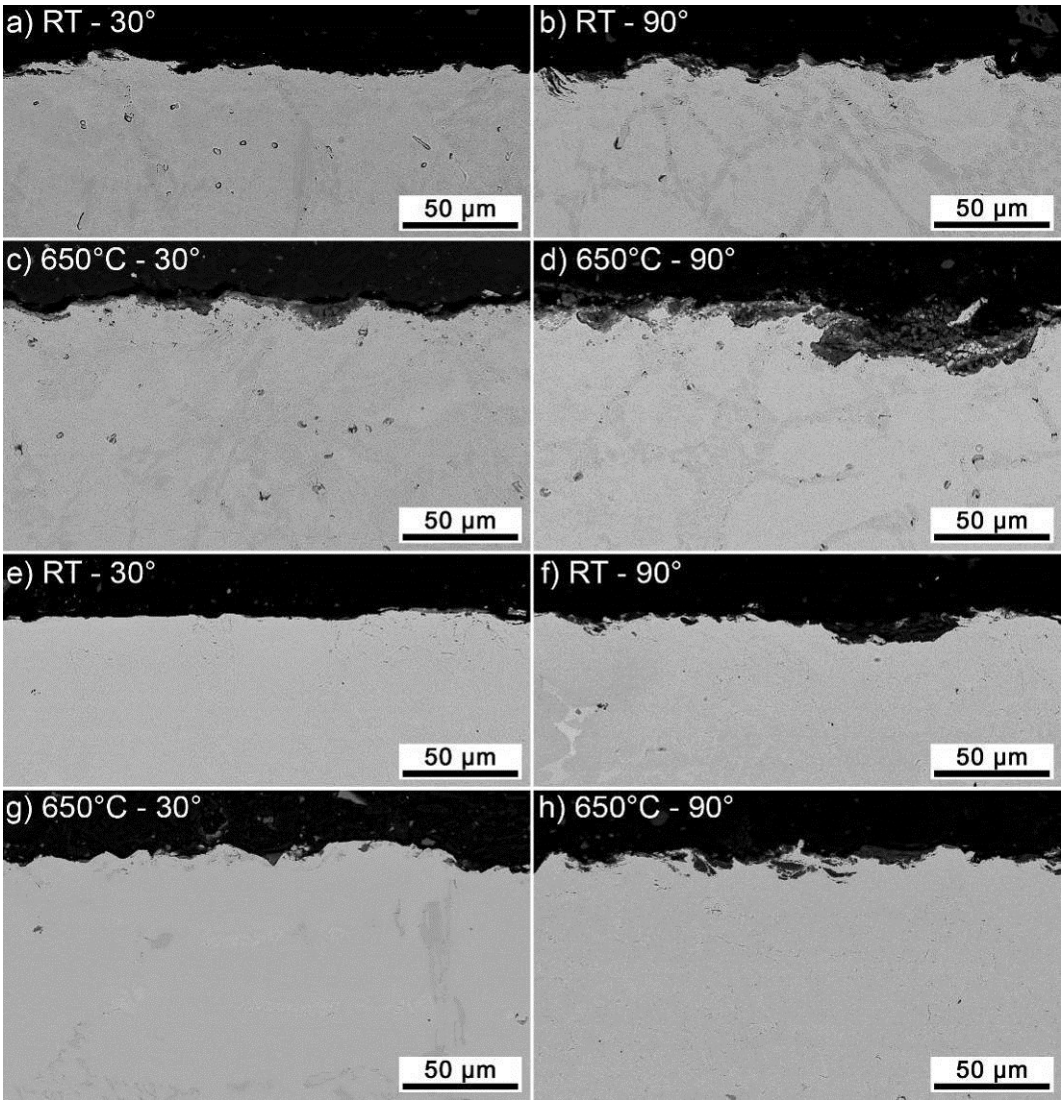

Fig. 62: SEM of cross sections through the HT-ET wear scars of the cast materials:
FeCrC: a) RT-30°, b) RT-90°, c) 650°C-30°, d) 650°C-90°;
NiCrW: e) RT-30°, f) RT-90°, g) 650°C-30°, h) 650°C-90°

The cast alloys are shown in Fig. 62. The FeCrC reveals some sticking particles (42 % coverage) at oblique impact for RT. Carbide breakage reaches ~20 µm depth. At normal impact, particle embedding is covering nearly the entire surface area (95 %) and some inter-mixing takes place, albeit penetration depth is still small. Carbide breakage can be detected up to ~55 µm depth. At 650°C (Fig. 62c-d) affected zones are generally thicker. At oblique impact sticking particles penetrate ~6 µm. MML formation is not pronounced, albeit covered surface is 78 %. The shallow impact angle may hinder intermixing. Carbide breaking does not proceed significantly further: The last cracks can be found in ~30 µm depth. Although the load regime does not promote MML formation at normal impact clear signs of intermixing can be observed and the whole surface is covered. The zone of mixed broken abrasive, oxide,

matrix and carbides is up to ~30 µm deep, especially in carbide-free matrix zones. Carbide breakage reaches ~55 µm deep. So the MML protects the material definitely.

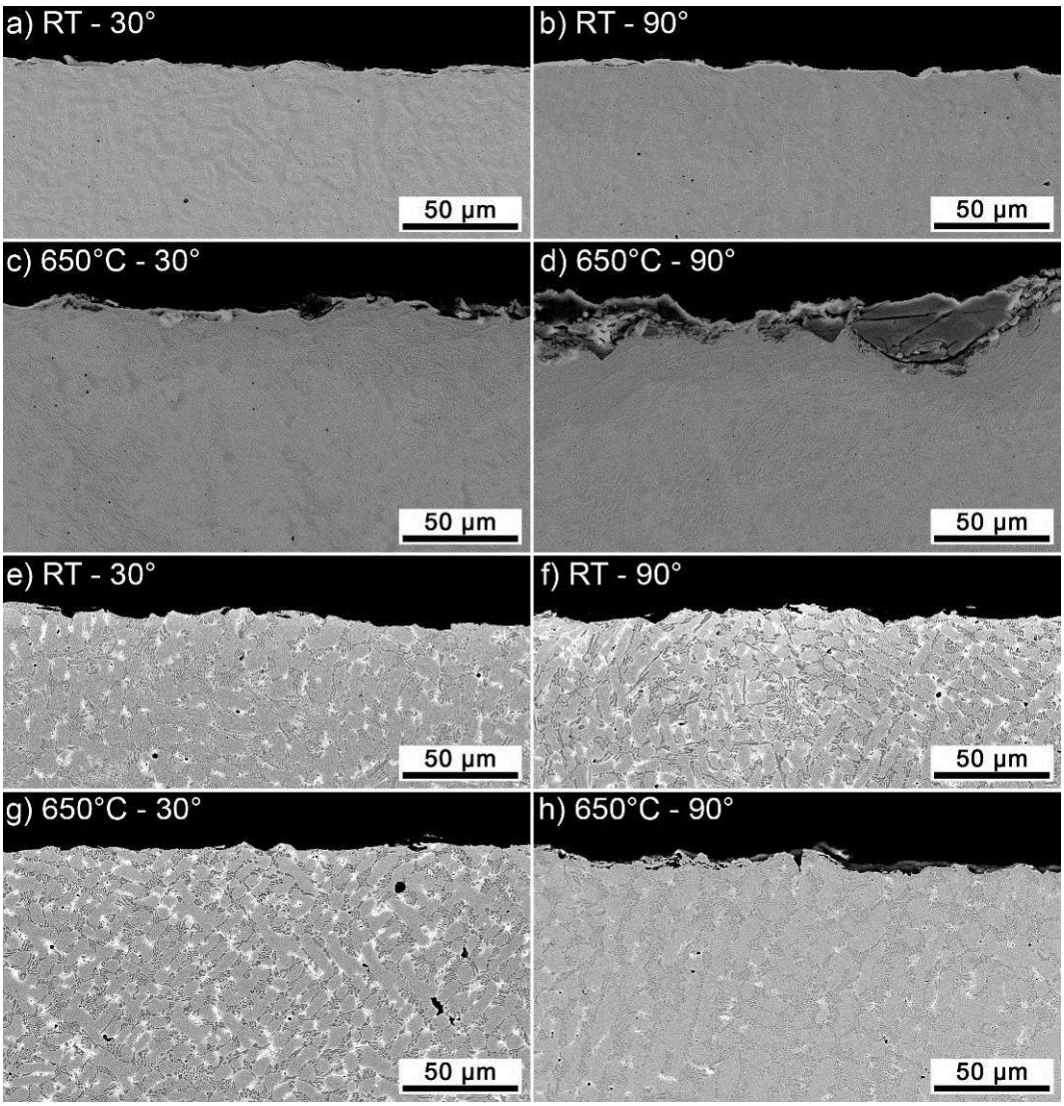

Fig. 63: SEM of cross sections through the HT-ET wear scars of the Co-containing alloys: FeCrCoC: a) RT-30°, b) RT-90°, c) 650°C-30°, d) 650°C-90°; CoCrWC: e) RT-30°, f) RT-90°, g) 650°C-30°, h) 650°C-90°

The two Co containing alloys are shown in Fig. 63. The martensitic FeCrCoC shows no pronounced MML formation at all conditions but 650°C-normal impact. At RT-oblique impact some plastic deformation can be seen in the first micrometres, at normal impact plastic deformation is less pronounced. At 650°C-oblique impact (Fig. 63c) some sticking particles can be found (~80 % covered surface) and oxides. Plastic deformation is slightly more extensive than at RT. A complete different behaviour can be seen at normal impact (Fig. 63d), where a thick layer of abrasive and oxide covers the surface. Some intermixing with the substrate takes place. The thickness of this layer is up to ~30 µm covering 97 % of the

surface. Plastic deformation also is obvious in this range beneath the surface/embedded abrasive particles. Thus, this protective layer makes the difference between highest erosion rates at oblique impact and good results at normal impact.

The Co-base alloy CoCrWC is given in Fig. 63e-h. At RT-oblique impact some randomly sticking particles in matrix zones can be found, but their penetration depth is <5 µm. Carbide breaking can be detected up to ~10 µm depth at this condition. Wear behaviour is very similar at normal impact, albeit cracking reaches 15-20 µm depth and slightly more abrasives stick to the surface (33 % coverage). At 650°C matrix and carbide zones wear uniformly as at RT. At oblique impact carbide breakage can be found up to ~8 µm depth, occasional abrasive sticking and overlapping matrix can be detected, covering 32 % of the surface. At normal impact penetrating abrasive is covering the majority of the surface (72 %), but thickness is limited to 4-8 µm. In some small carbide free areas intermixing can take place in the first micrometres. Due to its frequent carbide precipitations the MML formation is hindered in this alloy significantly.

Cross sections of the wear zones of the PTA welded hardfacings are given in Fig. 64 and GMAW in Fig. 65. Quantitative results are shown in Tab. 14.

Tab. 14: Quantitative results of wear mechanisms during HT-ET
at oblique and normal impact: carbide-rich hardfacings

		30° erosion				
		Crack depth [µm]			MML	
		Large HP	Small HP	Matrix	Depth [µm]	Coverage [%]
FeCrNbC-PTA	RT	9±2 max. 11	-	-	-	-
	650°C	18±2 max. 21	-	-	-	-
FeCrNbBWC-PTA	RT	5±1 max. 5	max. 1	-	-	-
	650°C	6±0 max. 6	3±2 max. 5	-	max. 2	17
FeCrNbBWC-GMAW	RT	5±3 max. 8	-	-	-	-
	650°C	21±10 max. 32	7±3 max. 9	max. 5	-	-
FeCrNbBC-GMAW	RT	7±5 max. 10	-	-	-	-
	650°C	28±2 max. 30	-	-	-	-

		90° erosion				
		Crack depth [µm]			MML	
		Large HP	Small HP	Matrix	Depth [µm]	Coverage [%]
FeCrNbC-PTA	RT	10±6 max. 16	-	-	-	-
	650°C	40±3 max. 43	-	-	4±2 max. 6	36
FeCrNbBWC-PTA	RT	17±4 max. 20	3±1 max. 3	-	-	-
	650°C	19±6 max. 24	max. 16	max. 8	max. 5	14
FeCrNbBWC-GMAW	RT	16±8 max. 25	-	max. 2	-	-
	650°C	40±8 max. 45	7±2 max. 8	8±2 max. 10	-	-
FeCrNbBC-GMAW	RT	17±6 max. 22	-	-	-	-
	650°C	27±15 max. 43	-	-	max. 3	20

Brittle behaviour dominates the wear of FeCrNbBWC-PTA (Fig. 64e-h). At RT oblique impact cracking can be identified in all hardphases. Large and small Cr-carboborides break until ~5 µm depth. Smaller Nb-precipitations are scarcely harmed, but also there cracks were

observed. At 90° impact cracking is far more extended and reaches ~20 µm depth in large Cr-precipitations. Small Nb- and W-carbides are affected <5 µm depth. At HT the surface is much more scattered than at RT. At oblique impact cracking reaches ~6 µm depth, also smaller hardphases and the W-rich matrix zones are cracked, especially directly on the surface all phases are affected. At normal impact cracking reaches 20-25 µm depth. Especially large Cr-carboborides reaching the surface are widely cracked. Smaller precipitations within the matrix are broken until ~15 µm depth. A single sticking particle was observed.

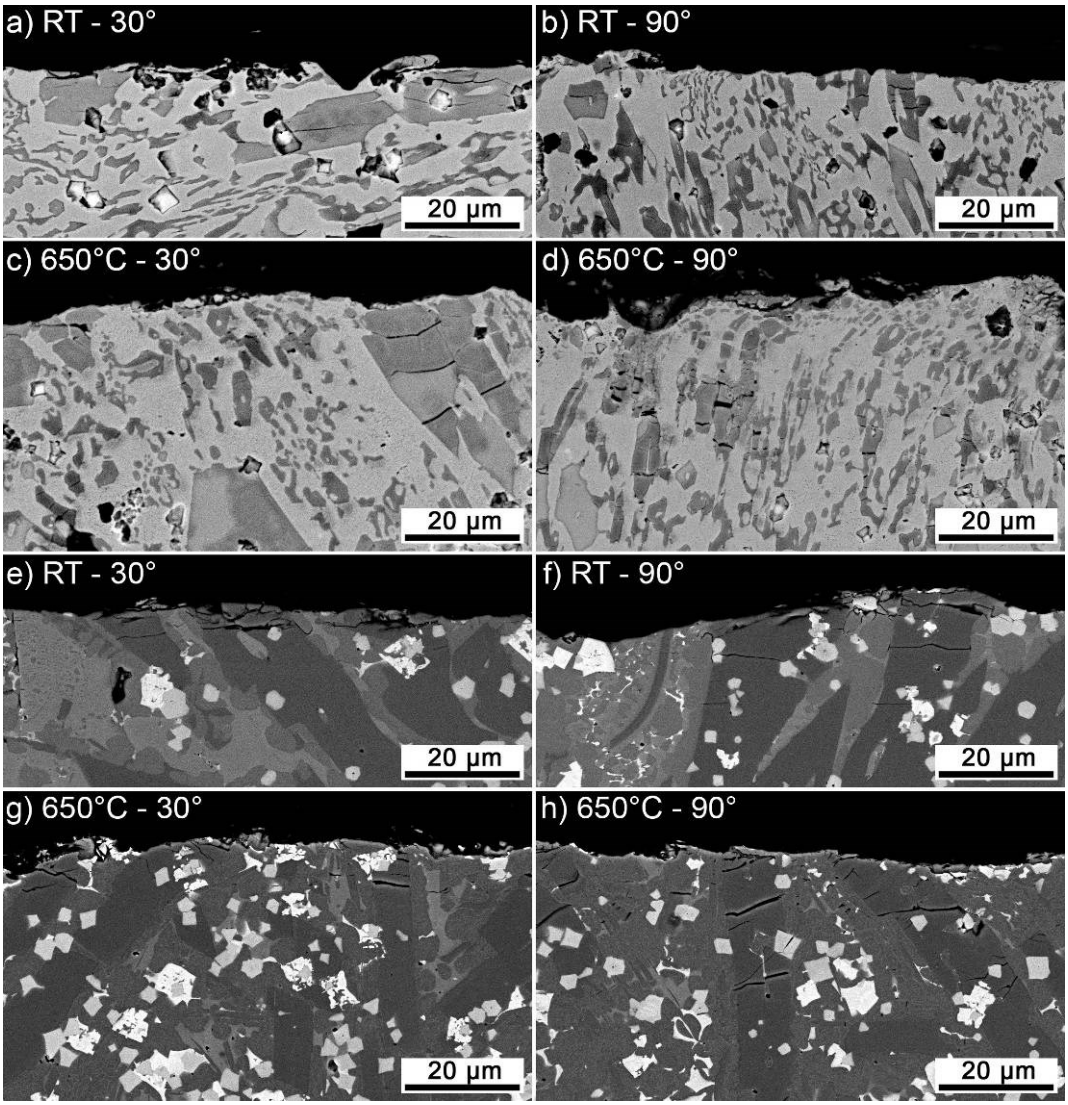

Fig. 64: SEM of cross sections through the HT-ET wear scars of the PTA welded carbide-rich hardfacings: FeCrNbC: a) RT-30°, b) RT-90°, c) 650°C-30°, d) 650°C-90°; FeCrNbBWC: e) RT-30°, f) RT-90°, g) 650°C-30°, h) 650°C-90°

The GMAW alloys are displayed in Fig. 65. In contrast to the PTA welded alloys cracking at FeCrNbBWC-GMAW is limited at RT to the first ~5 µm of Cr-carboborides. Also smaller Cr-precipitations are involved, but no other hardphases or matrix zones. At normal impact

also mainly the large Cr-precipitations are affected. Parallel cracking can there be found until ~25 µm, while frequent cracks concentrate up to ~15 µm depth. Also W-rich matrix zone show scarcely cracks in the first micrometres. At 650°C oblique impact (Fig. 65c) widespread scattering is obvious. All hardphases break and also some cracks in matrix zones can be found. Cracking of large Cr-carboborides reaches ~20 µm depth, while other phases crack mostly in the first 10 µm. At normal impact cracking can be detected until ~45 µm in large Cr-precipitations. In the first 8 µm all phases are involved and show frequent cracks. Larger areas detach by the connection of cracks in this region.

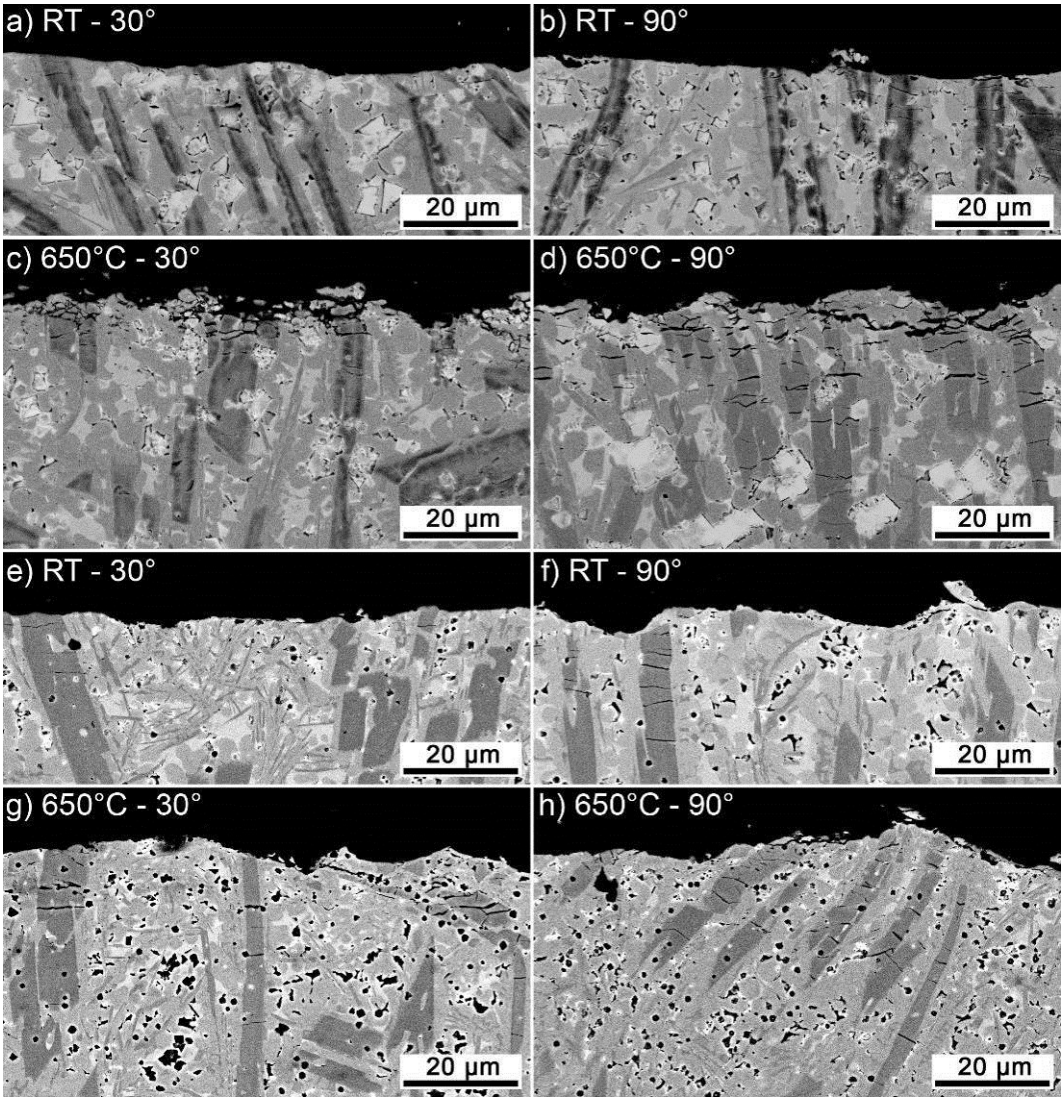

Fig. 65: SEM of cross sections through the HT-ET wear scars of the GMAW carbide-rich hardfacings: FeCrNbBWC; a) RT-30°, b) RT-90°, c) 650°C-30°, d) 650°C-90°; FeCrNbBC: e) RT-30°, f) RT-90°, g) 650°C-30°, h) 650°C-90°

The FeCrNbBC-GMAW is shown in Fig. 65e-h. Wear behaviour is similar as at FeCrNbBWC. At RT oblique impact cracking of the large hardphases can be observed. Cracks parallel to the

surface can be found until ~10 µm depth in large Cr-carboborides, the other phases show no cracking. At normal impact cracks in these phases reach ~20 µm depth. At this condition also other phases seems not affected of cracking, but limited plastic deformation can be observed. At 650°C-oblique impact cracking of large Cr precipitations reaches ~30 µm. Also smaller hardphases and W-rich matrix zones are affected in surface near zones. At normal impact cracks can be found until ~40 µm depth. Also some plastic deformation, particle sticking and oxides on the surface can be found at this highest testing temperature.

5. Discussion

In this chapter, the relevance of tribological research of abrasive phenomena for sinter plants is discussed, followed by a comparison of wear mechanisms achieved in the tests with real wear phenomena from practical application. Then, a comparison of the various abrasion modes is done, aiming at the identification of most effective wear protection; materials sensitive to specific forms of abrasion are identified. The competitiveness of the materials investigated here is evaluated and compared to data from literature. A discussion of wear phenomena at the various abrasion modes is given and beneficial microstructures as well as in-situ built layers are given. Correlations of material properties with wear rates and phenomena are discussed. Finally, an economic evaluation of the different materials for specific applications is given.

5.1. Tribological assessment of maintenance data

Tab. 15 gives an overview of the maintenance data presented in chapter 4.1. Percentages of total costs/tasks within the sinter plant in the period 4.2008-3.2011 are given for the categories maintenance and –frequency, downtime and –frequency and total costs. Further total costs are split into maintenance and downtime expenses. Additionally to the sum, components of the main plants/aggregates are given. Expenses/frequency above 5 % are highlighted yellow, >10 % orange and >15 % red.

Important components/failure causes within the plants/aggregates exceeding 1 % of total were presented in chapter 4.1. Now it should be evaluated which of them is due to tribological malfunction and may be improved by tribological research/improvement.

Beginning with the section sinter belt, the crusher system and the sinter wagons are of highest importance concerning total costs. Although the crusher system causes nearly no downtime, the maintenance costs are extreme, which is mainly caused by wear. The crusher system is constantly crushing the ~700°C abrasive finished sinter after the sintering process. The main wear component is the spike crusher, followed by the crusher grate. Adjacent components in the crusher area, like the pre-breaker or even side walls, are also constantly worn. Details on the dominant failure mechanisms are given in chapter 2.3.2. It can be concluded that the **crusher system** is of major tribological concern because of **HT abrasive wear**.

The main transport components within the sinter process are the sinter wagons. They cause high maintenance expenses as well as downtime, the downtime frequency is exorbitant. This is due to the major relevance of the grate bars for the sinter process. The grate bars support the

sinter mixture, but also the spacing between the bars is essential for optimal air flow, which is necessary for the sinter process. The grate bars suffer two main degradation mechanisms. The first is HT corrosion: in the sinter process aggressive components from the sinter mixture (ore, limestone, etc.) are dissolved and corrode following components in the air flow. Major attack can be found on the grate bars, as there is still very HT. Corrosion leads to material loss of the grate bars, but also deposit build-up, which is especially detrimental, as it closes the ventilation spacing between the bars. This makes a cyclic cleaning of the bars necessary, which is normally done during the maintenance standstills. However often during the working period, a cleaning of the closed spacings becomes necessary to keep the sinter process in optimal process conditions. The cleaning during production may lead to unplanned downtime, e.g. when the cleaning stuff breaks a rod. The second major failure mechanism of the grate bars is material loss due to wear. At the end of the sinter process the sinter is dropped into the crusher system. During this drop-off the hot finished sinter abrades over the grate bars, which especially damages the edge of the wagon, where highest load occurs during sliding of the sinter cake. Grate bars are replaced when their thickness in this region is too low. I.e. the **grate bars** suffer a **combined HT-abrasive and corrosive load**. At side walls with no contact to the sinter mixture HT corrosion dominates, while at the drop edge HT abrasion dominates. Details are given in chapter 2.3.1.

Tab. 15: Overview of the maintenance records evaluation (sorted by total costs), [%] of total

	Plant priority	Mainten-ance	Mainten-ance frequency	Downtime	Downtime frequency	Total costs	Total costs	
							mainten-ance	+ downtime
Sinter belt	A	19.6	8.8	23.1	48.8	17.6	12.0	5.6
Sinter belt remains	A	7.8	6.3	17.7	14.8	9.0	4.7	4.3
Crusher system	A	7.1	0.4	1.1	0.1	4.7	4.4	0.3
Sinter wagons	A	4.7	2.2	4.3	33.9	4.0	2.9	1.1
Electronics	A	10.7	18.2	20.1	0.6	11.5	6.6	4.9
Electrical installation	A	3.5	5.4	19.9	0.4	7.1	2.2	4.9
Measurement and control systems	A-B	7.2	12.8	0.2	0.2	4.5	4.4	0.1
Emission control	A-B	13.3	10.7	10.0	3.1	10.5	8.1	2.4
Meros	B	4.6	3.9	3.0	0.8	3.5	2.8	0.7
Filter	B	5.9	4.8	0.1	0.1	3.6	3.6	0.0
Ventilation	A	2.8	2.0	6.9	2.3	3.4	1.7	1.7
Conveyor belts	A	11.3	23.2	7.2	10.4	8.7	6.9	1.8
HT sieve and chutes	A	8.2	4.3	10.2	8.4	7.5	5.0	2.5
Apron conveyor	A	2.3	1.2	6.6	7.2	3.0	1.4	1.6
Pug mills	A	2.0	0.9	3.0	6.3	1.9	1.2	0.7
Sinter mixture transport	A	1.5	0.3	3.9	4.1	1.9	0.9	1.0
Belt weighers	A	2.8	4.6	0.2	0.9	1.8	1.7	0.1

Further maintenance causes within the sintering belt are the electric drive and clutch, leading to some downtime. Malfunctions were mainly due to electrical failures, i.e. tribological relevance is minor. The rails of the sinter wagons also caused some downtimes. Here a tribological influence cannot be excluded, but records mainly report misalignment of the wagons.

The electronics come in second place, mainly because of frequent measurement tasks, controlling key parameters of the processes and exhaust emissions on one hand, and an unfortunate cable fire entailing many hours downtime on the other hand. Tribological influence is not discernible within this section.

The **emission control** is an essential part for meeting the environmental constraints, but ventilation is also crucial to keep the sinter process running. A majority of the costs can be attributed to electrical malfunction, but also component wear cannot be neglected. Transportation of sinter remains in the exhaust gas leads to **erosive wear**, also a combination with **corrosion** and deposit build-up is possible due to the aggressive components in the emissions.

Conveyor belts are necessary for transportation of (cold) goods. Their summed maintenance costs are high, because many belts are in use. Also downtime is detrimental, as they are seldom redundant. One of the main issues, especially from a tribological point of view, is the wear of the rubber belt. The filling and the acceleration of goods lead to relative motion between belt and goods, resulting in wear. This can be minimised by proper design of the loading unit. At the other end of the conveyor belt, the drop-off, cleaning of the belt is necessary in order to avoid dirt all over the length of the belt. Scrapers are used for removal of attaching goods. This section represents an interesting tribosystem: on the one hand, the belt should be cleaned as well as possible to avoid dirt at the plant. On the other hand, high loading of the scraper leads to increased conveyor belt wear, limiting its lifetime. I.e. an optimisation between wear loss and cleaning efficiency is necessary. Abrasive wear at the scrapers is different from wear at the interaction of the free-rolling goods: scrapers feature aggressive two-body conditions limited to a small area. Free movement of the goods leads to less aggressive three-body conditions, but affecting almost the entire length of the conveyor belt with a load concentration at the filling station. As rubber wear is very different from steel wear, it will not be discussed within this work. **Two- and three-body abrasive wear of conveyor belts** is investigated, e.g. in [MOL14]. However, not only wear of conveyor belts causes high maintenance costs. Frequent tasks are control of the conveyor belts and repair of conveyor belt misalignment, i.e. the conveyor belt moves to one side and needs to be centred. Thousands of rolls support the conveyor belts and alignment stations should centre them, but

the dusty environment due to transportation goods impairs the movement of the rolls and stations. Frequent control should ensure operation of the conveyor belts; also lubrication of the components is checked. However, stuck rolls do not lead to a plant downtime, this happens when the sharp parts enter the conveyor belt system by accident. Resulting repair leads often to plant downtime.

A large amount of HT sieve and chutes maintenance constitutes a major renovation. Also the electrical drive causes some problems. Of greater tribological relevance are bearing failures entailing downtimes: the vibrating screen stresses especially the bearings. The flooring of the HT sieve and chutes costs also reasonable maintenance. Wear of the flooring due to the abrasive HT sinter makes frequent replacement of the **flooring** necessary [VAR15-2, chapter 2.3.3]. Knowledge of **HT abrasive wear** and wear-protective solutions are necessary to obtain adequate lifetime of the flooring and screens.

The apron conveyor for returned sinter is prone to unplanned downtime. Break of axes and brackets, loss of components, etc., are frequent failures and may be caused due to tribological malfunction. The apron conveyor for the sinter carries much higher tonnage, also at higher temperature, but does not suffer unplanned downtimes because of a major renovation done lately. This may also be advisable for the other apron conveyor instead of frequent repair.

Bunkers are on one hand a tribological issue: the walls are protected by wear resistant ceramics or metal solutions. On the other hand, bunkers cause a measurement and control challenge: the exhaustion or overfilling must be avoided. Problems with the filling level lead to frequent control tasks and some downtimes, but of minor duration.

The pug mills for homogenisation of the sinter mixture cause substantial downtime frequency. Mechanical/tribological failure is seldom found, main causes are the water sprinkler and deposit build-up. Wear of the pug mills is negligible due to a very effective structuring of the mills' surface, allowing the deposit of sinter mixture and preventing wear of the mills by a self-protecting sinter mixture layer.

The drum loader caused downtimes because of problems with the electric drives. Belt weighers are also mainly affected by electrical problems and misalignment/ belt drift. The latter is similar to the conveyor belts.

Interestingly the lubrication of components did not cause major problems or consume notable maintenance efforts. I.e. an effective lubrication of components can be done at relatively low costs. Control activities of components often include lubrication at certain intervals, therefore

the costs are hidden within these control tasks. Control tasks were only of higher costs for the conveyor belts. It has to be noted, that due to CIP frequent problems are consitantly addressed and maintenance evaluations may show different results when repeated later.

Tab. 16 gives a schematic summary of the maintenance tasks evaluation with a colour code for the tribological relevance in the period investigated. The crusher system is dominated by HT abrasive wear due to the falling and crushing of hot sinter. The sinter wagons suffer HT corrosion in combination with abrasive wear at the end of the sinter belt at the drop-off. The HT sieve and chutes are adjacent aggregates to the sinter belt and also have to sustain HT abrasive wear by the broken sinter which still has HT. The ventilation and exhaust emission system experiences erosive wear (sometimes in combination with corrosion). Conveyor belts are also mainly worn due to abrasion, temperatures here are low and materials are different (rubber). The apron conveyor and pug mills show some components with tribological interaction, but main problems have different focus.

More than ten percent of total maintenance costs of the sinter plant can be directly assigned to HT abrasive wear of components (sinter crusher, sinter wagons, HT sieve and chutes). The motivation of this work is to understand these HT abrasive wear mechanisms, in order to design improved wear protection solutions and reduce maintenance efforts in the future.

Tab. 16: Schematic of maintenance expenses and tribological relevance

	Plant priority	Maintenance	Maintenance frequency	Downtime	Downtime frequency	Total costs
Sinter belt	A	↑↑		↑↑	↑↑↑↑	↑↑
Sinter belt remains	A	~	~	↑	↑	↑
Crusher system	A	~				~
Sinter wagons	A	~			↑↑↑	
Electronics	A	↑	↑	↑↑		↑
Electrical installation	A		~	↑↑		~
Measurement and control systems	A-B	~	↑			
Emission control	A-B	↑	↑	↑		↑
Meros	B					
Filter	B	~				
Ventilation	A		~			
Conveyor belts	A	↑	↑↑	~	↑	~
HT sieve and chutes	A	~		↑	~	~
Apron conveyor	A			~	~	
Pug mills	A				~	

Abrasive wear dominated
High tribological relavance
Medium tribological relavance
Low tribological relavance

5.2. Comparison of wear phenomena in field with lab-scale abrasion tests

Abrasive conditions in the production of iron ore sinter are inevitable, as well as HT for the processing of the sinter. Grain size and abrasivity increases from the mixing of raw materials (ore fines, limestone, coke breeze) to the processed sinter [CAP73]. At the end of the sinter belt the sinter block size is the area of a sinter wagon by the filling height. The finished iron ore sinter is very abrasive and at HT after production. The sinter then is broken by the sinter crusher and fines are removed by the HT sieve. Especially these HT components are the subject of this work, namely the flooring of the sinter belt (grate bars), the sinter crusher and the HT sieve were different abrasion modes are suspected.

5.2.1. Sinter belt – grate bars

The grate bars are the flooring of the sinter belt and exposed to the high processing temperatures of the sintering as well as the corrosive gases produced during the process. At the end of the sinter belt, the finished sinter slides over the edge of the grate bars into the crusher system. The material of these grate bars is a HT and corrosion-resistant white cast iron and referred to as FeCrC within this work. Lifetime of the grate bars is limited by a minimal thickness: when the grate bars get too thin, they break during cleaning. The material loss of the grate bars can be put down to the abrasion at the drop-off edge as well as to HT corrosion. To maintain proper sinter conditions especially the ventilation slots between the grate bars must not close, which can happen due to oxide scale formation and deposit build-up.

High-stress abrasion or gouging is suspected at the grate bars, as loads are very high due to the large block of sinter at the drop-off. A comparison of a grate bar after seven weeks in plant service with a wear scar is given in Fig. 66. Wear behaviour is clearly different. In the plant, almost no signs of abrasion can be found in the middle of the grate bars. Neither abrasive embedding nor carbide breakage can be detected, but massive corrosive attack of the ferritic matrix, while the carbides are unaffected. At HT high-stress abrasion, on the other hand, intermixing with the abrasive is evident, as well as carbide breakage due to the high loads. Thus clearly abrasion is not the main failure criterion for the grate bars, but HT corrosion. The corrosives set free during the sinter process attack the grate bars, which leads to corrosion loss, scale formation and closing of the ventilation slots. HT corrosion in the sintering plant is a serious problem limiting the lifetime of the grate bars, but is beyond the scope of this work. A comprehensive study can be found in [ROJ15]. It is expected that the corroded surface has poor resistance against abrasion and is removed easily by the movement of the sinter, exacerbating wear loss.

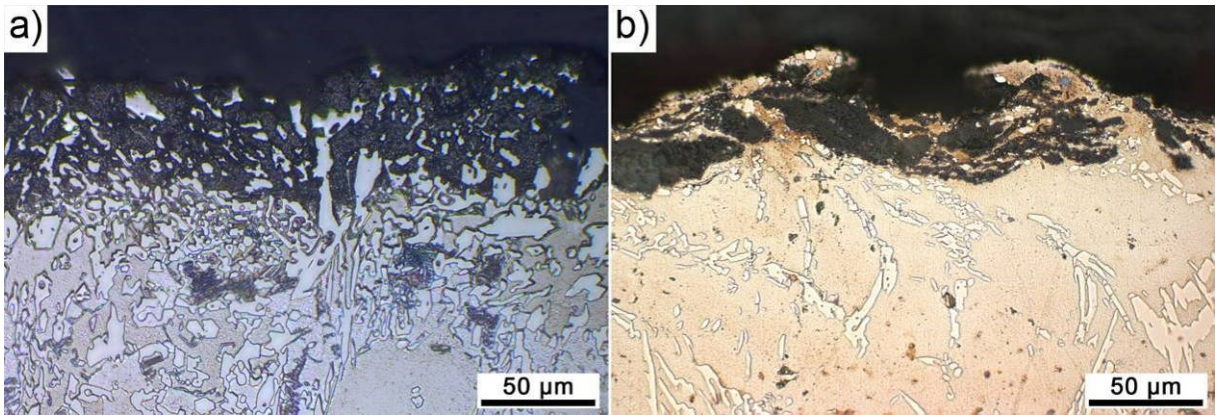

Fig. 66: LM cross sections comparing the wear on the sinter belt with HT-CAT specimen:
a) grate bar (FeCrC) after 7 weeks in service; b) wear scar of FeCrC after 550°C HT-CAT testing

At the drop-off edge of the sinter wagons, clear signs of abrasion can be found, as seen in Fig. 5. However also at this position similarities with HT-CAT testing are poor. From the deep wear grooves which are tens of mm long, it is suspected that loads there are even higher than in high-stress abrasion testing, and that the wear mechanism is gouging.

5.2.2. Crusher system

In the crusher system, the finished sinter is crushed to chunks <200 mm for further use in the blast furnace. The block of sinter in the size of the wagon is dropped from the sinter belt and hits the crusher grate and parts of the sinter crusher, while the impact energy is reduced by the pre-breakers. Suspected load conditions for the crusher are presented in Fig. 9 [SHA14]. On the backside of a crusher tooth impact occurs through the falling sinter cake, while the crushing is done by the opposite of the tooth. On the flanks, high-stress abrasion is suspected, as the sinter is pressed through the crusher grate and broken. At the counter part, the crusher grate, impact load on the top surface is present combined with abrasion. The side flanks are loaded by high-stress abrasion like the teeth flanks.

The impact-abrasion test HT-CIAT was especially designed to simulate the highest loaded surface of the crusher grate where the sinter impacts and the crusher presses it through the grate [WIN09-1, WIN09-3]. Damage analyses given in [KAT07, WIN09-3] indicate temperatures of 650-700°C in this application. The hypereutectic hardfacing applied as wear protection in the crusher grate (Fig. 10, Fig. 67a) shows brittle fracture of the large Cr-precipitations up to ~30 µm depth. Nb-carbides are affected until ~10 µm depth, and the behaviour of the matrix cannot be seen after this etching procedure. Some adhering sinter particles can be seen (reddish).

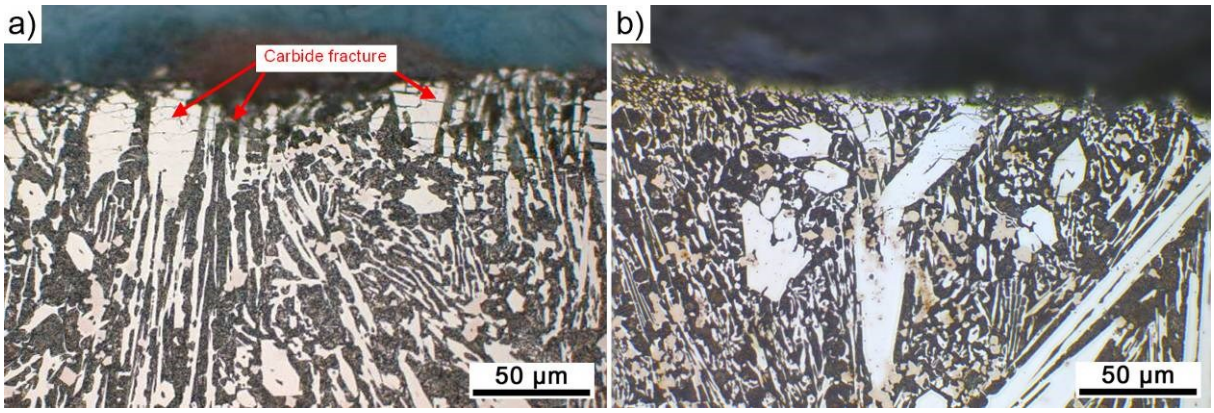

Fig. 67: LM cross sections (etched with Fe_3Cl) comparing the wear of the grate bar and HT-CIAT: a) crusher grate [cf. WIN09-3] after service; b) FeCrNbC after 700°C HT-CIAT

Direct comparison with the similar hardfacing FeCrNbC after HT-CIAT testing in Fig. 67b shows much related wear behaviour. After the HT-CIAT at 700°C large Cr-carbides also show cracking up to ~30 µm depth. Breaking of smaller Nb-precipitations was found in the first micrometres. Also some sticking abrasive particles on the surface can be seen on the far right of Fig. 67b. Although cracking is more pronounced after field usage, the wear mechanisms are very similar in the HT-CIAT. The more frequent cracking in the field may be entailed by ageing effects due to long-term use.

On the side flanks, wear of mild steel substrate of hardfacings is published [KAT07]. In Fig. 10b clear signs of plastic deformation and intermixing with abrasive and oxide can be seen, extending >100 µm depth. This indicates high-stress abrasion. The mild steel is not oxidation resistant at these HT, very soft and also poor abrasion resistance can be suspected. Unfortunately no direct comparison with any material of this work can be done. Thus choice of test load for HT-CAT cannot be directly related to the real system. The most similar alloy FeCrC with ferritic matrix but significant hardphase amount shows MML formation up to ~30 µm depth. As FeCrC has significantly higher hot hardness and hardphases, both limiting MML formation, the chosen load may be in the correct range simulating high-stress abrasion on the crusher grate and –teeth.

5.2.3. Sinter sieve

The HT sieve for screening the crushed sinter is a necessary aggregate to deliver the correct size of sinter to the blast furnace. The fraction <5 mm is returned to the sinter process. [CAP73] The sieve is generally located directly after the crushing (cf. Fig. 1). A detailed damage analysis by the author et al. is published in [VAR15-2]. Temperatures in the observed sieve are in the range of 200-300°C, larger sinter chunks may have up to 600°C. Due to the

long transport route in the investigated plant temperatures are moderate. Other steel plants with the sieve located directly after crushing may have to deal with average temperatures up to 700°C, like in the crusher system.

Wear loss on the sieve's surface was found to be minor; the lifetime limiting factor is the widening of the sieve cavities. I.e. the low-stress abrasive wear on the surface is insignificant compared to erosive wear of the cavities. The angle of impact varies from the cavity edge downwards. First contact may be normal impact, following impacts within the cavity have to be shallower. The energy of the impacts is difficult to estimate, as both particle speed and size can vary in a wide range. Hence comparability with the parameters from the erosion test is difficult to prove. Test temperature of 300°C is in the correct range for the investigated sieve. Particle size in the test is much smaller than 5 mm (0.1-0.3 mm), therefore the speed was chosen high to obtain higher impact energies. Estimations taking the different abrasives into account lead to impact energies one order of magnitude higher in the test, which was necessary to obtain results within reasonable times.

A similar alloy as used in the real-field was chosen for testing (FeCrNbC). Comparison of wear mechanisms and extent of wear is nearly impossible, because the microstructure in the loaded zone of the cavities is altered by the cutting process as seen in Fig. 12. The hardphase-rich complex alloyed microstructure is diluted with the substrate and hardphases are fused. I.e. the wear resistance of the alloy is locally impaired by the processing of the cavities. Nevertheless, some positions on the sieve were found, where, after the thermal cutting process, grinding to the desired cavity width was necessary, entailing unaltered micro-structure. The extent of wear at these positions is significantly smaller than at the altered microstructure. Hence, in order to maintain wear protection at the cavities where it is needed, non-thermal cutting techniques are necessary.

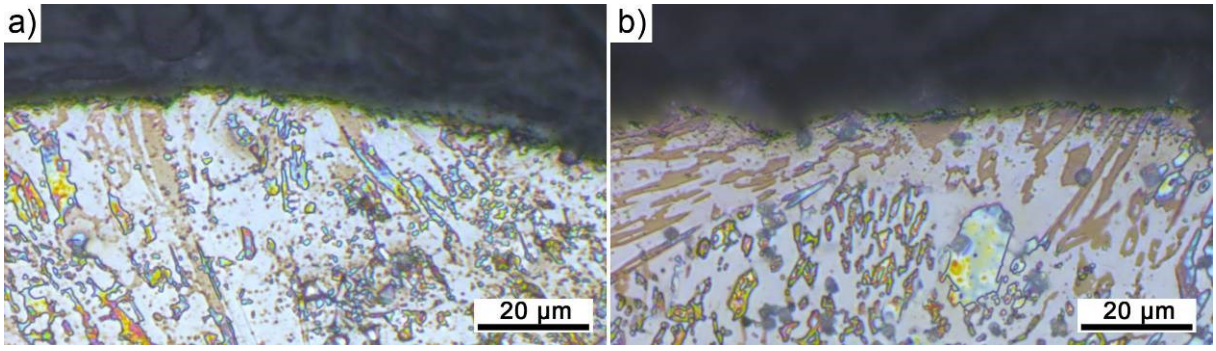

Fig. 68: LM cross sections comparing the wear of sinter sieve cavity edge and oblique HT-ET:
a) cavity edge after 7 weeks in service; b) wear scar of FeCrNbC after 300°C oblique ET (30°, 80 m/s)

Fig. 68 compares the grinded position of a sieve cavity with the 300°C oblique ET of FeCrNbC. Wear mechanisms are very similar for the field sample and after ET: hardphases and matrix are worn uniformly at both conditions. Cracking of the large hardphases is hardly visible at this magnification and limited to the first micrometres for both conditions. Hence, it can be concluded that the ET simulates the conditions at the sinter sieve cavities sufficiently. Further applications with high erosive component within the sinter plant are e.g. the side walls of the crusher system, the suction boxes of the sinter belt or generally the exhaust gas system.

5.3. Wear rates for various abrasion modes

Volume loss for various abrasion modes was found to be very different for the materials and temperatures investigated. As chapter 4.3 gives wear rates of the materials in detail, a direct comparison of abrasive wear loss under the various loads should be discussed here. For this purpose, the wear rates of the materials were normalised to the best-performing alloy at a condition, i.e. the best relative wear rate is one and all others are worse by a certain factor.

5.3.1. Comparison of abrasion modes at room temperature

This is plotted for RT in Fig. 69. The best-performing material at high-stress abrasion is FeCrCoC. At impact-abrasion, material FeCrNbBC-GMAW is superior so that the results had to be plotted on the second y-axis. Best material at oblique erosion is FeCrNbBWC-PTA, and at normal erosion FeCrC. Generally at all abrasion modes (except impact-abrasion), wear rates of the materials are maximally doubled compared to the best alloy. Due to the superior performance of FeCrNbBC-GMAW at impact-abrasive condition, the worst wear rates are 17× higher (FeCrC).

At RT, the material **FeCrC** shows best wear resistance at **normal erosion** (90°), also high-stress abrasion resistance is in a good range. Oblique erosive (30°) wear is nearly doubled compared to the best material, and impact-abrasive wear is worst of all materials (factor 17 to the best performance). The Ni-base cast material NiCrW is not superior at any condition. Normal erosion resistance is comparable to FeCrC. High-stress abrasion wear loss is ~35 % higher than the best (FeCrCoC), impact abrasive wear is ~16× higher than FeCrNbBC-GMAW, and oblique erosion 70 % higher than the best. The martensitic **FeCrCoC** has the best performance at **high-stress abrasion**, nevertheless, performance at other conditions is relatively unbeneficial. It is 10× higher at impact-abrasive wear, 80 % higher at oblique erosion, and ~50 % higher at normal erosion compared to the best materials at these conditions. The Co-base CoCrWC shows good behaviour in high-stress abrasion. At oblique

erosion (30°) wear rates are ~35 % higher and normal erosion 50 %. Wear rates at impact-abrasion are about 10× higher than the best alloy.

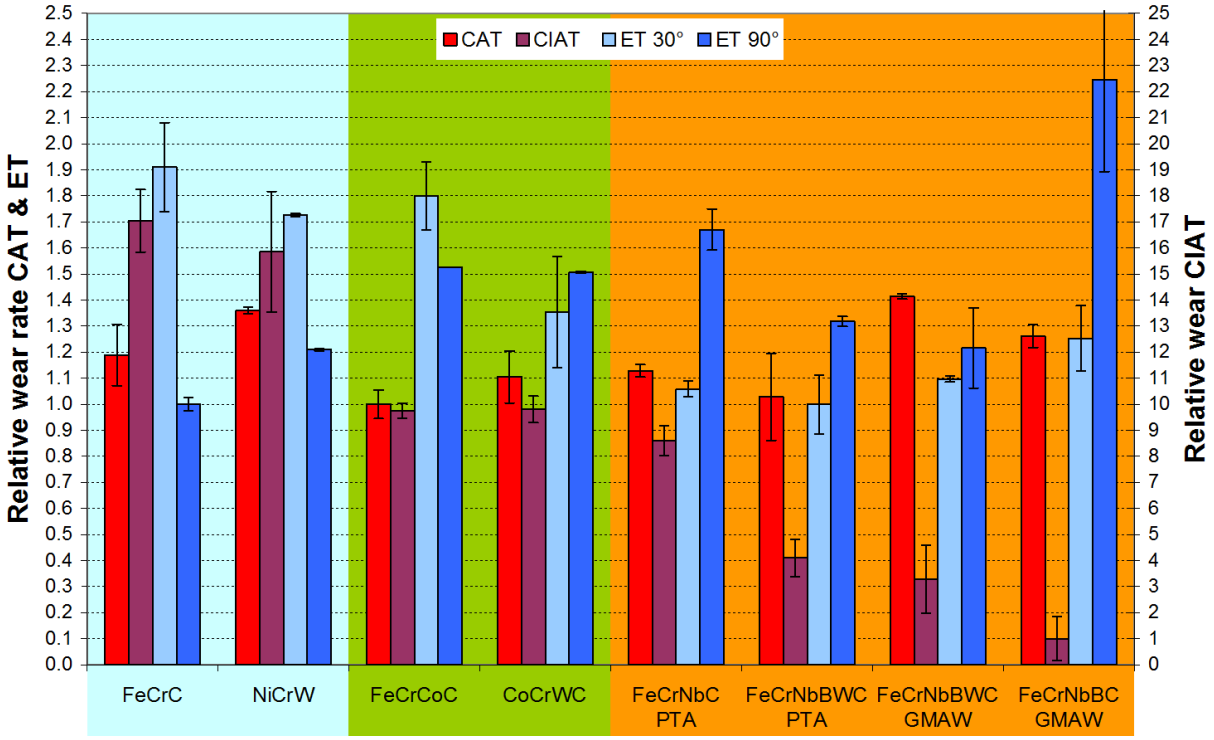

Fig. 69: Relative wear rates at RT for high-stress abrasion, impact-abrasion and 80 m/s erosion

The PTA-welded hardfacings **FeCrNbC and FeCrNbBWC** show very good behaviour at **oblique erosion** (30°), also high-stress abrasion rates are low at RT. Impact abrasive wear of FeCrNbC-PTA is ~8.5× higher and of FeCrNbBWC-PTA ~4× higher as FeCrNbBC-GMAW. Normal erosive wear is relatively high at FeCrNbC-PTA (65 % increase) and moderate at FeCrNbBWC-PTA 30 % higher. Both oblique and normal erosive wear performance is relatively good for FeCrNbBWC-GMAW. On the other hand, high-stress abrasive wear is worst in the test field. Impact-abrasive wear resistance is good, 3× the FeCrNbBC-GMAW wear rate. **FeCrNbBC-GMAW impact-abrasion** wear resistance is best at RT. Both high-stress abrasion and oblique erosion are about 25 % higher than the best materials. On the other hand, the normal impact abrasive wear of this material is the highest in the test field with more than doubled wear rate of the best material.

5.3.2. Comparison of abrasion modes at elevated temperatures

Comparison of wear rates at highest testing temperatures at the various tests are given in Fig. 70. Like before, data are normalised to the lowest wear rate measured at the certain abrasion mode and temperature. With the exception of HT impact-abrasion, wear rates have higher

differences between the materials investigated. High-stress abrasion covers a range of ~2.5× (FeCrNbBWC-GMAW) higher rate than the best material (CoCrWC). The factor at impact-abrasion at HT is 2.9 (compared to 17 at RT) with FeCrNbBWC-GMAW being the best and FeCrC the worst alloy tested. Differences at oblique erosion are smallest, FeCrNbBWC-PTA featuring best performance and FeCrCoC worst, but just by 60 %. On the other hand, at normal erosion, differences are largest: FeCrC shows best wear resistance and FeCrNbBWC-PTA worst by a factor of ~3.1.

HT wear behaviour of **FeCrC** cast alloy is generally very good, except at impact-abrasion. Wear resistance at erosive wear is superior at both conditions: FeCrC showed to be the best of all materials investigated **at normal erosion** (90°) and only ~10 % worse than the best (FeCrNbBWC-PTA) at oblique impact. Also high-stress abrasive wear results lie in a very good range with just ~30 % higher wear rates than the best (CoCrWC). These beneficial behaviour stands in contrast to having the worst HT impact-abrasive wear behaviour of all materials tested, i.e. 2.9× higher wear rate than the best FeCrNbBWC-GMAW.

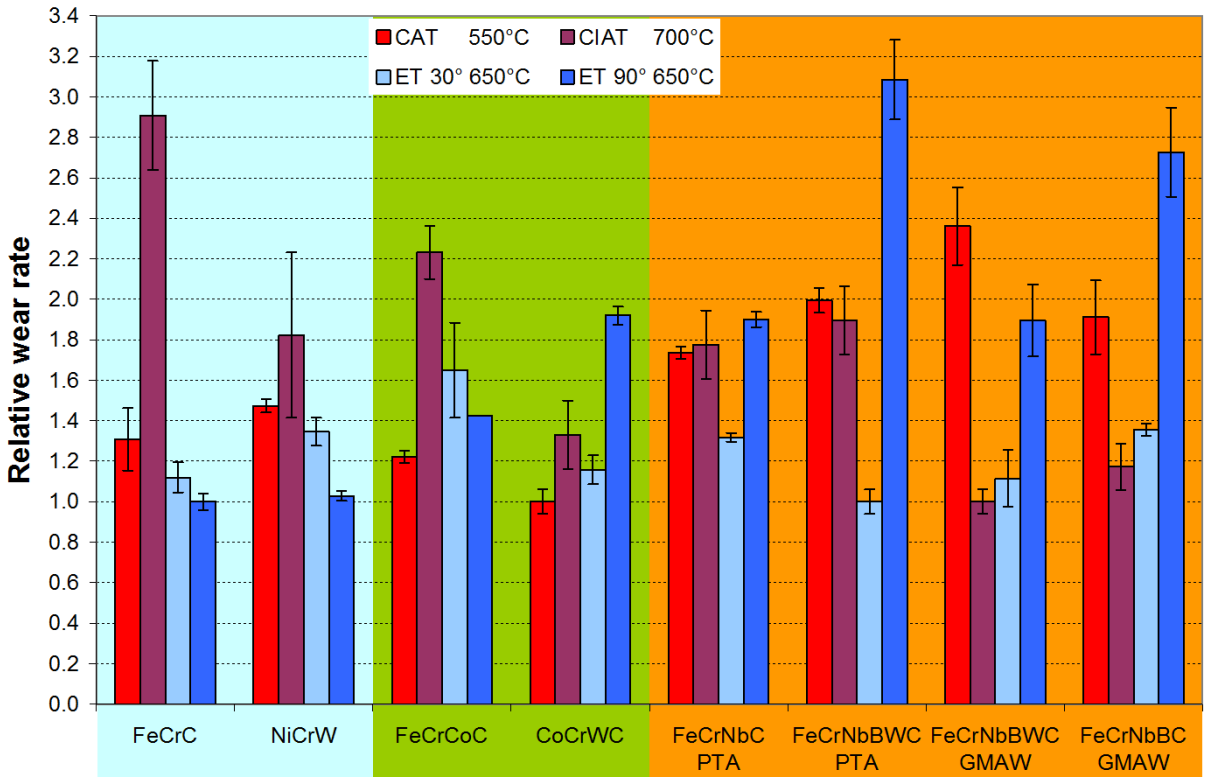

Fig. 70: Relative wear rates at HT for high-stress abrasion (550°C), impact-abrasion (700°C) and erosion (650°C)

NiCrW shows just insignificantly higher wear rates at **normal erosion** (90°), and can be set equal to the best FeCrC. Oblique erosion (30°) results are higher with ~30 % wear increase

compared to the best. High-stress abrasive results are slightly worse than FeCrC. NiCrW on the other hand shows much better performance in impact-abrasion than the other cast alloy FeCrC. Wear at this condition is ~80 % higher than the best FeCrNbBWC-GMAW. HT wear behaviour is not superior at any condition for FeCrCoC, but high-stress abrasion shows about 20 % higher wear rates than the best. Impact-abrasive results are worse by a factor of 2.2 compared to the best material, oblique erosion by 60 % and normal erosion by 40 %. The Co-base alloy **CoCrWC** shows best **high-stress abrasion** wear resistance of all materials investigated. Furthermore, impact-abrasive and oblique erosive wear resistance are good for this alloy. Impact-abrasion leads to ~30 % higher wear rates compared to the best alloy and oblique erosion ~15 % higher. Normal erosion on the other hand shows higher wear rates by a factor of 1.9 compared to the best material.

FeCrNbC-PTA shows unbeneficial wear behaviour at all abrasion conditions investigated. High-stress abrasion and impact-abrasion results are both 70-75 % higher than the best alloys. Oblique erosion is 30 % higher, and normal erosion is 90 % higher. Nevertheless, the normal erosion result is the best for the carbide-rich hardfacings. **FeCrNbBWC-PTA** shows the best **oblique erosion** wear resistance of all materials investigated. However, the material does not tolerate high-stress abrasion, leading to doubled wear rate compared to the best. The same can be said for impact-abrasion with 90 % increase. Most detrimental is normal erosion, resulting in the highest wear loss measured, i.e. 3.1× higher than the wear rate measured for the best material FeCrC. The same alloy welded by GMAW (**FeCrNbBWC-GMAW**) shows best performance in **impact-abrasive** environment. Also oblique erosion results are just 10 % higher than for the best alloy. By contrast, the high-stress abrasion leads to worst wear rates of all materials investigated with ~2.4× higher wear rate than the best material. Normal erosion resistance is substantially better than for the PTA welded alloy of the same type, nevertheless the wear rate is 90 % higher than for the best material. The other GMAW-welded alloy FeCrNbBC-GMAW also shows very good impact-abrasion wear resistance, wear rates are ~15 % higher than for the best alloy. Oblique erosion is significantly higher than for FeCrNbBWC-GMAW and has ~35 % increased wear than the best alloy. High-stress abrasion is ~90 % higher than for the best CoCrWC. Normal erosion is detrimental for the material resulting in ~2.7× higher wear rates than for FeCrC.

5.3.3. Range of wear rates of the materials investigated

At certain conditions, variations in the wear rates between the materials are high, especially at low temperatures in impact-abrasive environment. Fig. 71 quantitatively compares the best materials with the worst for a certain abrasion mode and test temperature.

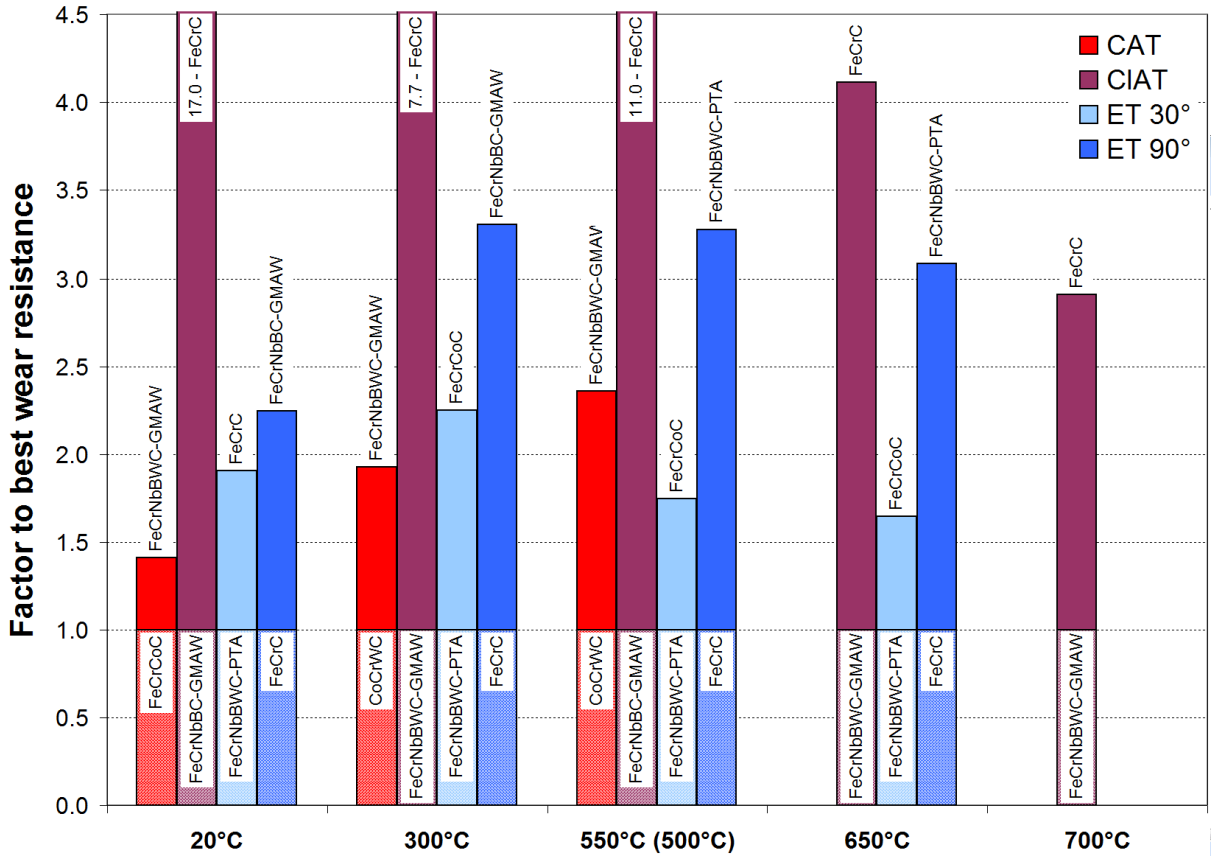

Fig. 71: Comparison of best wear resistant materials (bottom) with highest wear rates at the various tests and temperature conditions

The materials in the bottom row of Fig. 71 represent the best material for each condition and the bars factor of the increased wear rate for the worst material. This is plotted for the various tests and temperature steps. (Testing of HT-CIAT was carried out at 500°C, while the other tests were performed at 550°C.) It can be seen clearly that the best as well as worst materials can change with temperature increase. The deviation range for oblique erosion (30°) is the smallest, also high-stress abrasion is in the same range (but was limited to 550°C). Differences in impact-abrasion are extreme, especially at temperatures up to 500°C. Also the deviation range for normal erosion (90°) is high. From this range it can be concluded that for impact-abrasive condition a high hardphase content is necessary to withstand wear, whereas especially at normal erosion a high hardphase content is detrimental.

It is interesting to observe the evolution with temperature of the range between best and worst materials. At high-stress abrasion, differences increase from 40 % at RT to a factor of 2.4 at 550°C. This means that the MML forming materials keep their high wear resistance, while the brittle hardfacings become much worse with temperature. Contrary is the evolution at impact-abrasion, which starts with a very high factor of 17 and decreases to 4.1 at 700°C. Here the outstanding performance of the very hard GMAW alloys at low temperatures lead to the high range for the soft cast materials. At very high testing temperatures, the microstructural changes of the hardfacings are much more pronounced than for the heat resistant cast materials, leading to weaker wear protection entailing smaller variations of the wear rates.

At oblique erosion, wear rates show the largest deviation at 300°C, 2.3× times the best wear resistance. At RT, FeCrC shows the worst behaviour, while it is FeCrCoC at higher temperatures. I.e. the material without hardphases show unbeneficial behaviour in this environment, but differences at oblique erosion are the smallest for all of the abrasion modes investigated. For normal erosion, variation peaks at 300°C testing with 3.3×. At all temperatures, FeCrC shows the best performance, although it nearly doubles its wear rate in this field. I.e. wear loss of the hardfacings increases faster with temperature than the cast alloy.

5.3.4. Competitiveness of wear-protective solutions investigated

Comparison of the results found within this work with other HT materials reported in literature is challenging as there is no standardised HT test procedure for any of the abrasion processes investigated. This means that even if the same test rig is used, test parameters may be chosen differently, which can lead to different wear mechanisms and wear rates.

5.3.4.1. Erosive wear

Best comparison can be made for erosion testing as test parameters are chosen in accordance with a GOST standard [GOS79] extended to HT testing. Katsich et al. [KAT09] uses the same test conditions (30°, 90° impact; 80 m/s velocity; 0.1-0.3 mm quartz; RT-650°C) on two of the same carbide-rich hardfacings, but deposited with other welding parameters, e.g. on mild steel substrate. The materials used there were hypereutectic FeCrNbC and complex alloyed FeCrNbBWC. A direct comparison at normal impact is given in Fig. 72, and oblique erosion in Fig. 73.

Wear rates obtained at RT-normal impact were in the range of 30-35 mm³/kg in [KAT09], which is slightly higher than results of materials tested here (20-27 mm³/kg). Results at 650°C are much higher for FeCrNbC in [KAT09] than for the similar material presented here.

Material FeCrNbBWC shows about 80 mm³/kg, while in the experiments here 55 mm³/kg was reached for GMAW (but ~90 mm³/kg for PTA). The wear rate for FeCrNbC is almost doubled compared to the results here. Results at oblique erosion for FeCrNbBWC are almost identical to wear rates found in this work for FeCrNbBWC-GMAW, the 650°C wear rate is ~10 % higher in [KAT09]. This is also similar for FeCrNbC, but with 10 % less wear loss in [KAT09] than FeCrNbC-PTA in this work. So it can be expected that the wear resistance of materials investigated here is at a very good level for this type of hardfacings.

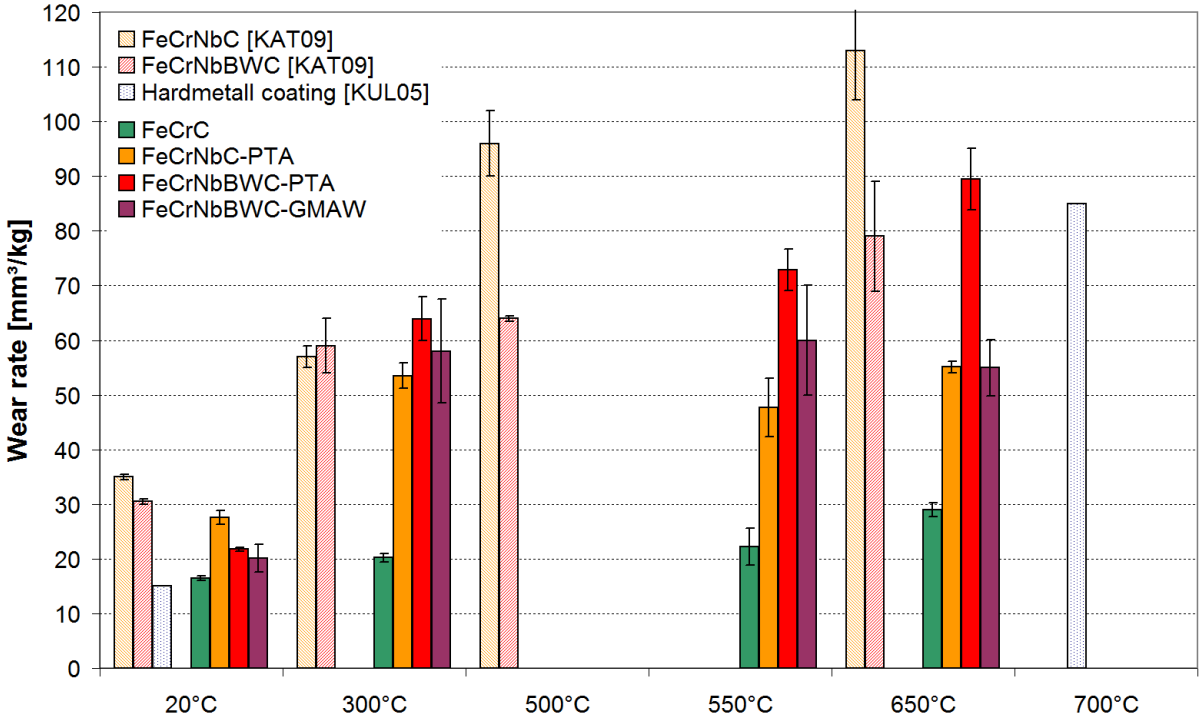

Fig. 72: Direct comparison of normal erosion (90°) wear rates at 80 m/s of best materials in [KAT09, KUL05] with best alloys tested within this work

Similar hardfacings were also investigated by Badisch et al. in [BAD10], and the influence of thermal ageing on the wear rate in [WIN09-2]. Wear rates of FeCrNbBWC are higher (30 mm³/kg) for RT normal impact. The reported RT wear rate for FeCrNbC is about double than in this work. At 650°C wear rate of FeCrNbBWC is also higher in [WIN09-2] and FeCrNbC is tripled compared to FeCrNbC-PTA. It can be assumed that with the choice of ideal deposition parameters during welding of the hardfacing wear rates can be optimised in a wide range. Thermal ageing was not studied within this work, however, its influence on the wear rate was studied by Katsich [KAT07] and Winkelmann et al. [WIN09-2]. Especially for the hardfacings, thermal ageing increases HT oblique erosion wear rates. Best normal erosion results of the alloys investigated in [BAD10] were found for austenitic steel with values <30 mm³/kg at all test temperatures (RT-650°C) because of MML formation.

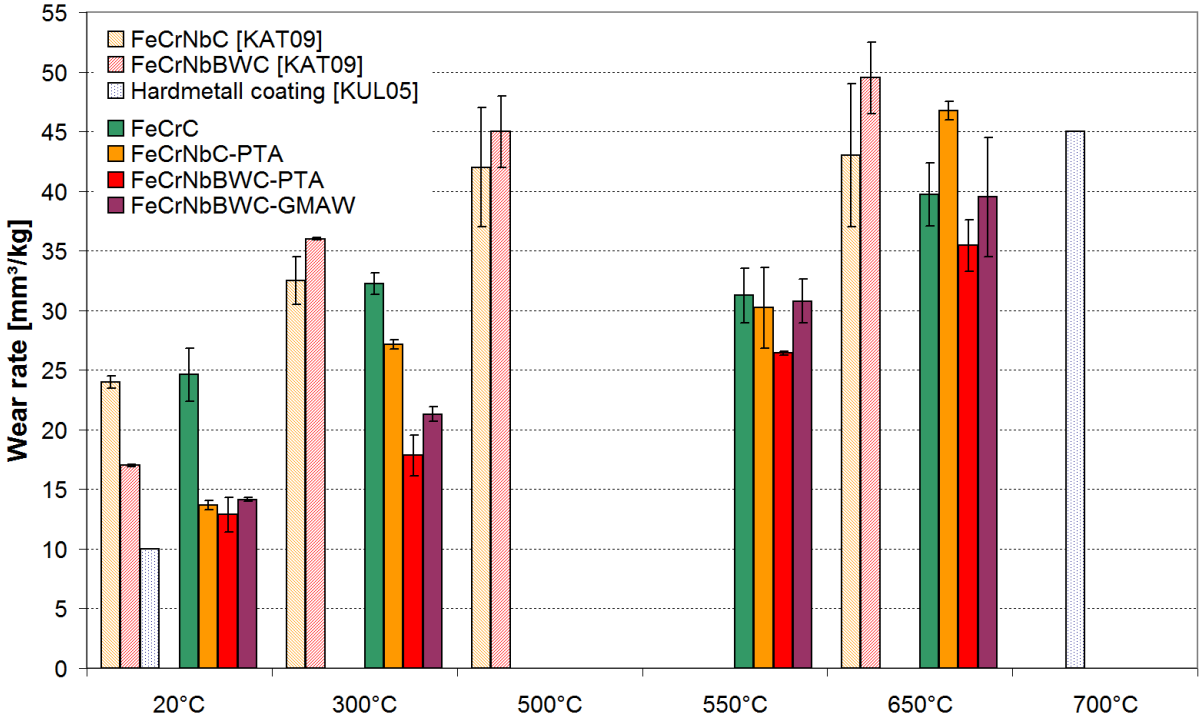

Fig. 73: Direct comparison of oblique (30°) erosion wear rates at 80 m/s of best materials in [KAT09, KUL05] with best alloys tested within this work

Similar test parameters (with 700°C HT testing instead of 650°C) are chosen in the work of Kulu et al. in [KUL05], applied to various hard coatings (spray coated, including hardmetals). Best erosive wear resistance was found for the hardmetal coatings with 10 mm³/kg at oblique and 15 mm³/kg at normal impact, RT (see Fig. 72 and Fig. 73). At 700°C 45 mm³/kg at oblique and 85 mm³/kg at normal impact are measured. That means that RT values are slightly lower for this hardmetal coating, as best values measured at the materials in this research reach ~13 mm³/kg at oblique impact (FeCrNbBWC-PTA) and 16.5 mm³/kg at normal impact (FeCrC). Assuming that wear rates will not increase drastically from 650°C to 700°C, the behaviour of the HT tests can be compared. At oblique impact, also FeCrNbBWC-PTA shows the best results with 35 mm³/kg at 650°C testing. Still, equal performance of this material at 700°C cannot be guaranteed, as a distinct hardness drop was measured in this region. For normal impact on the other hand, very good values of 29-30 mm³/kg were measured for FeCrC and NiCrW, where especially for the Ni-base alloy no significant change in wear behaviour can be suspected for 700°C. This means an almost 3× better wear resistance than the hardmetal spray coating.

Cermets are known for their extraordinary erosion resistance. This was studied on various cermets by Hussainova et al. in [HUS01], but only at RT. Best performance was shown by a WC-Co cermet with wear rates <0.001 mm³/kg, which is orders of magnitude superior to all

the alloys tested in this work. However for these materials, the temperature behaviour of the tungsten carbides must be kept in mind, as they easily oxidise at HT [WIN10]. Also the TiC based cermets, which can withstand HT, showed excellent erosion resistance at RT with 0.002 mm³/kg for oblique and 0.006 mm³/kg for normal impact.

5.3.4.2. Impact-abrasive wear

Different impact-abrasive wear tests cannot be successfully compared. E.g. the impeller-tumbler impact-abrasion test [RAT13] aims at the evaluation of the blunting resistance, while the HT-CIAT utilised here investigates surface damage. Nevertheless some publications are available since the paper of Winkelmann et al. [WIN09-1] first introduced the test in 2009 for experimental simulation of HT impact-abrasive wear in crusher systems of sinter plants. Test conditions are kept constant for most of the related papers known and are therefore directly comparable with the results of this work. In [WIN09-1], hardfacings of the FeCrNbBWC and FeCrNbC type, which are similar to both materials in this work, are tested at RT and 600°C. The lowest wear loss there was measured as ~3 mm³ for FeCrNbBWC at RT, which is slightly higher than FeCrNbBWC-GMAW in this work (2 mm³). RT wear loss of FeCrNbC in [WIN09-1] is much lower at 3.5 mm³ than FeCrNbC-PTA at 5.2 mm³, which can be put down to the lower hardness of ~780 HV10 of the 1-layer PTA welded sample compared to 880 HV10 in [WIN09-1]. HT values cannot be directly compared, as in this work a temperature of 650°C was used, but differences in this temperature regime are thought to be minor. FeCrNbBWC wear was measured as 7.5 mm³ in [WIN09-1], which is much higher than 4.9 mm³ here. FeCrNbC with 11.5 mm³ at 600°C in [WIN09-1] is higher than 9 mm³ of this work. It is not known if hot hardness of the alloy in [WIN09-1] drops faster than the material within this work, as no hardness data are given there.

An alloy of FeCrNbBWC was again tested by Winkelmann et al. in [WIN10]. This time at various temperature steps up to 750°C, and also the first hot hardness data of such alloys are presented there. Wear loss of best performing materials is directly compared to the two alloys with the best wear resistance of this work in Fig. 74.

The FeCrNbBWC from [WIN10] is of the same chemical composition as in this work, but welding parameters may be different (RT hardness is 900 HV10 compared to 765 HV10 for the PTA welded and 1070 HV10 for the GMAW in this work). Also shown in Fig. 74 is the best material of the test series in [WIN10], a Ni-base alloy with 60 wt.% of synthetic WC added during welding. For RT the alloys of this work show less wear, especially the FeCrNbBC-GMAW with superior wear resistance to impact-abrasive wear under this condi-

tion. The wear rate of the FeCrNbBWC in [WIN10] rises much faster with temperature than the hardfacings deposited here. Even the PTA welded FeCrNbBWC alloy of this work (with much higher wear loss than the FeCrNbBWC-GMAW) shows lower wear at all temperatures investigated. Interesting in [WIN10] is the Ni-base alloy with the synthetic WC hardphases, which shows excellent HT-wear resistance, comparable to FeCrNbBWC-GMAW of this work. Nevertheless, the WC reinforced material shows massive oxidation at the highest testing temperature, i.e. despite its temperature-stable Ni-matrix it cannot be used at these HT conditions. This direct comparison of three welding conditions of FeCrNbBWC shows clearly the importance of optimisation of the welding procedure. With the very same alloy wear can be more than halved at enhanced temperatures for this impact-abrasive condition.

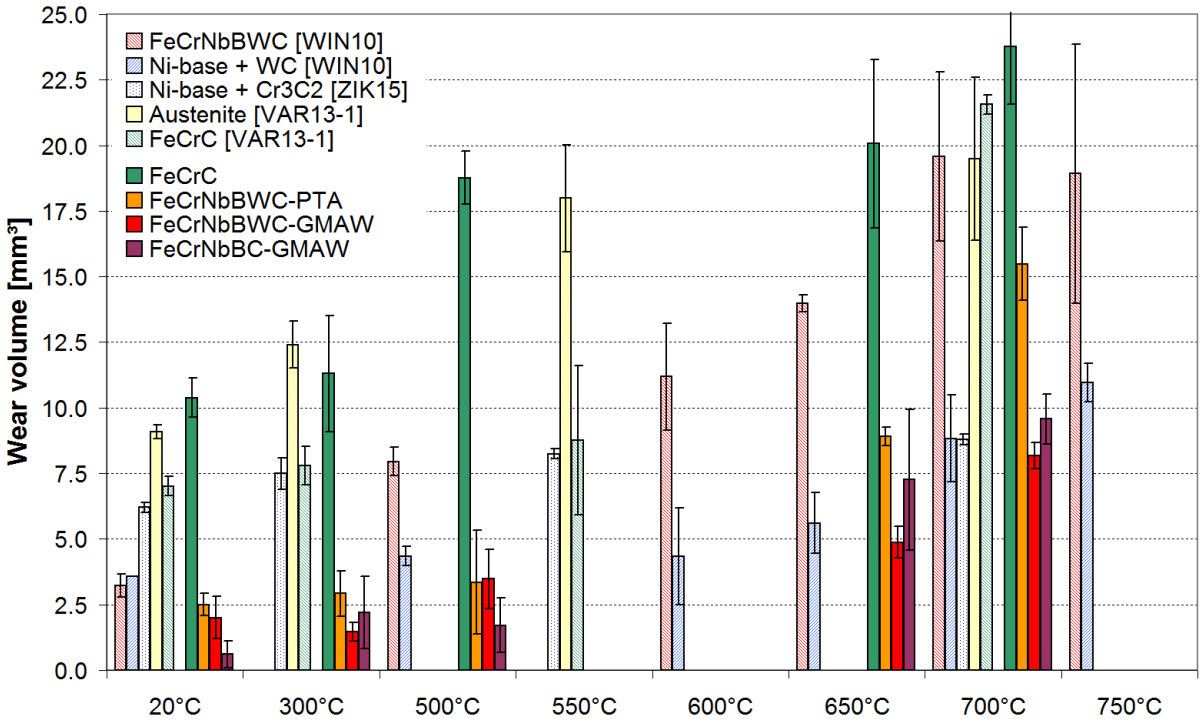

Fig. 74: Direct comparison of HT-CIAT wear of best materials in [WIN09-1, ZIK15, VAR13-1] with alloys tested within this work

Zikin et al. studies in [ZIK15] PTA welded hardfacings with addition of Cr-carbides. The least wear loss at RT of 6 mm³ was found for a Cr-carbide reinforced Ni-matrix. Values are significantly higher than the WC reinforced Ni-base of [WIN10] until 550°C testing, but at 700°C testing the Cr-carbide reinforced material becomes superior with just ~9 mm³ wear loss (because of the pronounced oxidation of WC at this temperature). This is at the same level as the best alloy within this work (FeCrNbBWC-GMAW).

Wear loss of austenite was found to be significantly higher in impact-abrasive conditions as reported by the author et al. in [VAR13-1]. Still, the investigation is of interest as MML formation is studied in great detail there for austenitic steel grade, grey cast iron and FeCrC-type cast steel. The FeCrC-type shows lower wear rates at low temperatures (~7 mm³ at RT, ~9 mm³ at 550°C) than in this work, which increases to the same level at 700°C (22 mm³ in [VAR13-1] versus 23.8 mm³). Hardness after this casting procedure was found to be ~420 HV10 at RT, which is significantly higher than the material tested here (275 HV10), this may be the reason for the lower wear loss in [VAR13-1]. MML thickness was very limited due to the high hardness at RT. At 700°C higher values were measured (~60 µm compared to ~20 µm in this work). I.e. MML formation is strongly dependent on the material condition (as the chemical composition within the two studies is nearly identical). MML formation for the austenitic grade was found to be very pronounced reaching 90 µm at 700°C testing. The grey cast iron shows very high wear loss of 18 mm³ at RT, which is far worse than the worst material within this study (10.4 mm³-FeCrC). Wear of the cast iron further increases to 35 mm³ at 700°C testing (23.8 mm³-FeCrC). MML formation was found to be hindered by the microstructure of the grey cast iron: the hard cementite phase makes it impossible to embed abrasive as wear protection.

5.3.4.3. Three-body abrasive wear

HT high-stress abrasive wear investigation by use of an modified ASTM G65 apparatus was first published by the author in 2011 [VAR11]. Shortly afterwards, a similar test rig was introduced by Antonov et al. [ANT12]. There the wheel diameter is significantly lower (85 mm) and 10 mm wide (instead of ø 232 × 12 mm). A more angular abrasive is used as well. Loads in [ANT12] were chosen as 9.8 N and 196 N, respectively, i.e. different contact parameters compared to the setup used in this work. It can be suspected that loading conditions are subcritical for the low load while the pressures at 196 N load are far higher, leading to higher wear loss compared to this work. The difference in wear rates can also be due to the different abrasive used, which is of more angular shape than the Ottawa sand used in this work. Sharp edged abrasives are known for their increased abrasivity [KEL01].

Direct comparison can be done with the previous works by the author et al. [VAR11, VAR13-1, VAR13-4]. Gray cast iron was found to behave very unbeneficial under HT high-stress abrasion. Wear rates of 0.14 mm³/m at RT up to 0.17 mm³/m at 550°C were measured in [VAR13-1, VAR13-4], which means an almost 5× higher wear rate than best alloys of this work. In [VAR11] a Ni-base alloy with synthetic WC deposited via PTA-technology, as well

as a FeCrNbBWC type were investigated. A direct comparison of reported wear rates with findings of this work is shown in Fig. 75. HT wear rates of FeCrNbBWC-PTA of this work are identical with values found at [VAR11], but RT wear rate is significantly lower with 0.2 mm³/m as reported in [VAR11]. This may be put down to slightly higher hardness. The Ni-base with WC reinforcement shows significantly higher wear rates than the complex alloyed material, i.e. ~0.06 mm³/m at RT, but lower temperature dependence, entailing ~0.075 mm³/m at 550°C. Also abrasive embedding is studied in [VAR11], but is limited for these two alloys with <40 % surface coverage at the highest testing temperature.

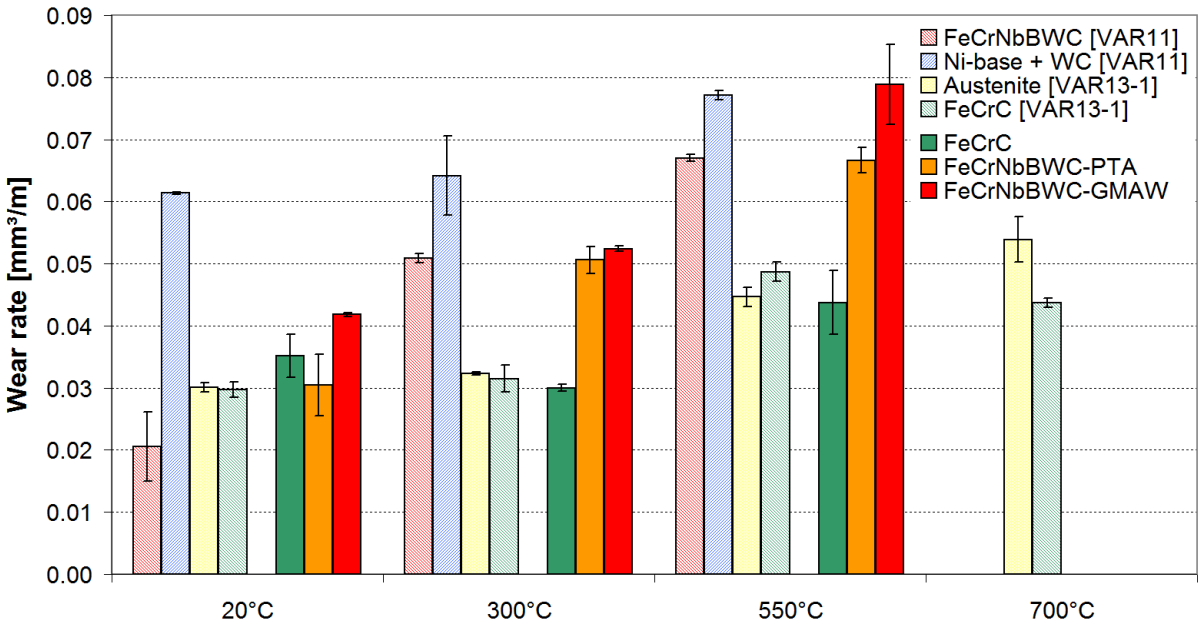

Fig. 75: Direct comparison of HT-CAT wear rates of best materials in [VAR11, VAR13-1] with alloys tested within this work

An austenitic steel tested in [VAR13-1] shows excellent wear resistance up to HT (Fig. 75). It is at the same level as FeCrC-type (similar material as in this work) up to 550°C testing, albeit no hardphases are present within the austenitic steel. Just at very HT of 700°C the austenite is outpaced by the FeCrC-type (0.055 mm³/m austenite; 0.044 mm³/m FeCrC). MML formation was found to improve wear resistance of these two materials and was most pronounced for the austenite, reaching a thickness of 37 µm at 550°C. At FeCrC ~25 µm thickness was found, which is on the same level as in this work (23±11 µm). This means that MML formation is repeatable for certain abrasive conditions.

5.4. Wear phenomena in abrasive contact and influence of MML

Wear behaviour of softer materials, i.e. the cast group and Co-family, is shown to be different than the carbide-rich hardfacings for all of the abrasive conditions investigated within this

work. While for the carbide-rich hardfacings brittle behaviour dominates the wear process, the materials with low hardphase content show plastic behaviour and formation of MML, which may lower material removal during abrasive process.

5.4.1. Wear phenomena in high-stress abrasive environment

As example, FeCrC and FeCrNbBWC-PTA after HT-CAT testing are compared in Fig. 76. FeCrC stands for one of the softest materials in the test matrix with low amount of hardphases and FeCrNbBWC-PTA for one of the carbide-rich materials with high hardness for all temperatures investigated, as visible in the hot hardness measurements (Fig. 49). The softer materials, also containing low amount of hardphases, experience the embedding of abrasive for all test conditions, while the hardphase-rich materials do not show this behaviour.

Under high-stress abrasion the cast alloys FeCrC and NiCrW as well as FeCrCoC show the formation of a MML already at RT. The extent of the MML increases with ascending temperature. As found in [VAR13-1] MML formation is impeded by carbide regions. This is also clearly visible in Fig. 76a, where the MML could only be found in matrix regions, but not at the carbide network. Polak et al. [POL08] reported a strong influence of the inter-particle distance between the hardphases on low-stress abrasive wear rates, but due to the formation of MML in the high-stress environment investigated here, the inter-particle distance (Fig. 44) was of minor importance. At higher temperatures also the small carbides of this alloy get intermixed in the MML and almost the whole surface is covered by this in-situ formed layer. Despite the high hardness of the martensitic hardfacing FeCrCoC, pronounced MML formation (90-97 % coverage) is present at all temperatures. This may be put down to the high hardness of the abrasive, which is for all conditions tested harder as the martensite (Fig. 26). CoCrWC shows first signs of MML formation at RT, which is more pronounced at HT. Nevertheless, compared to the alloys with less hardphases, the MML coverage is much smaller. This may be put down to the very fine structure of the carbide network in CoCrWC, with matrix areas of ~10 µm extent hindering embedding of larger abrasive particles. An extreme example is grey cast iron: despite its low hardness, MML formation was found to be impossible because of the pearlitic structure with its fine alternating substructure of cementite and ferrite, where the cementite renders abrasive penetration and embedding very difficult [VAR13-1]. So the hardphase content of ~20 % may be a critical threshold for MML formation under high-stress abrasion. This gets clearer when further observing the carbide-rich hardfacings, where now signs of MML formation could be found. Even for FeCrNbBC with just some percent more hardphases than CoCrWC MML was now detected.

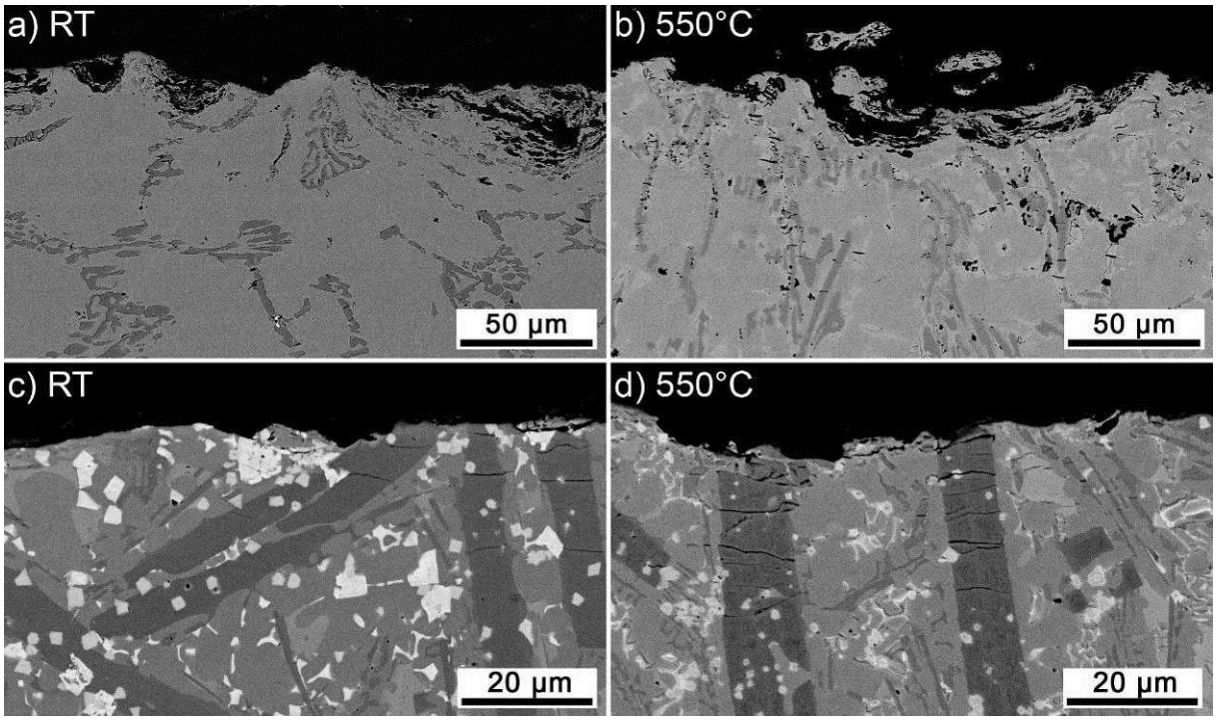

Fig. 76: Wear mechanisms at HT-CAT (SEM-BSE) at the example of FeCrC:
a) RT, b) 550°C; and FeCrNbBWC-PTA: c) RT, d) 550°C

The carbide-rich materials show brittle behaviour and carbide cracking. Already at RT, where the example of Fig. 76c (FeCrNbBWC-PTA) shows one of the lowest wear rates, with carbide cracking at the large Cr-carbides up to a depth of ~20 µm. Smaller Nb and W-carbides as well as the ledeburitic matrix are not concerned. When approaching HT also smaller carbides show cracking, which reaches up to ~25 µm depth (Fig. 76d). Similar behaviour could be found for the other carbide-rich hardfacings. GMAW alloys show worse behaviour compared to the PTA welded ones. This may be attributed to their higher hardness and even more brittle behaviour in high-stress abrasion.

As proposed by Winkelmann et al. [WIN10] matrix softening at HT impairs hardphase backup and gives rise to carbide breakage. Furthermore, the high-stress abrasion with its countless single abrasive events leads to fatigue wear, whereto especially the hard carbides are sensitive [65], which may be most detrimental for the GMAW alloys with highest hardness. NI measurements of the different phases present in the carbide-rich hardfacings (Fig. 48) clearly point out the low hardness of the matrix compared to the hardphases. As measured by Berns (ed.) [BER98], Fig. 26, hardness decrease with temperature of the matrix will be much more pronounced than hardness loss of the hardphases.

The main damage mechanism for the materials with low hardphase content is abrasive removal of material, but it is drastically impaired by the protecting MML, which increases signi-

ficantly in extent at HT. For the other hardphase-rich hardfacings, brittle breakage of carbides and further material removal were observed. This dramatically increases at HT, because carbide backup fails due to matrix softening. Further, the carbides are sensitive to fatigue wear, which is especially present under high-stress abrasion with its multiple abrasive interactions and even more pronounced for the hardest GMAW alloys. Hence, it can be assumed that carbide-rich hardfacings are unbeneficial for HT high-stress abrasive environment.

5.4.2. Wear phenomena in impact-abrasive environment

This chapter concentrates on the cyclic impact-abrasive behaviour of the alloys. Microstructural analysis of typical representatives of a ductile-behaving material and a hardphase-rich material are displayed in Fig. 77. For the ductile-behaving alloys, i.e. cast- and Co-family, some MML-formation at the matrix occurs at low temperature testing (Fig. 77a-d). No pronounced difference in wear loss between matrix areas and carbide regions can be detected; the whole surface is worn uniformly in this impact-dominated environment, although larger abrasive particles are embedded in matrix zones. At 700°C testing the affected zone is much deeper and pronounced intermixing and MML-formation can be detected for the cast alloys. Also oxides were found in the MML of FeCrCoC, so oxidation was present in HT-CIAT due to the longer testing duration of 1 h (plus heating and cooling down), while no significant oxidation was found in HT-CAT. Also annealing of the martensitic microstructure was found, which is supposed to reduce wear resistance. For the CoCrWC alloy (Fig. 77c-d), which show good wear resistance at highest testing temperature, some intermixing could be detected and the whole surface was covered with abrasive particles and MML, albeit the depth was limited to 12 µm. So it can be assumed that the fine structured carbide network controls the formation of the MML structure and also limits its extent. It can be concluded that in impact-dominated environment MML-formation occurs at materials with low hardphase content, but has limited effect for wear protection in this environment.

For the hardphase-rich group representative images are given in Fig. 77e,f. Similar to abrasion testing, brittle carbide breakage is obvious. Also large Cr-carbides show cracks up to a certain depth. Comparing the RT wear marks in detail, the extent in depth of the breakage is lower in the impact environment compared to high-stress abrasion testing. On the other hand, most of all of the present phases are affected by cracking, i.e. also small carbides and even ledeburitic and W-rich matrix zones, while in abrasion testing this was limited mostly to large Cr-carbides at RT. This is more pronounced at 700°C testing (Fig. 77f), where the whole surface is scattered through the impact load. Nevertheless, overall wear loss of the carbide-rich alloys

is much lower than for the other two material groups. It can be concluded that high hardness at application temperature plays a major role in impact-dominated environment. Despite its small disadvantages in HT hardness, a ductile, temperature-resistant matrix can offer good wear resistance through particle sticking and embedding as seen for CoCrWC.

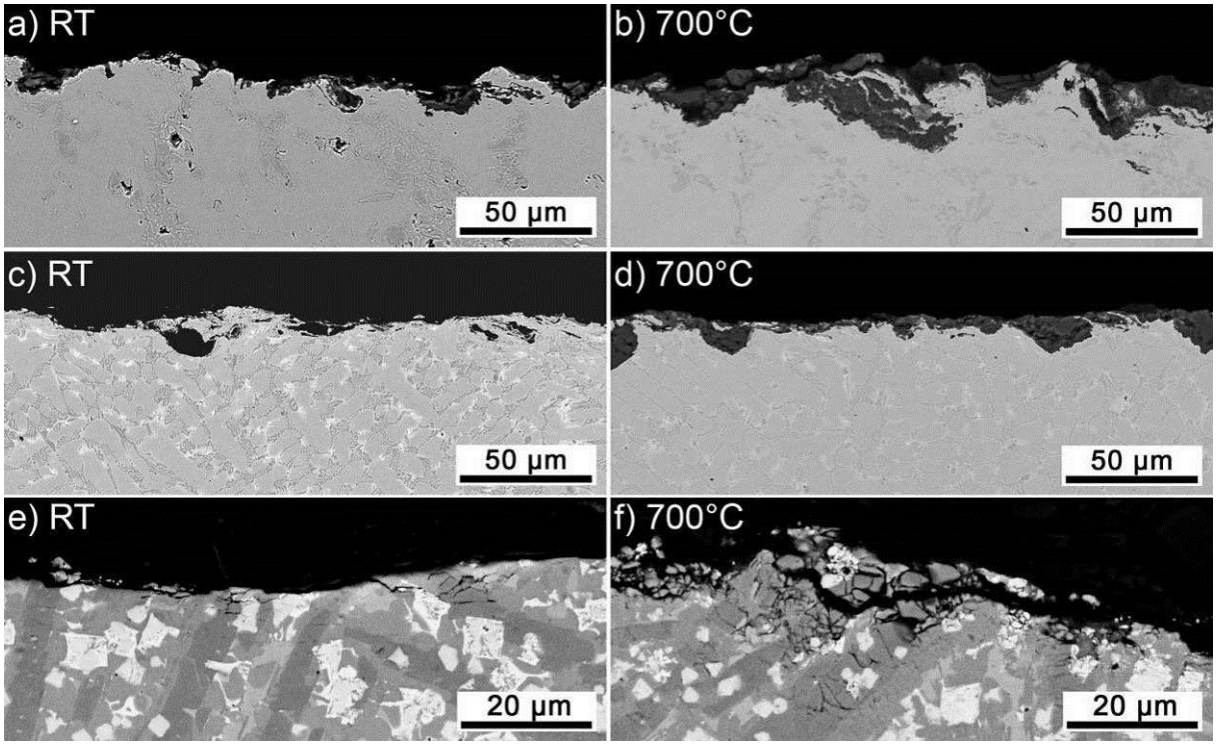

Fig. 77: Wear mechanisms at HT-CIAT, impact zone (SEM-BSE) at the example of FeCrC: a) RT, b) 700°C; CoCrWC: c) RT, d) 700°C and FeCrNbBWC-GMAW: e) RT, f) 700°C

5.4.3. Wear phenomena in solid particle erosive environment

Wear mechanisms in erosive environment are similar to impact-abrasive environment, therefore no additional figures are given here. However, depending on the angle of incidence materials may show totally different wear resistance. This is especially evident for oblique erosion for the cast materials, showing high wear rates. MML formation is present, but the angle of incidence leads to pronounced plastic deformation and material is worn easily. I.e. despite impact energy of the abrasive particles is much lower than at normal impact (halved), these materials wear more under oblique condition. The other phenomenon which can be observed under normal impact is the brittle wear mechanism of the carbide-rich materials. Wear is exacerbated compared to oblique erosion, resulting in the highest wear rates for materials with highest hardphase content. On the other hand, the ductile alloys, especially FeCrC, show the formation of a surface covering MML, entailing excellent wear protection at this condition.

Plotting the normal erosion results against the oblique erosion results is a common technique to differentiate ductile and brittle wear behaviour: materials with higher wear rates under oblique impact tend to plastic wear loss, while materials with higher normal erosion rates show brittle wear behaviour. To that end oblique and normal impact results are displayed together in Fig. 78. Values above the dotted line show higher wear rates for normal impact (brittle behaviour) and below the line for oblique impact (ductile behaviour), respectively. For reasons of simplification just RT and 650°C values are displayed: the blue circle marks the RT values and the red circle the 650°C values. Opposing behaviour of the materials to the angle of impact can be figured out: while the cast alloys and FeCrCoC show lower wear rates for normal impact, this is contrary at the other alloys.

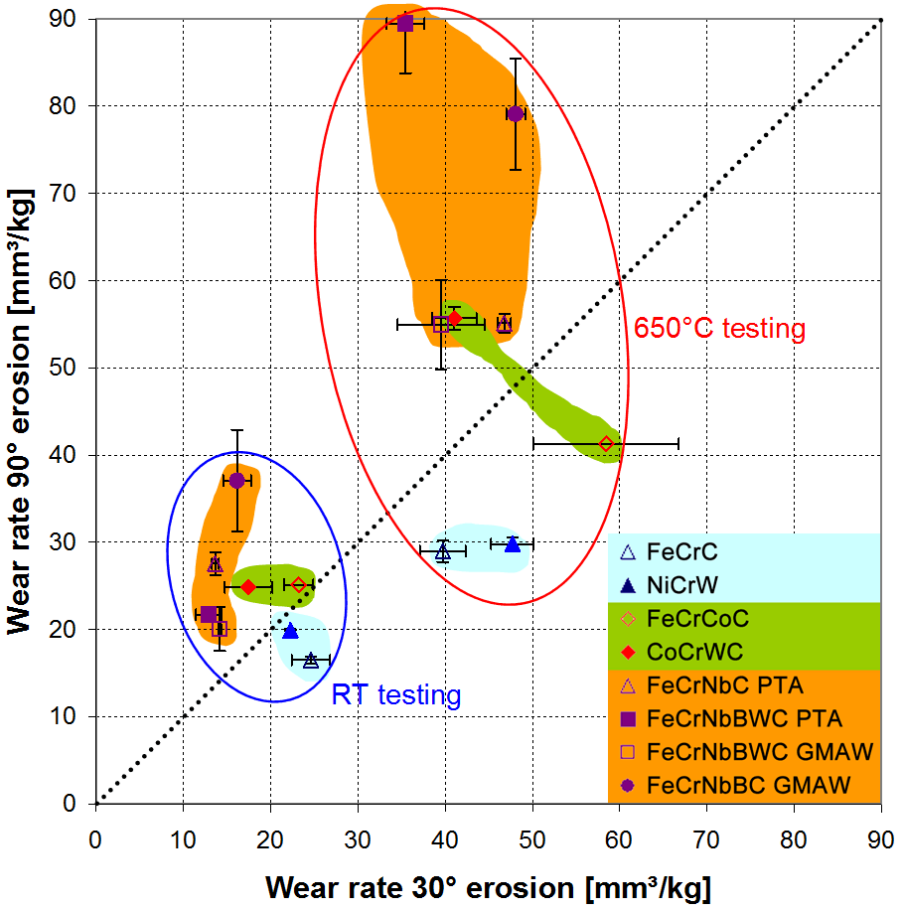

Fig. 78: Erosion results for oblique (30°) and normal (90°) impact

Lowest RT wear rates for oblique impact were measured for the PTA hardfacings and FeCrNbBWC-GMAW with <15 mm³/kg. The FeCrC cast alloy shows similar low wear rates at normal impact. Wear rate increase with temperature is dramatic, especially for the carbide-rich hardfacings at normal impact. E.g. FeCrNbBWC-PTA increases from 22 mm³/kg at RT, normal impact to nearly 90 mm³/kg at 650°C, the highest value measured. Nevertheless, for

oblique impact at this temperature, this alloy was the best in the investigation with 35 mm³/kg. Hence, the impinging angle has crucial influence on erosive wear loss of all materials investigated.

Wear rates for the cast alloys are excellent for normal impact, especially at HT. On the other hand, they were detrimental for oblique impact. Differences in MML formation are especially evident for the FeCrC alloy with 5 µm depth at 42 % coverage for RT oblique impact and 7 µm but 95 % coverage for normal impact. Similar trend was found for NiCrW and FeCrCoC. It can be assumed that the shallow impact angle prevents intermixing. On the other hand, the much higher coverage at normal impact and good wear results lead to the conclusion that the MML formation protects the material from wear loss in normal impact environment. Hence, these cast alloys with relative low hardphase content are best suited for HT normal erosion. Like in high-stress abrasion, MML formation is not pronounced at CoCrWC, which leads to the assumption that also in this solid particle erosive environment the carbide-network is too dense to allow the effective formation of a protective MML.

All carbide-rich hardfacings show very good oblique erosion resistance in the investigated temperature range. Although low values at RT normal impact are obtained for FeCrNbBWC-PTA and -GMAW, the carbide-rich alloys could not be recommended for normal impact usage at HT. Also the high standard deviations indicate the presence of large outbreaks occurring. Temperature dependency for normal impact conditions is interesting for these alloys. Relative low values at RT rocket to high values already at 300°C, which are then staying almost constant up to the highest temperature investigated. On the other hand, temperature dependency is more regular for oblique impact with a gradual increase.

When varying impact angles are present with a distinct normal impact component, the cast alloys, especially FeCrC, should be preferred to carbide-rich hardfacings.

The diagonal in Fig. 78 marks the transition from ductile to brittle behaviour: materials with higher erosion rates for normal impact compared to oblique impact show brittle wear behaviour, materials under this line ductile behaviour. The cast alloys are in the ductile region for all temperatures investigated, while the carbide-rich hardfacings are clearly in the brittle zone. The FeCrCoC moves changes to clearly ductile behaviour with increasing temperature, while the CoCrWC changes to more brittle behaviour with ascending temperature.

5.4.4. Influence of MML formation on wear at different abrasion modes

From the different forms of layers which can form in tribological contacts according [PAU03] the types “mechanically mixed layers” (MML) and “composite layers” are relevant for this work. The MML consists of a mixture of wearing and mating material, without oxidation, whereas the composite layer also includes oxides, which may form at HT. Clear distinction for the materials within this work is difficult. Although at HT the latter is preferred, oxidation plays an insignificant role for most of the HT resistant materials investigated (with the exception of FeCrCoC, which showed some oxidation at CIAT). Further, the short test durations also impede pronounced oxidation, hence the formed layers are considered mainly as MML.

The extend of the MML formed under various conditions is summarised in Fig. 79, Fig. 80 and Fig. 82, Fig. 83, where the first two plot the covered surface according to microscopic analyses of the wear scares and the latter two the depth of penetration. Clearly **MML coverage increases at highest testing temperatures** compared to RT testing for all materials, which are forming MMLs. Even the hardfacings show some coverage at HT, especially for normal erosion. No correlation of hardness to the amount of covered surface was found. Most probable is a microstructure-related effect leading to MML: especially in high-stress abrasion and impact-abrasion FeCrCoC, the material without hardphases, shows very high coverage already at RT, when it still has a high hardness. Differences at HT are minor for this material at CAT and CIAT. The cast materials show slightly lower coverage compared to the martensite at CAT and CIAT, which leads to the assumption that the carbide network hinders the embedding of abrasive to some extent. This is especially evident at CoCrWC with its fine carbide network, entailing low coverage at CAT and ET.

On the other hand, the CIAT’s impact energy seems to be high enough to break the carbide network, leading to high MML coverage at this condition for CoCrWC. At normal erosion at HT, coverage is high for all materials with low hardphase content. Even most hardfacings with high hardphase content show some coverage at 650°C. This is similar to the findings of Olsson et al. [OLS15] who studied rock drilling tools from cemented carbide. Also at the very high hardphase content of cemented carbide some transfer of rock material to the surface was found. It is assumed that cyclical loading and fatigue weaken the carbide compound and lead to penetration of abrasive.

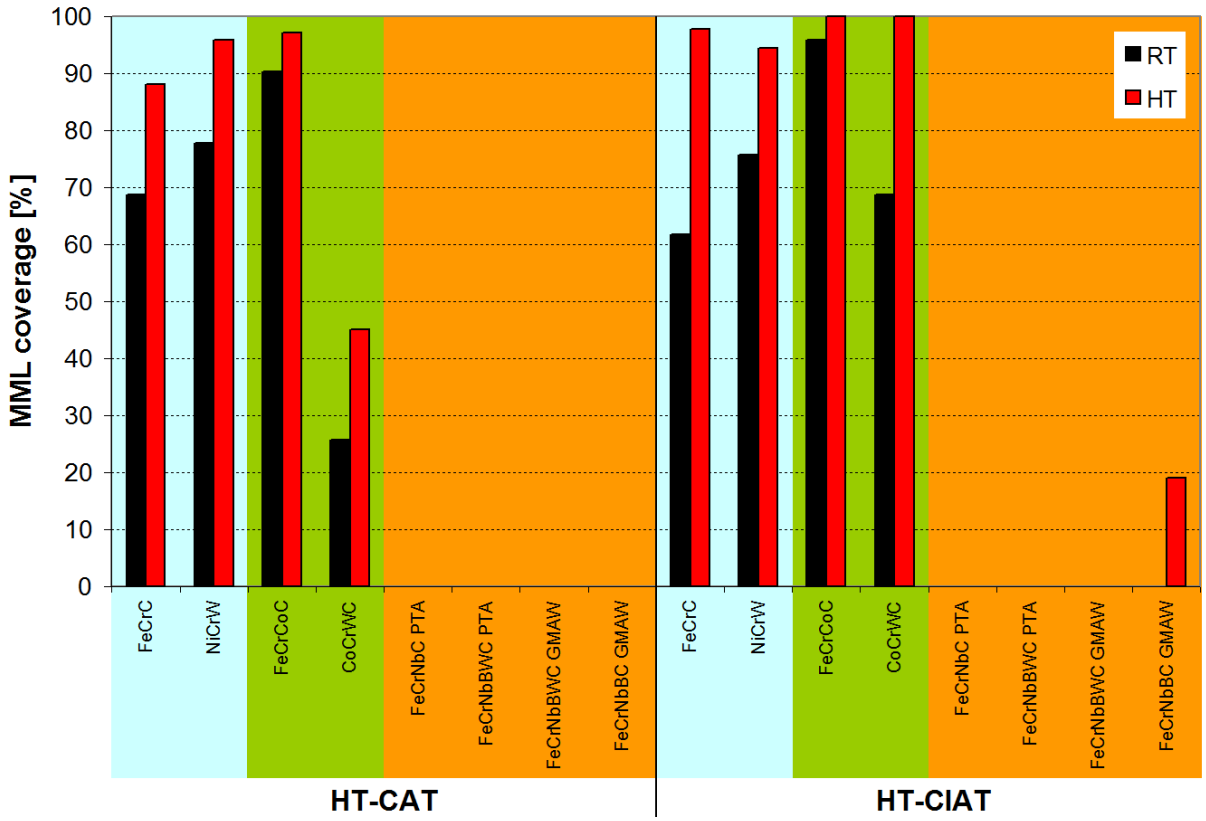

Fig. 79: MML coverage after HT-CAT testing at RT and 550°C;
HT-CIAT testing at RT and 700°C

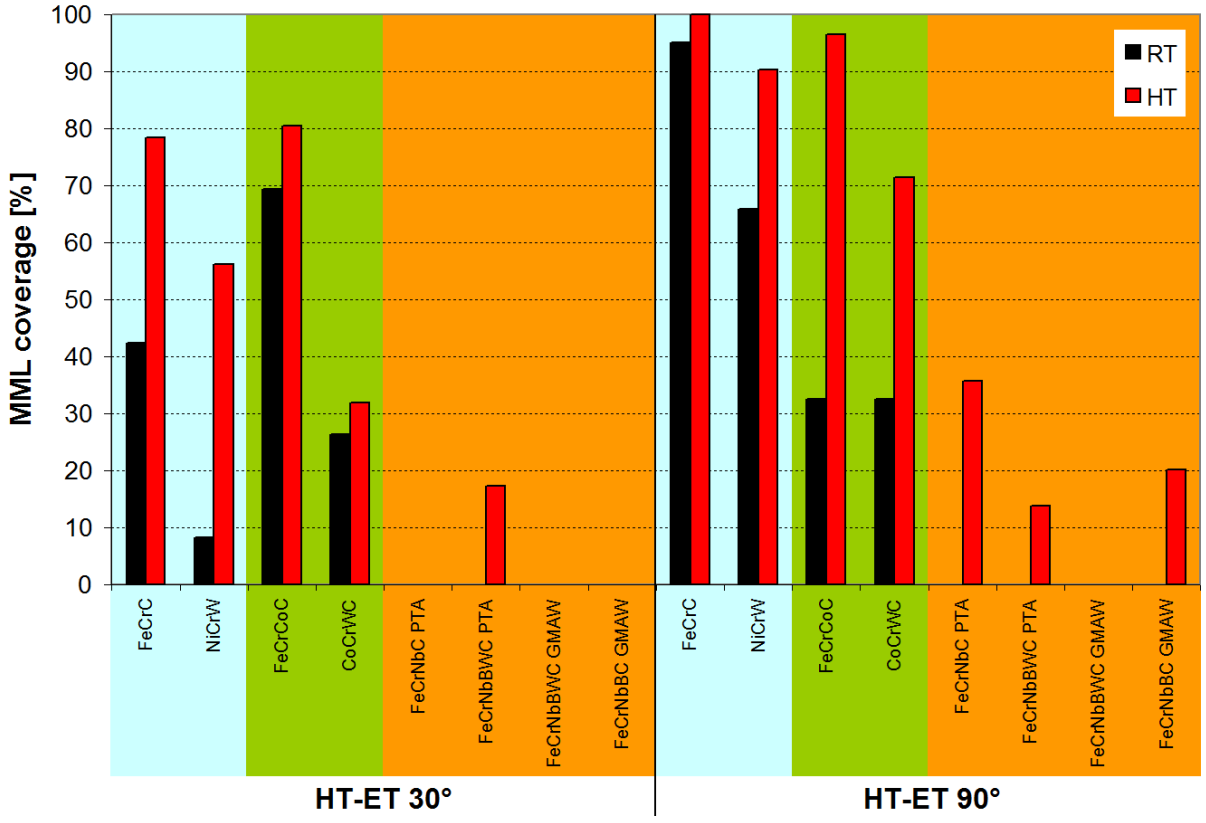

Fig. 80: MML coverage after erosion testing at RT and 650°C for oblique and normal impact

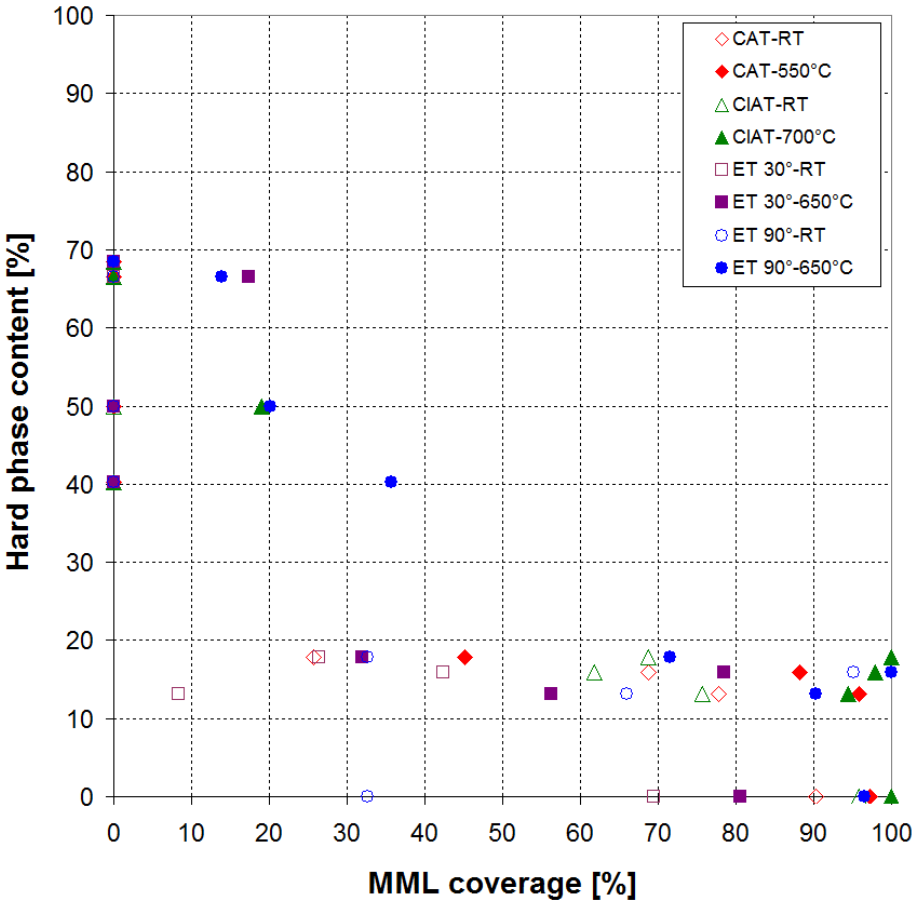

Fig. 81: Dependence of MML coverage on hardphase content for several test conditions

Fig. 81 displays the influence of hardphase content (area %) on the **MML coverage** at the different tests and temperatures. Obviously a high coverage (>40 %) **requires a low hardphase content**. According to the investigated materials a hardphase content <20 % is sufficient. Nevertheless, a high MML coverage does not necessarily go conform with low abrasive wear loss. At certain conditions MML formation was found to increase wear resistance, especially at HT [ANT12, FIS92, KAT09, VAR13-1, VEN97, WIN10, WIN09-2]. MML formation was observed for various HT abrasive conditions within this work and is also reported in literature for e.g. erosion [KAT09, WIN09-2], high-stress abrasion [ANT12, FIS92, VAR13-1] and impact-abrasion [WIN10, ZIK13]. Especially **high-stress abrasion and normal erosion rates** were found to be **lowered by MML formation** in this work. Wear at this condition was also reported in [KAT09, WIN09-2] to be significantly lower due to MML formation than the hardness or low hardphase content of the alloy let suspect. Although MML formation was also observed at impact-abrasion, the effectiveness as wear protection was found to be insufficient. Highest effect was found for high-stress abrasion [FIS92, VAR13-1] and could be also confirmed within this work for ductile materials. MML formation was found to entail superior HT high-stress wear resistance for soft austenites

without hardphases by the author [VAR13-1], which is lower than highly sophisticated hardfacings with hardphase contents >50 % [VAR11]. Within this work no austenitic steel was tested, as it is not commonly used as wear protection, nevertheless, materials with low hardphase content promoted formation of MML, which was found to serve as effective wear protection. Newest work of the author et al. [VAR15-1] suggest that the performance of austenite can further be increased by small amount of hardphases (material FeCrC), which was tested here, especially at very HT [VAR13-1].

The depth the MML is penetrating the microstructure at the various tests is displayed in Fig. 82 and Fig. 83. Standard deviations are high as the inhomogeneous microstructure and wear process leads to a wide range of penetration depths at the materials. Further, just a single section out of the wear track can be analysed on the cross section (no standard deviation means just a single penetrating abrasive was found). Nevertheless, differences between the materials and abrasion modes are observable.

Like before, also penetration depth generally increases at HT testing; highest depths were found after CIAT 700°C testing. Although the material properties can be assumed to be equal at the same testing temperature, especially at erosion testing, penetration depth is minor at oblique impact. That indicates that the severity of the contact has great influence on the formation of thick MML layers and is discussed in the next chapter 5.4.5. When the abrasive contact is very severe, like in high-stress abrasion and normal erosion, and MML formation is pronounced (especially at HT), a direct correlation of hot hardness on the penetration depth can be seen, albeit a general correlation at all materials and tests remains elusive (Fig. 84).

Penetration depth of MML was found to be hardness dependent for high-stress abrasion by the author [VAR15-1]: temperature-induced material softening entails higher penetration depth for the materials investigated. Load influence on MML formation on FeCrC and FeCrNbBWC-GMAW is presented in [VAR16]. No hardness difference between stressed surface near regions and bulk could be measured (360±12 HV1 for all regions). A clear influence of load on the surface coverage was found for FeCrC, i.e. increasing loads lead to significantly higher coverage. Temperature influence of coverage was especially found for medium loads (45 N), while low and high loads show less temperature influence. Penetration depth was not found to be significantly load dependent, here the main influence is temperature induced softening.

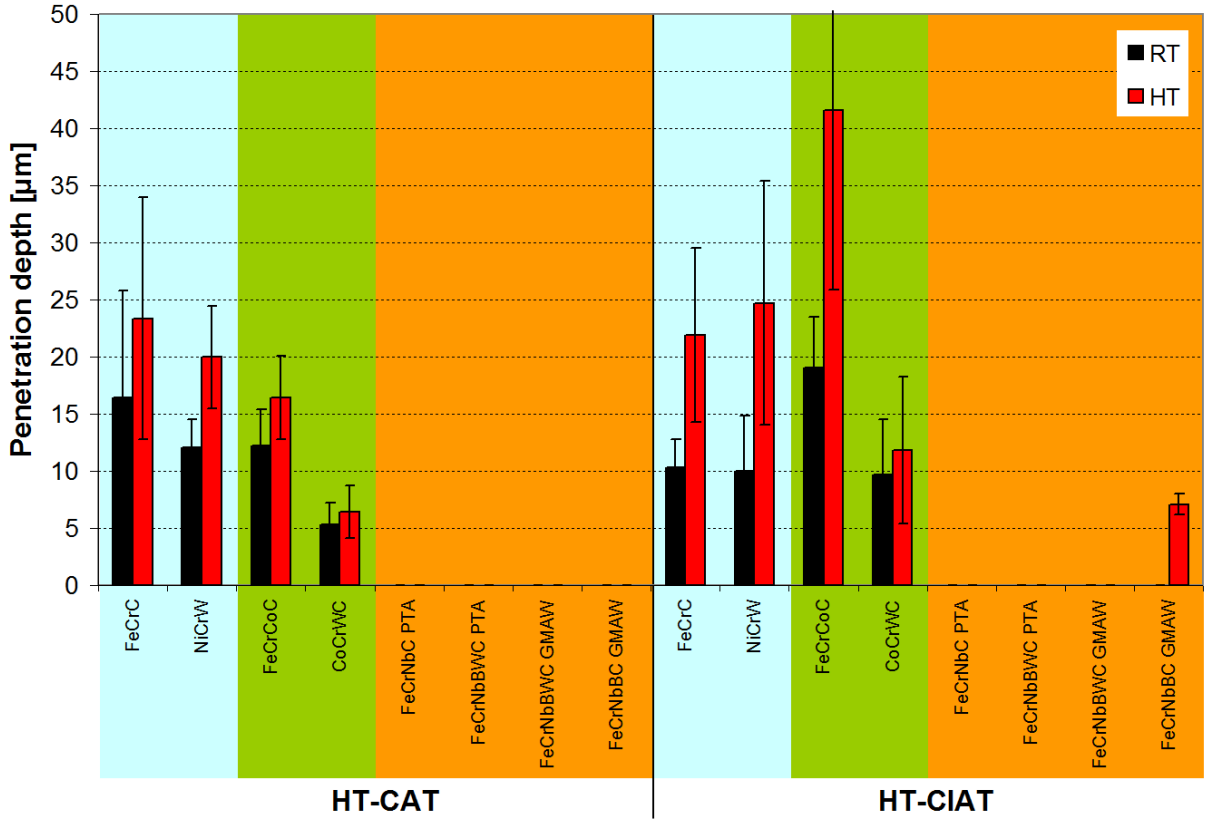

Fig. 82: MML penetration depth after HT-CAT testing at RT and 550°C;
HT-CIAT testing at RT and 700°C

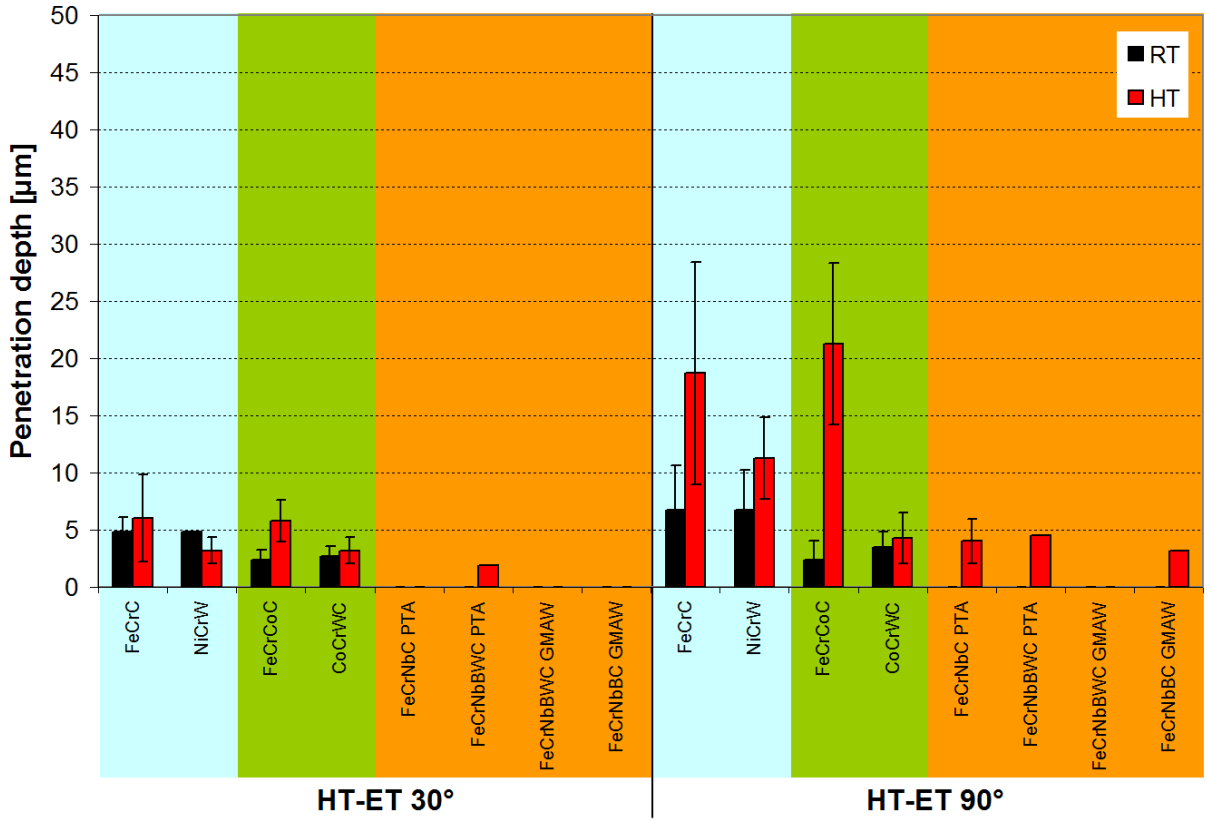

Fig. 83: MML penetration depth after erosion testing at RT and 650°C at oblique and normal impact

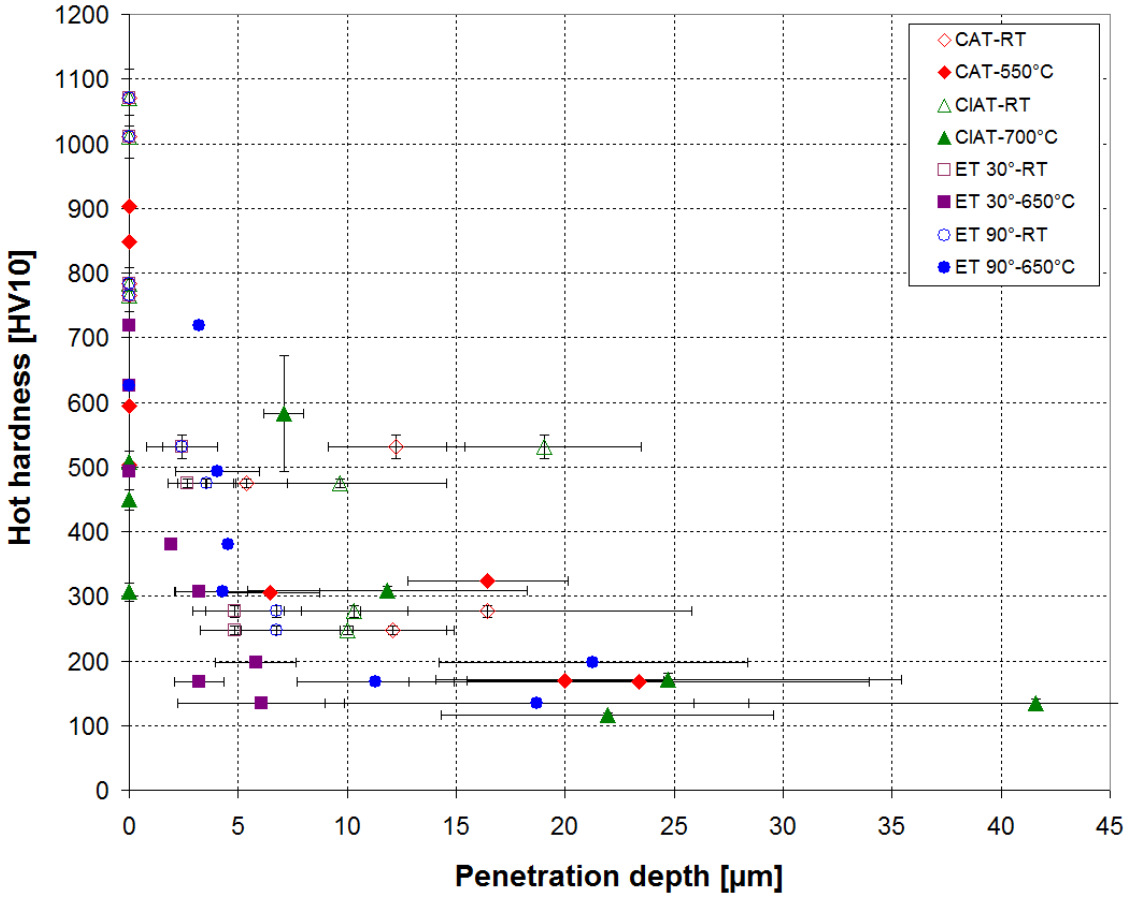

Fig. 84: Dependence of MML penetration depth on hot hardness at the various tests

5.4.5. Influence of contact severity on MML formation

As discussed in the previous chapter, the MML formation is not only material dependent, but shows significant differences at the various abrasion modes. In this chapter an attempt to correlate the MML formation with the contact severity is undertaken. For this purpose, the energy transferred through the contact zone is taken as measure and broken down to the single abrasive contacts based on the assumption that the load is carried homogenously by all particles in the contact zone. The time for the wear process is not considered here, as all tests were performed at steady-state conditions and MML establishment is thought to be complete.

In three-body abrasive contact (HT-CAT) the energy set free in the tribocontact is assumed as:

$$E_{CAT} = F \cdot s = 45\ N \cdot 15\ mm = 0.675\ J \qquad \text{Eq. 3}$$

where F is the applied load and s the sliding distance of the sample at the end of the test run. This is a simplification, as the contact length steadily increases from a line contact at the begin of the test run to a length of ~15 mm (dependent on temperature and material) at the end of the test. It is assumed that the energy transfer per abrasive particle has the most influence on the MML formation, hence the amount of particles has to be estimated. To

calculate the worst possible case, the largest diameter of the CAT-abrasive is taken (300 µm) and arranged in sphere close-packing in the contact zone of 12 mm × 15 mm (wheel width × contact length). This results in ~1880 abrasive particles carrying the load in the contact (under the assumption that they do not break [cf. ANT12]). Hence, the energy transferred by one single abrasive particle is ~0.36 mJ at HT-CAT.

In an impact-abrasive environment the energy is applied by a free falling plunger of m = 2 kg weight and h = 40 mm dropping height. Additionally, the abrasive component has to be taken into account. From tested samples a sliding distance of s = 2.5 mm was measured at an impact angle α of 45°, i.e. the normal component of the load is smaller by cos 45°. Adding these two components, the energy transferred through the impact-abrasive contact is:

$$E_{CIAT} = m \cdot g \cdot (h + \cos\alpha \cdot s) = 2\ kg \cdot 9.81\ m/s^2 \cdot (40\ mm + \cos 45° \cdot 2.5\ mm) = 0.819\ J \quad \text{Eq. 4}$$

From high speed videos the particle load was estimated: in the impact area a coverage of about 40 % can be assumed. With the largest possible abrasives of 900 µm ~17 particles are in the tribocontact. Like in abrasive contact the breakage of the abrasives has to neglected for simplification. Furthermore, the dynamic wear process by the impact load cannot be assessed with this simple calculation. From these assumptions ~47 mJ per abrasive particle are calculated for HT-CIAT.

Erosion testing was performed at v = 80 m/s abrasive particle speed. Hence, the energy transferred by one particle can be assessed directly, when the mass of one single particle is known. For this purpose, a spherical quartz particle with the maximum diameter at ET of 300 µm was taken. With the density of quartz (2.65 g/cm³) a mass of m ~37 µg can be calculated per particle. In normal erosion the particle energy is then:

$$E_{ET\ 90°\ particle} = \frac{m \cdot v^2}{2} = \frac{37\ \mu g \cdot (80\ m/s)^2}{2} = 0.12\ mJ \quad \text{Eq. 5}$$

At oblique erosion, only the normal component is thought to affect MML formation, hence the particle energy at the oblique angle of α = 30° is:

$$E_{ET\ 30°\ particle} = \frac{m \cdot v^2}{2} \cdot \sin\alpha = \frac{37\ \mu g \cdot (80\ m/s)^2}{2} \cdot \sin 30° = 0.06\ mJ \quad \text{Eq. 6}$$

With the knowledge of energy per abrasive particle at the various abrasion tests, the MML formation can be ranked by increasing energy. While the three-body abrasion test and the erosion tests feature relatively low particle energies below 1 mJ, the massive impact of the impact-abrasion testing entails ~47 mJ, which is two orders of magnitude higher. Hence the

energy effect on the MML formation is of especial interest. Fig. 85 depicts the MML penetration depth at the MML forming alloys (cast- and Co-group) at RT and HT sorted by abrasive particle energy as calculated above.

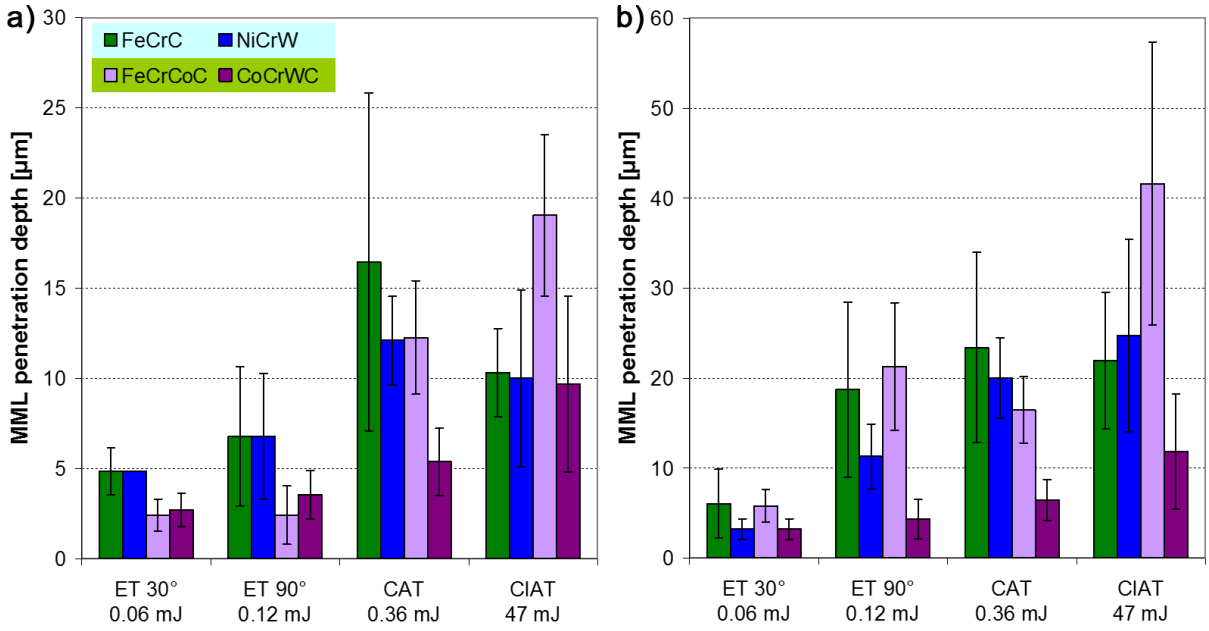

Fig. 85: Abrasive particle energy influence on the MML penetration depth for the MML forming alloys: a) RT testing; b) HT testing: ET at 650°C, CAT at 550°C and CIAT at 700°C

As the maximum test temperatures were not identical for the various tests, this discussion will concentrate on the RT results in Fig. 85a. With the exception of CIAT testing with high impact energies per particle, the **thickness of the MML increases with increasing energy input**, i.e. the more severe the contact, the deeper the MML penetrates the wearing surface. For the Fe-base FeCrC and the Ni-base NiCrW the values at RT are similar and the increase is nearly linear, whereas the FeCrCoC alloy shows a steep increase at CAT testing (0.36 mJ). The Co-base alloy CoCrWC also shows a nearly linear increase until 0.36 mJ, albeit at a significantly lower level than the cast-family. Nevertheless, direct relation with the matrix structure is challenging to assess, as the hardphase network is also much finer in the Co-base alloy compared to the cast alloys.

Increase of penetration depth at CIAT testing is not in direct correlation with the energy increase. At RT, values for the cast-family are in the same range as at CAT, albeit the energy level is two orders of magnitude higher. The Co-group on the other hand shows drastic increase in MML penetration depth. This means that the penetration depth has some limit and further increasing the particle energy does not lead to deeper penetration.

At HT testing, the Ni-base NiCrW shows lower penetration depths at ET (energy <0.2 mJ) compared to the Fe-base of similar structure (FeCrC), while at higher energies they are in the same range. The relatively stable temperature behaviour of Ni-base matrix may be beneficial against penetration at low impact energies. On the other hand the fcc-structure may be beneficial for MML formation, if impact energies are high enough to entail significant plastic deformation. The Co-base also shows similar behaviour, albeit the critical threshold is assumed at higher energies, as a significant rise in penetration depth was observed only in CIAT.

Fig. 88 shows the influence of particle energy on surface coverage at RT and HT testing. Contrary to the penetration depth, influence of particle impact energy is not clearly visible. At the Ni-base alloy NiCrW, both at RT and HT, an increasing coverage with increasing abrasive particle energy is visible. A threshold seems to be reached at CAT energy, as the coverage does not grow further at CIAT. Coverage at the Co-base alloy CoCrWC is fluctuating in the low energy regime, but relatively high at CIAT. As found in the wear scars, penetration and intermixing was significant at CIAT, while the other tests entailed limited MML formation for this alloy. The energy level at CIAT is therefore thought to destroy the carbide network and lead to massive MML formation, while the severity at the other tests is too low.

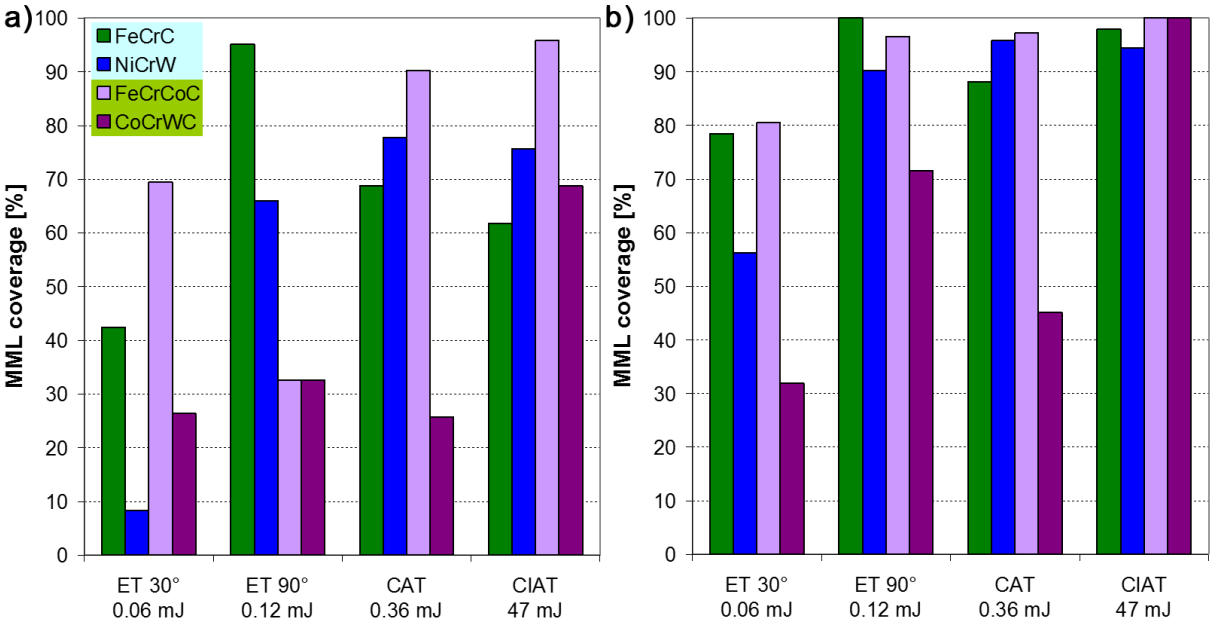

Fig. 86: Abrasive article energy influence on the MML coverage for the MML forming alloys: a) RT testing; b) HT testing: ET at 650°C, CAT at 550°C and CIAT at 700°C

It can be concluded that particle energy has significant influence on the MML formation, especially on the penetration depth [cf. WIN09-2]. Generally MML penetration depth increases with increasing abrasive particle energy. Critical thresholds were found for the

various materials, on one hand limiting the further propagation of the MML coverage, i.e. a saturation level is reached. On the other hand, FeCrCoC showed over-proportional increasing MML penetration over a certain threshold energy.

5.5. Correlation of abrasive wear rates with material properties

A correlation of wear rates with microstructural or mechanical properties of the materials is the goal of every tribologist. Correlations presented in various publications are just valid in a very narrow field, for identical wear mechanisms and very similar materials. So abrasion resistance as a material property remained elusive [ZOK07]. Within this work, a new attempt is undertaken to find correlations for defined abrasion modes and different material groups, which is especially challenging, as the various materials are of very different type. Correlations with microstructure parameters like carbide content and distribution, or mechanical properties of the single phases were evaluated, but no breakthrough could be reached with these parameters. Microstructure and carbide distribution was found to especially influence the MML formation, as discussed in the chapter 5.4.4. This in turn lowers wear at certain conditions, but no mathematical modelling for this effect could be found. Most successful was the **correlation with the hot hardness of the materials**. The measured HV10 hot hardness is a parameter describing the whole microstructural compound, including matrix- and hardphase-areas as well as their statistic distribution. The novelty within this work is the availability of the hardness-temperature progress, enabling the correlation of HT wear results with the corresponding hardness. The correlation of wear rates therefore was started with the simple Archard's wear law (Eq. 1) [ARC53], where the hardness is the only material property linearly influencing the material loss, while load and sliding distance are system properties.

Following this approach, high-stress abrasive wear rates were plotted against the material's hardness at testing temperature in Fig. 87 and linear correlations were calculated when possible. At first sight no general correlation can be seen, as also materials with very low hardness show good wear resistance, especially at HT. However when evaluating the various material groups separately some good correlations can be found. Especially the high-stress wear rates *WR* of the PTA welded alloys (on the left side in the orange cloud) follow a linear relation with the hardness *H* at a good coefficient of determination R^2 of 0.96:

$$WR\,HT - CAT_{PTA\,hardfacing} = -1 \cdot 10^{-4} \cdot H + 0.1337 \qquad \text{Eq. 7}$$

Despite their similar microstructure, the correlation of the GMAW alloys (on the right side in the orange cloud) is less pronounced: the wear rates under conditions where material

FeCrNbBWC-GMAW exceed 1000 HV10 do not fit the correlation. Nevertheless, the other results meet a linear correlation quite good, but at a steeper slope than the PTA welded ones:

$$WR\,HT-CAT_{GMAW\ hardfacing\ <1000HV10} = -2\cdot10^{-4}\cdot H + 0.2702 \qquad \text{Eq. 8}$$

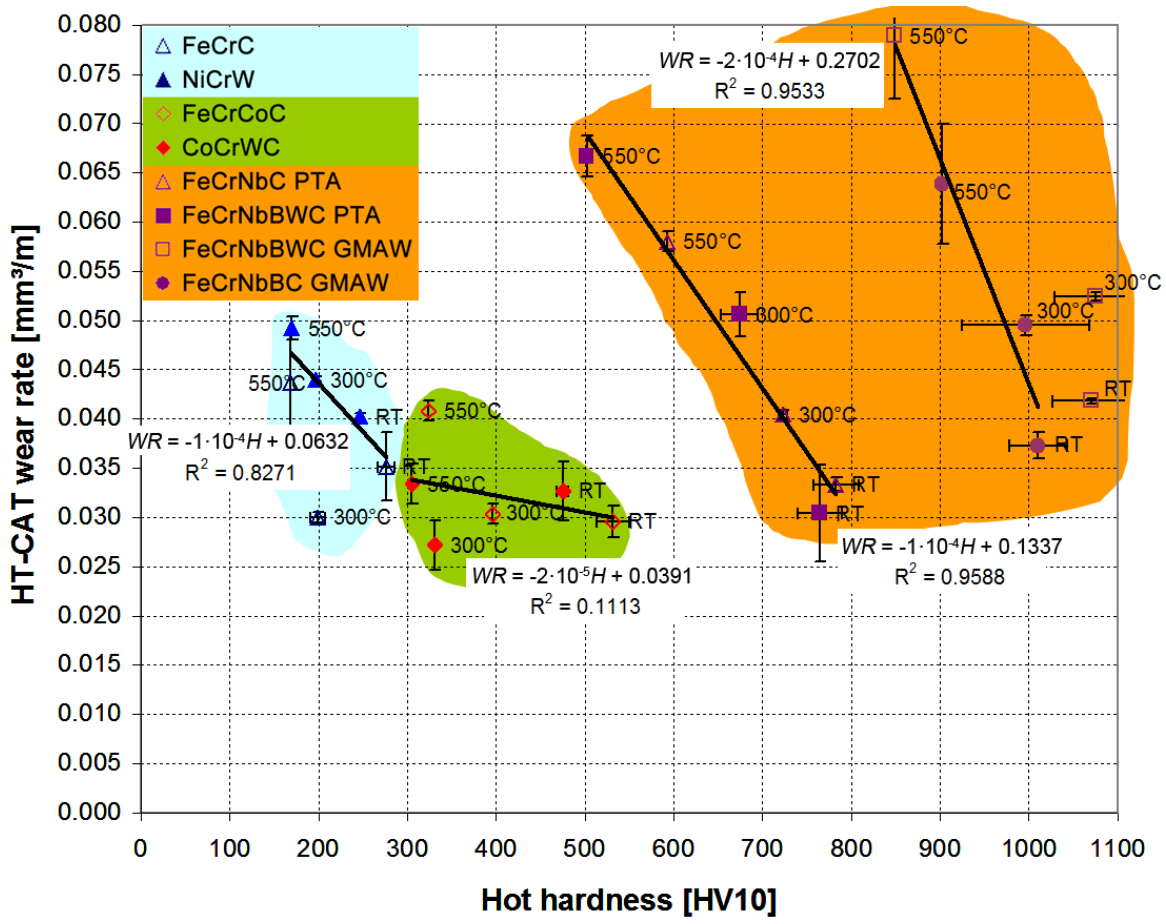

Fig. 87: Correlation of abrasive wear with hardness with trend lines for material groups (outliers excluded: >1050 HV10; FeCrC 300°C)

Linear relation was also tried for the two other material groups (formulas given in Fig. 87), but correlation is not sufficient. Some linear fit was found for the cast materials when excluding the 300°C value of FeCrC, maybe also the HT wear rates of CoCrWC fit to this correlation. At the Co-group no linear fitting was possible. It is suspected that the formation of the wear protecting MML, albeit influenced by hardness, makes it impossible to correlate the wear rate to materials hardness. Factors influencing the MML formation and its wear-protective effect were discussed in the previous chapter 5.4.4. Correlations of the HT-CAT wear rate with hardphase content were not successful.

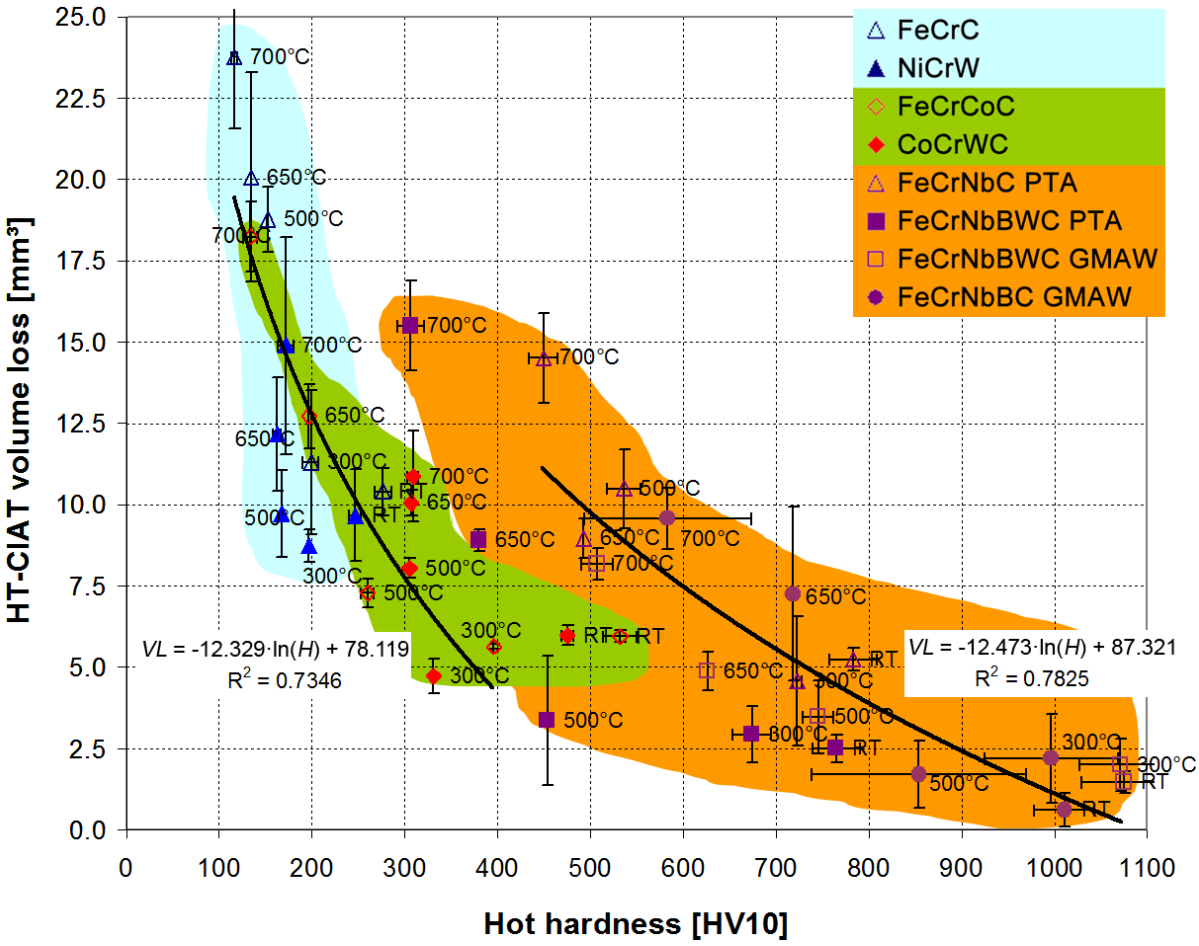

Fig. 88: Correlation of impact-abrasive wear with hardness with trend lines for material groups (outliers excluded: Co-group RT; FeCrNbBWC-PTA >300°C)

HT-CIAT wear is plotted against the material hardness in Fig. 88. Generally it can be seen that the higher the hardness, the lower the wear will be, albeit there is no linear correlation. Within the diagram two trend lines for the volume loss *VL* are given: one for the low hard-phase containing materials and a second for the carbide-rich hardfacings. Logarithmic trend was best suited for the data, albeit no explanation for a logarithmic dependency can be given. Despite the split in the two groups, determination of the fit is poor. Nevertheless, the hardness dependency cannot be neglected. The two different slopes of the carbide-rich hardfacings compared to the low hardphase containing materials may be directly linked to the formation of MML, albeit its wear protection in impact-abrasive environment is of minor importance.

Oblique erosion wear rates showed significant hardness dependency as it can be seen in Fig. 89. Although no general hardness correlation can be found for material groups, the hardness dependency within one single material is pronounced. Two materials show a coefficient of determination of over 0.99, namely FeCrCoC and FeCrNbBWC-PTA. Further, the materials CoCrWC, FeCrNbC-PTA and FeCrNbBWC-GMAW show R^2 in the range of 0.9 or above.

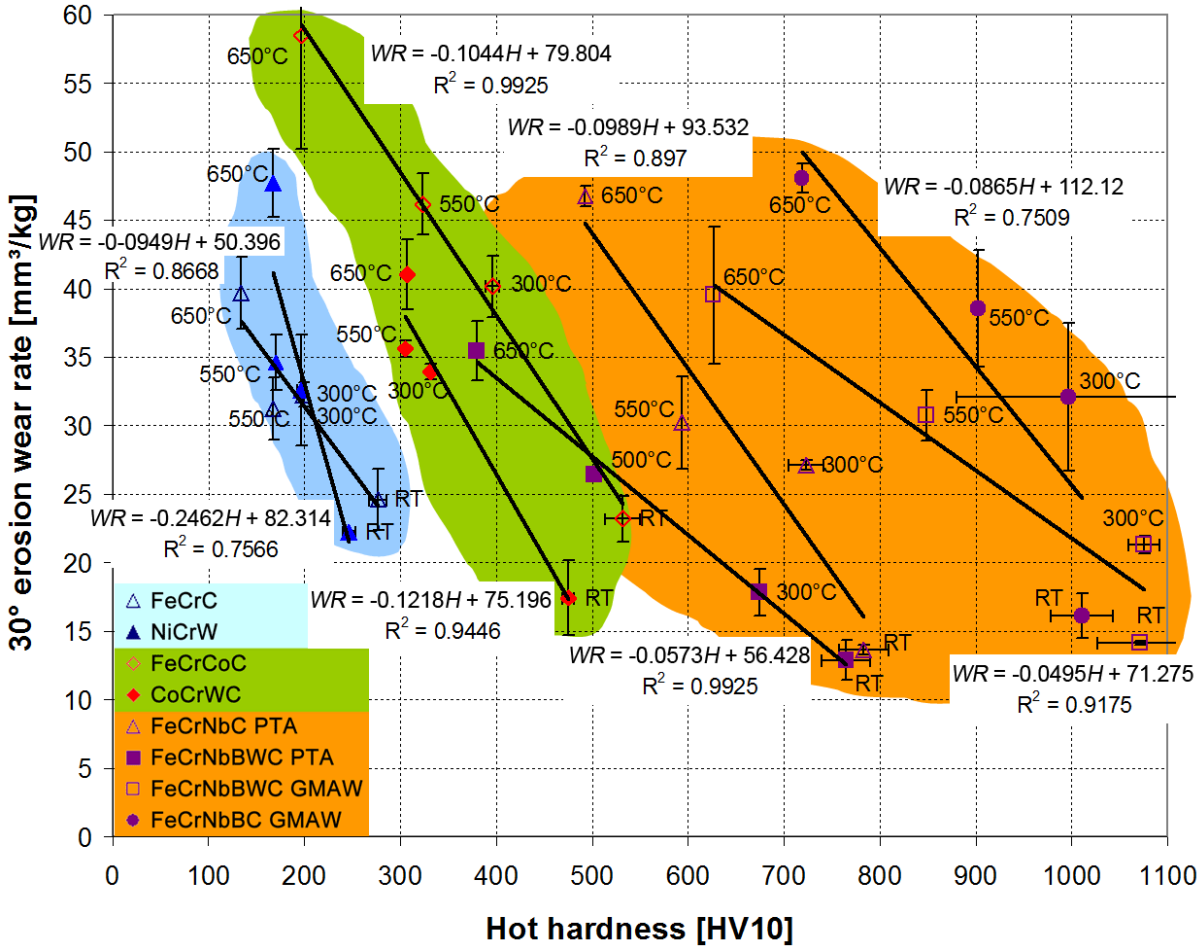

Fig. 89: Correlation of oblique erosion wear rates with hardness with trend lines for materials

Normal erosion wear rates are plotted against hardness in Fig. 90. In contrast to oblique impact, the correlations are insufficient for most materials. Linear trend lines are given for the materials showing the highest correlation. A very good correlation was obtained for NiCrW, which is especially outstanding, as this material forms also a thick MML. So this linear correlation is a product of temperature induced softening and increased MML formation with increasing plasticity of the material influencing the wear loss. Also a noteworthy linear relationship can be seen for the martensitic material FeCrCoC and cast FeCrC. Despite its similar hardphase content, the Co-based CoCrWC does not follow this strong hardness dependency, and also does not show significant MML formation and penetration depth at this condition, respectively (Fig. 83). That means that all materials forming significant MML for this wear mode follow a linear relation of wear rate with material softening.

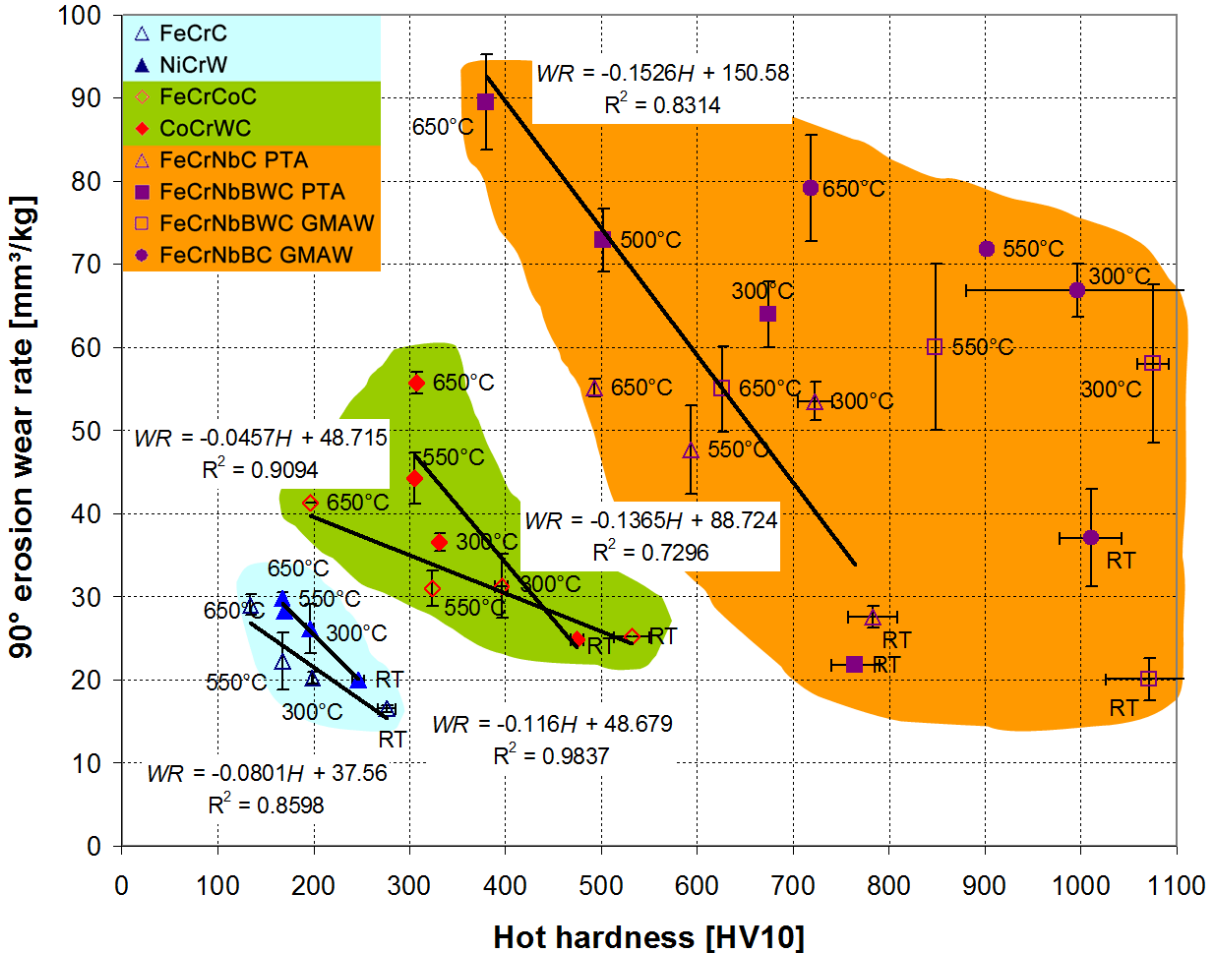

Fig. 90: Correlation of normal erosion wear rates with hardness with trend lines for materials

The most interesting correlation with hardness was found combining oblique with normal erosion wear rates, as depicted in Fig. 91. **The ratio of normal erosion / oblique erosion** (erosion response [cf. KAT09]) **follows a linear trend with hardness** throughout all materials and temperatures. Only the FeCrNbBWC alloys do not follow this trend as well as the other alloys: HT results from the PTA welded one are outlaying, just as the RT value of the GMAW alloy. The general equation:

$$\frac{90°\,erosion}{30°\,erosion} = 0.0019 \cdot H + 0.3683 \qquad \text{Eq. 9}$$

describes the behaviour of all other tested materials in the temperature range of RT-650°C with a coefficient of correlation of nearly 0.9, which means an outstanding accuracy for the variety of materials tested. With the aid of this equation, one unknown parameter in erosion can be calculated. E.g. by measuring the hot hardness and normal erosion, the behaviour at oblique erosion can be predicted.

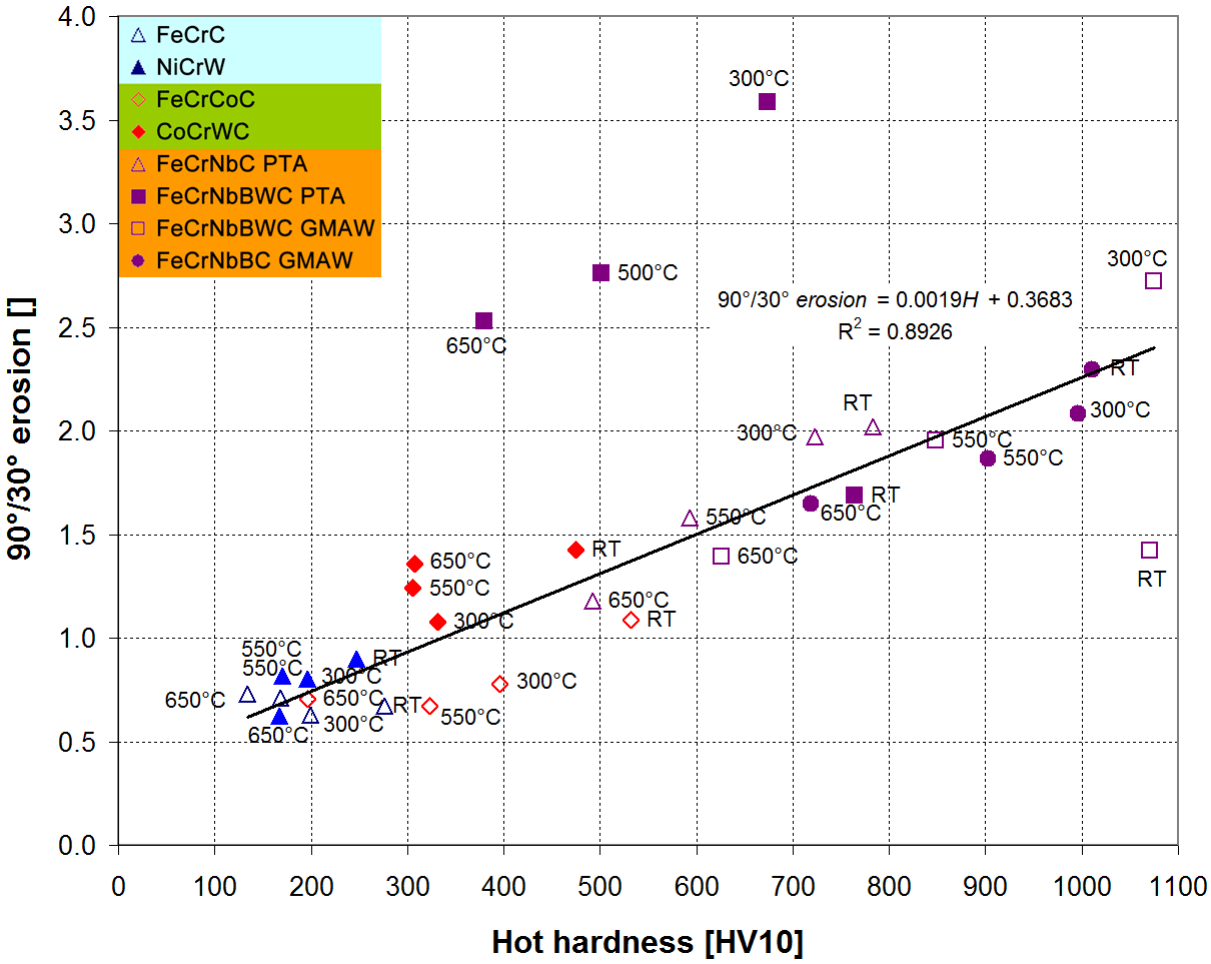

Fig. 91: Correlation of the ratio of normal erosion / oblique erosion wear rates (erosion response) with hardness with a general trend line for the materials investigated (outliers excluded: FeCrNbBWC-PTA at HT; FeCrNbBWC-GMAW RT)

5.6. Wear map for abrasive conditions at enhanced temperatures

Summarising all wear results for the different abrasion modes is attempted within this chapter, in order to aid material selection for abrasive wear conditions at various temperatures. Naturally it is difficult to display all results within one graph, so following data are limited to the three best materials at the certain condition.

Fig. 92 displays the wear resistance of the three best alloys (four if they are close together) at the various conditions investigated. The height of the bar represents the performance of the best alloys investigated compared to the worst, i.e. a high bar means that the best alloy is far better than the worst for this certain condition. The range of wear rates is discussed in detail in chapter 5.3.3 and can be very different at the various abrasion modes. This is also visible in Fig. 92 as, e.g. impact-abrasion results show very high bars, meaning that the best alloys are far better than the worst (FeCrNbBC-GMAW is 17× better than FeCrC, see Fig. 71). Within

the bars the three (four, if close together) best alloys are indicated. The alloy on top stands for the best material and at a distance, representing the variation in wear resistance, the second and third alloy is named. E.g. at RT impact-abrasive wear condition the best alloy is FeCrNbBC-GMAW, followed by FeCrNbBWC-GMAW with a large distance. Another example are the RT results of oblique erosion, where the three best alloys are very close to each other.

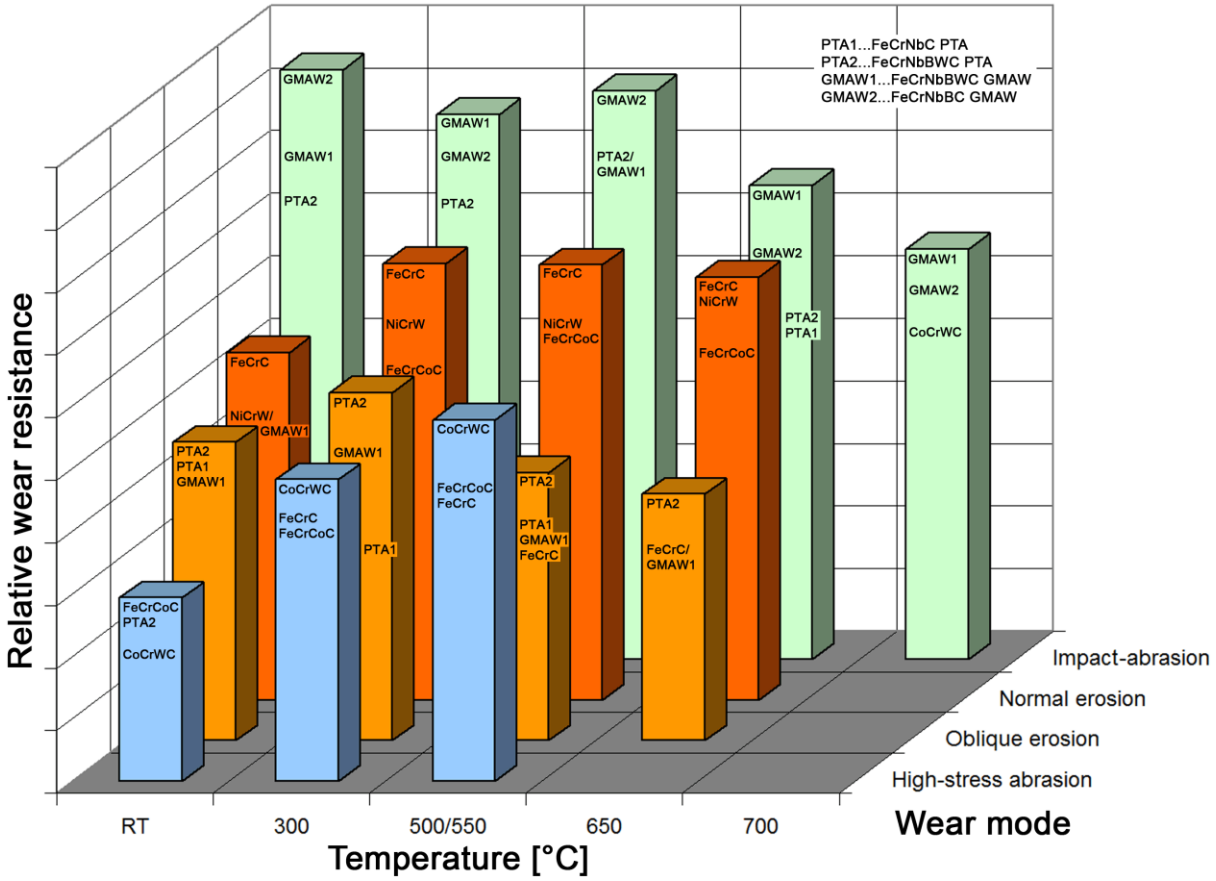

Fig. 92: Wear map of the different materials for various abrasion modes at temperatures investigated (500°C for impact-abrasion; others 550°C)

If a certain wear mode is dominating at a specific plant component, the plant engineer can directly choose the best materials from Fig. 92. If mixed conditions are present, e.g. erosion with an impact component of coarser particles, the choice of the wear protection has to be done thoughtfully and the summarising figure here may be not sufficient. In this case, the whole set of data presented in chapter 4.3 needs to be considered. This is especially important when wear protection is driven by the formation of MML, as, e.g. in high-stress abrasion or normal erosion. In combination with impact component, where MML formation does not guarantee sufficient wear resistance, material choice has to be done according impact-abrasive wear resistance.

5.7. Economic effect of wear protection

Within the previous chapter 5.6 materials with best wear resistance are presented, independent of the costs. Plant maintenance is not based on the scientific choice of the materials with best wear resistance, but on the solution offering lowest maintenance costs in a long-term view. Hence within this chapter an attempt is done to combine the wear results with the costs for the wear protection.

A first step to evaluate the costs of wear protection is to evaluate the costs for the materials used. Material cost is usually given per kilogram and the relative costs (normalised by the cheapest) are displayed in Fig. 93. Generally, hardfacing alloys are much more expensive than cast materials, because a huge amount of processing is necessary to obtain the powder or welding wire for deposition. On the other hand, the mixture for cast alloys is more easily and pre-alloys, e.g. ferrochromium, are mixed to obtain the desired chemical composition in the alloy. As evident from Fig. 93, huge differences in the material costs are present. The Ni-base cast alloy is ~3× more expensive than the Fe-base FeCrC. Most expensive within the test field is the Co-base powder, followed by the Co-containing Fe-base FeCrCoC. The carbide-rich hardfacings FeCrNbC and FeCrNbBC are less expensive as their alloying content of expensive elements is lower. Further, their production to flux core wires is less expensive than power production of the Co-group.

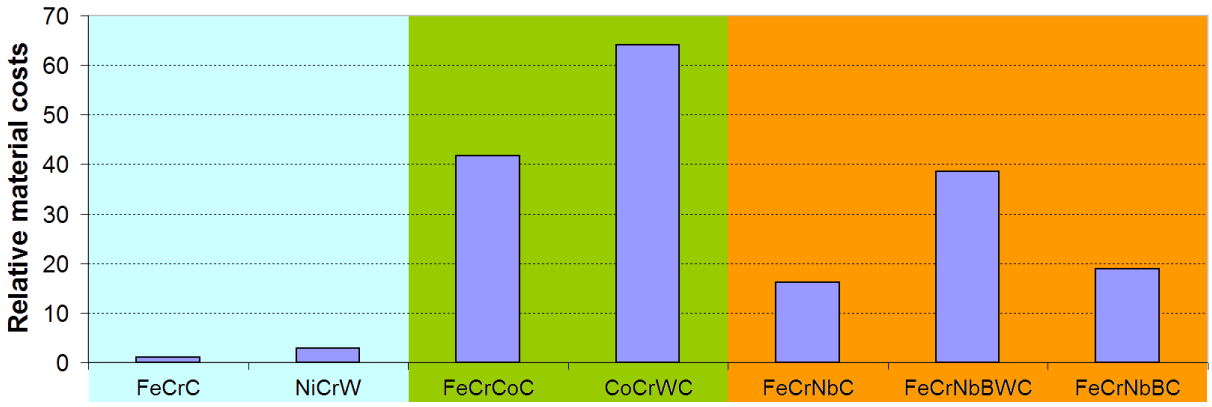

Fig. 93: Relative material costs for the alloys investigated [HOR15]

Additionally to the material cost the processing costs for applying component wear protection are added. For the cast alloys the processing was included within the material costs of Fig. 93. For the hardfacings the processing costs are strongly dependent on the welding technique utilised. With PTA welding approximately 0.8-2 kg can be deposited per hour [FAH14], therefore, welding parameters can be controlled very accurately and hardfacing quality can be optimised. On the other hand, by GMAW 3-15 kg can be deposited per hour [FAH14], but

welding cannot be controlled with the same accuracy as at PTA welding. An alternative deposition technique, which is currently strongly researched is laser welding technique. With this novel technique 10-16 kg/h can be reached with well controlled parameters [TUO14]. Further cost efficient hardfacing deposition may be reached thereby in the future.

In order to estimate cost for wear protection, a hypothetical component of the size of a grate bar is chosen, which should be protected by the various materials. This means for the cast alloys a material weight of 7 kg for FeCrC and 8.2 kg of NiCrW is necessary. By hardfacing only the areas exposed to wear need to be protected, this means the top surface and the side walls, entailing 0.07 m² surface. In this assumption a wear protection of 2 mm thickness hardfacing is applied. Depending on the density of the hardfacing this means ~1.1-1.3 kg needs to be deposited. With the PTA welding technique on a simple geometry (~1.5 kg/h deposition rate) approximately 45 min working time (technician plus device) are necessary, while at GMAW with ~7 kg/h deposition rate it is just ~10 min. So these processing costs are added to the material costs resulting in costs for the wear protection.

With these costs for wear protection, the costs of material loss can be further assessed for the hypothetic component by use of the experimentally found wear rates: if the wear rate is high at the certain condition, also the material loss is high. This material loss is weighted with the cost of wear protection as described above. As material and processing costs vary in a wide range may a cheap wear protection wearing rapidly is still cheaper than a pricy material wearing slowly. As wear of a cheap material may be considered as best solution for the application, it has to be noted that the component may fail because of excessive material loss and a higher replacement frequency is necessary.

Hence, in a second step also the available amount of wear protection is taken into account. For hardfacings this is maximally the thickness of the hardfacing. For cast alloys theoretically the whole component can be worn, but in application in the most cases it will be replaced earlier before its function is lost. Continuing the hypothetic maintenance of the grate bar it is assumed that the component is designed assuming low wear loss (best wear protection). That means higher wear loss leads to more frequent replacement of the component. For this replacement during regular maintenance intervals (no additional plant downtime) one hour of working time (labourer) is assumed. Change intervals are set according the wear rate of the materials: for every 30 % higher wear of hardfacings than the best alloy one exchange is added to the hypothetic maintenance costs. For the cast alloys 50 % was chosen as threshold,

as generally higher wear volume is allowable for these materials. This additional replacement costs may lead to significant higher costs for maintenance than only the costs of material loss.

The following diagrams Fig. 94-Fig. 97 display the costs for wear loss and the costs for maintenance (wear loss + replacement) at the various abrasion modes according the assumptions described above. Above the abscissa costs of wear loss are plotted, i.e. material costs plus eventually processing costs for deposition. Below the abscissa the hypothetic maintenance costs are given, i.e. costs of wear loss plus eventually necessary frequent replacement as described above. All costs are normalised to the best performing material that differences can be seen directly, e.g. if relative wear costs are 30, this means the solution will cost 30× more than the best alloy for this wear mode and temperature. Solutions which require more frequent replacement will have significant higher maintenance costs.

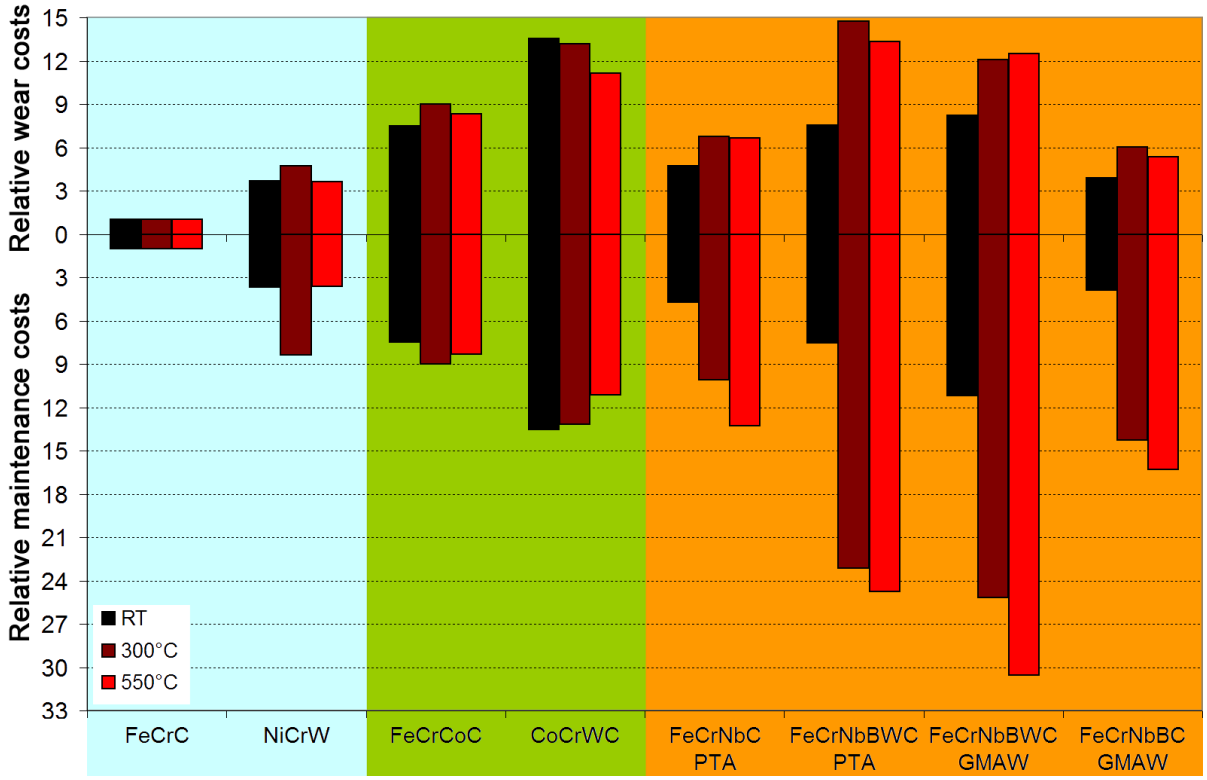

Fig. 94: Relative costs for wear protection in high-stress abrasive environment

Data for high-stress abrasive environment are displayed in Fig. 94. As the FeCrC cast alloy has highest wear resistance at all temperatures and least material costs it also will entail least maintenance efforts. Costs of the Co-family are mainly driven by the higher material costs, wear loss on the other hand, is not so high that additional replacement will be necessary. HT components made of carbide-rich hardfacings in high-stress abrasive condition have two

combined disadvantages: high material costs and high wear loss making frequent replacement necessary. For the grate bar up to ~30× higher maintenance costs may arise.

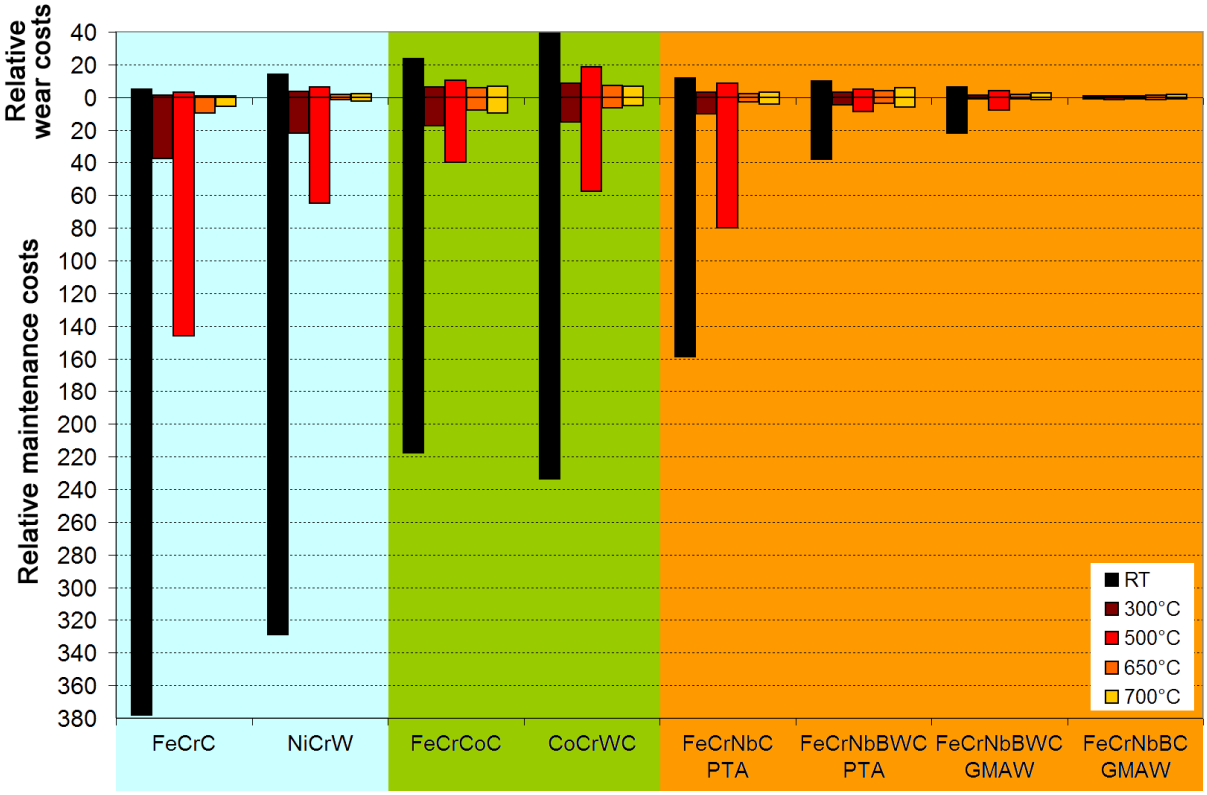

Fig. 95: Relative costs for wear protection in impact-abrasive environment

Impact-abrasive wear mode is the most critical mechanisms regarding maintenance efforts as displayed in Fig. 95. The two best alloys at all temperatures are FeCrNbBC-GMAW and FeCrNbBWC-GMAW due to their superior wear resistance. Although their high material costs, such alloys are necessary for impact-abrasive environment. At very HT the differences between the materials get less pronounced as material degradation of the carbide-rich hard-facings lowers their superior wear resistance observed at lower temperatures. Taking also the theoretical costs of frequent repair into account, especially the cast materials and Co-family result in dire performance. For the cast alloys, due to their inferior wear resistance, at the Co-family additionally the high material costs have to be considered. Summarising the view on possible maintenance costs in HT impact-abrasive environment, the correct choice of wear protection is essential, as wrong material selection makes frequent replacement necessary. This replacement costs cannot be compensated by the low material costs of the cast alloys and may lead to maintenance efforts up to >300× higher than for the best carbide-rich hardfacings.

Cost and maintenance estimations for oblique erosion are given in Fig. 96. The range of possible relative maintenance costs for the materials investigated goes up to ~20× of the most

cost efficient wear protection. Although the wear resistance of FeCrC is less than for carbide-rich hardfacings, the costs of wear loss are little because of the low material costs. Due to these data in oblique erosion environment, the application of highly sophisticated hardfacings cannot be recommended. Albeit wear resistance of carbide-rich hardfacings is slightly higher than for FeCrC cast alloy, their material costs are multiple times higher.

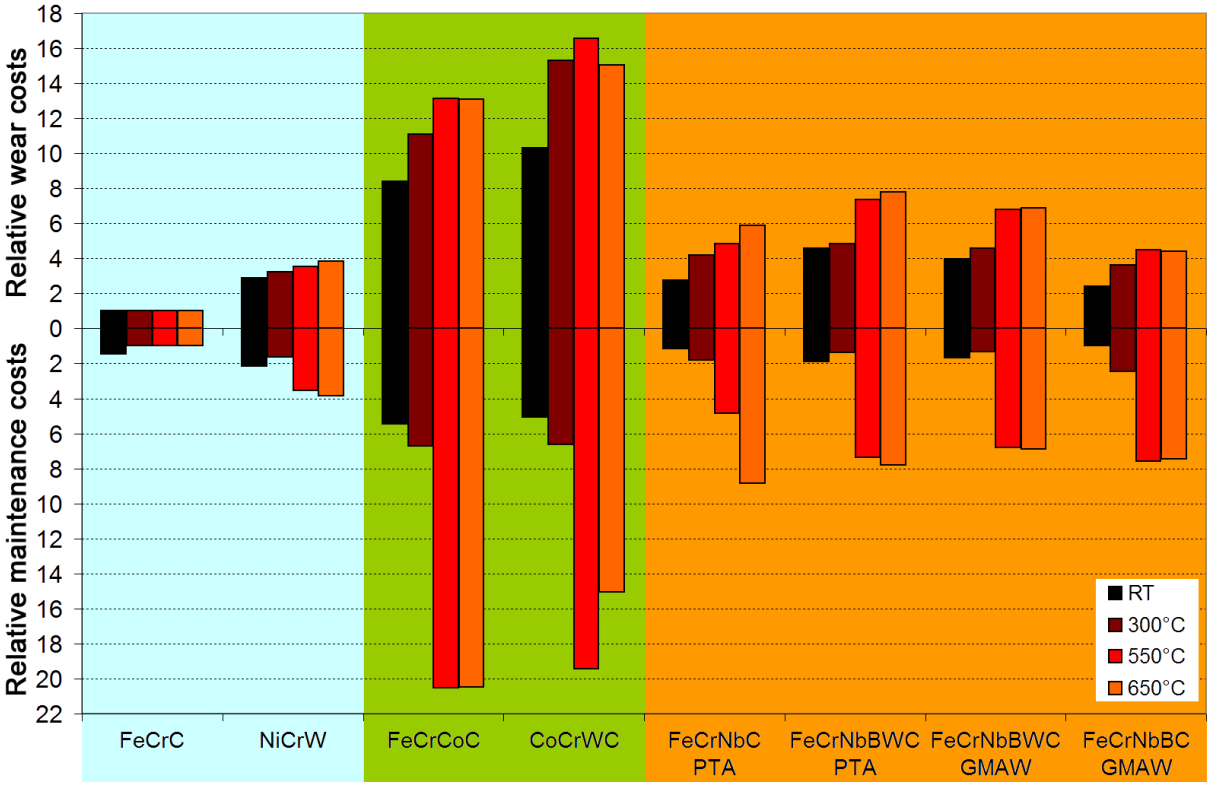

Fig. 96: Relative costs for wear protection in oblique erosion (30°) environment

Maintenance expenses in normal erosive environment are depicted in Fig. 97. This wear mode is significantly influenced by MML formation for the materials with low hardphase content leading to good performance of the cast alloys. As these alloys are also low in material and processing costs, their superiority is reasonable. The FeCrC cast alloy shows best wear resistance at all temperatures investigated, hence it is serving as reference of material loss costs and maintenance costs. Also wear rates of NiCrW are low, but concerning the higher material costs, maintenance efforts are 3-4× higher. The Co-family also shows good wear resistance, nevertheless, the very high material and processing costs render their application uneconomic. The carbide-rich hardfacings show combined disadvantages like high material costs and high wear rates entailing up to ~80× higher maintenance costs.

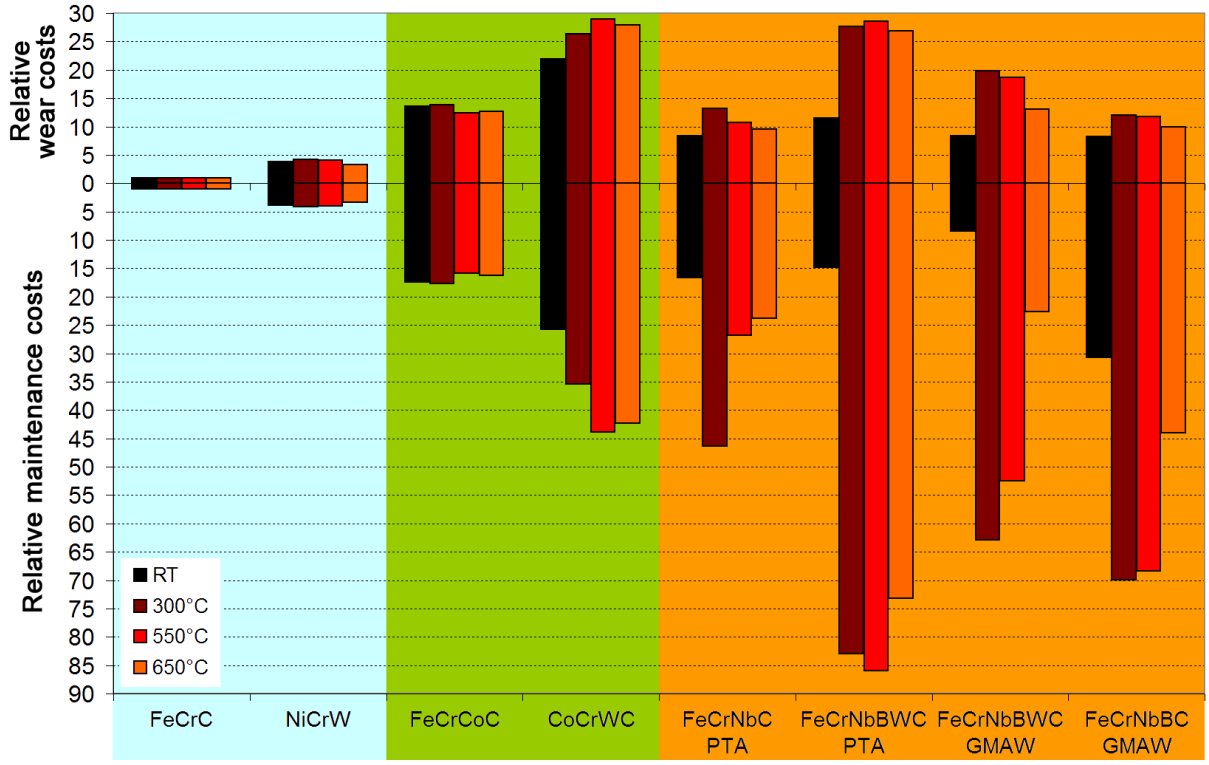

Fig. 97: Relative costs for wear protection in normal erosion (90°) environment

Concluding the maintenance evaluations of the hypothetic grate bar with application of the various wear resistant alloys, a wide range of possible maintenance costs was found. A factor of 10× costs compared to the most economic solution can easily be present, but this can go up to disastrous >100× at certain wear modes (especially impact-abrasion).

If replacement of the component is relatively easy, as in the example discussed here, and no plant downtime results by high wear loss, the cheapest material **FeCrC** was **most economic in most abrasive wear situations** except impact-abrasion. That means that even if higher wear loss is present, this is compensated by the relative cheap material and processing costs for the cast component. In case of **impact-abrasion** this is different, as here the **carbide-rich hardfacings** have many times lower wear rates than the cast alloys. Hence if the cheap cast alloy is applied, frequent replacement is necessary, leading to rocketing maintenance costs. So in impact-abrasive environment a carbide-rich hardfacing is inevitable to obtain low maintenance costs in a long-term view.

6. Summary

In steel production, many plants are exposed to high temperature (HT) wear. In this work, common tribological failures were investigated using the example of the sinter plant for iron ore refining. Sinter plants are necessary to provide optimal raw material size for the blast furnace, as too small particles will block the reduction process.

State of the art **sinter plants** are working according to the continuous Dwight-Lloyd sinter process. Here, ore fines, limestone, coke breeze and returned sinter are placed on a moving sinter belt and ignited from the top. A downward air flow guarantees the sintering of the whole sinter bed by the length of the sinter belt. High process temperatures in the range of 1200-1400°C are present in the sinter mixture. At the end of the sinter belt, the finished sinter cake is dropped into the crusher system, which is used to break up the sinter into smaller chunks. An HT sinter sieve is then necessary to remove fine parts from the crushed sinter. With the following sinter cooler, the HT components of the sinter plant are complete.

Evaluations of maintenance costs were utilised to identify core components exposed to tribological loading. For this purpose, maintenance costs (material costs and staff) and downtimes due to component failure are investigated. Combining these two data sources, the sinter belt was found to cause the highest costs due to expensive maintenance and frequent downtime. Grate bars of the sinter wagons are responsible for frequent downtimes, as broken bars need to be replaced immediately. The crusher system causes almost no unplanned downtimes, but is very expensive in maintenance, mainly due to material and repair costs of the wear protection. The second-highest maintenance costs are caused by the electronics, but their tribological improvement is not possible. Emission control causes the third-highest costs, followed by conveyor belts. These can both be improved by tribological measure, but as they are operating at ambient temperatures, they were not the key topic of this work. The last HT components causing remarkable maintenance costs are the HT sieves and chutes.

Additionally to the high maintenance costs of the HT components, they collectively suffer from **abrasive wear loss**. Grate bars are exposed to high-stress abrasive and corrosive wear at up to 800°C. The crusher system is stressed by the impacting hot sinter cake and the movement of the crusher causes additional abrasion. Temperatures of the sinter in this region are ~700°C. The screening of the sinter is done in the HT sieve, where an erosive wear mechanism dominates at the sieve cavities, with temperatures in the range of 300-500°C.

Core components of the sinter plant operating at HT were found to fail due to various forms of abrasion. To systematically investigate HT wear behaviour, various **materials for HT wear environment** were chosen for testing. A Fe-base and Ni-base cast alloy with ~15 % of hardphases, two hardfacings with Co content (no content of large hardphases and ~15 % carbides in Co-base matrix) and three hardphase-rich hardfacings were selected (~40-55 % hardphases). For the last group, the influence of welding technique was also investigated, comparing plasma transferred arc welding (PTA, one-layer) with gas metal arc welding (GMAW). At GMAW the deposition of two layers was necessary, due to the high dilution at one-layered structures.

The highest **hot hardness** of >900-1000 HV10 up to 500°C was found at two-layered GMAW alloys. The PTA-welded one-layered hardfacings show significantly lower hardness due to longer cooling times and some dilution with the matrix. The Ni- and Co-base materials keep their hardness nearly unchanged up to 800°C (maximum investigated temperature).

High-stress abrasive wear rates are lowest for the Fe-base cast alloy and the Co-family in the temperature range investigated (room temperature (RT) - 550°C). The carbide-rich hard-facings show very unbeneficial wear behaviour, especially at elevated temperatures. The good wear resistance of the relatively soft alloys can be put down to the in-situ formation of mechanically mixed layers (MML) with the abrasive, leading to excellent wear protection. For the carbide-rich hardfacings, on the other hand, brittle breaking of the hardphases dominates, which is exacerbated at higher temperatures. A linear relationship of the wear rate with hot hardness of the hardphase-rich hardfacings was found for both investigated PTA-welded and GMAW alloys.

In **impact-abrasive wear** condition, a high hardphase content and hardness was found to be indispensable for sufficient wear protection. Although the softer alloys form pronounced MMLs, their wear-protective effect at impact-abrasive condition is insufficient in the test field of RT-700°C. Within this abrasion mode, the highest range of wear rates was observed. This is especially evident comparing the best GMAW hardfacing and worst alloy (Fe-cast) at RT, which are separated by a factor of 17. A strong hardness dependency was found for this impact-abrasive environment. Hence, in applications with impact component, high hardness and hardphase content is inevitable in order to reach sufficient wear resistance.

Solid particle erosive wear was tested at oblique impact (30°) and normal impact (90°) at RT-650°C. Best wear resistance at oblique impact was found for the hardphase-rich materials at temperatures up to 550°C. At the highest testing temperature, the Fe-base cast alloy and

Co-base hardfacing are close to the carbide-rich hardfacings. Oblique erosive wear rates follow a linear relationship with the hot hardness of the materials. Merging of different materials to material groups was not successful; nevertheless, the wear rates of single materials can be calculated by knowing their hardness-temperature progress. Generally, the range of measured wear rates between the various materials under oblique erosion is low. Deviation is much higher at normal erosion, where the two cast alloys show the best wear resistance. The hardphase-rich hardfacings exhibit detrimental wear behaviour at elevated temperatures under this abrasion mode. The formation of MML was proven to efficiently aid wear protection for the materials with low hardphase content in normal erosion. A hardness dependency of normal erosive wear rates was observed for the cast materials and the hardphase-free material despite their massive MML formation. Thus the combined effect of material softening and increasing MML formation leads to a linear relationship with the hardness progress of these materials. The ratio of normal erosion results and oblique erosion results of almost all materials interestingly follows a linear dependency with the hot hardness of the materials within this investigation.

Two different **wear mechanisms** were observed, when taking all abrasion modes for the materials investigated into account. Materials with low hardphase content wear due to plastic deformation and a cutting wear mechanism, while hardphase-rich materials wear mainly by brittle fracture of the hardphases.

The **formation of MML** can significantly increase the wear protection of the surface by addition of hard wear resistant abrasives. This MML formation was observed for all abrasive wear modes for the materials with low hardphase content (<20 %). Nevertheless, the extent of MML is very microstructure-, temperature- and abrasion mode- (stress-) dependent. Highest abrasive coverage (MML) and penetration depth was found in impact-abrasive and high-stress abrasive environment, albeit not for the Co-base alloy with its fine hardphase network. So it is assumed that a too fine hardphase network impedes the embedding of abrasive particles, while it was easier for the Fe- and Ni-base alloy with 15 % carbides and the hardphase-free material. In erosive environment, significantly higher coverage and abrasive penetration depth was found for normal impact, while for oblique impact MML formation plays a minor role. This also explains the differences in the wear rates: while MML wear protection at oblique impact is minor, material loss due to plastic deformation and cutting is pronounced for the materials with low hardphase content. On the other hand, pronounced MML formation at normal impact entails superior wear resistance for these materials. Surface coverage is

strongly dependent on the microstructure, temperature and severity of contact: abrasives are easily embedded in matrix zones, which becomes more pronounced with temperature induced material softening and high-stress contact conditions (e.g. impact-abrasion). A fine carbide network hinders MML formation, until the severity of the contact exceeds a threshold leading to carbide network breakage and allowing MML formation. MML formation was found to be dependent on the abrasive particle energy in the contact. While erosion and three-body abrasion are in a range of small particle energies (<1 mJ), impact-abrasion is much severer. The thickness of MML was found to be strongly particle energy dependent, although a saturation level was observed in most materials, limiting further growth of the MML.

Brittle fracture of the hardphases is the major wear mechanisms for the hardphase-rich materials, especially for large Cr-carbides/carboborides. MML formation plays a minor role, as softer matrix areas are scarce. The affected depth increases with ascending temperatures, i.e. the cracks in the large hardphases reach deeper zones. This is put down to the differences in temperature-induced material softening between the hardphases and matrix: the hardness of the present hardphases is very stable within the investigated temperature range, while the Fe-base matrix suffers pronounced softening. It is assumed that this softening weakens the back-up of the hardphases entailing more pronounced cracking.

Lowest maintenance costs do not necessarily go conform with the best-performing alloys for certain wear modes and temperatures. Material and processing costs of highly sophisticated hardfacings may be much higher than of cast alloys. Hence, the life cycle costs of the wear components need to be assessed, i.e. material and processing costs, as well as costs for (frequent) exchange in the plant, if necessary. If replacement is easily possible, it was found that cheap cast alloys are often the most economic solution, also in a long-term view. Additionally, at certain wear modes the formation of MMLs put the cast alloys within the most wear-resistant materials. Nevertheless, one specific environment, namely impact-abrasion, makes the application of highly sophisticated hardphase-rich hardfacings inevitable. Wear rates of the cast alloys are much higher at this condition, which would make frequent replacement necessary, leading to rocketing maintenance costs if the wrong material is chosen in such environments with impact component.

7. Outlook

After performing this scientific study, implementation of the gained knowledge in the daily routine is sought. Nevertheless, also new questions arose and weaknesses of current techniques are revealed during research, which should be addressed in further studies:

- Due to the current design of the abrasion test equipment, maximum temperatures were limited to 550°C-700°C. For Fe-base materials, the critical temperature range in which microstructure and wear mechanisms might change is 500°C-700°C. Hence, updates of the heating systems of the devices are intended, in order to reach 700°C at the various abrasion modes. Metallic Ni- and Co-base alloys are often implemented in applications up to 1000°C or beyond. Therefore, a future goal is to reach this temperature range.
- The proposed analytical techniques of HT abrasive wear are a prospective measure to identify abrasive wear mechanisms quantitatively and may be implemented in a routine for evaluation of future wear results.
- In industrial plants, mostly a combined attack of various tribological and chemical loads take place. Within this work a combined impact-abrasive load was studied exemplarily, which showed significantly higher wear loss compared to the presence of solely abrasive wear. This points out the necessity to study combined interaction when present in the application. Especially at the grate bars addressed in this work HT-corrosion was found to exacerbate abrasive wear, hence the study of combined tribo-corrosion at HT is a task for future research.
- Commercially available materials were studied in this work. Wear results showed beneficial behaviour for different materials at certain abrasive conditions. Further improvement of materials and deposition techniques on the basis of found wear mechanisms, especially the formation of MMLs, is an ongoing goal for research.

8. Figures

9. Tables

10. Formulas

11. List of publications

- M. Varga, H. Winkelmann, E. Badisch: Impact of microstructure on high temperature wear resistance, Procedia Engineering 10 (2011) 1291-1296
- M. Varga, H. Rojacz, H. Winkelmann, H. Mayer, E. Badisch: Wear reducing effects and temperature dependence of tribolayer formation in harsh environment, Tribology International 65 (2013) 190-199
- M. Varga, C. Goniva, K. Adam, E. Badisch: Combined experimental and numerical approach for wear prediction in feed pipes, Tribology International 65 (2013) 200-206
- M. Varga, M. Buranich, K. Adam, R. Wimberger, E. Badisch: Cost efficient tribological systems in steel production based on life cycle optimisation, Proceedings 5th World Tribology Congress 8.-13.9.2013, Torino (2013)
- M. Varga, E. Badisch, H. Winkelmann, K. Adam: High temperature wear phenomena in steel production plants on the example of a coke quenching car, Proceedings 5th World Tribology Congress 8.-13.9.2013, Torino (2013)
- M. Varga, AMF. Azhaarudeen, E. Badisch: Influence of in-situ formed tribolayer on abrasive wear reduction, Materials Science Forum 825-826 (2015) 85-92
- M. Varga, L. Widder, M. Griesinger, K. Adam, E. Badisch: Wear progress and mechanisms in high temperature sieves, Engineering Failure Analysis in press (2015)
- M. Varga, M. Flasch, E. Badisch: Introduction of a novel tribometer especially designed for scratch, adhesion and hardness investigation up to 1000°C, Proceedings of the Institution of Mechanical Engineers Part J: Journal of Engineering Tribology in press (2015)
- M. Varga, AMF. Azhaarudeen, K. Adam, E. Badisch: Influence of load and temperature on abrasion of carbidic cast steel and complex alloyed hardfacing, Key Engineering Materials 674 (2016) 313-318

- H. Winkelmann, M. Varga, E. Badisch, H. Danninger: Wear mechanisms at high temperatures: Part 2: Temperature effect on wear mechanisms in the erosion test, Tribology Letters 34/3 (2009) 167-175
- H. Winkelmann, M. Varga, E. Badisch, H. Danninger: Wear mechanisms at high temperatures. Part 3: Changes of the wear mechanism in the continuous impact abrasion test with increasing testing temperature, Tribology Letters 37/2 (2010) 419-429
- H. Winkelmann, M. Varga, E. Badisch: Disquisition on material parameters and their influence on wear rates at high temperatures, Tribologia 30/1-2 (2011) 12-20
- H. Winkelmann, M. Varga, E. Badisch: Influence of secondary precipitations in Fe-based MMCs on high temperature wear behaviour, Tribology Letters 43/2 (2011) 229-234
- W. Molnar, M. Varga, P. Braun, K. Adam, E. Badisch: Correlation of rubber based conveyor belt properties and abrasive wear rates under 2- and 3-body conditions, Wear 320/1 (2014) 1-6
- H. Torres, M. Varga, F. Widder, U. Cihak-Bayr, O. Viskovic, M. Rodríguez Ripoll: Experimental simulation of high temperature sliding contact of hot rolled steel, Tribology International 93B (2016) 745-754

12. References

ADA03 K. Adachi, IM. Hutchings: Wear-mode mapping for the micro-scale abrasion test, Wear 255 (2003) 23-29

ADA05 K. Adachi, IM. Hutchings: Sensitivity of wear rates in the micro-scale abrasion test to test conditions and material hardness, Wear 258 (2005) 318-321

ALL01 DN. Allsopp, IM. Hutchings: Micro-scale abrasion and scratch response of PVD coatings at elevated temperatures, Wear 251 (2001) 1308-1314

ANT09 M. Antonov, I. Hussainova: Experimental setup for testing and mapping of high temperature abrasion and oxidation synergy, Wear 267 (2009) 1795-1803

ANT12 M. Antonov, I. Hussainova, R. Veinthal, J. Pirso: Effect of temperature and load on three-body abrasion of cermets and steel, Tribology International 46 (2012) 261-268

ARC53 JF. Archard: Contact and rubbing of flat surfaces, Journal of Applied Physics 24 (1953) 981-988

AST10 ASTM G65-04: Standard test method for measuring abrasion using the dry sand/rubber wheel apparatus, American Society for Testing and Materials (2010)

AST11 ASTM E384-11e1: Standard test method for Knoop and Vickers hardness of materials, American Society for Testing and Materials (2011)

AST13 ASTM G76-13: Standard test method for conducting erosion tests by solid particle impingement using gas jets, American Society for Testing and Materials (2013)

AST15 ASTM D3389-15: Standard test method for coated fabrics abrasion resistance (Rotary Platform Abrader), American Society for Testing and Materials (2015)

AVE61 HS. Avery: The measurement of wear resistance, Wear 4 (1961) 427-449

AVH61 Akademischer Verein Hütte, E.V. in Berlin: Hütte - Taschenbuch für Eisenhüttenleute, Verlag von Wilhelm Ernst & Sohn, Berlin; Verlag Stahleisen mbH, Düsseldorf (1961) 522-524

AXE94 N. Axén, S. Jacobson, S. Hogmark: Influence of hardness of the counterbody in three-body abrasive wear-an overlooked hardness effect, Tribology International 27/4 (1994) 233-241

AXE97 N. Axén, S. Jacobson, S. Hogmark: Principles for the tribological evaluation of intrinsic coating properties, Wear 203-204 (1997) 637-641

BAD03 E. Badisch, C. Mitterer: Abrasive wear of high speed steels: Influence of abrasive particles and primary carbides on wear resistance, Tribology International 36 (2003) 765-770

BAD08 E. Badisch, M. Kirchgaßner: Influence of welding parameters on microstructure and wear behaviour of a typical NiCrBSi hardfacing alloy reinforced with tungsten carbide, Surface & Coatings Technology 202 (2008) 6016-6022

BAD09 E. Badisch, M. Kirchgaßner, F. Franek: Continuous impact-abrasion testing: influence of testing parameters on wear behaviour, Proceedings of the Institution of Mechanical Engineers Part J: Journal of Engineering Tribology 223/5 (2009) 741-750

BAD10 E. Badisch, C. Katsich, H. Winkelmann, F. Franek, M. Roy: Wear behaviour of hardfaced Fe-Cr-C alloy and austenitic steel under 2-body and 3-body conditions at elevated temperature, Tribology International 43 (2010) 1234-1244

BEA14 B. Beake, A. Harris, M. Davies, et al.: The use of high temperature nanomechanics in designing coatings with improved wear resistance in high-speed machining, 16th Nordic symposium on tribology, Aarhus, Denmark, 10-13. June 2014, paper 13

BER01 H. Berns, B. Wewers: Development of an abrasion resistant steel composite with in situ TiC particles, Wear 251 (2001) 1386-1395

BER95 H. Berns: Microstructural properties of wear-resistant alloys, Wear 181-183 (1995) 271-279

BER97 H. Berns, SD. Franco: Effect of coarse hard particles on high-temperature sliding abrasion of new metal matrix composites, Wear 203-204 (1997) 608-614

BER98 H. Berns (ed.): Hartlegierungen und Hartverbundwerkstoffe, Springer Berlin, Heidelberg (1998)

BER99-1 H. Berns, S. Koch: High temperature sliding abrasion of nickel-base alloy and composite, Wear 225-229 (1999) 154-162

BER99-2 H. Berns, S. Koch: Influence of abrasive particles on wear mechanisms and wear resistance in sliding abrasion tests at elevated temperatures, Wear 233-235 (1999) 424-430

BIR10 Y. Birol: High-temperature abrasive wear testing of potential tool materials for thixoforming of steels, Tribology International 43 (2010) 2222-2230

BOG71 L. Bogdandy, HJ. Engell: The reduction of iron ores - scientific basis and technology, Verlag Stahleisen mbH, Düsseldorf; Springer-Verlag Berlin, Heidelberg, New York (1971) 374-383

BRI21 JA. Brinell: Researches on the resistance of iron, steel and some other materials to wear, Jernkontorets Ann (1921)

CAP73 F. Cappel, H. Wendeborn: Sintern von Eisenerzen, Verlag Stahleisen mbH, Düsseldorf (1973)

CES06 L.Ceschini, G. Palombarini, G. Sambogna, D. Firrao, G. Scavino, G. Ubertalli: Friction and wear behaviour of sintered steels submitted to sliding and abrasion tests, Tribology International 39 (2006) 748-755

CHA10 JG. Chacon-Nava, A. Martinez-Villafañe, F. Almeray-Calderon, JA. Cabral-Miramontes, MM. Stack: Some remarks on particle size effects on the abrasion of a range of Fe based alloys, Tribology International 43 (2010) 1307-1317

CHE98 H. Chen, IM. Hutchings: Abrasive wear resistance of plasma-sprayed tungsten carbide-cobalt coatings, Surface & Coatings Technology 107 (1998) 106-114

COZ11 RC. Cozza, DK. Tanaka, RM. Souza: Friction coefficient and wear mode transition in micro-scale abrasion tests, Tribology International 44 (2011) 1878-1889

DAN08 R. Danzer, T. Lube, P. Supancic, R. Damani: Fracture of ceramics, Advanced Engineering Materials 10/4 (2008) 275-298

DIN79 DIN 50320:1979-12: Wear; Terms, systematic analysis of wear processes, classification of wear phenomena, Deutsches Institut für Normung (1979)

DIN99 DIN EN ISO 5470-1: Rubber- or plastics-coated fabrics - Determination of abrasion resistance – Part 1: Taber abrader, Deutsches Institut für Normung (1999)

DOG95-1 Ö.N. Doğan, G. Laird II, J.A. Hawk: Abrasion resistance of the columnar zone in high Cr white cast irons, Wear 181-183 (1995) 342-349

DOG95-2 Ö.N. Doğan, J.A. Hawk: Effect of carbide orientation on abrasion of high Cr white cast iron, Wear 189 (1995) 136-142

DUB99 NB. Dube, IM. Hutchings: Influence of particle fracture in the high-stress and low-stress abrasive wear of steel, Wear 233-235 (1999) 246-256

FAH14 H. Fahrenwaldt, V. Schuler, J. Twrdek: Praxiswissen Schweißtechnik - Werkstoffe, Prozesse, Fertigung, Springer Vieweg, Wiesbaden, 5th edition (2014)

FIS92 A. Fischer: Mechanisms of high temperature sliding abrasion of metallic materials, Wear 152 (1992) 151-159

GAH87 Zum Gahr: Microstructure and Wear of Materials, Elsevier Science Publishers, Tribology Series 10 (1987)

GAL97 R. Gåhlin, M. Larsson, P. Hedenqvist, S. Jacobson, S. Hogmark: The crater grinder method as a means for coating wear evaluation - an update, Surface & Coatings Technology 90 (1997) 107-114

GAT98 JD. Gates: Two-body and three-body abrasion: A critical discussion, Wear 214 (1998) 139-146

GEI05 P. Geiderer: Testing of combined impact-abrasion wear, FH-diploma thesis, FH Wiener Neustadt (2005)

GOR97 GJ. Gore, JD. Gates: Effect of hardness on three very different forms of wear, Wear 203-204 (1997) 544-563

GOS79 GOST 23.201-78: Products wear resistance assurance. Gas abrasive wear testing of materials and coatings with centrifugal accelerator, Euro-Asian Council for Standardization, Metrology and Certification (1979)

HAW01 JA. Hawk, RD. Wilson: Tribology of earthmoving, mining and minerals processing, in B. Bhushan (ed.), Modern Tribology Handbook, CRC Press, Vol. 2 (2001) 1331-1370

HOR15 J. Hornung: private communication with the author on the costs of hardfacing powders per kg, from the price list of Castolin, 25.09.2015

HUS01 I. Hussainova, J. Kubarsepp, J. Pirso: Mechanical properties and features of erosion of cermets, Wear 250 (2001) 818-825

HUT92 IM. Hutchings: Ductile-brittle transitions and wear maps for the erosion and abrasion of brittle materials, Journal of Physics D 25 (1992) A212-A221

HUT98 IM. Hutchings: Abrasive an erosive wear tests for thin coatings: a unified approach, Tribology International 31/1-3 (1998) 5-15

ISO95 ISO 6507-1:2005: Metallic materials - Vickers hardness test - Part 1: Test method, International Organization for Standardization (2005)

JAC92 S. Jacobson, M. Olsson, P. Hedenqvist, et al.: Scratch testing. In: P. Blau (ed.), ASM Handbook 18 (1992) 820-837

JAH75 S. Jahanmir, NP. Suh, EP. Abrahamson: The delamination theory of wear and the wear of a composite surface, Wear 32 (1975) 33-49

JON09 LC. Jones, RJ. Llewellyn: Sliding abrasion resistance assessment of metallic materials for elevated temperature mineral processing conditions, Wear 267 (2009) 2010-2017

KAO00 K. Kato: Wear in relation to friction - a review, Wear 241 (2000) 151-157

KAO01 K. Kato, K. Adachi: Wear mechanisms, in B. Bhushan (ed.), Modern Tribology Handbook, CRC Press, Vol. 1 (2001) 273-300

KAT07 C. Katsich: Hochtemperatur-Werkstoffverhalten von Eisen-Basislegierungen bei Kombination von Schlag und Abrasion, Master Thesis, MUL Leoben (2007)

KAT09 C. Katsich, E. Badisch, M. Roy, GR. Heath, F. Franek: Erosive wear of hardfaced Fe-Cr-C alloys at elevated temperature, Wear 267 (2009) 1856-1864

KAT11 C. Katsich, E. Badisch: Effect of carbide degradation in Ni-based hardfacing under abrasive and combined impact/abrasive conditions, Surface & Coatings Technology 206 (2011) 1062-1068

KEL01 DA. Kelly, IM. Hutchings: A new method for measurement of particle abrasivity, Wear 250 (2001) 76-80

KEN01 FE. Kennedy, PJ. Blau: Glossary, in B. Bhushan (ed.), Modern Tribology Handbook, CRC Press, Vol. 2 (2001) 1645-1659

KIR08 M. Kirchgaßner, E. Badisch, F. Franek: Behaviour of iron-based hardfacing alloys under abrasion and impact, Wear 265 (2008) 772-779

KLE05 I. Kleiss, P. Kulu: Solid particle erosion - occurrence, prognostification and control, TUT Press, Tallinn (2005)

KUL05 P. Kulu, I. Hussainova, R. Veinthal: Solid particle erosion of thermal sprayed coatings, Wear 258 (2005) 488-496

LIN13 M. Linz, H. Winkelmann, K. Hradil, E. Badisch, F. Mücklich: Directional development of residual stress and surface fatigue during sliding contact, Engineering Failure Analysis 35 (2013) 678-685

LIU01 H.-N. Liu, M. Sakamoto, M. Nomura, K. Ogi: Abrasion resistance of high Cr cast irons at an elevated temperature, Wear 250 (2001) 71-75

MAR14 HP. Martin: Material characterization-hot hardness test at 1500°C, Fraunhofer IKTS http://www.ikts.fraunhofer.de/content/dam/ikts/de/doc2/Sintern-Charakt/Mechanische_Werkstoffpruefung/IKTS_Materialcharakterisierung_Härte.pdf (retrieved 31.12.2014)

MIS80 A. Misra, I. Finnie: A classification of three-body abrasive wear and design of a new tester, Wear 60 (1980) 111-121

MOL14 W. Molnar, M. Varga, P. Braun, K. Adam, E. Badisch: Correlation of rubber based conveyor belt properties and abrasive wear rates under 2- and 3-body conditions, Wear 320/1 (2014) 1-6

MOO80 MA. Moore, FS. King: Abrasive wear of brittle solids, Wear 60 (1980) 123-140

MUT88 PJ. Mutton: Abrasion resistant materials for the Australian minerals industry, Australian Minerals Industries Research Association Limited (1988)

NOR80 TE. Norman: Wear in ore processing machinery, Wear Control Handbook (1980)

OEN98 ÖNORM EN 13306, 1998: Maintenance terminology, Austrian Standards Institute (1998)

OLS15 M. Olsson, J. Heinrichs, K. Yvell, S. Jacobson: Initial degradation of cemented carbides for rock drilling-Model studies of the tribological contact against rock, International Journal of Refractory Metals and Hard Materials 52 (2015) 104-113

PAU03 A. Pauschitz, M. Roy, F. Franek: Comparative analysis of high temperature wear of Chrome by the formation of alloying of Fe and Ni basis alloys, Tribologie und Schmierungstechnik 5 (2003) 40-49

POL08 R. Polak, S. Ilo, E. Badisch: Relation between inter-particle distance (L_{IPD}) and abrasion in multiphase matrix-carbide materials, Tribology Letters 33/1 (2008) 29-35

QIA97 M. Qian, W. Chaochang: Impact-abrasion behavior of low alloy white cast irons, Wear 209 (1997) 308-315

RAB61 E. Rabinowicz, LA. Dunn, PG. Russell: A study of abrasive wear under three-body conditions, Wear 4 (1961) 345-355

RAT13 V. Ratia, I. Miettunen, VT. Kuokkala: Surface deformation of steels in impact-abrasion: The effect of sample angle and test duration, Wear 301 (2013) 94-101

REN09 J. Rendón, M. Olsson: Abrasive wear resistance of some commercial abrasion resistant steels evaluated by laboratory test methods, Wear 267 (2009) 2055-2061

ROJ15 H. Rojacz, L. Krabac, M. Varga, K. Adam, G. Fafilek: The behaviour of steels exposed to the high temperature corrosive environment of a sintering plant for pig iron production, Corrosion Science submitted 14.9.15 (2015)

ROY06 M. Roy: Elevated temperature erosive wear of metallic materials, Journal of Physics D 39 (2006) R101-R124

RUT96 KL. Rutherford, IM. Hutchings: A micro-abrasive wear test, with particular application to coated systems, Surface & Coatings Technology 79 (1996) 231-239

SAT05 T. Satoh, H.-N. Liu, M;. Sakamoto: High temperature properties of a high-chromium cast iron and its composites fabricated via powder metallurgy process, Journal of Materials Science 40 (2005) 3283-3286

SCH10 M. Schenk: Instandhaltung technischer Systeme, Berlin, Heidelberg: Springer (2010)

SHA14 B. Shah, R. Kirchmayer, J. Luster, M. Varga, E. Badisch: Increasing the product life cycle of sinter crusher components by systematic analysis of complex combined wear phenomena, Poster European Steel Environment and Energy Congress, 15.-17.9.2014, Teesside University, UK (2014)

SHI95 PH. Shipway, IM. Hutchings: Measurement of coating durability by solid particle erosion, Surface & Coatings Technology 71 (1995) 1-8

SLA15 K. Slater: http://www.reliabilityweb.com/art07/advanced_maintenance.htm, Reliabilityweb.com (retrieved 27.10.2015)

STO02 FH. Stott: High-temperature sliding wear of metals, Tribology International 35 (2002) 489-495

SUH73 NP. Suh: The delamination theory of wear, Wear 25 (1973) 111-124

SUN01 A. Sundström, J. Rendón, M. Olsson: Wear behaviour of some low alloyed steels under combined impact-abrasion contact conditions, Wear 250 (2001) 744-754

TOR16 H. Torres, M. Varga, F. Widder, U. Cihak-Bayr, O. Viskovic, M. Rodríguez Ripoll: Experimental simulation of high temperature sliding contact of hot rolled steel, Tribology International 93B (2016) 745-754

TRE99 RI. Trezona, DN. Allsopp, IM. Hutchings: Transition between two-body and three-body abrasive wear: influence of test conditions in the microscale abrasive wear test, Wear 225-229 (1999) 205-214

TUO14 J. Tuominen, T. Ristonen, J. Näkki, T. Peltola, H. Pajukoski, T. Nyyssönen, P. Vuoristo: High performance wear and corrosion resistant coatings by novel cladding techniques, Proceedings 28th conference on Surface Modification Technologies 16-18.6.2014, Tampere (2014) 105-117

TYL92 Tylczak, Oregon: Friction, Lubrication and Wear Technology-Abrasive wear, ASM Handbook, 337-351 (1992)

VAR10 M. Varga: Konzeption und Entwicklung eines Prüfstandes zur Messung der Warmhärte, Master thesis, FH Wiener Neustadt (2010)

VAR11 M. Varga, H. Winkelmann, E. Badisch: Impact of microstructure on high temperature wear resistance, Procedia Engineering 10 (2011) 1291-1296

VAR13-1 M. Varga, H. Rojacz, H. Winkelmann, H. Mayer, E. Badisch: Wear reducing effects and temperature dependence of tribolayer formation in harsh environment, Tribology International 65 (2013) 190-199

VAR13-2 M. Varga, C. Goniva, K. Adam, E. Badisch: Combined experimental and numerical approach for wear prediction in feed pipes, Tribology International 65 (2013) 200-206

VAR13-3 M. Varga, M. Buranich, K. Adam, R. Wimberger, E. Badisch: Cost efficient tribological systems in steel production based on life cycle optimisation, Proceedings 5th World Tribology Congress 8.-13.9.2013, Torino (2013)

VAR13-4 M. Varga, E. Badisch, H. Winkelmann, K. Adam: High temperature wear phenomena in steel production plants on the example of a coke quenching car, Proceedings 5th World Tribology Congress 8.-13.9.2013, Torino (2013)

VAR15-1 M. Varga, AMF. Azhaarudeen, E. Badisch: Influence of in-situ formed tribolayer on abrasive wear reduction, Materials Science Forum 825-826 (2015) 85-92

VAR15-2 M. Varga, L. Widder, M. Griesinger, K. Adam, E. Badisch: Wear progress and mechanisms in high temperature sieves, Engineering Failure Analysis in press (2015)

VAR15-3 M. Varga, M. Flasch, E. Badisch: Introduction of a novel tribometer especially designed for scratch, adhesion and hardness investigation up to 1000°C, Proceedings of the Institution of Mechanical Engineers Part J: Journal of Engineering Tribology in press (2015)

VAR16 M. Varga, AMF. Azhaarudeen, K. Adam, E. Badisch: Influence of load and temperature on abrasion of carbidic cast steel and complex alloyed hardfacing, Key Engineering Materials 674 (2016) 313-318

VDE71 Verein deutscher Eisenhüttenleute: Gemeinfassliche Darstellung des Eisenhüttenwesens, Verlag Stahleisen mbH, Düsseldorf (1971) 29-32

VDI02 VDI: VDI-Guideline Technical availability of machines and production lines, VDI 3423, Beuth Berlin (2002)

VDI06 VDI: Maintenance-Guidelines, VDI 2885-2899, Beuth Berlin (2006)

VEN97 K. Venkatesan, C. Subramanian, E. Summerville: Three-body abrasion of surface engineered dies steel at elevated temperatures, Wear 203-204 (1997) 129-138

WIN09-1 H. Winkelmann, E. Badisch, M. Kirchgaßner, H. Danninger: Wear mechanisms at high temperatures. Part 1: Wear mechanisms of different Fe-based alloys at elevated temperatures, Tribology Letters 34 (2009) 155-166

WIN09-2 H. Winkelmann, M. Varga, E. Badisch, H. Danninger: Wear mechanisms at high temperatures: Part 2: Temperature effect on wear mechanisms in the erosion test, Tribology Letters 34/3 (2009) 167-175

WIN09-3 H. Winkelmann: Wear mechanisms at high temperatures as acting at the industry application sinter grate, Dissertation, TU Wien (2009)

WIN10 H. Winkelmann, M. Varga, E. Badisch, H. Danninger: Wear mechanisms at high temperatures. Part 3: Changes of the wear mechanism in the continuous impact abrasion test with increasing testing temperature, Tribology Letters 37/2 (2010) 419-429

WIN11-1 H. Winkelmann, M. Varga, E. Badisch: Disquisition on material parameters and their influence on wear rates at high temperatures, Tribologia 30/1-2 (2011) 12-20

WIN11-2 H. Winkelmann, M. Varga, E. Badisch: Influence of secondary precipitations in Fe-based MMCs on high temperature wear behaviour, Tribology Letters 43/2 (2011) 229-234

WIR00 S. Wirojanupatump, PH. Shipway: Abrasion of mild steel in wet and dry conditions with the rubber and steel wheel abrasion apparatus, Wear 239/1 (2000) 91-101

XUX13 X. Xu, W. Xu, FH. Ederveen, S. Zwaag: Design of low hardness abrasion resistant steels, Wear 301 (2013) 89-93

ZIK13 A. Zikin, M. Antonov, I. Hussainova, L. Katona, A. Gavrilovic: High temperature wear of cermet particle reinforced NiCrBSi hardfacings, Tribology International 68 (2013) 45-55

ZIK15 A. Zikin, I. Hussainova, C. Katsich, E. Badisch, C. Tomastik: Advanced chromium carbide-based hardfacings, Surface & Coatings Technology 206 (2015) 4270-4278

ZOK07 FW. Zok, A. Miserez: Property maps for abrasion resistance of materials, Acta Materialia 55 (2007) 6365-6371